UNIVERSITÀ DEGLI STUDI FIRENZE

DOTTORATO DI RICERCA IN
SCIENZE BIOMEDICHE

CICLO XXXII

COORDINATORE Prof. Massimo Stefani

Study of the relationship between structure and toxicity of different α-synuclein aggregates and related cellular dysfunctions

Settore Scientifico Disciplinare **BIO/10**

Dottoranda
Dott.ssa Alessandra Bigi

Tutore
Prof.ssa Cristina Cecchi

Coordinatore
Prof. Massimo Stefani

Anni 2016/2019

TABLE OF CONTENTS

INDEX OF FIGURES

LIST OF TABLES

LIST OF ABBREVIATIONS

3-MA – 3-Methyladenine

AADC – Aromatic amino acid decarboxylase

AD – Alzheimer's disease

AFM – Atomic force microscopy

ALP – Autophagy-lysosome pathway

AMPAR – α-Amino-3-hydroxy-5-methyl-4-isoxazolepropionic acid receptor

ANS – 8-Anilino-1-naphthalenesulfonate

Atg – Autophagy-related genes

Aβ – Amyloid beta

BBB – Blood-brain barrier

Calcein-AM – Calcein-acetoxymethyl ester

CaM – Calmodulin

CaMKII – Ca^{2+}/CaM-dependent protein kinase II

CD – Circular dichroism

CM-H2DCFDA – 5-(and-6)-Chloromethyl-2',7'-dichlorodihydrofluorescein diacetate

CMA – Chaperone-mediated autophagy

CNQX – 6-Cyano-7-nitroquinoxaline-2,3-dione

COMT – Catechol-O-methyltransferase

Cryo-EM – Cryo-electron microscopy

CSF – Cerebrospinal fluid

CTX-B – Cholera toxin subunit B

D1R/D2R – Dopamine D1/D2 receptors

DAT – Dopamine transporter

DBS – Deep brain stimulation

DLB – Dementia with Lewy bodies

DMEM – Dulbecco's Modified Eagle's Medium

DTI – Diffusion tensor imaging

EGCG – Epigallocatechine gallate

EM – Electron microscopy

ER – Endoplasmic reticulum

FAM-FLICA – Fluorescent carboxyfluorescein - Fluorescent-labeled inhibitor of caspases

FAM-DEVDFMK – Fluorescent carboxyfluorescein - Aspartic acid-glutamic acid-valine-aspartic acid fluoromethyl ketone

FBS – Fetal bovine serum

Fluo 4-AM – Fluo 4-acetoxymethyl ester

FT-IR – Fourier Transform Infrared Spectroscopy

GM1 – Monosialotetrahexosylganglioside 1

HATs - Histone acetyltransferases

HDACs – Histone deacetylases

HEK – Human embrionic kidney

HEPES – 4-(2-Hydroxyethyl)piperazine-1-ethanesulfonic acid

Hoechst 33342 – (2'-[4-ethoxyphenyl]-5-[4-methyl-1-piperazinyl]-2,5'-bi-1H benzimidazole trihydrochloride trihydrate

HSPGs – Heparan sulfate proteoglycans

IDP – Intrinsically disordered protein

InsP3R – Inositol 1,4,5-trisphosphate receptor

IRE – Internal reflection element

L-DOPA – Levodopa

LAG3 – Lymphocyte activation gene 3

LAMP2A – Lysosome-associated membrane protein type 2A

LB – Lewy body **LBs** – Lewy bodies

LF – Long fibrils

lncRNA – Long non-coding RNA

LNs – Lewy neurites

LTP – Long term potentiation

M – Monomer

MAM – Mitochondrial-associated ER membrane

MAOB – Monoamine oxidase type B

MCU – Mitochondrial calcium uniporter

MCT – Mercury cadmium telluride

Mem – Memantine

mGluR5 – Metabotropic glutamate receptor 5

miRNA – Micro RNA

mRNA – Messenger RNA

MSA – Mutliple system atrophy

MSR – Methionine sulfoxide reductase

MTT – 3-(4,5-Dimethylthiazol-2-yl)-2,5-diphenyltetrazolium bromide

NAC – Non-Aβ-amyloid component

NCX – Na^+/Ca^{2+} exchanger

NKA – Na^+/K^+-ATPase

NMDAR – N-methyl-D-aspartate ionotropic glutamatergic receptor

NMR – Nuclear magnetic resonance

OA* – Type A* oligomers

OB* – Type B* oligomers

PBS – Phosphate buffered saline

PD – Parkinson's disease

PDMP – D-threo-1-phenyl-2-decanoylamino-3-morpholino-1-propanol

PET – Positron emission tomography

PFFs – Pre-formed fibrils

PGC-1α – Peroxisome proliferator–activated receptor γ coactivator-1α

PKC – Protein kinase C

PMCA – Protein-Misfolding Cyclic Amplification

PMCA – Plasma membrane Ca^{2+} ATPase

POPS – 1-Palmitoyl-2-oleoyl-sn-glycero-3-phospho-L-serine

PP2A – Protein phosphatase 2A

PrP^C – Cellular prion protein

PTP – Permeability transition pore

PTM – Post-translational modification

ROC – Receptor-operated channel

ROS – Reactive oxygen species

RPMI medium – Roswell Park Memorial Institute medium

RT-QuIC – Real-Time Quaking- Induced Conversion

RyR – Ryanodine receptor

SDS – Sodium dodecyl sulfate

SERCA – ER/SR Ca^{2+}-ATPase

SF – Short fibrils

SLBs – Supported lipid bilayers

SN – Substantia nigra

SNAP25 – Synaptosomal-associated protein 25

SNARE – Soluble N-ethylmaleimide-sensitive factor attachment protein receptor

SNAREpin – SNARE protein complex

SNpc – Substantia nigra pars compacta

SNRIs – Serotonin-norepinephrine reuptake inhibitors

SPCA – Secretory pathway Ca^{2+}-ATPase

SPECT – Single photon emission computed tomography

SR/ER – Sarco/endoplasmic reticulum

SSRIs – Selective serotonin receptor inhibitors

SUVs – Small unilamellar vesicles

TBS – Tris-buffered saline

TEM – Transmission electron microscopy

TH – Tyrosine hydroxylase

ThT – Thioflavin T

TNT – Tunneling nanotubes

UPR – Unfolded protein response

UPS – Ubiquitin/Proteasome System

UPSIT – University of Pennsylvania's smell identification test

VAMP2 – Vesicle associated membrane protein 2

VDAC1 – Voltage-dependent anion channel 1

VMAT2 – Vesicular monoamine transporter 2

VOC – Voltage-operated channel

WT – Wild-type

αS, βS, γS – α-, β- and γ-Synuclein

α3-NKA – α3-subunit of Na^+/K^+-ATPase

ABSTRACT

α-Synucleinopathies are a vast group of neurodegenerative disorders characterized by the abnormal accumulation of insoluble aggregates, both in neurons and in oligodendrocytes, whose major component is the protein α-synuclein (αS). Among them, Parkinson's disease (PD) is the most widespread; it is defined by the progressive loss of dopaminergic neurons in the *substantia nigra*, responsible for several motor disturbances, such as bradykinesia, muscular rigidity and resting tremor.

This work is focused on αS, whose abnormal self-assembly gives rise to insoluble inclusions called Lewy bodies and neurites, the most relevant neuropathological hallmarks of PD. The aggregation process of αS is extremely complex and leads to the formation of a wide range of assemblies such as oligomers, protofibrils and fibrils. To define the nature of the species responsible for neuronal damage and their mechanism of action, in the first part of this work we have evaluated the evolution in time of different readouts of cellular dysfunction in neuronal cells. We found that, at early incubation times, small oligomeric species with a rudimentary cross-β structure and high solvent exposed hydrophobicity are by far the most toxic to cells, whereas unstructured monomers and hydrophilic and disordered oligomers are unable to cause any cellular dysfunction. We also found that αS fibrils induce the same cascade of events as toxic oligomers, but more slowly and at a rate dependent on their length, despite their inability to be internalized by the cells. Thus, we associated the toxic capacity of αS fibrillar assemblies with their ability to release small hydrophobic oligomers with a cross-β architecture, particularly effective in crossing neuronal membranes and in inducing neurotoxicity. Our results indicate that oligomers are the most toxic among the analysed αS species, but fibrillar assemblies can generate neurotoxicity through the release of small oligomeric aggregates, that can in turn contribute to the toxicity associated with their well-characterized ability to transfer from neuron-to-neuron, causing the spreading of Lewy body pathology.

In the second part of this study we focused on the ability of αS species to interact with neuronal membranes and we analysed the involvement of the different membrane components, in particular the exposed proteins, on this interaction. Our study revealed that αS oligomers accumulate on the plasma membrane in close proximity to the cellular prion protein (PrP^C), subsequently inducing an increase of intracellular Ca^{2+} influx in

cells by both channel-independent and channel-dependent mechanisms, with the N-methyl-D-aspartate receptor-channels (NMDARs) triggering a prompt and transient Ca^{2+} influx, followed by a massive Ca^{2+} dysregulation due to the disruption of the plasma membrane integrity. Accordingly, the pharmacological inhibition of NMDARs, as well as the PrP^{C} blockade and the removal of the proteins exposed on the cell membrane transiently delayed the early Ca^{2+} influx, but not the sustained late one caused by αS oligomers. Furthermore, αS fibrils caused Ca^{2+} dyshomeostasis with slower kinetics with respect to the oligomers, and the observed ionic alterations were not rescued by the blockade of NMDARs or by the removal of the proteins exposed in neuronal membranes. Thus, the experimental evidences accumulated in the second part of this work shed light into the interplay between αS aggregates and the plasma membrane of neuronal cells, thus expanding the range of molecular targets for the therapeutic intervention in PD.

Overall, the data presented in this work provide a robust body of evidence on the prominent role of oligomeric species with high solvent exposed hydrophobicity and cross-β structure, formed either during the aggregation process of αS, or released from mature fibrils, in the neurotoxicity of αS, giving a detailed description of the toxic effects they evoke. The experimental evidences accumulated in this study also emphasize the importance of the membrane binding properties of such species for their pathological features, proposing possible strategies with therapeutic value in PD.

1 INTRODUCTION

1.1 α-Synucleinopathies

α-Synucleinopathies are a vast group of neurodegenerative diseases characterized by the abnormal accumulation of insoluble aggregates, both in neurons and glial cells, whose major filamentous component is the protein α-synuclein (αS). These pathologies include Parkinson's disease (PD), dementia with Lewy bodies (DLB), multiple system atrophy (MSA), together with other rare neuroaxonal dystrophies (McCann *et al*., 2014). Among them, PD is far away the most widespread, and DLB is the second most common neurodegenerative dementia, affecting the 0.7% of the population above 60 years of age (Hogan *et al*., 2016). It is characterized by the progressive decline of cognitive functions, that has been linked to the presence of insoluble αS assemblies in the cortex (McKeith *et al*., 2017). MSA is a rare and fatal neurodegenerative condition, in which αS predominantly accumulates in oligodendroglial cells, thus forming cytoplasmic inclusions known as Papp–Lantos bodies (Roncevic *et al*., 2014). It is characterized by a wide range of clinical manifestations, including autonomic failure, motor disturbances such as akinesia, rigidity, postural tremor and, less commonly, resting tremor (Wenning *et al*., 1994).

1.2 Parkinson's Disease

PD, firstly described in 1817 by James Parkinson as the "shaking palsy" (Parkinson, 1817) is the second most common neurodegenerative disorder, affecting 1% of the population above 65 years in industrialized countries, and increasing exponentially in subsequent decades of life (Lee *et al*., 2016). The symptomatology is mainly motor, and includes bradykinesia, muscular rigidity, resting tremor, postural instability and gait impairment (Kalia and Lang, 2015). There are also various nonmotor features, frequently present in PD before the onset of the motor symptoms (Postuma *et al*., 2012), such as olfactory dysfunction, cognitive impairment, psychiatric symptoms, sleep disorders, constipation, autonomic dysfunction, pain and fatigue (Simuni *et al*., 2008; Kalia and Lang, 2015).

PD is characterized by the massive death of dopaminergic neurons in the *substantia nigra pars compacta* (SNpc), especially in the ventrolateral tier of SNpc, containing pigmented dopaminergic neurons that project to the dorsal putamen of the striatum (**Figure 1A**). Their loss is responsible for the massive decrease of the neurotransmitter dopamine in the synaptic terminals of the dorsal striatum, responsible for the motor symptoms of PD (**Figure 1B**). Neuronal loss is also observed in many other brain regions, including the locus coeruleus, nucleus basalis of Meynert, pedunculopontine nucleus, raphe nucleus, dorsal motor nucleus of the vagus, amygdala, and hypothalamus (Dickson, 2012).

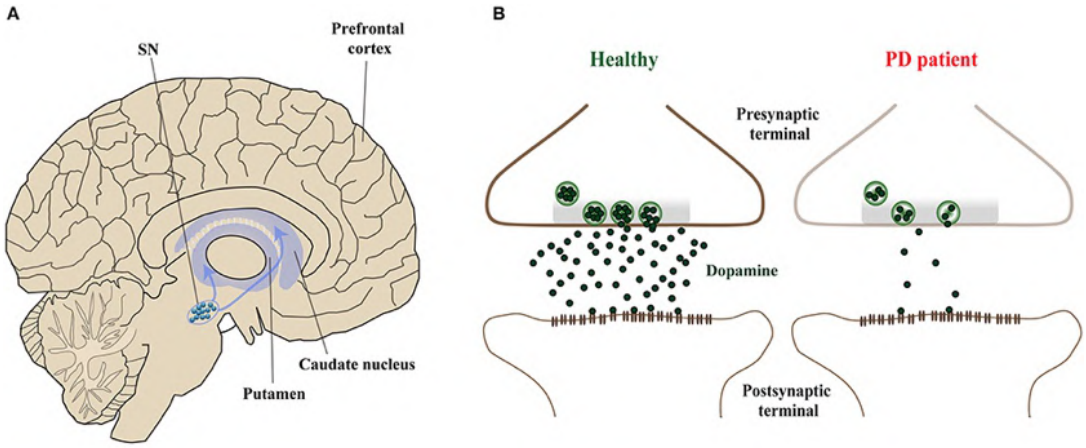

Figure 1 - Dopaminergic neurons of SNpc are involved in PD. (A) The death of dopaminergic neurons in the *substantia nigra* (SN). **B**. Nigrostriatal degeneration in PD patients results in the loss of the neurotransmitter dopamine on synaptic terminals of striatal neurons, as compared to healthy controls (Adapted from Bridi and Hirth, 2018).

The main neuropathological hallmark of PD is Lewy pathology, characterized by the presence of inclusion with a dense eosinophilic core and a pale surrounding halo, known as Lewy bodies (LBs) and neurites (LNs), located in the cell body and in the axonic extensions, respectively (Forno, 1996). These inclusions derive from the abnormal deposition and accumulation, in several different brain areas, of the neuronal protein αS (Spillantini *et al*., 1998). The role of LBs and LNs in causing PD is not completely understood; however, the evidence that specific mutations in the gene *SNCA*, encoding for αS, can lead to an increased protein aggregation, provide a direct connection between protein aggregation and the disease (Lashuel *et al*., 2013). In physiological conditions, αS is mostly found at presynaptic terminals in its native, unstructured and soluble monomeric state; neurotoxic properties are acquired when monomers progressively combine to form oligomers, small protofibrils and finally large, insoluble fibrils, that are

the major components of LBs and LNs (Melki *et al*., 2015). Oligomers and protofibrils are actually considered the most cytotoxic species, responsible for the synaptic disfunction, that is the first step of neurodegeneration, followed by axonal degeneration and, finally, by the complete loss of neuronal connectivity, thus leading to the death of dopaminergic neurons (**Figure 2**) (Scott *et al*., 2010; Lu *et al*., 2014; Morales *et al*., 2015; Calo *et al*., 2016; Grosch *et al*., 2016; Feng *et al*., 2017; Roy, 2017).

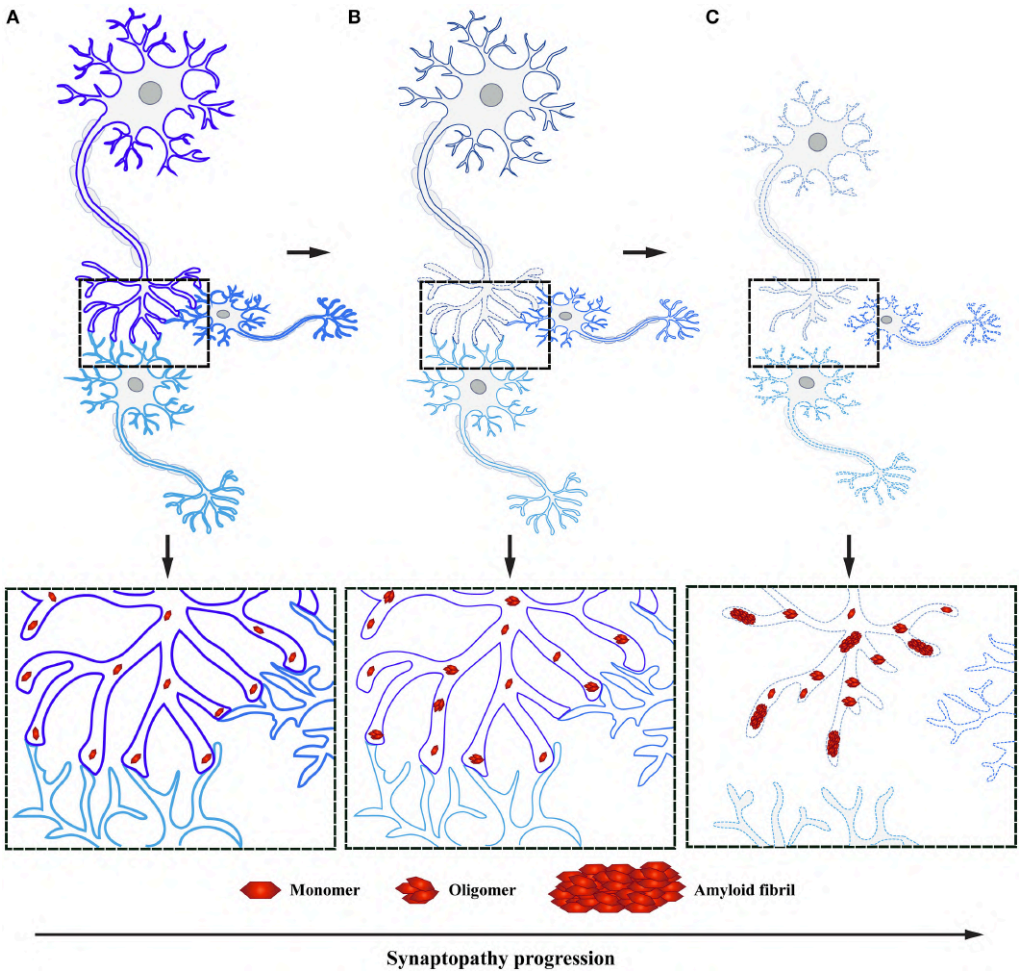

Figure 2 - αS aggregation and accumulation in presynaptic terminals cause synaptic dysfunction and neurodegeneration. (A) Under physiological conditions, αS is in its monomeric state at the presynaptic terminals. **(B)** The accumulation of toxic αS at the presynaptic terminals is responsible for synaptic dysfunction. **(C)** Affected synapses progressively undergo a deconstruction process, leading to a complete loss of neuronal connections and subsequent neuronal cell death (Bridi and Hirth, 2018).

After αS aggregation and deposition, other proteins are captured and accumulated into LBs and LNs, such as structural elements, αS-binding proteins, synphilin-1-binding proteins, components of the ubiquitin-proteasome system, proteins implicated in cellular

responses, or associated with phosphorylation and signal transduction, cytoskeletal elements, cell cycle proteins, cytosolic proteins and many others (Wakabayashi *et al*., 2007; Longhena *et al*., 2019).

1.2.1 Risk factors

The etiology of PD remains largely unknown. This neurodegenerative disorder is actually considered to result from a combination of genetic and environmental risk factors and to be sporadic in about 90% of cases, with 10-15% of patients having a positive family history of PD (Papapetrulopulos *et al*., 2007). The most relevant risk factor for PD is aging; in fact, the incidence increases nearly exponentially with age and joins a peak after 80 years (Driver *et al*., 2009). However, in the last two decades it became clear that the exposure to different environmental factors could strongly contribute to the majority of the late-onset sporadic PD cases, alone or in combination with genetic factors. Several environmental risk factors were identified, such as pesticide exposure (Ascherio *et al*., 2006), prior traumatic brain injury (Fang *et al*., 2012) or β-blockers use (Noyce *et al*., 2012). Opposite, an inverse association was found with the exposure to tobacco smoking (Chen *et al*., 2010), coffee drinking (Ascherio *et al*., 2004), physical exercise (Chen *et al*., 2005), ibuprofen anti-inflammatory use (Gao et al., 2011). Moreover, several epidemiological studies revealed the male sex as a prominent risk factor for developing PD, with the male-to-female ratio being approximately 3:2 (De Lau *et al*., 2006). This strongly dimorphic pattern could be related to a differential frequency of exposure to the previously reported risk factors and to their different interactions with sex variables such as genes located in sexual chromosomes X or Y, effects of sex hormones, or pregnancy (Rocca, 2018).

1.2.2 Genetics

Over the past two decades, scientists identified the genetic basis of PD, especially monogenic disease-causing genes. The missense mutation A53T in the exon 4 of the gene *SNCA*, encoding αS, was the first to be found in association with an adult-onset autosomal-dominant PD phenotype (Polymoropulous *et al*., 1997); afterwards, other pathogenic missense mutations in the same gene were identified, such as A30P, E46K,

H50Q, and G51N (Krüger *et al*., 1998; Zarranz *et al*., 2004; Lesage *et al*., 2013). Missense mutations result in amino acid substitutions and, together with multiplications of the gene locus (such as duplications and triplications) render αS prone to aggregation (Devine *et al*., 2011; Kalia and Lang, 2015). Interestingly, while missense mutations have been found only in familial PD (Mizuta *et al*., 2006), *SNCA* multiplications, in particular triplication, were identified in both familial (Singleton *et al*., 2003; Ibañez *et al*., 2004) and sporadic PD patients (Ahn *et al*., 2008).

Besides *SNCA*, other five genes have been reported to cause autosomal dominant forms of PD: *LRRK2*, *VPS35*, *EIF4G1*, *DNAJC13*, and *CHCHD2* (**Table 1**).

	Protein	Pathogenic mutation(s)
Autosomal dominant		
SNCA	α-synuclein	Missense mutations (Ala18Thr, Ala29Ser, Ala30Pro, Glu46Lys, His50Gln, Gly51Asp, Ala53Glu, Ala53Thr); multiplications (duplications, triplications)
LRRK2	Leucine-rich repeat kinase 2	Missense mutations (Ile1371Val, Asn1437His, Arg1441Cys, Arg1441Gly, Arg1441His, Tyr1699Cys, Gly2019Ser [most common], Ile2020Thr)
VPS35	Vacuolar protein sorting 35	Missense mutation (Asp620Asn)
EIF4G1	Eukaryotic translation initiation factor 4-γ 1	Missense mutations (Arg1205His, Ala502Val)
DNAJC13	Receptor-mediated endocytosis 8 (REM-8)	Missense mutation (Asn855Ser)
CHCHD2	Coiled-coil-helix-coiled-coil-helix domain containing 2	Missense mutations (Thr61Ile, Arg145Gln); splice-site alteration
Autosomal recessive		
Parkin	Parkin	Exon rearrangements, including exon deletions or multiplications (most common); missense mutations, nonsense mutations, small deletions or insertions; splice-site alterations
PINK1	PTEN-induced putative kinase 1	Missense or nonsense mutations (most common); exon rearrangements, including exon deletions or duplications
DJ-1	DJ-1	Missense mutations or exon rearrangements (most common); splice-site alterations

Table 1: **Monogenic forms of Parkinson's disease, by gene**

Table 1 - The main mutations associated with monogenic forms of PD (Kalia and Lang, 2015).

LRRK2 encodes the leucine-rich repeat kinase 2, a multidomain protein encompassing two different enzymatic functions at its core (GTPase and serine-threonine kinase), involved in many physiological functions, such as synaptic morphogenesis, membrane trafficking, autophagy, and protein synthesis (Cookson et *al*., 2012a; Lee *et al*., 2012; Sanna *et al*., 2012; Martin *et al*., 2014). *LRRK2* mutations are the most frequent cause of genetic PD, present in about 4% of familial PD and in 1% of sporadic disease (Healy *et al*., 2008). Among the mutations occurring to this gene, the G2019S is the most frequent

pathogenic one (Singleton *et al*., 2013), responsible for the increase of the kinase activity (West *et al*., 2007). *VPS35* codify for the vacuolar protein sorting 35 and its mutation associated to autosomal dominant PD was recently identified by the next-generation sequencing technique (Vilariño-Güell *et al*., 2011); *EIF4G1* encodes a scaffold protein involved in translation initiation factor complex assembly (Villa *et al*., 2013); mutations in this gene have been identified and linked to PD (Chartier-Harlin *et al*., 2011), but several negative results have been reported, and the first identified mutation was also found in negative controls, and so considered a rare but benign genetic polymorphism (Lesage *et al*., 2012; Tucci *et al*., 2012). *DNAJC13* encodes a chaperone protein called receptor-mediated endocytosis 8 (REM-8), that regulates endosomal trafficking and protein recycling (Popoff *et al*., 2009); the pathogenic mutation N855S has been associated to late-onset autosomal dominant PD (Vilariño-Güell *et al*., 2014). Finally, *CHCHD2* encodes the mitochondrial protein coiled-coil-helix-coiled-coil-helix domain containing 2; mutations and polymorphic variants of this protein have been associated with PD (Funayama *et al*., 2015). However, the pathogenicity of the reported mutations is still debated (Tio *et al*., 2017).

Autosomal recessive forms of PD are associated with mutations to *Parkin*, *PINK1*, and *DJ-1* genes (Kalia and Lang, 2015). Unlike autosomal dominant PD, whose age of onset is quite similar to the sporadic one, monogenic forms of recessive parkinsonism are an important cause of early-onset pathology (before 40 years of age) (Schrag *et al*., 2006). Parkin protein is an E3 ubiquitin ligase, so it is involved in the degradation of targeted proteins through the Ubiquitin/Proteasome System (UPS). Mutations in the Parkin encoding gene have been associated with ubiquitin ligase-activity dysfunction, finally resulting in accumulation of proteins that cause neuronal toxicity, particularly in the SN (Kalinderi *et al*., 2016). *PINK1* encodes the PTEN-induced putative kinase 1, a serine-threonine protein kinase, that was found to interact with Parkin to promote the selective autophagy of damaged mitochondria (Seirafi *et al*., 2015). Finally, the precise function of the DJ-1 protein has not been completely understood, but many evidences indicate its involvement in the oxidative stress response (Taira *et al*., 2004). Missense mutations, exon rearrangements and splice site mutations in *DJ-1* gene have all been recently associated to an autosomal recessive, early-onset familial PD (Cookson *et al*., 2012b).

1.2.3 Epigenetics

The term "epigenetics" refers to the complex mechanisms explaining the effects of multiple environmental factors on genes, thus creating a new heritable phenotype, without changing the DNA sequence (Portela and Esteller, 2010; Waddington, 2012). These mechanisms play a crucial role in the central nervous system, where they control many neurobiological and cognitive functions, such as brain development and neurogenesis, but also learning and synaptic plasticity (Day and Sweatt, 2010; Guo *et al*., 2011). Primary epigenetic mechanisms are DNA methylation, post-transcriptional modifications of histones and gene expression changes modulated by noncoding RNA (Marques *et al*., 2011; Ammal Kaidery *et al*., 2013). The most relevant epigenetic modification is DNA methylation, resulting from the covalent addition of methyl groups to cytosines adjacent to guanines (CpG islands); this process exerts a great impact on the interaction between histones and DNA, thus changing chromatin structure and gene expression (Chao *et al*., 2013) and generally inducing gene silencing: highly methylated areas of the genome are usually weakly active at a transcriptional level (Labbé *et al*., 2016). This epigenetic mechanism has been widely investigated for its implications in PD. First of all, αS expression (*SNCA* gene) is strongly regulated by DNA methylation (Singleton *et al*., 2003; Edwards *et al*., 2010), and a very low methylation of the intron 1 and of the CpG-2 island in the promoter of *SNCA* have been observed in PD patients (Ai *et al*., 2014; Tan *et al*., 2014), thus contributing to αS overexpression. It has also been found that many other genes involved in neurogenesis, such as *Wnt*, *neurogenin 2*, *sprouty RTK signaling antagonist 1*, and *catenin beta 1* are hypermethylated in PD brain with respect to healthy controls, thus indicating the possible involvement of these genes in the progression of PD pathogenesis (Zhang *et al*., 2016; Jang *et al*., 2017).

Gene expression is strongly regulated by histone acetylation dynamics and subsequent chromatin remodeling, operated by a wide range of histone acetyltransferases (HATs) and histone deacetylases (HDACs) (Gräff and Tsai, 2013). The addition of negatively charged acetyl groups weakens their interaction with DNA, thus resulting in a general increase of gene expression (Bannister and Kouzarides, 2011). Higher levels of histone acetylation have been found in dopaminergic neurons from PD patients, if compared to healthy controls (Park *et al*., 2016). αS expression is highly regulated by histone acetylation, but, interestingly, αS can also regulate histone acetylation, possibly with a feedback loop. In the nucleus of dopaminergic neurons, αS directly interacts with

histones, thus accelerating its fibrillation and toxicity (Goers *et al*., 2003). Subsequently, Kontopoulos and colleagues not only confirmed these evidences, but they also demonstrated that αS binds directly to histones, inhibiting histone H3 deacetylation by interacting with the deacetylase SIRT2, so inducing neurotoxicity. In the same study, researchers revealed that A30P and A53T missense mutations lead to a significant increase of the nuclear localization of the protein, thus enhancing this mechanism (Kontopoulos *et al*., 2006).

Finally, other important epigenetic regulation mechanisms have been associated with the activity of a wide range of long noncoding RNAs (lncRNAs) and micro RNA (miRNAs). While lncRNAs and their involvement in PD are only beginning to be elucidated, many evidences have been accumulated about the role of miRNAs. These small noncoding RNAs bind to the 3′ untranslated region (3′UTR) of target mRNAs (Cannell *et al*., 2008), thus inhibiting the expression of the proteins they encode (Valencia-Sanchez *et al*., 2006). miRNAs have shown to be crucial in the regulation of PD related gene expression. In 2007, Kim and colleagues investigated the role of miRNAs in midbrain, reporting that MiR-133b, crucial for neuronal maturation and functionality, was highly expressed in dopaminergic neurons of the SN of healthy subjects, and present at much lower levels in PD brains (Kim *et al*., 2007). Similar results were obtained in two different PD mice models (Smidt *et al*., 2004; Martinat *et al*., 2006). *SNCA* expression resulted to be regulated by two different miRNAs, miR-7 and miR-153, that work in concert, producing an additive effect. Both bind to the 3′-untranslated region of αS mRNA and downregulate its protein levels (Doxakis, 2010). *SNCA* expression is also controlled by miR-34b and miR-34c: their reduced levels have been observed in many brain areas of PD patients (Villar-Menendez *et al*., 2014). The effect of their downregulation was investigated *in vitro* in SH-SY5Y human neuroblastoma cells, and was associated with an increase in αS expression, possibly contributing to PD pathogenesis (Kabaria *et al*., 2015). More recently, miR-155 has been found to be upregulated in a mouse PD model overexpressing αS (Thome *et al*., 2016). The most relevant epigenetic modifications involved in PD are reported in **Figure 3**.

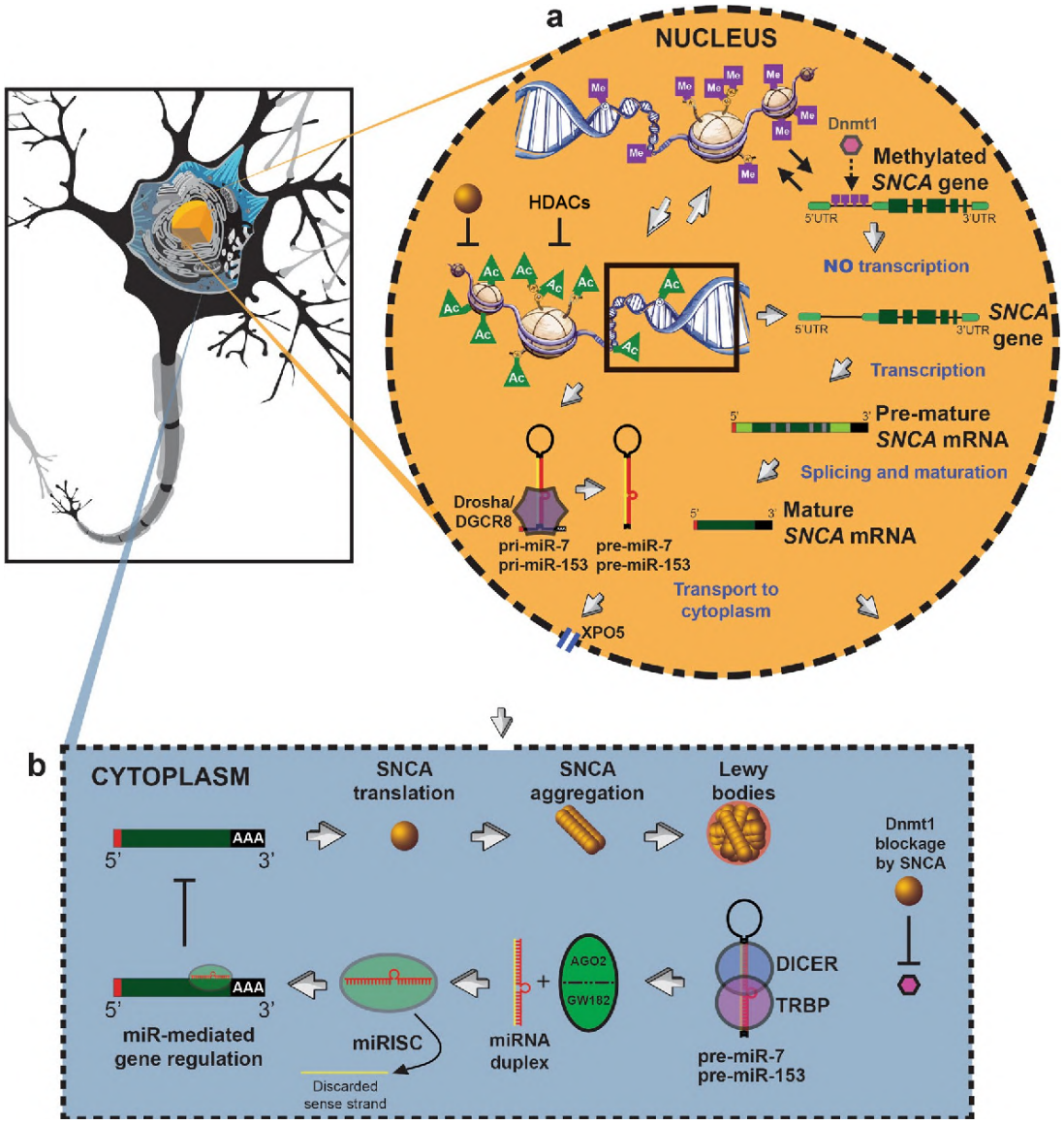

Figure 3 - Epigenetic mechanisms in αS pathology. (A) In the nucleus, histones methylation leads to their compression and to chromatin condensation. Opposite, acetylation decreases their affinity for DNA, allowing *SNCA* transcription. HDACs remove acetyl groups from histones, thus repressing gene expression. DNA methylation by the Dnmt1 enzyme at the CpG island also represses *SNCA* transcription, whereas its demethylation promotes *SNCA* transcription. The microprocessor complex (formed by Drosha and DGCR8) starts to process primary miRNAs, that are then transported to the cytoplasm **(B)** by XPO5. Here, *SNCA* mRNA is translated into αS that, in pathological conditions, can form β-sheet-rich oligomers and fibrils. The DICER/TRBP complex processes the pre-miRNAs that are further incorporated to the AGO2/GW182 complex to generate mature miRISCs. MiRISCs containing miR-7 or miR-153 can bind to the 3'UTR of *SNCA* mRNA, thus inducing its translational repression. Abbreviations not cited in the main text - 3′UTR: 3′ Untranslated region; AAA: poly(A) tail; Ac: acetylated residue; AGO2: argonaute-2; DICER: endoribonuclease Dicer or helicase with RNase motif; Dnmt1: DNA (Cytosine-5-)-Methyltransferase 1; GW182: trinucleotide repeat-containing gene 6A (TNRC6A); Me: methylated residue; miRISC: miRNA-mediated silencing complex; mRNA: messenger RNA; pre-miR: precursor microRNA; pri-miR: primary microRNA; TRBP: Transactivation-responsive binding protein; XPO5: exportin-5 (adapted from Labbé *et al*., 2016).

Taken together, all these evidences clearly indicate that abnormalities in the epigenetic regulation mechanisms play a key role in the etiology of PD. However, further research will be essential for understanding the interplay among all the risk factors (genetic, epigenetic, and environmental) associated with disease pathogenesis.

1.2.4 Diagnosis and screening

PD diagnosis is actually primarily clinical, and involves a wide range of neurological, psychological and physical screenings. The UK Parkinson's Disease Society Brain Bank, proposed a three-step process for PD diagnosis, based on cardinal criteria with a diagnostic accuracy of up to 90% (Huges *et al*., 2001; Jankovic, 2008; Kalia and Lang, 2015). Clinically, PD is primarily defined by the presence of parkinsonian symptoms i.e. bradykinesia and at least another one of the major motor symptoms (muscular rigidity, resting tremor and postural instability not caused by primary visual, vestibular, cerebellar, or proprioceptive dysfunction). The second diagnostic step is the evaluation of several exclusion criteria, possibly indicating an alternative diagnosis, such as repeated head injury, history of repeated strokes with progression of parkinsonian features, presence of a cerebral tumor or communicating hydrocephalus, and many others (Kalia and Lang, 2015). Finally, the third step is based on the presence of three or more supportive prospective positive criteria, such as unilateral onset, disorder progressiveness, rest tremor, clinical course of at least 10 years and others (Gibb *et al*., 1988). All these criteria are based on signs and symptoms emerging in the later stage of disease, in fact the early diagnosis of PD remains extremely difficult and insufficient. For such purpose, there are several studies underway with the aim to identify biomarkers to enhance the diagnosis in early disease, or at least in the prodromal stage (Kalia and Lang, 2015; Poewe *et al*., 2017). Potential clinical markers could be represented by the evaluation of the olfactory impairment (the Lewy pathology also occurs in neurons located in the olfactory system) measured by standardized methods, such as the well characterized University of Pennsylvania Smell Identification Test (UPSIT) (Doty *et al*., 1984). Regarding imaging markers, there are several techniques, such as positron emission tomography (PET) and single photon emission computed tomography (SPECT) that can be used for the evaluation of the reduction in dopaminergic nerve terminals of the SN (Brooks and Pavese, 2011). These markers can be used to distinguish PD from other clinical conditions

mimicking its symptoms, but that are not associated with striatal dopamine depletion (Stoessl *et al*., 2014; Politis, 2014; Kalia and Lang, 2015; Poewe *et al*., 2017). Several studies have focused on the evaluation of possible early biochemical biomarkers of PD, such as the presence of differential levels of many proteins, first of all αS, but also DJ-1, tau, and β-amyloid$_{1-42}$, as well as β-glucocerebrosidase activity in the cerebrospinal fluid (CSF) of PD patients versus healthy subjects (Hong *et al*., 2010; Parnetti *et al*., 2013). Different immunoassays, such as ELISA and electrochemiluminescence, have been employed for the measurement of total αS levels in the CSF. Although many studies converged on the idea that its concentration was lower in PD patients as compared to healthy controls (Gao *et al*., 2015; Eusebi *et al*., 2017; Abbasi *et al*., 2018), total αS measurement cannot be considered a reliable diagnostic marker for PD, because low CSF levels have been also observed in other synucleinopathies, such as MSA and DLB, and also in other neurodegenerative diseases, such as frontotemporal dementia, thus rendering these pathological conditions indistinguishable from each other (Wennström *et al*., 2013). CSF oligomeric αS has also been measured, as these small aggregates are widely considered to play a crucial role in PD pathogenesis (Conway *et al*., 2000); their concentrations were found to be significantly higher in PD patients with respect to healthy controls, but the sensitivities and specificities of the employed immunoassays resulted to be not completely satisfactory (Eusebi *et al*., 2017; Zhou *et al*., 2018). Furthermore, high sensitivity protein amplification assays, such as Protein-Misfolding Cyclic Amplification (PMCA) and Real-Time Quaking- Induced Conversion (RT-QuIC) has been used for the identification of pathogenic aggregates in biological fluids, including αS (Fairfoul *et al*., 2016). The technique is based on the exponential amplification, monitored by a fluorophore, of the protein aggregates contained in the sample of interest, such as CSF (Parnetti *et al*., 2019). However, the employment of these techniques is actually limited by the impossibility of discriminating between different synucleinopathies, so further studies are needed to improve their employment for the early and differential diagnosis of PD (Parnetti *et al*., 2019).

As constipation represents a relevant symptom frequently present in the very early stages of PD, researchers tried to evaluate αS accumulation in the enteric nervous system; however, positive αS staining has been observed in biopsies arising from the enteric system of both PD patients and control populations, thus indicating that colonic αS deposition is not a useful diagnostic test for PD (Gold *et al*., 2013; Visanji *et al*., 2014; Scheperjans *et al*. 2015).

Finally, specific genetic screenings are carried out in families characterized by cases of monogenic parkinsonism, in order to find mutations that could lead to disease development. However, because of the reduced penetrance of the monogenic mutations causing PD, genetic testing cannot provide a definitive diagnosis (Poewe *et al*., 2017). A complete list of possible early biomarkers for PD diagnosis is given in **Figure 4**.

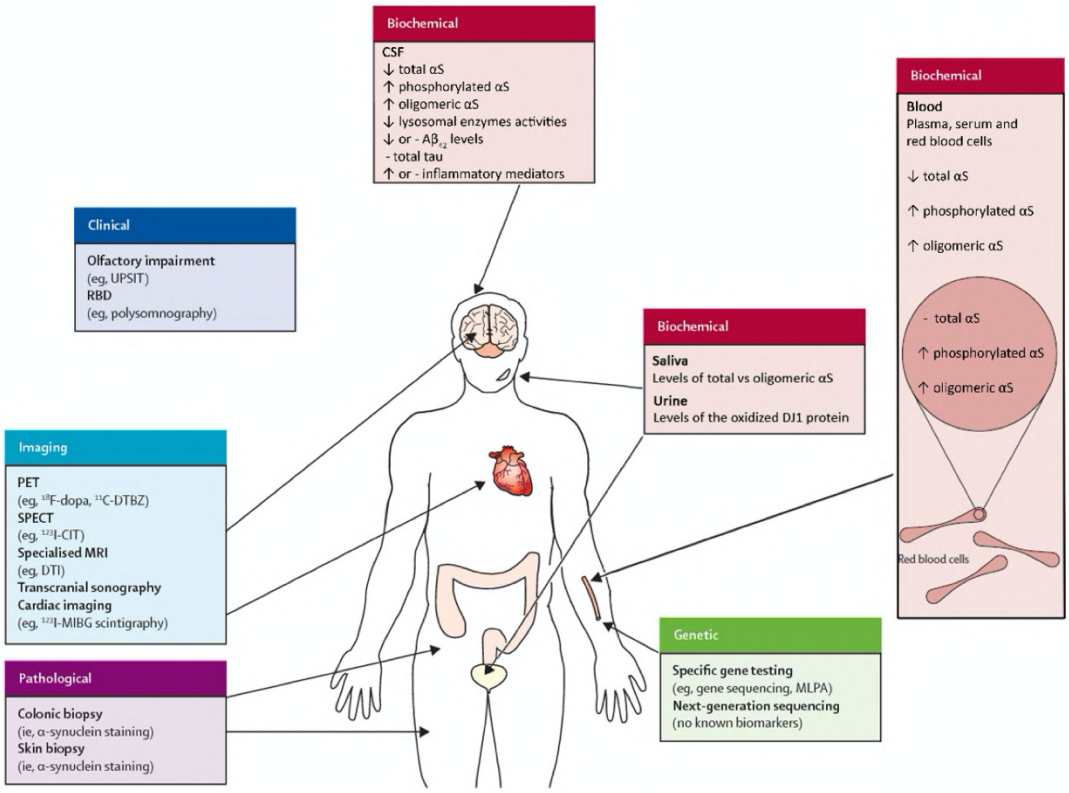

Figure 4 - Potential biomarkers for PD diagnosis. Several biomarkers for PD diagnosis have been recently proposed. They can be classified as clinical, imaging, pathological, biochemical, and genetic. Abbreviations not cited in the main text - ^{11}C-DTBZ: ^{11}C-dihydrotetrabenazine. DTI: diffusion tensor imaging. ^{123}I-CIT: ^{123}I-2β-carbomethoxy-3β-(4-iodophenyl) tropane. ^{123}I-MIBG:^{123}I-metaiodobenzylguanidine. MLPA: multiplex ligation-dependent probe amplification. RBD: rapid eye movement sleep behavior disorder. ↑ = Increased; ↓ = Decreased; - = Equivalent. (Adapted from Kalia and Lang, 2015; Parnetti *et al*., 2019).

1.2.5 Therapy

The causative pathogenic mechanism underlying the motor symptoms of PD is the massive dopamine depletion caused by the death of the dopaminergic neurons in the SN. Actually, there are no disease-modifying treatments, the only possible therapy is symptomatic and consists of the administration of different drugs able to enhance the intracerebral dopamine concentrations, or to stimulate dopamine receptors. These drugs, together with their action mechanisms, are all represented in **Figure 5**.

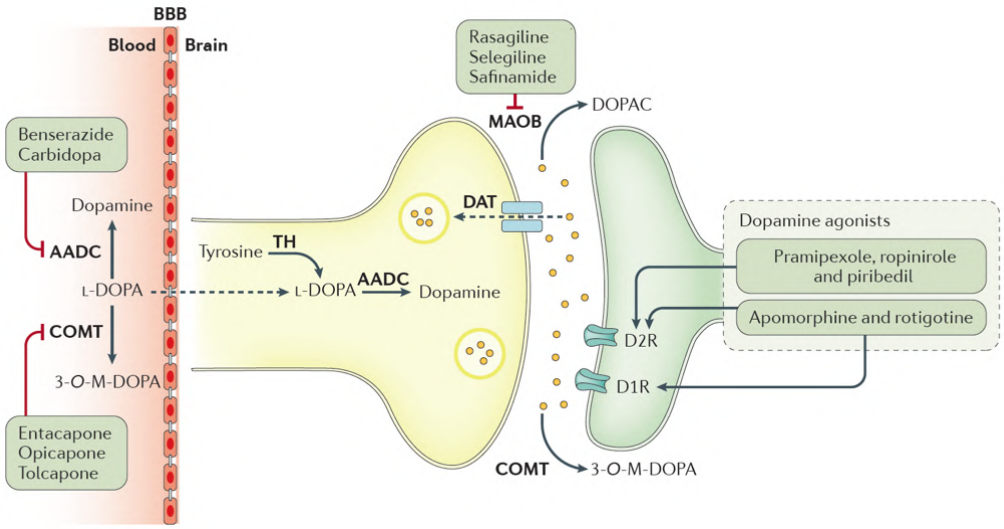

Figure 5 - Dopaminergic targets for therapeutic intervention in PD. Levodopa (L-DOPA) can cross the blood–brain barrier (BBB), and its substitution at presynaptic terminal is usually combined with the inhibition of aromatic amino acid decarboxylase (AADC) or catechol-O-methyltransferase (COMT). Monoamine oxidase type B (MAOB) inhibitors enhance the synaptic availability of dopamine; whereas dopamine agonists act at the postsynaptic terminal. Dashed arrow through the dopamine transporter (DAT) indicate dopamine reuptake from the synaptic cleft. Abbreviations - 3-*O*-M-DOPA: 3-*O*-methyl-DOPA; D1R and D2R: dopamine D1 and D2 receptors; DOPAC: 3,4-dioxy-phenylacetic acid; TH: tyrosine hydroxylase (Poewe *et al*., 2017).

L-DOPA is the most used, effective and tolerated drug for symptomatic treatment of PD; it is the precursor of dopamine, able to cross the blood-brain barrier (BBB); once inside the neurons, L-DOPA is converted in dopamine by the AADC enzyme. However, its prolonged administration frequently leads to motor complications, such as dyskinesias, with mechanisms that are not fully understood (Cenci *et al*., 2014). Furthermore, its availability for uptake into the brain is significantly diminished by peripheral metabolism;

for this reason, L-DOPA preparations are frequently combined with AADC inhibitors, such as carbidopa and benserazide, in order to enhance its bioavailability (Poewe *et al*., 2017). As a consequence, when AADC is inhibited, L-DOPA peripheral metabolism is shifted towards another pathway, consisting in ortho-methylation by COMT, and the inhibition of this enzyme with specific drugs, such as opicapone and tolcapone, further enhances L-DOPA half-life and bioavailability (Muller *et al*., 2015).

Another therapeutic strategy for the management of PD, used as monotherapy or in concert with L-DOPA, is the administration of MAOB inhibitors, that block dopamine degradation, thus prolonging and increasing its synaptic concentration. As monotherapy, MAOB inhibitors, such as selegiline and rasagiline, are effective at the early stages of PD and they possibly delay L-DOPA administration. Dopamine agonists are another class of drugs used for PD therapy, as they directly stimulate postsynaptic dopamine receptors (D1R and D2R represented in **Figure 5**). Dopaminomimetics have a longer half-life with respect to L-DOPA, and their administration seems to be less likely associated with the the motor complications evoked by L-DOPA, but their antiparkinsonian effect is weaker (Lewis and Spillane, 2019).

As already stated, PD is primarly caused by the massive dysfunction of dopaminergic neurons and, for this reason, the dopaminergic therapy has remarkable effects on PD symptoms; however, it may lead to several complications, such as motor fluctuations and L-DOPA-induced dyskinesia, but also nonmotor complaints such as pain, anxiety and depression. For these reasons, there is a clear need for therapies targeting other pharmacological systems, previously shown to be affected in PD pathogenesis, such as glutamatergic, adenosinergic, noradrenergic, serotonergic, GABAergic and cholinergic pathways (Kalia *et al*., 2013a). The treatment of psychiatric complaints is necessary to improve the quality of life of the patients, thus allowing a better coexistence with the disease (Seppi *et al*., 2011, Connolly and Lang, 2014). In particular, it has been reported that depression is present in 40–50 % of PD patients (Reijnders *et al*., 2008), in which is treated with triciclic antideprassants, SSRIs (selective serotonin receptor inhibitors) and SNRIs (serotonin-norepinephrine reuptake inhibitors) (Barone *et al*., 2010; Richard *et al*., 2012).

In many cases, the pharmacological therapy is not sufficient for the management of both motor and nonmotor symptoms of PD; recently, surgical treatment, and the subsequent deep brain stimulation (DBS), have shown to be effective in the treatment of moderate and severe motor symptoms (Kalia and Lang, 2015). DBS consists on the implantation of

electrodes in specific brain areas (subthalamic nucleus or globus pallidus internus), followed by the high-frequency electrical stimulation of these targets, made by a pacemaker (Kalia and Lang, 2015; Poewe *et al*., 2017; Lewis and Spillane, 2019). However, surgical treatment cannot be applied in all PD patients; after many clinical trials, it became clear that patients with motor symptoms who do not respond to L-DOPA are unlikely to respond to DBS (Poewe *et al*., 2017).

1.3 α-Synuclein

1.3.1 Structure

α-Synuclein (αS) is a 14-kDa intrinsically disordered protein (IDP), originally identified in the electric organ of *Torpedo californica* (Maroteaux *et al*., 1988). Maroteaux and colleagues found this protein not only at presynaptic terminals, but also on the nuclear envelope, even if this evidence was not confirmed in the largest part of subsequent studies (Burré *et al*., 2018). At the same time, a specific αS fragment (residues 61-95) was identified as the non-Aβ-amyloid component (NAC) of senile plaques of Alzheimer's disease (AD) patients (Ueda *et al*., 1993). The discovery of this protein was soon followed by the identification of two other members of the synuclein family, β- and γ-synuclein (βS and γS, respectively) (Nakajo *et al*., 1990; Jakes *et al*., 1994; Lavedan *et al*., 1998; Burré *et al*., 2015; Burré *et al*., 2018). βS was identified at presynaptic terminals in rat and bovine brains (Nakajo *et al*., 1990), whereas γS was initially found to be present in breast cancer cells (Ji *et al*., 1997). These three proteins have a high degree of sequence homology (55–60%), a very similar domain organization and they are all highly expressed in the human central nervous system (Goedert, 2001). In particular, αS was found to be highly expressed in the neocortex, hippocampus, striatum, thalamus, and cerebellum (Nakajo *et al*., 1994), and also in many other organs and cell types, such as muscle, kidney, liver, lung, heart, blood vessels, platelets, blood cells, or body fluids including cerebrospinal fluid (CSF) and plasma (Ueda *et al*., 1993; Jakes *et al*., 1994; Hashimoto *et al*., 1997; Askanas *et al*., 2000; Shin *et al*., 2000; Li *et al*., 2002; Tamo *et al*., 2002; Kim *et al*., 2004a; Ltic *et al*., 2004; Nakai *et al*., 2007).

αS started to be extensively investigated in 1997, when the missense mutation A53T was found to be associated with familial cases of PD (Polymeropoulos *et al*., 1997). In the last

two decades, researches accumulated many evidences about its structural characteristics. The primary structure of αS is represented in **Figure 6**.

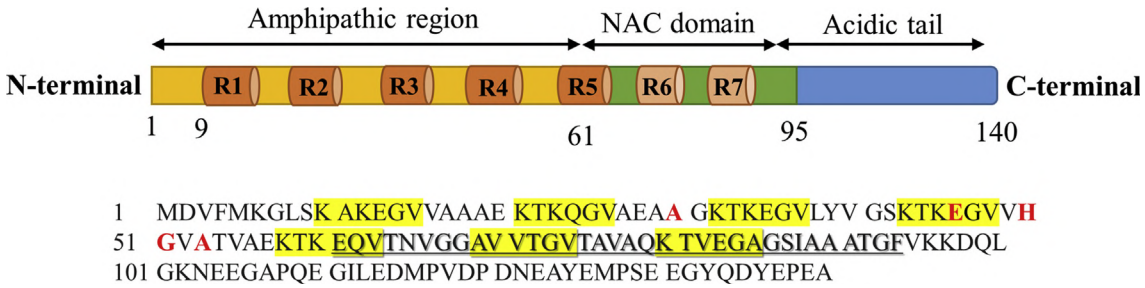

Figure 6 - Schematic representation of the primary structure of wild-type full-length monomeric αS. The primary sequence of human αS is reported, with clinically relevant mutations (A30P, E46K, H50Q, G51D, A53T, and A53E) marked in red. The seven imperfect lysine-rich highly conserved motif repeats (KTKEGV), are highlighted in yellow, and the NAC domain is underlined (Oliveri, 2019).

The primary structure of αS can be divided into three different major regions:

- The positively charged N-terminal region (residues 1-60), presenting four imperfect 11 residue repeats with a KTKGEV consensus sequence; this region mediate αS association with membranes (George *et al*., 1995; Bussell *et al*., 2003) and, after binding, form amphipathic α-helical structures with 3 turns (Chandra *et al*., 2003; Burré *et al*., 2018). This domain is subjected to many point mutations that accelerate the aggregation kinetics of the protein, and so the development of PD (Polymeropoulos *et al*., 1997; Kruger *et al*., 1998; Pasanem *et al*., 2014).
- The hydrophobic non-Aβ-amyloid component of AD (NAC) region (residues 61-95), presenting three imperfect KTKEGV repeats; it is responsible for αS aggregation (Giassonn *et al*., 2001) and is able to modulate the affinity of the protein for the membrane, also in dependence to the lipid composition of the bilayers (Fusco *et al*., 2014).
- The highly acidic C-terminal region (residues 96–140), that remains largely unstructured (Wu *et al*., 2008); it is involved in many different interactions, such as ion, polycation, and polyamine binding (Paik *et al*., 1999; Nielsen *et al*., 2001; Hoyer *et al*., 2004; Brown 2007), and, together with the NAC region, in the modulation of membrane binding (Chandra *et al*., 2003; Bussell *et al*., 2005; Fusco *et al*., 2014). This domain seems to protect αS from aggregation: many *in*

vivo and *in vitro* experimental evidences revealed that there is a strong correlation between C-terminal truncated variants and PD pathology (Li *et al*., 2005; Ulusoy *et al*., 2010; Games *et al*., 2014); moreover, aggregates obtained from C-terminally truncated αS are more cytotoxic than those formed from the wild-type protein (Sung *et al*., 2005)

A wide range of biophysical studies of monomeric αS in aqueous solution revealed the lack of persistent secondary or tertiary structures (Eliezer *et al*., 2001; Uversky *et al*., 2002). These finding, together with the previously reported primary structure charachteristics, clearly explain that αS belongs to the family of intrinsically disordered proteins (IDPs), and, more specifically, to the subfamily of the natively unfolded proteins, characterized by a combination of low hydrophobicity, low sequence complexity and high net charge (Lee *et al*., 2007; Breydo *et al*., 2012).

In neuronal cells, there is a dynamic equilibrium between the soluble unfolded state assumed by cytosolic αS, and the membrane-bound one, in which a partial α-helix secondary structure is assumed upond binding to lipid bilayers, such as those of synaptic vesicles involved in neurotransmitter release (Chandra *et al*., 2003; Bussell *et al*., 2005; Burré *et al*., 2013). Upon membrane binding, αS multimerizes, giving rise to a complex structure that has been proposed as the functional form of αS (Burré *et al*., 2014). A stable folded αS tetramer has been purified from human erythrocytes upon analytical centrifugation (Bartels *et al*., 2011), but this structure was neither detected by electron microscopy (EM) in the same work, nor by NMR (nuclear magnetic resonance) experiments (Wang *et al*., 2011). Furthermore, αS tetrameric structures were not found in other preparations (Burré *et al*., 2013). In contrast, αS adopts a β-sheet secondary conformation in pathological conditions, associated to the formation of oligomers, protofibrils, fibrils and their subsequent deposition in LBs and LNs (Conway *et al*., 1998, 2000; Lashuel *et al*., 2002; Uversky, 2007). The possible conformations assumed by αS are represented in **Figure 7**.

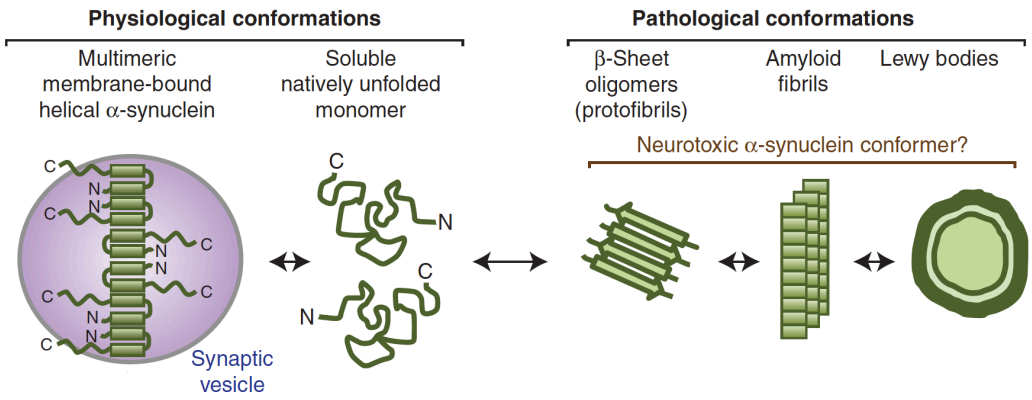

Figure 7 - Different conformations assumed by αS. Monomeric soluble αS is natively unstructured. After binding to curved membranes, such as synaptic vesicles, αS undergoes a conformational change and folds into an amphipathic α-helix. Opposite, under pathological conditions, soluble αS forms a wide range of β-sheet-rich oligomers (protofibrils), that further aggregate forming amyloid fibrils, that are the major constituents of LBs. (Adapted from Burré *et al*., 2018).

αS is susceptible to a wide range of post-translational modifications (PTMs), that alter protein charge, hydrophobicity and structure, affecting both its physiological and pathological functions. Among them, phosphorylation is the most investigated, because of its close relationship with pathology (Villar-Piqué *et al*., 2016). In particular, more than 90% of αS present in LBs is phosphorylated at residue S129 (pS129), whereas only 4% of the cytosolic protein is phosphorylated at the same position (Anderson *et al*., 2006). It is not clear whether phosphorylation occurs at the monomeric or fibrillar stage of the aggregation pathway (Stephens *et al*., 2019), but it has been reported that αS aggregation rate is decreased by S129 phosphorylation (Waxman *et al*., 2008). An aggregation-reducing effect was also associated with the phosphorylation at the tyrosine residues Y125, Y133, and Y135 (Ellis *et al*., 2001; Nakamura *et al*., 2001; Ahn *et al*. 2002; Negro *et al*., 2002; Takahashi *et al*., 2003; Chen and Feany, 2005; Chen *et al*., 2009). These amino acid residues were also found to be major nitration targets, but this PTM has been supposed to induce αS oligomerization (Giasson *et al*., 2000).

Many other post-translational modifications have been reported, such as acetylation, associated to an increased affinity for lipid membranes, and so to a higher propensity to form α-helix secondary structures, that avoid aggregation (Kang *et al*., 2012; Bartels *et al*., 2014); many studies are also focused on ubiquitination, whose role in modulating αS aggregation is not yet understood, even if αS strongly colocalize with ubiquitin in LBs and LNs (Gomez-Tortosa *et al*., 2000).

1.3.2 Physiological functions

The physiological functions of αS have not been yet defined uniquely. Firstly, αS is considered an important regulator of membrane biogenesis, composition and lipid transport; thanks to its affinity for fatty acids (Sharon *et al*., 2001), it may serve as their transporter between the cytosol and the various membrane compartments, even if other reasearchers reported the contrary (Lucke *et al*., 2006). It is widely accepted that αS, as expected for a protein with lipid-binding properties, produce membrane curvature, thus converting large vesicles into highly curved membrane tubules and vesicles (Varkey *et al*., 2010; Westphal and Chandra, 2013; Shi *et al*., 2015). The capacity of controlling membrane lipid composition has been associated with the binding and the subsequent inhibition of phospholipase D, which hydrolyzes phosphatidylcholine to phosphatidic acid and choline, observed both *in vitro* and *in vivo* (Jenco *et al*., 1998; Ahn *et al*., 2002; Payton *et al*., 2004; Gorbatyuk *et al*., 2010), even if these data are still controversial (Rappley *et al*., 2009). Finally, αS has been described as a lipid-packing sensor and controller (Kamp and Beyer, 2006; Ouberai *et al*., 2013).

αS was found to contain regions with a high degree of homology with 14-3-3 family of molecular cytosolic chaperones (Ostrerova *et al*., 1999), and also to bind to the targets of 14-3-3 (Emamzadeh, 2016). It has been reported that, under thermal and chemical stress coditions, αS is overexpressed and prevent the aggregation of denatured proteins, by binding them with the N-terminal domain, while the C-terminal one is responsible for the solubilization of the forming protein complexes (Park *et al*., 2002). αS has also been described for its capacity to protect dopaminergic neurons from apoptotic cell death through the downregulation of protein kinase C (PKC) expression (Jin *et al*., 2011). Interestingly, it has been reported that αS can interact with calmodulin (CaM), a messenger protein activated by Ca^{2+} binding, involved in many neuronal mechanisms, such as short- and long-term memory formation (Emamzadeh, 2016). Some researchers suggested that this interaction could play a role in Ca^{2+}-triggered events in neurons (Grushus *et al*., 2013), but further analysis are needed to clarify the biological relevance of this interaction.

αS is also involved in the control of dopamine synthesis, by downregulating TH activity (Masliah *et al*. 2000; Kirik *et al*. 2002; Perez *et al*. 2002); TH is the enzyme catalyzing the rate-limiting step of dopamine biosynthesis, the conversion of the amino acid L-tyrosine to L-3,4-dihydroxyphenylalanine (L-DOPA). In this case, αS probably acts by

inhibiting TH phosphorylation and stabilizing its dephosphorylated inactive state (Perez *et al*., 2002; Peng *et al*., 2005; Wu *et al*., 2011). This effect is due to the interaction between αS and the protein phosphatase 2A (PP2A), with the subsequent dephosphorylation of TH-Ser 40 residue (Peng *et al*., 2005). Furthermore, αS acts on the vesicular dopamine transporter 2 (VMAT2), responsible for dopamine uptake from the cytoplasm into the synaptic vesicles (Lotharius and Brundin, 2002) by using the proton gradient across the vesicular membranes as a driving force (Wimalasena, 2011). Both αS overexpression and knockdown resulted *in vitro* in the loss of dopamine homeostasis (Guo *et al*., 2008). αS is also involved in the regulation of membrane trafficking (Prankle *et al*., 2011) and of the interaction of the GTP-binding protein rab3 with membranes, especially synaptic vesicles (Chen *et al*. 2013).

Due to its capacity to bind synaptic vesicles (Maroteaux *et al*., 1988; Perrin *et al*., 2000) and synaptobrevin-2 (Burré *et al*., 2010), and its SNARE (Soluble N-ethylmaleimide-sensitive factor Attachment Protein Receptor) complex chaperoning activity (Burré *et al*., 2010), αS has been associated with neurotransmitter release and synaptic plasticity, even if its precise function remains to be elucidated. The molecular mechanism of neurotransmitter release requires the fusion of the vesicles with the presynaptic plasma membrane, and it is mediated by SNARE proteins: target plasma membrane (t-) SNAREs, such as syntaxin 1A and SNAP-25 (synaptosomal-associated protein-25), and vesicle (v) SNARE synaptobrevin/vesicle-associated membrane protein (VAMP) 2 associate each other to form the SNAREpin (SNARE protein complex), which facilitates the fusion (Poirier *et al*., 1998; Sutton *et al*., 1998). The formation of the SNAREpin is highly regulated by different proteins, such as the Ca^{2+}-sensor synaptotagmin-1 (Chapman, 2002) and, as a consequence, neurotransmitter release from a large number of vesicles is fast and syncronized (Sabatini and Regehr, 1987). The role of αS has been widely investigated, both in knockout and overexpressing conditions, but there are still many controversies, as it has been reported to promote (Steidl *et al*., 2003; Liu *et al*., 2004; Gureviciene *et al*., 2007, 2009; Greten-Harrison *et al*., 2010; Anwar *et al*., 2011; Vargas *et al*., 2014), but also to inhibit neurotransmitter release (Abeliovich *et al*., 2000; Cabin *et al*., 2002; Yavich *et al*., 2004, 2006; Larsen *et al*., 2006; Senior *et al*., 2008; Greten-Harrison *et al*., 2010), or to have no effect at all on this process (Chandra *et al*., 2004; Watson *et al*., 2009; Burré *et al*., 2010). Despite these controversies, probably associated to the inconsistence of the experimental models, there is general concordance on the fact that αS is not necessary for basal neurotransmission, but its role could be attributed to

neuronal maintenance during activity (Burré *et al*., 2015). The absence of αS in worms, flies, and yeast corroborate this hypothesis. At the synapse, αS has been reported to interact with the VAMP2, thus promoting SNARE complex assembly (Burré *et al*., 2010). It has been recently reported that αS also interacts with the neuronal phosphoprotein synapsin III (syn III), thus cooperating in the control of dopamine release (Zaltieri *et al*., 2015); interestingly, it has also been demonstrated that syn III is present, in complex with αS, in insoluble LBs fibrils from PD brains and that its silencing could prevent αS aggregation both *in vitro* and *in vivo* (Faustini *et al*., 2018; Longhena *et al*., 2018).
Furthermore, Scott and Roy proposed a function in the modulation of vesicle motility, thus contributing to the mantainment of dopaminergic vesicles between the recycling and the resting pools (Scott and Roy, 2012). The binding of αS to synaptic vesicles is Ca^{2+}-dependent and requires the amino acid portions 1–25 and 65–97 (Fusco *et al*., 2016; Lautenschlager *et al*., 2018). Experimental evidence has indicated that αS is present not only at the presynaptic terminal, but also in mitochondria (Li *et al*., 2007; Cole *et al*., 2008), endoplasmic reticulum (ER) (Colla *et al*., 2012a) and nuclei (Pinho *et al*., 2019), even if at lower concentrations. Here, the precise functions of αS are not completely clarified and are still matter of debate. In addition, it has been proposed that αS can function as an antioxidant, preventing the oxidation of unsaturated membrane lipids; in this process, the N-terminal methionine (Met) residues of the protein are oxidized, and the oxidation is then promptly reversed by the enzyme methionine sulfoxide reductase (MSR), which catalyzes the reduction of Met sulfoxide residues back to Met (Zhu *et al*., 2006). αS putative major functions are all reported in **Figure 8**.

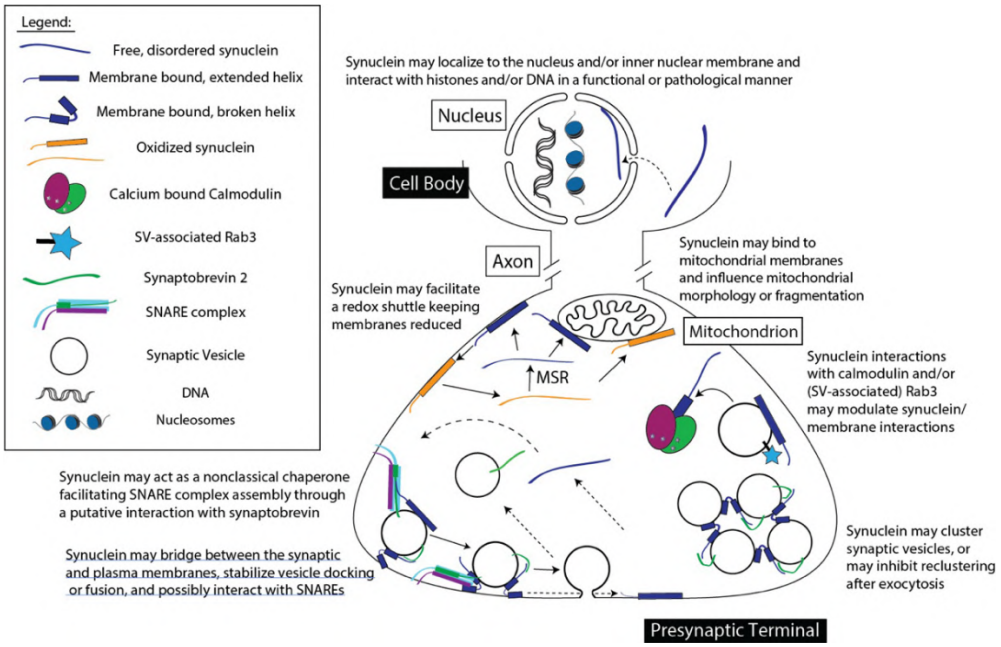

Figure 8 - αS physiological functions. Cellular organelles, pathways, and other targets potentially implicated in αS functions. (Snead and Eliezer, 2014).

As previously reported, αS is also expressed outside of the CNS, in peripheral blood cells and hematopoietic elements, where its functions remain to be completely elucidated, but some reports proposed a role in the development and function of the immune system (Shameli *et al*., 2016). Interestingly, it has also been proposed that αS could contribute to tumorigenesis (Israeli *et al*., 2011), and its expression has been observed in a range of cancers, such as tumors with neuronal differentiation, melanomas and meningiomas (Kawashima *et al*., 2000; Matsuo *et al*., 2010; Ge *et al*., 2016).

1.3.3 Aggregation process

A range of about 50 distinct human pathologies has been linked to the accumulation of amyloid deposits, primarily composed of one specific type of peptide or protein (Chiti and Dobson, 2017). Such conditions are collectively referred to as protein misfolding or amyloid diseases (Chiti and Dobson, 2006). Among these pathologies, neurodegenerative disorders, including AD and PD, represent nowadays very common and debilitating medical conditions of the industrialized countries.

Aggregation is a complex mechanism consisting on the transition of peptides or proteins from their functional soluble state to the amyloid one, in dependence not only to the

intrinsic characteristics of the protein, but also to the environmental conditions under which aggregation occurs, giving rise to stable and highly ordered β-sheet-rich aggregates (Cremades *et al*., 2017; Cremades and Dobson, 2018; Oliveri, 2019). The pathogenicity of these aggregates has been associated with a loss of function of the involved proteins, but more likely to a gain of toxic functions through the generation and accumulation of misfolded aggregated forms (Cremades and Dobson, 2018); this hypothesis has been initially linked to the evidence that amyloid aggregates are located in the damaged regions of affected patients (Yabkner *et al*., 1990); however, especially in neurodegenerative conditions, there is not a well-established correlation between the accumulation of protein aggregates and the severity of disease-associated symptoms (Ross and Poirier, 2005; Kalia *et al*., 2013b).

Among amyloid aggregates, the most representative are fibrils, usually composed of many protofilaments twisting around each other and characterized by a secondary cross-β structure, in which β-strands are aligned perpendicularly to the fibril axis, thus generating inter-molecular β-sheets that run parallel to fibril axis (Sunde *et al*., 1997; Sawaya *et al*., 2007; Eisenberg *et al*., 2012; Fitzpatrick *et al*., 2013). Amyloid fibrils arising from different proteins share these generic structural features, that are independent of the protein sequence, but more likely attributed to intramolecular and intermolecular interactions within the β-sheets, common to all peptide and protein molecules, primarly hydrogen bonds between the main-chain atoms of the polypeptide chains, that are also responsible for the extremely high stability of these structures (Fandrich and Dobson, 2002; Knowles *et al*., 2007). The structural differences between amyloid fibrils generated from different proteins arise from the manner in which the various side chains are incorporated into their structure (Serpell *et al*., 1995; Jimenez *et al*., 1999; Serpell and Smith, 2000a; Serpell *et al*., 2000; Zhang *et al*., 2009; Fitzpatrick *et al*., 2013). The representative structure of an amyloid fibril is reported in **Figure 9**.

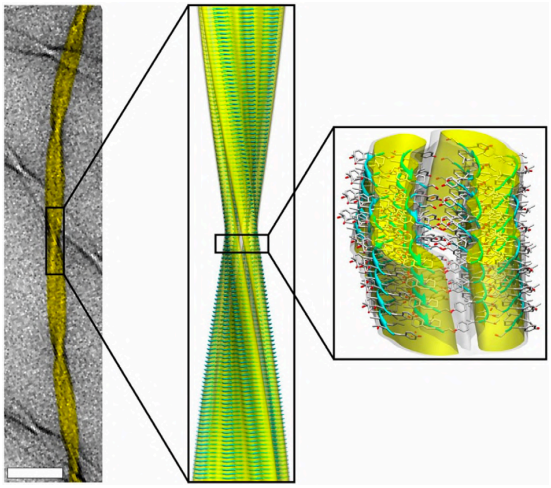

Figure 9 - Representative structure of an amyloid fibril. Atomic-resolution structure of amyloid fibrils formed by an 11-residue fragment of transthyretin. In the left, the image obtained using transmission electron microscopy (TEM) (scale bar 50 nm); in the center is reported the cryo-electron microscopy (cryo-EM) reconstruction. In the right, the fibril surfaces are shown, with oxygen, carbon, and nitrogen atoms represented in red, gray, and blue, respectively (Adapted from Fitzpatrick *et al*., 2013).

Interestingly, some studies revealed that the native state of folded or natively unfolded proteins is metastable, whereas the amyloid one is thermodynamically more stable than the functional conformation (Baldwin *et al*., 2011); in addition, the thermodynamic stability of the amyloid state has been reported to increase together with protein concentration. As a consequence, there is a critical concentration at which the stability of the native state is the same as that of the amyloid one; at higher concentrations, the protein will acquire the amyloid conformation, even though the high kinetic barriers for the conversion (Cyriam *et al*., 2013). There are some proteins with an *in vivo* concentration very close to the critical one; in those cases, even small changes in expression levels could lead to the conversion into the amyloid conformation (Cremades *et al*., 2017).

Protein aggregation, culminating in the formation of high ordered and stable amyloid fibrils, is a complex process in which, especially in the early stages, a wide range of low molecular weight oligomeric species that vary in size, β-sheet content, and stability, is generated. These assemblies are actually widely recognised as the key neurotoxic agents responsible for neurodegeneration (Bucciantini *et al*., 2002; Dobson, 2003; Chiti and Dobson, 2006; Walsh and Selkoe, 2007; Sakono and Zako, 2010; Ferreira and Klein, 2011; Winner *et al*., 2011; Benilova *et al*., 2012; Hayden and Teplow, 2013). In addition, several biochemical studies have demonstrated a strong correlation between the levels of

soluble amyloid oligomers in the brains of AD and PD patients and the severity of the symptomps (Winner *et al*., 2011; Ferreira *et al*., 2014). Due to their pathological relevance, many studies have focused on the molecular mechanisms of amyloid formation, and there is general agreement on a nucleation–conversion–polymerization model, at least for the intrinsically disordered proteins, in which most studies have been focused. According to such model, monomers start to assemble into relatively disordered oligomers with little or no stable β-sheet structure. These rudimental species subsequently convert into more highly ordered and compact oligomers with higher stability; these aggregates, with futher growth and β-sheet rearrangement, finally form amyloid fibrils (Auer *et al*., 2008; Orte *et al*., 2008; Qi *et al*., 2008; Carulla *et al*., 2009; Bleiholder *et al*., 2011; Lee *et al*., 2011; Cremades *et al*., 2012), as reported in **Figure 10**. In particular, oligomeric species initially acquire an antiparallel β-sheet configuration, that further convert into a parallel one, that is necessary for their elongation, culminating in the generation of the typical amyloid structure under physiological conditions (Cremades and Dobson, 2018).

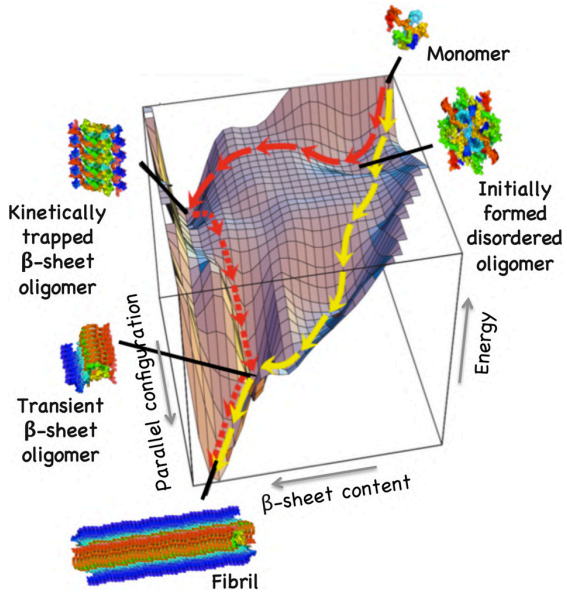

Figure 10 - Representative energy landscape for the amyloid aggregation process. The formation of amyloid assemblies is characterized by a wide range of degenerate energy states with high energy barriers between different regions of conformational space. The consequence of such a landscape is the existence of multiple pathways each with distinct oligomeric species. Some pathways will generate oligomeric species that are only transient and that rapidly elongate and convert into fibrils (such as the one indicated with yellow arrows). Other pathways give rise to kinetically trapped oligomeric species (red arrows), possessing a structural configuration that is not optimal for their further elongation; as a consequence, they only transform into fibrils after many structural slow rearrangements (dashed red arrows) (Cremades and Dobson, 2018).

αS abnormal aggregation has been associated not only with PD, but also with DLB and MSA, collectively referred to as synucleinopathies (McCann *et al*., 2014). In PD and DLB, αS inclusions are predominantly located inside the neurons and are commonly called LBs and LNs, whereas in MSA, inclusions are poorly organized bundles of αS fibrils, mostly present in the cytoplasm of oligodendroglial cells and, to a lesser extent, also inside neurons (Papp *et al*., 1989; Spillantini *et al*., 1998). Finally, αS has also been found to be a component of the amyloid inclusions found in the brain of AD patients (Ueda *et al*., 1993). Physiological intracellular αS levels are finely regulated and depend on the balance between protein synthesis, aggregation, and clearance. Any imbalance in these pathways can cause αS accumulation and toxicity.

αS has been defined as a protein-chameleon, because of its high conformational plasticity, which allows the acquisition of many different conformations, depending on the environmental conditions (Uversky, 2003), such as the presence of neighboring proteins, lipid membranes, but also one redox state, and the local pH (Uversky 2001; Eliezer *et al*., 2001; Janowska *et al*., 2015; Fusco *et al*., 2016; Lv *et al*., 2016). Under *in vivo* and *in vitro* physiological conditions, in the absence of amphipathic molecules or lipid vesicles, αS populates a range of disordered conformations, including structures that are slightly more compact than expected for a completely unfolded chain (Eliezer *et al*., 2001). Instead, in the fibrillar form, αS reaches a stable and compact cross-β structure in about two/thirds of the amino acid sequence (Chen *et al*., 2007, Comellas *et al*., 2011). Thus, as discussed earlier, the transition from the natively unfolded monomeric state to the fibrillar conformation is defined by the acquisition of a persistent secondary structure in the largest part of the polypeptide chain. During this complex conformational transition, several oligomeric species are formed; they can be “on-pathway”, that means that they are on a direct pathway to protofibrils and fibrils formation, but also off-pathway, if they do not form fibrils *in vivo* (Fagerqvist *et al*., 2013).

The many conformational states acquired by αS are represented in **Figure 11**.

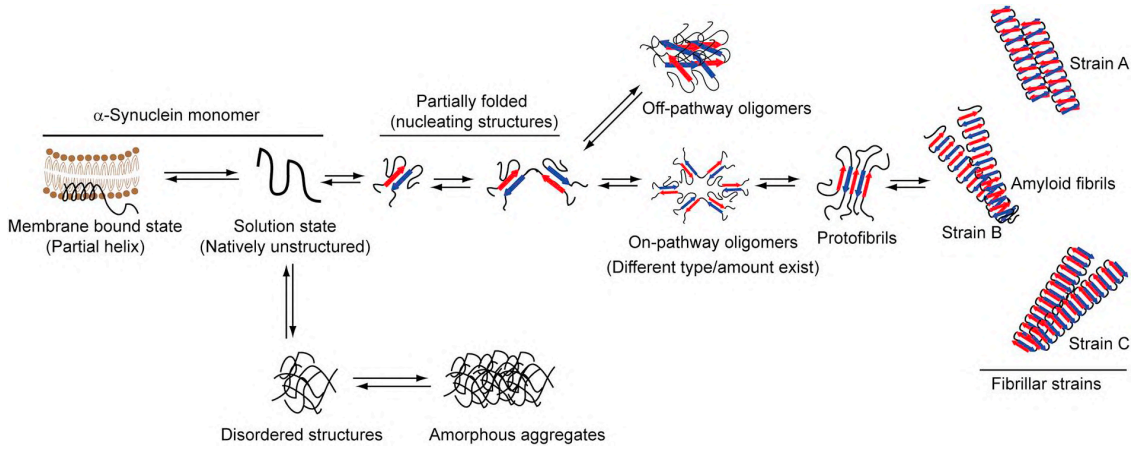

Figure 11 - Overview of the possible αS conformational states. αS monomer is natively unstructured in solution, but once bound to membranes it acquires a partial helical conformation. Under specific conditions, the natively unstructured monomer can convert into oligomers (on-pathway or off-pathway). Only the on-pathway oligomers can further aggregate into highly ordered cross-β-sheet fibrils. αS can also form disordered structures and amorphous aggregates (Mehra *et al*., 2019).

αS aggregation pathway has been extensively studied *in vitro* and its kinetic has been described as a sigmoidal curve, consisting of three main phases: the initial lag phase, also called nucleation, that represents the rate-limiting step of the whole process, characterized by the presence of monomers, transient small oligomers and an extremely low amount of fibrils; this step is followed by the elongation exponential phase, in which the nucleus converts into protofibrils and fibrils, whose concentration rapidly increase; finally, the third phase is the stationary one, where the largest part of the soluble protein is converted into amyloid fibrils (Wood *et al*., 1999; Narkiewicz *et al*., 2014; Li *et al*., 2019). However, the acquisition of the amyloid structure is a much more complex process, described in detail with two different models. The first one is the nucleation–polymerization model (**Figure 12A**), according to which the structural conversion from the natively unfolded conformation to the β-sheet structure takes place into monomeric αS. This step is followed by the formation of intermolecular hydrogen bonds, thus generating oligomers with a folded nucleus and composed of sections rich in β-sheet domains (Cremades *et al*., 2017). The limiting case of this model is monomeric αS with a fully formed β-sheet structure, that must encounter other monomers with the same structural characteristics for giving rise to oligomeric asseblies, a very unlikely situation. Given the weakness of this model, another one has been proposed, the so called nucleation–conversion–polymerization model (**Figure 12B**), according to which monomeric αS gets only

partially a β-sheet structure and subsequently self-assemblies; the acquisition of the fully-formed β-sheet structure takes place in the aggregated species resulting from the self-assembly of such partially-folded oligomeric species.

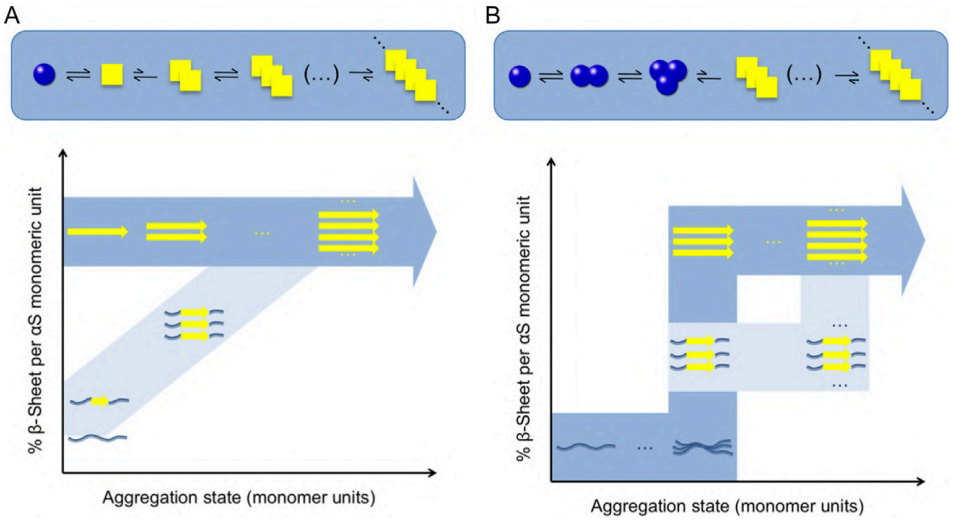

Figure 12 - Models proposed for the conversion of αS from its intrinsically disordered monomeric form to the cross-β structure characteristic of the amyloid form. Schematic representation of the nucleation–polymerization model **(A)** and the nucleation–conversion–polymerization one **(B)** (Cremades and Dobson, 2017).

1.3.4 αS oligomeric assemblies

"Oligomer" is an unspecific term widely used for indicating aggregated αS that has not joined a fibrillar conformation, so including a wide range of species with different structural and biophysical properties, such as molecular weight, β-sheet content and exposed hydrophobicity (Bengoa-Vergniory *et al*., 2017; Cremades *et al*., 2017). This great variety of species reflects a plethora of preparation methods, and morphological studies have revealed a great diversity of apparent structures. Despite these observed differences, both atomic force microscopy (AFM) and TEM revealed that oligomers have mostly a spherical shape (Conway *et al*., 1998; 2000a; 2000b) and that their further incubation gives rise to elliptical rings (Conway *et al*., 2002b), or to mature fibrils in the presence of an excess of the monomeric protein (Lashuel *et al*., 2002). Different oligomeric assemblies have been found to be dissimilar in secondary structure, which changes during the aggregation process, converting from an α-helical to a β-sheet (Apetri *et al*., 2006; Ghosh *et al*., 2015). Due to their transient nature, several tecniques have been

employed for the isolation and the stabilization of oligomeric assemblies *in vitro*, during fibrillar formation. One of the most commonly used technique is lyophilization, that strongly promotes, under agitation, the generation of oligomeric assemblies recognised by the oligomer-specific A11 antibody; these species seem to be unable to further aggregate and form fibrils (Celej *et al*., 2012; Chen *et al*., 2015). They have an antiparallel β-sheet secondary structure and are able to associate with lipid bilayers (Chen *et al*., 2015). Furthermore, these oligomers resulted to be toxic to neuronal cells, because of their ability to induce a significant production of reactive oxygen species (ROS), eventually leading to caspase-3 activation and apoptotic cell death (Deas *et al*., 2016). Taken into account these observation, it has been speculated that such oligomers could strongly reproduce the species formed *in vivo*, as they induced the same cascade of toxic effects as those observed in human induced pluripotent stem cells (iPSC)-derived neurons with *SNCA* triplication (Deas *et al*., 2016). Furthermore, it has been reported that these antiparallel β-sheet rich oligomers are unable to seed fibril formation efficiently (Lorenzen *et al*., 2014; Chen *et al*., 2015).

Many compounds with the ability to selectively bind certain types of oligomeric assemblies, thus blocking their elongation, have been identified. Among them there are polyphenols such as curcumin, rosmarinic acid, baicalein and epigallocatechine gallate (EGCG) (Cremades *et al*., 2017). Many studies reported their ability to block the formation of αS fibrils and to destabilize the structure of pre-formed fibrils (PFFs); in this way, baicalein gives rise to nontoxic oligomers with high β-sheet content (Lu *et al*., 2011) and EGCG, interacting with both oligomeric and fibrillar aggregates, is able to disassembly their structure, thus producing harmless species (Bieschke *et al*., 2010). Many studies have been performed to understand whether dopamine, whose lack is associated with the cardinal motor sympomps of PD, could have the ability to modify αS assemblies, and all converged on the idea that dopamine inhibits fibrils formation and disaggregates PFFs, generating disordered αS oligomers (Conway *et al*., 2001). Furthermore, many drugs have the ability to inhibit fibril formation and to disaggregate PFFs, first of all selegiline, a MAOB inhibitor actually administered to PD patients alone or together with L-DOPA, for its ability to prolong and increase the synaptic dopamine concentrations. This drug has also been reported to promote the formation of nontoxic amorphous aggregates of αS, without interacting with the monomeric protein. Oligomers formation can be promoted *in vitro* also by metal ions, such as Ca^{2+} (Nielsen *et al*., 2001), and Cu^{2+} (Niensen *et al*., 2001; Wright *et al*., 2009), that was also found to induce the

formation of toxic oligomers in cellular models (Wang *et al*., 2010). Also chemical protein modifications, such as the oxidation of the methionine residues and the nitration of the tyrosine ones, have been reported to promote the generation of αS oligomeric assemblies (Cremades *et al*., 2017). Oligomers have been reported to form upon αS interaction with brain-derived membranes (Ding *et al*., 2002) or other phospholipid bilayers and vesicles that reproduce biological membranes; their interactions give rise to conformational modifications that lead to oligomerization (Eliezer *et al*., 2001; Volles *et al*., 2001). Finally, αS oligomers are also obtained from the cold denaturation of fibrils in supercooling conditions, giving rise to partially structured species able to disrupt lipid membranes. Furthermore, these oligomers are able to reassemble and elongate to form parallel β-sheet fibrils (Kim *et al*., 2009).

Recently, two relevant oligomeric species, called Type A* (OA*) and Type B* (OB*) oligomers, co-existing during the early phases of αS self-assembly and aggregation, and with significantly different toxic properties, have been identified (Chen *et al*., 2015; Fusco *et al*., 2017). These species closely match those of the previously identified unstable forms of nontoxic (Type A) and toxic (Type B) αS oligomers (Cremades *et al*., 2012). OA* and OB* have similar dimensions and molecular configuration, but they exhibit distinct abilities to disrupt lipid bilayers and to impair cell viability, closely associated with their different β-sheet content (Fusco *et al*., 2017). Thus, when incubated *in vitro* with small unilamellar vesicles (SUVs) composed of 1-palmitoyl-2-oleoyl-sn-glycero-3-phospho-L-serine (POPS) lipids, OA* evoked only a slight release of the encapsulated calcein molecules; opposite, OB* induced a significant calcein release, thus indicating an intrinsic ability to disrupt plasma membrane integrity (Fusco *et al*., 2017). Similar results were obtained when the two different oligomeric assemblies were added to the culture medium of SH-SY5Y human neuroblastoma cells and primary rat cortical neurons: OB*, but not OA*, evoked a significant perturbation of the plasma membrane integrity, together with other toxic effects, such as the increase of the intracellular ROS levels and the reduction of the mitochondrial activity (Fusco *et al*., 2017). The structural determinants of their toxicity have been identified by using sophisticated and innovative tecniques, such as solution and solid-state nuclear magnetic resonance. While OA* remain largely unstructured (like monomeric αS) and only bind to the membrane surface, OB* show a highly lipophilic N-terminal region, responsible for the interaction with the membrane surface and a structured and rigid core rich in β-sheet, able to insert into the lipid bilayer, thus causing the disruption of the plasma membrane integrity (Fusco *et al*.,

2017). The structural characteristics of these oligomeric assemblies are represented in **Figure 13**.

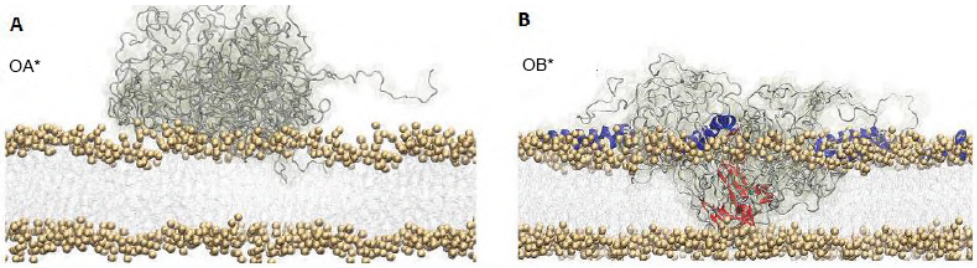

Figure 13 - Structural characteristics of αS OA* and OB*. **(A)** OA* (left) are mainly disordered and only bind to the membrane surface. **(B)** OB* present both structured (red) and disordered (gray) regions and bind the surfaces of the lipid bilayers via the folding of N-terminal regions into amphipathic α-helices (blue) upon membrane binding. Their rigid regions (red), rich in β-sheet structure, are able to insert into the lipid bilayers, thus inducing plasma membrane permeabilization (Fusco *et al*., 2017).

A recent study by Cascella and collaborators has further investigated the molecular determinants of OB* cytotoxicity. The use of a specific antibody targeting the N-terminal region of αS significantly reduced oligomers toxicity when they were incubated with primary cortical neurons and SH-SY5Y human neuroblastoma cells. These results corroborated the key role of αS N-terminal region in the interaction with the lipid bilayers, resulting in the observed cellular toxicity, as reported in **Figure 14** (Cascella *et al*., 2019).

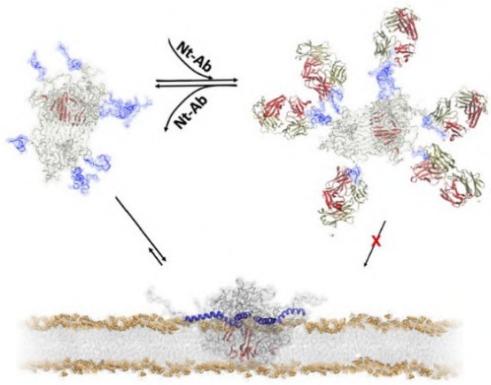

Figure 14 - Model of toxic αS OB*. Upon membrane binding, the N-terminal region of αS (blue) adopts an amphipathic α-helical conformation that anchors the oligomers to the membrane surface, whereas the structured core (red) inserts into the interior of the lipid bilayer and disrupts its integrity. The binding of an antibody targeting the N-terminal region (Nt-Ab, red and yellow chains) inhibits the crucial step leading to membrane binding and disruption (Cascella *et al*., 2019).

1.3.5 αS fibrils

αS self-assembly finally leads to the formation of highly compact and ordered fibrils that show the common amyloid features, such as the ability to bind Thioflavin T, the presence of a β-sheet structure and an elongated filamentous morphology (Serpell *et al*., 2000c; Qin *et al*., 2007; Celej *et al*., 2012) and that have been found to be morphologically and tinctorially almost identical to those extracted from patients (Crowther *et al*., 2000). Several techniques have been employed for the structural characterization of αS fibrils, such as EM, hydrogen exchange mass spectrometry, solid state NMR, or electron paramagnetic resonance (Cremades *et al*., 2017). Many accumulated evidences indicate that the core structure of αS fibrils generally includes residues 30–110, is resistant to proteases and completely buried (Miake *et al*., 2002; Chen *et al*., 2007; Vilar *et al*., 2008; Comellas *et al*., 2011; Gath *et al*, 2012), whereas both the C-terminus (residues 100–140) and the most N-terminal region of the protein (residues 1–30) remain largely unstructured, although both regions seem to be involved in the interactions between protofilaments (Vilar *et al*., 2008; Guilliams *et al*., 2013). Furthermore, αS fibrils adopt an antiparallel in-register β-sandwich fold; several polymorphs, which vary in the number and disposition of the protofilaments in the fibrils and in the strenght of the amino acid interactions responsible for the β-sandwich fold, have been identified (Vilar *et al*., 2008; Comellas *et al*., 2011; Tuttle *et al*., 2016). EM studies have shown that, independently of the fibril polymorphism, several αS fibrils possess a low electron density region in the center of their structure (Vilar *et al*., 2008), as they are formed by many protofibrils that, interacting each other, form a tubular-like ultrastructure, in both twisted and straight fibrils (Cremades *et al*., 2017). Cryo-EM studies revealed that the residues 50-57 of αS fibrils are located at the interface of the interacting protofilaments. Many familial point mutations associated with PD, such as H50Q, A53T, and G51D, are located in these residues, and they can give rise to different types of fibrils (Guerrero-Ferreira *et al*., 2018). Despite the increasing relevance given to αS oligomeric assemblies for their ability to induce cellular toxicity, many findings support the cytotoxic capacity of fibrillar αS species; the exposure of neuronal cells to αS fibrils has been reported to induce the aggregation of the endogenous αS and the formation of inclusions that are morphologically and biochemically similar to those found in the brain of PD patients. The presence of these Lewy body (LB)-like structures has been associated with the loss of dopaminergic neurons in the SN (Volpicelli-Daley *et al*., 2011; Luk *et al*., 2012; Masuda-

Sukake *et al*., 2014; Osterberg *et al*., 2015). Some researchers found that αS fibrils are toxic themselves, because of their ability to bind and permeabilize the plasma membrane, thus inducing several alterations in cultured cells, such as Ca^{2+} dyshomeostasis (Pieri *et al*., 2012) and mitochondrial dysfunction (Pemberton *et al*., 2011).

1.3.6 αS uptake, processing and release

Many studies performed both in humans and model systems clearly indicate that αS can be released from neurons (El-Agnaf *et al*., 2003), and subsequently taken up by nearby, thus inducing Lewy pathology. Accordingly, the so-called Braak hypothesis posits that αS from LBs and LNs spreads between synaptically-connected brain areas (Braak *et al*., 2002, 2003). This transmission would be responsible for the propagation of the pathology and strongly correlates with the progression and the severity of the disease-associated symptoms. According to this theory, Lewy pathology is initiated by an indefined pathogen (virus or bacterium) that enters in the nasal cavity, and subsequently reaches the gut (Braak *et al*., 2003b); this pathogen spreads via the olfactory tract or the vagus nerve, joining the central nervous system (CNS), and in particular the medulla oblongata and the olfactory bulb, thus causing olfactory deficits, that are early markers of the preclinical phases of PD (stages 1 and 2); the propagation carries on into the brainstem, and this causes sleep and motor disturbances (Braak stages 3 and 4), then into the limbic system, finally reaching the neocortical regions, thus determining cognitive impairment and emotional disturbances in Braak stages 5 and 6 (Halliday *et al*., 2011). The so-called Braak stages are reported, together with the associated sympoms, in **Figure 15**. It is, however, important to underline that the synaptic connection between different brain regions is necessary but not sufficient for causing neuronal cell death, that is strongly associated with the intrinsic vulnerability of specific neuronal populations (Henderson *et al*., 2019).

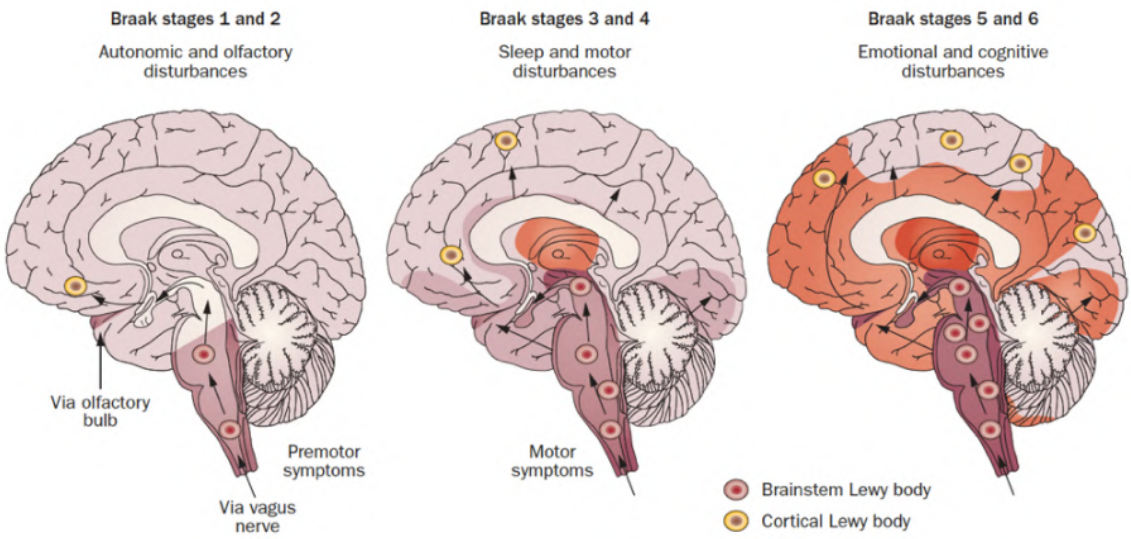

Figure 15 - The Braak staging system of PD. The initiation sites are located in the olfactory bulb and the medulla oblongata; Lewy pathology subsequently infiltrates into cortical regions. The red shading represents the pattern of pathology (Doty *et al*., 2012).

Many different cellular and animal models have been used to explain αS transmission. Some studies reported that αS PFFs, in the presence of a lipophilic agent, were internalized by non-neuronal cells overexpressing wild-type αS and, after internalization, they induced the misfolding of the endogenous αS and its aggregation in LB-like structures (Luk *et al*., 2009; Nonaka *et al*., 2010). Subsequent studies joined the same conclusions also in the absence of any agent able to augment the transfer of PFFs to the cytosol (Volpicelli *et al*., 2011). The so formed LB-like aggregates were found to induce neuronal impairment and, finally, cell death (Volpicelli-Daley *et al*., 2011; Froula *et al*., 2018; Luna *et al*., 2018). Similar results were obtained in primary dopaminergic neurons (Dryanowski *et al*., 2013; Henderson *et al*., 2018), in which LB-like aggregates were found to induce a massive mitochondial oxidative stress, having a central role in PD pathogenesis (Dryanowski *et al*., 2013).

Many studies have been performed in animal models, firstly with the injection of PFFs into the brains of transgenic mice overexpressing human A53T αS (Luk *et al*., 2012a), in which αS aggregation and LBs formation were exacerbated by the uptake of PFFs; these aggregates were also injected in mice brains overexpressing the wild-type protein, and LB-like inclusions were found to spread through the mouse brain following a precise spatiotemporal pattern (Luk *et al*., 2012b). Many other investigations have been performed in animal models, both in mice (Masuda-Sukake *et al*., 2013; Rey *et al*., 2018;

Steiner *et al*., 2018) and rats (Paumier *et al*., 2015). In all these cases, the injection of PFFs was confirmed to induce the formation of LB-like inclusions, thus leading to the spreading of αS pathology and, as a consequence, to the death of vunerable neuronal populations, thus reproducing the main features of PD. Taken together, all these evidences underline the importance of a better comprehension of the molecular mechanisms responsible for αS transmission, also for the indentification of potential targets for therapeutic intervention in PD. An overview of the whole process is given in **Figure 16**.

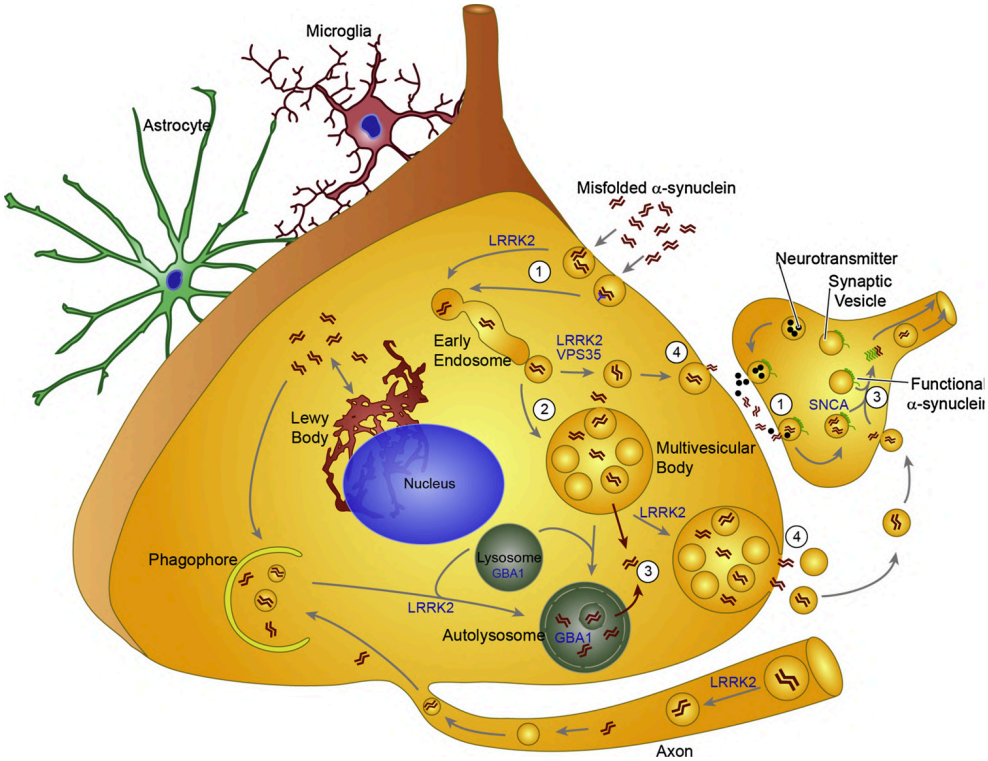

Figure 16 - Overview of the main mechanisms of pathogenic αS transmission. The 4 main steps are: uptake **(1)**, processing **(2)**, escape **(3)** and release **(4)**. The uptake of extracellular αS into neurons can take place either through non-selective endocytosis or receptor-mediated endocytosis **(1)**. The synaptic vesicle cycle, responsible for neurotransmitter release, may promote the uptake of extracellular αS. Misfolded αS is then processed through the endo-lysosomal pathway **(2)**: αS may be directly targeted back to the plasma membrane through recycling vesicles, or into multivesicular bodies, but αS seeds can also escape the endolysosomal pathway, thus becoming free in the cytosol **(3)**. This cause the recruitment of endogenous, functional αS into fibrillar structures. The autophagic pathway is implicated in the degradation of both cytosolic and vesicular αS; vesicles or multivesicular bodies containing αS can be also targeted for exocytosis, possibly to unburden the lysosomal degradation pathway. This leads to the release of pathogenic αS from the neuron **(4)**. LRRK2, VPS35 and GBA1 proteins are also reported, as their mutations have been associated to the development of PD. Astrocytes and microglial cells are also represented, as they have been shown to play some roles in αS transmission (Henderson *et al*., 2019).

Regarding αS uptake, it has been widely reported that different cell types easily internalize misfolded αS assemblies: this evidence was obtained in human embrionic kidney (HEK) and SH-SY5Y human neuroblastoma cells (Hansen *et al*., 2011), primary neurons (Karpowicz Jr *et al*., 2017; Froula *et al*., 2018), but also in oligodendrocytes (Kisos *et al*., 2012) and neurons *in vivo* (Luk *et al*., 2012b). In neurons, αS uptake takes place not only in the soma, but also in dendrites and axons, as observed by using microfluidic cell culture systems, a sophisticated tool that allows the separation of the different cellular compartments in fluidically isolated channels (Volpicelli-Daley *et al*., 2011; Tran *et al*., 2014; Brahic *et al*., 2016). Furthermore, once internalized in a specific compartment, αS misfolded aggregates can be transported through the axons, in both the anterograde and retrograde direction, even if with a different efficiency (Brahic *et al*., 2016). Interestingly, when new neurons were added to the axon channel of a previously established cell culture, αS assemblies were also transferred to second order neurons through anterograde transport, were they might work as a template for the aggregation of endogenous αS (Freundt *et al*., 2012; Mao *et al*., 2016).

Different molecular mechanisms have been proposed for αS uptake, such as micropinocytosis (Karpowicz Jr et al., 2017) and receptor-mediated endocytosis (Mao *et al*., 2016; Aulic *et al*., 2017). The extracelluar receptor LAG3 (lymphocyte activation gene 3), a member of the immunoglobulin superfamily of receptors, has been reported to bind prefibrillar αS and to mediate the endocytic process (Mao *et al*., 2016). Other researchers used a proteomic approach for the identification of possible membrane interactors of αS oligomers and fibrils, and they found that the α3-subunit of Na^+/K^+-ATPase (α3-NKA) was able to interact with both oligomeric and fibrillar forms of αS (Shrivastava *et al*., 2015). Accordingly, the gene encoding α3-NKA (*ATP1A3*), has been associated to rapid-onset dystonia-parkinsonism (de Carvalho *et al*., 2004). Furthermore, the Fc gamma receptor IIb (FcγRIIB) has been described as a receptor for αSyn fibrils, mediating their cell-to-cell transmission (Choi *et al.*, 2018). Two different studies reported that the cellular prion protein (PrP^C) is responsible for the uptake of misfolded αS assemblies (Aulić *et al*., 2017), and for the subsequent cellular dysfunctions and cognitive impairment (Ferreira *et al*., 2017). This protein was also reported to interact with amyloid-β oligomers (Salazar *et al*., 2017), thus representing a kind of cellular conformation-specific sensor for disease-associated proteins (Watts *et al*., 2018). However, in a recent study, La Vitola and collegues denied these evidence, as they indicated that PrP^C neither binds αS oligomers nor mediates their effects, both *in vitro*

and *in vivo* (La Vitola *et al*., 2019). Therefore, given that αS neurotoxicity is the result of a range of different molecular mechanisms, even not completely understood, both a PrP^C-dependent and PrP^C-independent pathways are thought to co-exist. Furthermore, Holmes and collegues reported that αS fibrillar aggregates bind to heparan sulfate proteoglycan (HSPGs) prior to internalization by micropinocytosis (Holmes *et al*., 2013). This evidence has been supported by the observation that soluble heparin added in cell culture media of primary neurons could competitively inhibit αS fibrils binding to cell surface and subsequent uptake by cells (Karpowicz *et al*., 2017). Finally, αS fibrils have been shown to interact with the amyloid-β precursor-like protein 1 (APLP1; Mao *et al*., 2016). An overview of the membrane proteins interacting with αS assemblies is proposed in **Figure 17**.

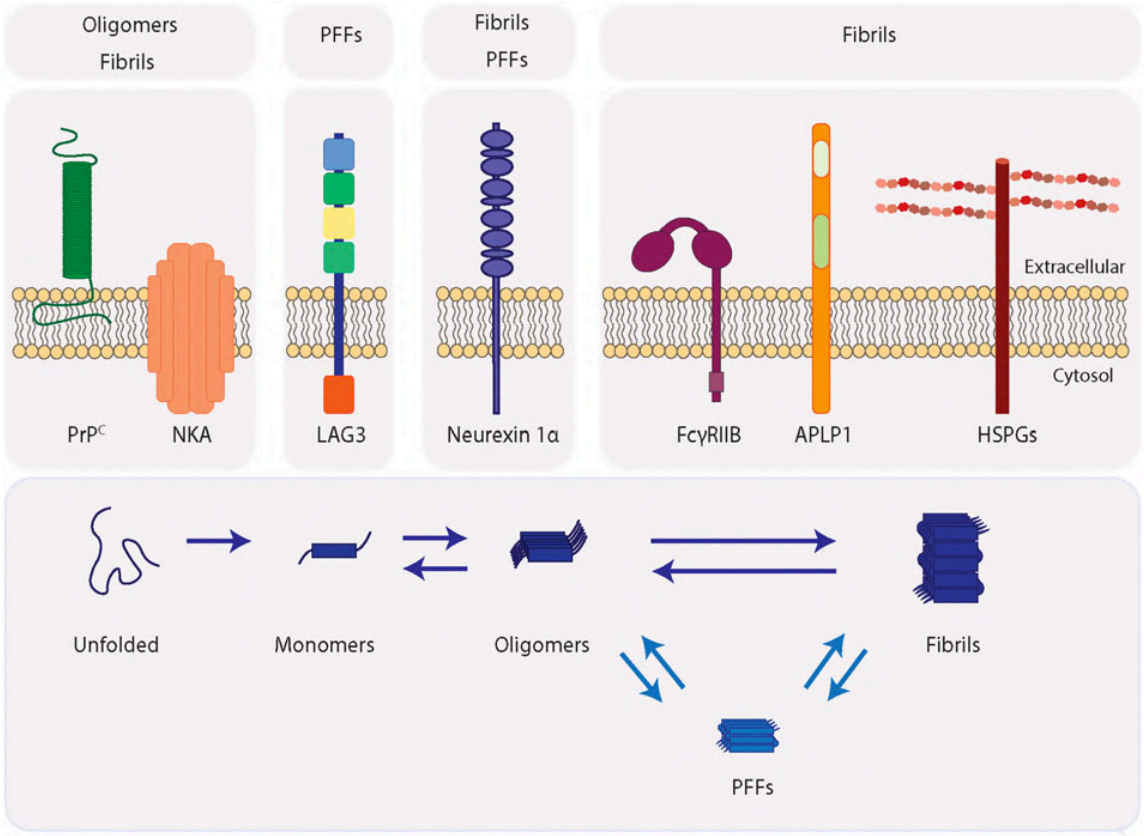

Figure 17 - Membrane proteins interacting with αS and mediating its internalization. Oligomeric and fibrillar αS have been reported to interact with both PrP^C and the α3 subunit of NKA. The cell surface receptor LAG3 can bind αS PFFs arising from the sonication of αS fibrils. Fibrillar αS can bind other surface receptors, such as FcγRIIB, APLP1, and HSPGs. Once internalized, αS aggregates can lead to the misfolding and fibrillization of the endogenous protein (Brás *et al*., 2018).

Once internalized, αS fibrils have been reported to colocalize with endogenous αS, in both neuronal and non-neuronal cell lines. This evidence suggests that exogenous αS assemblies could act as nucleating seeds, able to recruit intracellular αS, giving rise to the formation of large insoluble LB-like inclusions (Luk *et al*., 2009; Volpicelli-Daley *et al*., 2011), imprinting their structural characteristics onto endogenous protein, and so causing its misfolding (Bousset *et al*., 2013; Peelaerts *et al*., 2015). This process requires a direct contact between αS fibrils and the intracellular αS; for this reason, it has been supposed that misfolded aggregates are able to disrupt the integrity of endocytic membranes (Wiethoff *et al*., 2005).

Regarding αS clearance, it has been reported that misfodeld aggregates strongly colocalize with both early and late endosomal/lysosomal markers (Lee *et al*., 2008; Desplats *et al*., 2009; Brahic *et al*., 2016), thus indicating that αS is subjected to lysosomal degradation, even if there are some conflicting reports about the kinetics of this process, possibly because of differences in the experimental procedures applied for the preparation of the aggregates and their delivery to cells (Lee *et al*., 2008; Luk *et al*., 2009). Furthermore, the accumulation of aggregated αS has been associated with impairments of both the cellular protein catabolic systems, the ubiquitin-proteasome system (UPS) and the autophagy-lysosome pathway (ALP), represented by macroautophagy, chaperone-mediated autophagy (CMA) and microautophagy, all implicated in αS degradation, as reported in **Figure 18**.

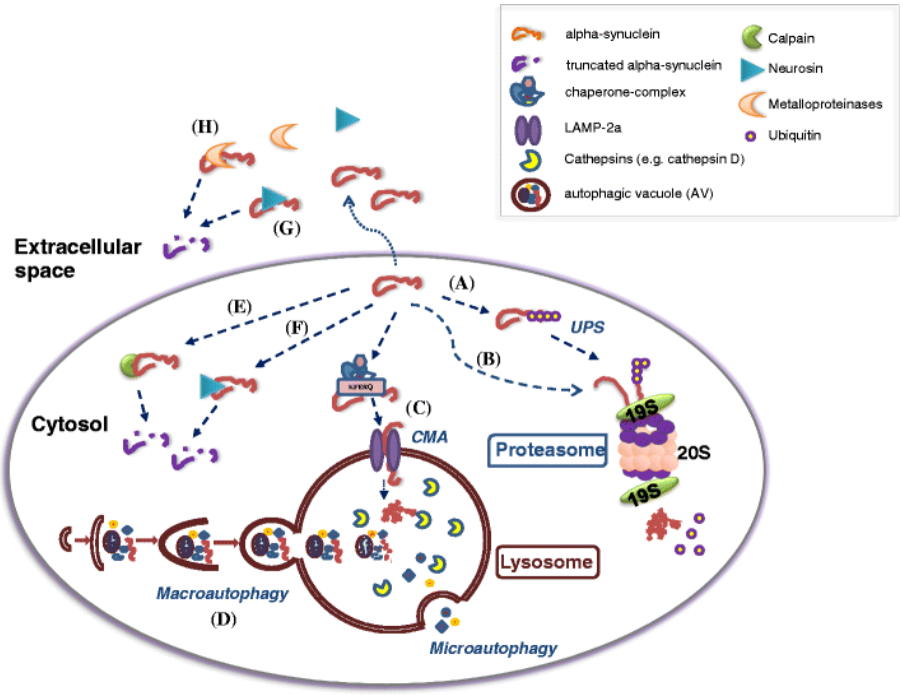

Figure 18 - Proteolytic pathways responsible for αS degradation. Intracellular proteins are degraded via the UPS and the ALP. αS can be degraded both with ubiquitin-dependent **(A)** and ubiquitin-independent **(B)** mechanisms. Three different lysosomal pathways have been described in mammalian cells: microautophagy, macroautophagy, and CMA. Both CMA **(C)** and macroautophagy **(D)** are involved in αS degradation: CMA is responsible for the degradation of monomeric wild-type αS, whereas macroautophagy can degrade wild-type, mutant and aggregated αS. Intracellular normal and aggregated αS can also be cleaved by proteases such as calpains **(E)** and neurosin **(F)**, potentially leading to the formation of truncated αS species with high pathogenic relevance. Secreted neurosin **(G)** and metalloproteinases **(H)** have been reported to cleave at selective sites extracellular αS, generating highly aggregation-prone fragments (Xilouri *et al*., 2013).

UPS is a cardinal proteolitic system targeting the vast majority of misfolded proteins. The process requires the poly-ubiquitylation of the target proteins in three different steps, catalyzed by ubiquitin-activating (E1), ubiquitin-conjugating (E2), and ubiquitin-ligase (E3) enzymes, respectively. After the first addition of ubiquitin to a lysine residue, other ubiquitin molecules are conjugated to the previous one; a minimum of four ubiquitins is required for proteasomal targeting of the protein (Layfield *et al*., 2001). After poly-ubiquitylation, substrate proteins are transferred to the 26S proteasome, a large multi-protein complex where they are degraded into oligopeptides; furthermore, ubiquitin molecules are released by ubiquitin recycling enzymes and can be reused for new poly-ubiquitylation reactions (Glickman *et al*., 2002). The main components of the 26S proteasome are the 20S core particle, where the proteolysis takes place, and two 19S

regulatory subunits, composed in turn by several ATPase subunits and by a number of subunits that lack of ATPase activity (Demartino *et al*., 2007). An ubiquitin-independent proteolysis, regulated by non-ATPase complexes, has also been described (Demartino *et al*., 2007). UPS has been associated to αS degradation as two UPS-related proteins, Parkin and UCH-L1, are encoded by genes whose mutations are associated to the development of PD (Kitada *et al*., 1998; Maraganore *et al*., 2004). A wide range of studies corroborated this hypothesis, demonstrating that αS is degraded by proteasome both by an ubiquitin-dependent (Bennett *et al*., 1999; Imai *et al*., 2000; Webb *et al*., 2003) and an ubiquitin-independent mechanism (Tofaris *et al*., 2001; Nakajima *et al*., 2005). As already announced, the largest amount of αS present in LBs is phosphorylated at residue S129 (pS129); it has been observed that the inhibition of the UPS pathway by MG132 or lactacystin led to a significant accumulation of pS129, without affecting the total amount of protein inside human neuroblastoma cells. Taken into account these evidences, it has been hypothesized a role for this post-translational modification in targeting the protein to the proteasome pathway, where a rapid degradation occurs through an ubiquitin-independent mechanism (Machiya *et al*., 2010). However, αS is predominantly degraded by lysosomes, acidic organelles containing a wide range of hydrolytic enzymes. In microautophagy, substrates are directly delivered into the lumen through invaginations of the lysosomal membrane (**Figure 18**). Macroautophagy is a catabolic process regulated by the expression products of a range of multiple autophagy-related genes (Atg); the degradation target is enveloped into double-membrane vesicles, that further merge with lysosomes. Its involvement in αS clearance has been demonstrated *in vitro*, as its inhibition with 3-methyladenine (3-MA) caused a significant increase of both soluble and aggregated αS levels in non-neuronal cells (Vogiatzi *et al*., 2008). Furthermore, the accumulation of A53T oligomers was observed in neuroblastoma cells following both the pharmacological and the molecular inhibition of the macroautophagic process (Yu *et al*., 2009). However, there are some conflicting works reporting that the 3-MA inhibition did not result in any accumulation of insoluble αS, both in neuronal cultured cells and in animal models, so suggesting that another lysosomal degradation mechanism probably occurs in αS clearance (Kluken *et al*., 2012). It has been proposed that macroautophagy could be the elective mechanism for the degradation of fibrillar assemblies and that oligomers are more likely degraded by chaperone-mediated autophagy. CMA is a complex catabolic pathway with a crucial role in the regulation of intracellular αS levels (Cuervo *et al*., 2004; Mak *et al*., 2010). It depends on the recognition of the so-called

CMA-targeting motifs, that is a consensus sequence present in the target-proteins (KFERQ), by Hsc70, with further translocation of the substrate into the lysosomal membrane. Hsc70, together with other co-chaperons, is able to unfold the target protein; once inside the lysosome, it interacts with the lysosome-associated membrane protein type 2A (LAMP2A); this step is responsible for the translocation of the substrate into the lysosomal lumen, where the degradation occurs (Cuervo *et al*., 2004; Lamb *et al*., 2013). A wide range of studies proved the relevance of this process in the degradation of monomeric and dimeric αS in isolated lysosomes *in vivo*, and that A30P and A53T αS mutations strongly inhibit CMA (Cuervo *et al*., 2004; Mak *et al*., 2010); furthermore, the central role of LAMP2A has been demonstrated, as its downregulation in cultured neuronal cells caused a significant increase of aggregated αS (Vogiatzi *et al*., 2008).

Through lysosomal rupture, a small amount of misfolded αS can escape the degradation pathway, thus becoming free in the cytosol (Jiang *et al*., 2017). Karpowicz Jr. and coworkers reported that the induction of lysosomal perturbation by chloroquine was resposible for a substantial increase of cytosolic misfolded αS (Karpowick *et al*., 2017). Importantly, is has been observed that lysosomal functionality is dramatically impaired with age, and this could be one of the most relevant mechanisms by which age could contribute to αS pathology (Flavin *et al*., 2017; Jiang *et al*., 2017). As a consequence, failures in the clearance of αS are responsible for the accumulation of toxic aggregates, as shown both in cultured cells and animal models (Lee *et al*., 2004; Ravikumar *et al*., 2008). Once inside the cells, αS forms perinuclear thread-like inclusions, further subjected to many modifications, such as phosphorylation and ubiquitination (Volpicelli-Daley *et al*., 2011); studies performed in mouse brains indicated that these pools of pathogenic αS can persist for months (Osterberg *et al*., 2015), but small oligomeric assemblies from these large inclusions could be released from cultured cells.

Finally, αS degradation can also occur through the activation of other proteases, such as calpain (Dufty *et al*., 2007), neurosin (kallikrein-6) (Iwata *et al*., 2003), and matrix metalloproteinases (Choi *et al*., 2011), both *in vitro* and *in vivo* (**Figure 18)**. The products of such cleavage are truncated forms of the protein with the ability to induce the aggregation of the full-length endogenous protein and, together with aggregated αS, they were found to be components of LBs and LNs (Liu *et al*., 2005).

The evidence of αS release from cells is given by the presence of both the soluble and the aggregated protein in CNS interstitial fluid and CSF (El-Agnaf *et al*., 2003). This process seems to be a consequence of the massive stress and subsequent impairment of the

proteostasis machinery, as shown by many studies performed in different cellular models (Bae *et al*., 2010; Jang *et al*., 2010; Lee *et al*., 2013; Fussi *et al*., 2018); thus, the release of harmful αS assemblies can be considered as a compensatory mechanism preventing the short-term toxicity on the individual cell, but it is responsible for the transmission of pathological αS to the nearby and sinaptically connected neurons (Henderson *et al*., 2019). The molecular mechanisms of secretion are not completely clear; Lee and collegues proposed the so-called misfolding-associated protein secretion pathway, showing that the protein USP19, an ER-bound deubiquitylase with chaperone activity, mediates the delivery of misfolded proteins to late endosomes, where they are incapsulated and subsequently secreted to the extracellular environment. These evidences have been accumulated in non-neuronal cells, and further investigations are needed to confirm whether this pathway takes place also in neurons (Lee *et al*., 2016).

Another recent study reported that the chaperone complex Hsc70/DnaJC5 binds to many neurodegenerative-associated proteins, such as αS, tau and TDP-43, thus driving their removal from neurons (Fontaine *et al*., 2016). Many aspects of these processes remain to be elucidated, as it is not clear in which conformation(s) (misfolded, oligomeric, or fibrillar) αS is secreted, and also if the two pathways are synergistic or work in parallel.

Very little amounts of oligomeric – but non fibrillar – αS have been found in exosomes, that could represent an alternative minor mechanism for release (Emmanouilidou *et al*., 2010). Finally, αS fibrils have been proposed to be transferred between cells also by tunneling nanotubules (TNTs), that are long, F-actin-based membranous channels connecting cells and allowing the transfer of many molecules (McCoy-Simandle *et al*., 2016); in this way, αS fibrils directly enter the cytosol of the acceptor cells, where they induce the aggregation of soluble αS. The cellular pathways implicated in αS release are represented in **Figure 19**.

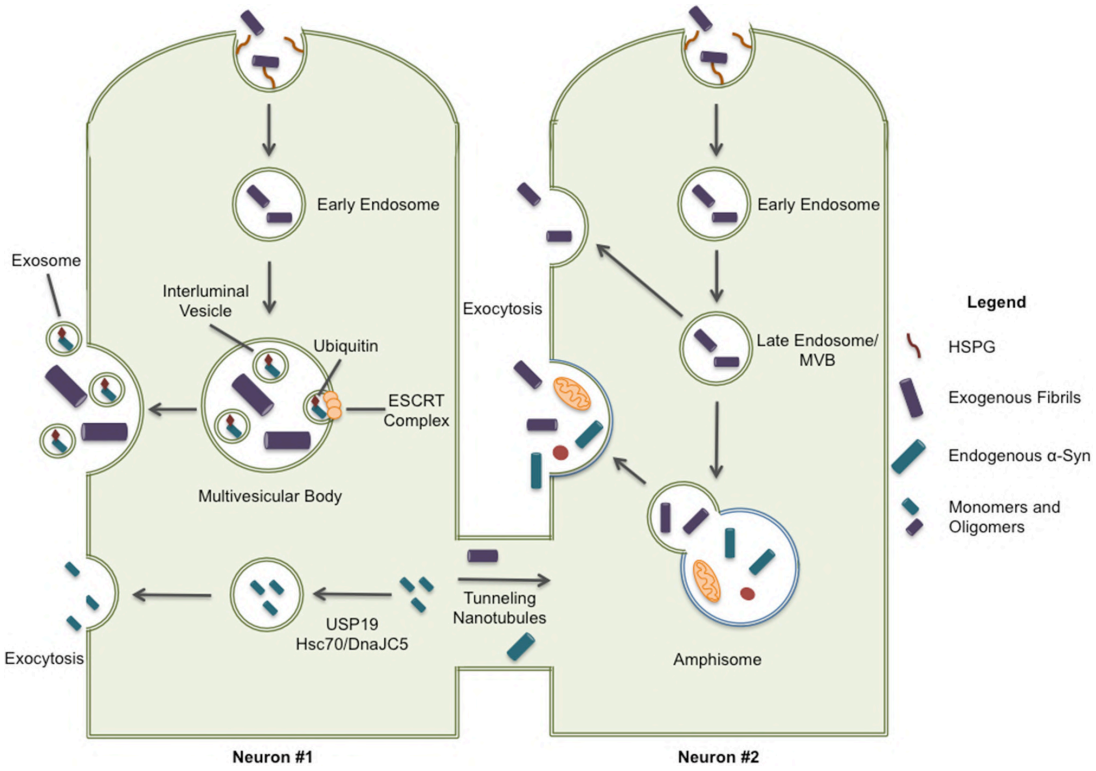

Figure 19 - Cellular pathways implicated in αS release and transmission to nearby cells. ESCRT (endosomal sorting complexes required for transport) is responsible for the excretion of αS through exosomal release. Cytoplasmic αS can be recruited to Rab9a-positive vesicles through chaperone-mediated pathways involving USP19 and Hsc70/DnaJC5, leading to exocytosis. Intracellular αS can also be secreted through TNTs and so transferred to neighboring cells, thus inducing the spreading of pathology. If internalized αS assemblies are not immediately directed to protein degradation systems, they may also be released through the exocytic system. This process can occur directly from late endosome/multivesicular bodies, but also from secretory autophagic vesicles (Rodriguez *et al*., 2018).

1.3.7 αS pathogenic pathways

αS neurotoxicity involves a wide range of different pathways, cellular functions and multiple organelles including cell membrane, synaptic vesicles, mitochondria, ER and Golgi, lysosomes, autophagosomes and nucleus, as reported in **Figure 20**.

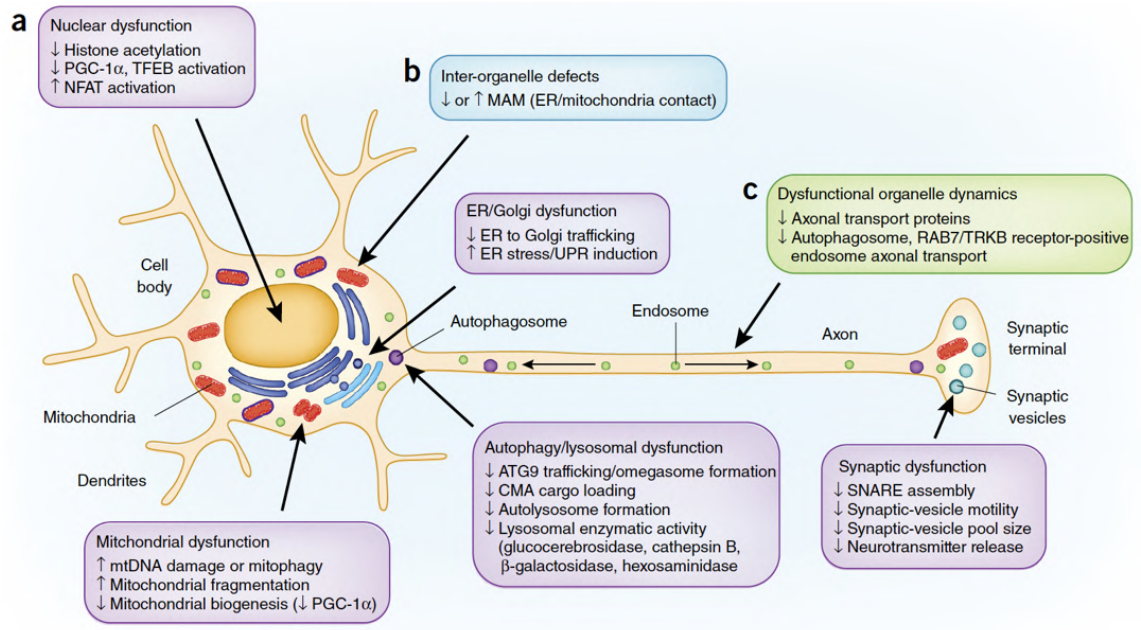

Figure 20 - Pathways implicated in αS cytotoxicity. (**a–c**) Organelle dysfunctions (**a, purple boxes**), defects in inter-organelle contacts (**b, blue box**) and dysfunctional organelle dynamics (**c, green box**) have been implicated in αS cytotoxicity (Wong and Kranic, 2017).

Synaptic-vesicle trafficking

As previously reported, one of the cardinal functions of αS is the regulation of neurotransmitter release by binding the VAMP2 protein, and so promoting synaptic-vesicle fusion at the presynaptic terminal (Burré *et al.*, 2010). Scott and coworkers showed that the overexpression of wild-type αS caused significant neurotransmitter release deficits in transgenic mice and that the derived cultured hippocampal neurons showed the absence of endogenous synaptic proteins, such as VAMP2 and the synaptic vesiscles (SV) proteins amphiphysin and synapsin I, that has been correlated with the observed synaptic pathology (Scott *et al.*, 2010). Accordingly, the depletion of the SNARE complex proteins VAMP2 and SNAP-25, but also that of the SV proteins CSPa and synapsin II has been observed *in vitro*, by exposing primary neuronal cultures to αS PFFs (Volpicelli-Daley *et al.*, 2011). Furthermore, studies *in vitro* reported that αS oligomers are able to bind the N-terminal domain of VAMP2, thus blocking SNARE-mediated vesicle docking (Choi *et al.*, 2013). A study from Garcia-Reitböck and coworkers showed that the overexpression of a truncated form of human αS caused its accumulation at the synapses, subsequently leading to a redistribution of the SNARE proteins to the striatum, together with an age-dependent reduction of dopamine release

(Garcia-Reitböck *et al*., 2010). αS has also a role in the regulation of vesicle trafficking, given by its ability to interact with Rab proteins. αS aggregates have been reported to abnormally interact with these proteins, thus causing defects in vesicular trafficking (Dalfò *et al*., 2004; Gitler *et al*., 2008). Taken together, these evidences indicate that the abnormal αS accumulation at the synapse is responsible for the gain of a toxic function, directly correlated with synaptic failure.

Mitochondrial functionality

Mithochondria are aboundant organelles where ATP synthesis takes place; they are also involved in the regulation of Ca^{2+} storage, lipid metabolism and neuronal survival (Nunnari and Suomalainnen, 2012). Dopaminergic neurons, due to their high synaptical connectivity, need high amounts of ATP and, as consequence, elevated mitochondrial activity. In physiological conditions, ATP is synthesized through an electron transport chain composed of four different complexes (I-IV), responsible for the formation of a protonic gradient over the mitochondrial inner membrane, required for ATP production. In the last step of the electron transport chain, complex IV, also called cytocrome *c* oxidase, reduces O_2 in water, thus causing a low formation of ROS. It has been reported that both in elderly people and in PD dopaminergic neurons, the activities of the complexes I and IV are altered, and that ROS production is significantly increased in such conditions (Blesa *et al*., 2015). This evidence was also supported by the discovery that a reduced activity of the complex I was also present in the skeletal muscle (Bindoff *et al*., 1989) and platelets of PD patients (Haas *et al*., 1995), supporting the hypothesis that systemic mitochondrial alterations are implicated in PD. Furthermore, the increase in ROS levels is responsible for the high degree of mutation of mitochondrial DNA (mtDNA), that, in a recent work, has been associated to complex I deficiency and increased ROS in PD (Giannoccaro *et al*., 2017). This complex is composed by several subunits, encoded both by nuclear and mitochondrial DNA, and mutations in mtDNA sequence are considered susceptibility factors for PD (Mizuno *et al*., 1989; Autere *et al*., 2004). Mitochondrial dysfunction in PD has been associated with the abnormal traslocation and accumulation of wild-type αS and its missense mutant A53T, from the cytosol to the mitochondrial membranes, both in PD patients and animal models, thus causing complex I impairment (Devi *et al*., 2008; Chinta *et al*., 2010), increased oxidative stress (Hsu *et al*., 2000; Parihar *et al*., 2008), reduced mitochondrial membrane potential, Ca^{2+} homeostasis impairment (Buttner *et al*., 2010; Rcom H'cheo-Gautier *et al*., 2016),

and, as a consequence, cytochrome *c* release, a critical early event in apoptotic cell death (Parihar *et al*., 2008, 2009). A bidirectional relationship between mitochondrial dysfunction and αS aggregation has been identified; the inhibition of mitochondrial complex I obtained in a rat model of PD with the pesticide rotenone led to the accumulation and the subsequent oligomerization of αS (Betarbet *et al*., 2000; Batarbet *et al*., 2006), causing in turn mitochondrial impairment and ROS production. Moreover, it has been observed that mutations in *PINK1*, encoding a mitochondrial kinase, and associated with a recessive form of PD, result in a severe inhibition of complex I and increased production of ROS in mitochondria (Gandhi *et al*., 2009). Di Maio and coworkers showed that oligomeric, dopamine-modified, and S129 phosphorylated αS can impair mitochondrial protein import, thus contributing to the dysfunction of these organelles (Di Maio *et al*., 2016). Interestingly, it has also been reported that αS oligomers are responsible for a massive disruption of the anterograde axonal transport of mitochondria in human neurons from PD patients, thus causing significant changes in transport-regulating proteins and energy deficits, finally culminating in synapse loss (Prots *et al*., 2017). In a recent work, Ludtmann and collaborators demontrasted that oligomeric αS aberrantly interacts with mitochondrial ATP sinthase, thus inducing the selective oxidation of his beta subunit. This oxidation, together with those of mitochondrial lipids and the other toxic effects previously reported, leads to the opening of the permeability transition pore (PTP) and, ultimately, to neuronal death (Ludtmann *et al*., 2018).

ER and Golgi functionality

ER plays an essential role in protein folding, traffiking to Golgi, regulation of Ca^{2+} homeostasis and unfolded protein response (UPR). The accumulation of misfolded proteins and their further aggregation in ER impair its normal functionality and evoke a cascade of toxic effects possibly culminating in cell death. In such conditions, the ER initiates a multi-signaling pathway called UPR, that restores its functionality (Walter and Ron, 2011). The accumulation of misfolded αS oligomers, followed by ER stress and activation of the UPR, has been demonstrated in mammalian cell cultures and in transgenic mouse and yeast models overexpressing A53T or C-terminal truncated αS (Smith *et al*., 2005; Cooper *et al*., 2006; Colla *et al*., 2012b; Heman-Ackah *et al*., 2017). Notably, Bellucci and coworkers showed that the overexpression of human full-lenght and truncated αS both in cultured cells and in transgenic mouse models of PD resulted in

the accumulation of the protein within the ER and, as a consequence, in the activation of the protein kinase R (PKR)-like endoplasmic reticulum kinase (PERK)-related pathway of the UPR (Bellucci *et al*., 2011). Furthermore, treatment with salubrinal, which alleviates ER stress, was found to reduce the accumulation of oligomeric αS in the ER (Colla *et al*., 2012 a,b). Accordingly, ER stress and the activation of the UPR have been observed in the brain of human PD patients, together with a significant accumulation of ER chaperones in LBs (Conn *et al*., 2004). αS oligomeric aggregates have also been reported to bind and activate the ER/SR Ca^{2+}-ATPase (SERCA), inducing Ca^{2+} release in the cytosol and so contributing to its dyshomeostasis (Betzer *et al*., 2018). Furthermore, Cooper and coworkers found that the overexpression of both wild-type and A53T αS caused the impairment of ER-to-Golgi transport, that is the first step in the biosynthetic protein secretory pathway, thus inducing further ER stress (Cooper *et al*., 2006). Dopaminergic nigral neurons from PD patients are characterized by a significant fragmentation of the Golgi apparatus (Gosavi *et al*., 2002; Fujita *et al*., 2006; Lazaro *et al*., 2016). In a recent study, Paiva and coworkers found that the overexpression of both wild-type and A30P αS caused a marked alteration of Golgi morphology, and that this effect was more evident in A30P αS overexpressing dopaminergic neurons (Paiva *et al*., 2018). Importantly, in recent years a subdomain of the ER, called mitochondria-associated ER membrane (MAM), linked to mitochondria with specific adaptor proteins, emerged for its involvement in a range of functions, such as autophagosome biogenesis, mitochondrial fission, Ca^{2+} homeostasis, and lipid transfer (Philips *et al*., 2016). Calì and coworkers reported that αS overexpression in HeLa cells was responsible for the increase of the MAM contact sytes and resulted in a marked increase in mitochondrial Ca^{2+} uptake (Calì *et al*., 2012). Opposite, Guardia-Laguarta and collaborators reported that wild-type αS was present not in mitochondria, but rather in MAM fractions; remarkably, a significantly decreased number of MAM contact sites was observed upon the overexpression of both wild-type and mutated (A53T and A30P) αS (Guardia-Laguarta *et al*., 2015).

Autophagy and lysosomal pathway impairment

As already mentioned, the accumulation of aggregated αS is strongly associated with the impairment of ALP and represents a crucial pathogenic event in PD. Wislow and coworkers reported that αS overexpression significantly impaired macroautophagy both in mammalian non-neuronal cells and in transgenic mouse models, by inhibiting Rab1a

protein, a key early mediator of the process; as a consequence, this inhibition causes in turn the mislocalization of the autophagy protein Atg9, and the decrease in omegasome formation, an early step of autophagosome maturation (Wislow *et al*., 2010). In CMA, the mutated forms of αS A53T and A30P have been reported to bind to the lysosomal receptor LAMP2A, thus preventing their own degradation, and also that of other target proteins (Cuervo *et al*., 2004). Finally, several proteolitic lysosomal enzymes, such as cathepsin and β-galactosidase, responsible for many degradation processes, have been found to be inhibited in induced pluripotent stem cells harbouring the *SNCA* triplication (Mazzulli *et al*., 2011, 2016).

Nuclear function

Since its discovery in 1988, αS has been localized in the nuclear envelope (Maroteaux *et al*., 1998), but its occurrence here remains controversial (Huang *et al*., 2011; Wales *et al*., 2013). Accumulating evidence supports the presence of different αS assemblies in the nucleus of neuronal cells of PD patients, where they exert toxic effects. Ma and coworkers reported that the nuclear import of αS could be mediated by importin α and that αS amino acid residues 1–60 and 103–140 are essential for its nuclear import. Once in the nucleus, αS resulted to be neurotixic by accelerating the cell cycle (Ma *et al*., 2014). Furthermore, in a recent study, Rousseax and collaborators proposed a role for the nuclear scaffold protein TRIM28, normally implicated in several post-transcriptional functions, as mediator of the nuclear localization of αS, given their strong colocalizion in dopaminergic neurons of PD patients (Rousseaux *et al*., 2016). Once in the nucleus, αS has been reported to bind to histones, and to modulate their acetylation level (Goers *et al*., 2003; Kontopoulos *et al*., 2006). The nuclear localization of αS has been reported to increase in the presence of PD-associated mutations such as A30P, A53T and G51D, as compared to the wild-type protein (Kontopoulos *et al*., 2006; Fares *et al*., 2014). Many alterations have been observed in the activation of transcription factors, such as the inactivation of the peroxisome proliferator–activated receptor γ coactivator-1α (PGC-1α): many genes expressed under its control, involved in cellular bioenergetics, are not expressed in PD patients (Zheng *et al*., 2010). Researchers found that the expression of the PGC-1α is in turn downregulated, because of the binding of αS oligomers to its promoter observed in a transgenic A30P αS mouse model (Eschbach *et al*., 2015).

Plasma membrane perturbation

The manteinance of the plasma membrane integrity is foundamental for every cell type, for osmotic homeostasis and survival. Several studies reported that αS aggregates, particularly oligomers, have the ability to aberrantly interact with the cell membrane, thus inducing its perturbation, followed by the loss of cellular homeostasis and finally culminating in cell death (Reynolds *et al*., 2011; Winner *et al*., 2011; Kalia *et al*., 2013b). The first crucial step for membrane permeabilization is the recruitment of αS on its surface and their further binding, mediated by negatively charged lipids that establish electrostatic interactions with the positively charged core of the oligomers (Stöckl *et al*., 2012). This step is followed by the permeabilization of the plasma membrane, explained with different models: the membrane thinning, also called the "carpet-like" mechanism (Sokolov *et al*., 2006; Ouberai *et al*., 2013); the leakage evoked by the extraction of lipids, or "detergent-like" mechanism (Reynolds *et al*., 2011), and finally the permeabilization through pore formation, or "poration" mechanism (Zakharov *et al*., 2007; Tosatto *et al*., 2012). According to the membrane thinning model, αS oligomers are incorporated among the packed lipids of the plasma membrane, thus inducing the thinning of the hydrophobic core of the lipid bilayer. The extraction mechanism has been proposed by Reynolds and coworkers, that observed that, when monomeric wild-type and mutated A53T and E57K αS was added on the surface of supported lipid bilayers (SLBs), was firstly adsorbed to the membrane, and then started to aggregate, causing both membrane thinning and lipid extraction around the growing aggregates. Mature αS fibrils has been observed after 24 h from the application to SLBs; at this time, membrane integrity was completely loss (Reynolds *et al*., 2011). Finally, the membrane poration model assumes that annular αS oligomers with a central pore embed into lipid bilayers forming transbilayer proteins, thus allowing the passage of small molecules (Stöckl *et al*., 2013). After the disruption of the plasma membrane integrity, several toxic downstream effects have been observed, such as the dysregulation of cellular ionic homeostasis (especially that of Ca^{2+}), ROS production, alterations in signal transduction, and finally synaptic degeneration and apoptotic neuronal cell death (Demuro *et al*., 2005; Furukawa *et al*., 2006; Roberts *et al*., 2015; Angelova *et al*., 2016). Furthermore, it has been demonstrated that the ability of recombinant αS oligomers to damage cellular membranes *in vitro* correlate with the consistent dopaminergic neuronal loss observed *in vivo* in the brain of rats expressing the same αS variants (Winner *et al*., 2011; Snead and Eliezer, 2014).

Ca^{2+} dyshomeostasis

Ca^{2+} is an essential intracellular metal ion, whose homeostasis is crucial for neuronal function and survival. It is involved in the control and modulation of almost all neuronal processes, such as gene transcription, membrane excitability, neurotransmitter release and synaptic plasticity, learning and memory (Berridge, 1998; Brini *et al*., 2014). Ca^{2+} signalling depends both on its influx from the extracellular space and its release from the intracellular stores. Furthermore, as neurons are excitable cells, they are continuously exposed to large Ca^{2+} fluctuations and, as a consequence, to a major risk of Ca^{2+} overload and dyshomeostasis. For these reasons, neuronal cells possess sophisticated mechanisms to control the duration, the localization in specific subcellular microdomains, the diffusion of Ca^{2+} signals and the subsequent reduction of its free cytoplasmic concentration, in order to specifically activate different cellular processes and, finally, to re-establish its basal level during the recovery from stimulation (Thayer *et al*., 2002; La Rovere *et al*., 2016).

All these processes are mediated by many different transport proteins such as channels, exchangers and pumps, that move the ions across the membranes. Ca^{2+} influx from the plasma membrane is mediated by voltage-gated (or voltage-dependent, VOC), receptor-operated (ROC) and store-operated (SOC) channels. ROC Ca^{2+} channels are particularly abundant in excitable cells, they rapidly open upon the binding of an external specific ligand (usually a neurotransmitter). The ionotropic glutamate receptors α-amino-3-hydroxy-5-methyl-4-isoxazolepropionic acid (AMPARs) and N-methyl-D-aspartate ionotropic glutamatergic receptors (NMDARs) are part of this group; they mediate the fast excitatory neurotransmission and play a crucial role in brain development and synaptic plasticity (Cull-Candy *et al*., 2001). Notably, NMDARs have been found to be often implicated in cellular pathophysiology, because of their high Ca^{2+} permeability (Vyklicky *et al*., 2014).

Ca^{2+} extrusion from the cytosol to the extracellular space depends on the activity of the plasma membrane Ca^{2+} ATPase (PMCA) and the Na^{+}/Ca^{2+} exchanger (NCX) (**Figure 21**). Furthermore, its release from the sarco/endoplasmic reticulum (SR/ER) is given by the inositol 1,4,5-trisphosphate receptor (InsP3R) and the ryanodine receptor (RyR); opposite, the re-uptake is operated by the SERCA and the secretory pathway Ca^{2+}-ATPase (SPCA) of the Golgi apparatus. Mitochondria contribute to Ca^{2+} homeostasis: the influx of Ca^{2+} ions from the cytosol is mediated by the mitochondrial Ca^{2+} uniporter (MCU), and their efflux is operated by the Na^{+}/Ca^{2+} exchanger NCX. Ca^{2+} passage in

and out of these organelles is also mediated by the voltage-dependent anion channel 1 (VDAC1), located in the inner mitochondrial membrane. However, an excess of mitochondrial Ca^{2+} can lead to the opening of the mitochondrial permeability transition pore, and so to cytochrome *c* release, that activates apoptotic cell death (Bernardi *et al*., 2015). Importantly, several Ca^{2+}-binding proteins buffer Ca^{2+} levels in neuronal cytosol, thus contributing to its homeostasis, the most important of which is calmodulin (CaM). CaM is highly expressed in the brain (but present at low concentrations in dopaminergic neurons of the SN), where it contributes to the regulation of synaptic plasticity (Xia and Storm, 2005). Many other Ca^{2+}-binding proteins are present both in neuronal cytosol (such as calbindin-D28, calretinin and parvalbumin) and in the ER lumen (calreticulin and calnexin). Their expression levels are cell-specific; in this way, they contribute to the selective activation of various biological processes in different cell types, but also to the intrinsic susceptibility to cell death of the specific neuronal populations in neurodegenerative disorders (Catoni *et al*., 2019).

The deregulation of Ca^{2+} homeostasis in dopaminergic neurons of the SNpc has been associated to neurodegeneration in sporadic PD (Zündorf and Rieser, 2011). These neurons are autonomous pacemakers, periodically generating action potentials (spikes) in the absence of any external excitatory input (Grace and Bunney, 1983), and Ca^{2+} plays a foundamental role in the regulation of the shape, the duration, the intensity, and the firing patterns of these action potentials (Surmeier *et al*., 2007; Calì *et al*., 2014). As a consequence, dopaminergic neurons are subjected to slow but significant oscillations in intracellular Ca^{2+} concentration, driven by the opening of voltage-dependent L-type $Ca_v1.3$ Ca^{2+} channels at hyperpolarized membrane potentials (Nedergaard *et al*., 1983; Puopolo *et al*., 2007; Guzman *et al*., 2009) (**Figure 21**). These mechanisms are responsible for dopamine release to the connected brain areas, and, as a consequence, they represent the molecular basis of coordinated movement (Surmeier *et al*., 2007). Furthermore, Ca^{2+} entry through $Ca_v1.3$ channels leads to its transfer in mitochondria, where it stimulates oxidative phosphorylation and ATP producion (Balaban *et al*., 2009); however, an abnormal Ca^{2+} influx could compromise mitochondrial functionality, leading to metabolic stress (Surmeier *et al*., 2013). As previously reported, all these processes must be finely regulated; an aberrant Ca^{2+} entry through $Ca_v1.3$ channels is a key early event inducing neurodegeneration in PD. Accordingly, it has been observed that, in the brain of PD patients, their expression and that of some buffer proteins, such as calmodulin and calbindin-D28, is strongly upregulated in vulnerable neurons (Hurley *et al*., 2013).

Their relevance in the susceptibility of dopaminergic neurons has been also corroborated by many epidemiological studies on patients under clinical trials with L-type channel antagonists for the treatment of hypertension, that resulted to have a significantly diminished risk of developing PD (Chan *et al*., 2007). Furthermore isradipine, an inhibitor of the voltage gated L-type Ca^{2+} channels, resulted to be neuroprotective in a mouse model of PD (Ilijic *et al*., 2011) and this molecule is now under evaluation in a phase III clinical trial for its possible ability to slow the progression of PD in humans (Liss and Striessnig, 2019). Ca^{2+} influx was also reported to be inhibited by N-type channel blockers in rat synaptoneurosomes incubated with extracellular αS (Adamczyk and Strosznajder, 2006).

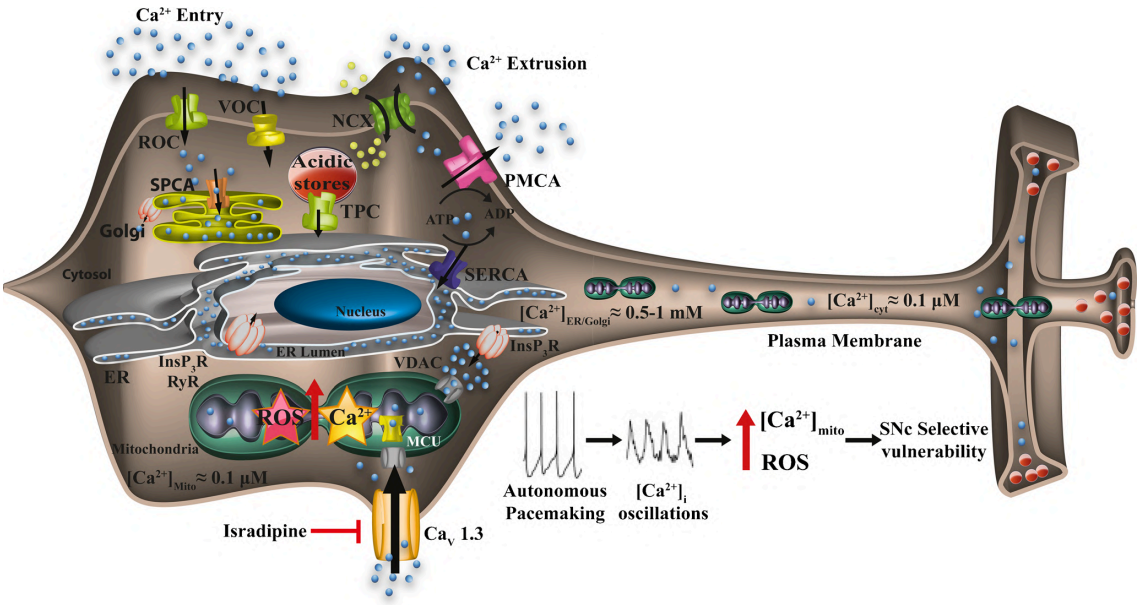

Figure 21 - The main Ca^{2+} transport systems in dopaminergic neurons. $Ca_V1.3$ L-type Ca^{2+} channels (efficiently blocked by isradipine) are strongly involved in the constitutive pacemaking activity of SNpc neurons. Their activity generates Ca^{2+} influx that requires the enhanced action of mitochondria for buffering its levels, thus exposing these organelles to increased oxidant stress by increased ROS production. The major Ca^{2+} transport proteins are also reported: the InsP3R, the RyR at the SR/ER membranes, the VOC and the ROC Ca^{2+} channels of the plasma membrane. Ca^{2+} extrusion is driven by the PMCA and the NCX on the plasma membrane. Its reuptake in the intracellular stores is given by the SERCA and the SPCA of the Golgi apparatus. The acidic compartments also act as Ca^{2+} stores, with the two pore channels (TPC) responsible for Ca^{2+} release (Calì *et al*., 2014).

The role of αS in Ca^{2+} dysregulation has been extensively investigated, given its ability to interact with lipid bilayers (Burré *et al*., 2010). Many studies demonstrated that αS aggregates, especially oligomers, are able to enhance plasma membrane permeability to Ca^{2+}, both by forming pore-like structures (Danzer *et al*., 2007; Surguchev and Surguchov, 2015; Angelova *et al*., 2016) and by interacting with several types of membrane channels, thus modulating their activity (Liu *et al*., 2013; Ronzitti *et al*., 2014). Moreover, an alteration in membrane conductance due to leak channel formation has been hypothesized (Feng *et al*., 2010), and it is substantially consistent with *in vitro* evidence demonstrating the formation of pore-like structures in synthetic membranes (Lashuel *et al*., 2002). Several observations have been performed after the addition of different αS species to the external medium of cultured cells. Angelova and coworkers reported that both monomeric and oligomeric αS is able to induce a massive influx of Ca^{2+} ions in neurons and astrocites, but only oligomers induce neuronal cell death (Angelova *et al*., 2016). Oligomeric assemblies have been reported to enhance plasma membrane permeability forming pore-like structures that fully perforate the plasma membrane, thus mediating an abnormal Ca^{2+} influx, with consequent toxicity (Tsigelny *et al*., 2012). It has been also demonstrated that A53T mutant and, to lesser extent, the A30P one, have a greater tendency to accumulate in plasma membranes with respect to the wild-type protein, thus inducing a much more consistent membrane permeabilization (Furukawa *et al*., 2006). Interestingly, extracellular added αS has been reported to increase the activity of the $Ca_v2.2$ channels, thus elevating cytoplasmic Ca^{2+} sufficiently to induce exocytotic dopamine release (Ronzitti *et al*., 2014). In this case, αS was not responsible for the upregulation of $Ca_v2.2$ expression, buth rather to the relocation of these channels, that move from lipid rafts to cholesterol-poor domains, thus inducing their abnormal activation. Adamczyk and Strosznajder observed that αS induced Ca^{2+} influx in rat synaptoneurosomes through N-type voltage-dependent Ca^{2+} channels, postulating the possibility of a protein-protein interaction (Adamczyk and Strosznajder, 2006). Furthermore, αS oligomers have been reported to alter the glutamatergic synaptic transmission in rat hippocampal slices, thus inducing the impairment of physiological stimuli. In particular, Diogenes and coworkers proposed a complex model in which αS oligomers are able to activate, directly or indirectly, the NMDARs. This has been associated with a significant increase in the intracellular Ca^{2+} ions that, once in the cytosol, bind to CaM; the Ca^{2+}/CaM complex is responsible for the activation of the Ca^{2+}/CaM-dependent protein kinase II (CaMKII), that in turn phosphorylates the GluR1

subunits of the AMPARs, so promoting the insertion into the postsynaptic membrane of higher conductance Ca^{2+}-permeable versus GluR2-containing AMPARs, involved in basal synaptic transmission, and thus leading to impaired long-term potentiation (Diógenes *et al*., 2012). Such impairment was also observed by Martin and collaborators, that reported that oligomeric αS, rather than monomeric or fibrillar assemblies was able to induce a massive influx of Ca^{2+} ions, responsible for the activation of the Ca^{2+}/CaM-activated serine/threonine phosphatase calcineurin, that dephosphorylates key signal transduction molecules essential for synaptic plasticity, learning and memory (Martin *et al*., 2012). More recently, Ferreira and coworkers proposed a complex mechanism for explaining the αS oligomers-induced impairment of long term potentiation (LTP): extracellular αS oligomers were reported to interact with PrP^C, thus leading to the activation of the metabotropic glutamate receptor 5 (mGluR5), a G-coupled receptor particularly abundant at postsynaptic terminals. This leads to the phosphorylation and activation of the Src kinase Fyn, that is soon followed by the phosphorylation of NMDARs, evoking a massive increase of intracellular Ca^{2+} levels, ultimately triggering synaptic dysfunction in hippocampal neurons (Ferreira *et al*., 2017).

αS oligomers were also reported to lead to Ca^{2+} dyshomeostasis upon their intracellular accumulation; once in the cytoplasm, they bind to SERCA and stimulate its activity, so triggering an initial reduction of cytosolic Ca^{2+} concentration and an overload in the ER. This phase is thought to be characterized by a significant imbalance of Ca^{2+}-dependent processes that is responsible for cellular dysfunction, and it is followed by a later increase in cytosolic Ca^{2+} levels, that precedes cell death (Betzer *et al*., 2018).

1.4 Aim of the study

The aggregation of αS, an intrinsically disordered protein involved in neurotransmitter release at presynaptic terminals, is associated with the onset and progression of PD and other debilitating neurodegenerative conditions. Intraneuronal inclusion bodies, called LBs and LNs, primarily composed of αS fibrils, are the main histopathological hallmarks of these diseases, although there is increasing evidence that small oligomeric assemblies, formed during the early phases of αS aggregation, or released from mature fibrils, play a crucial role in neuronal impairment. The cytotoxicity of these small aggregates seems to result from their ability to aberrantly interact with the plasma membrane of neuronal cells,

thus disrupting its integrity and causing the impairment of fundamental cellular pathways. However, the precise molecular mechanisms by which these species affect cellular functions remain largely unknown. Overcoming these knowledge gaps would be extremely important for clarifying the molecular basis of neurodegeneration in PD and to find new potential therapeutic strategies.

The aim of this project was to investigate the mechanisms of cell damage induced by an array of highly stable and defined αS species, differing each other in size and architecture, and including the monomeric form of the protein (M), together with four aggregated forms produced *in vitro*: type A* and type B* oligomers (OA* and OB*), short and long fibrils (SF and LF), whose structural and biophysical characterization has been recently performed by the research group headed by Professor Christopher Dobson at the University of Cambridge. These aggregates have a significant pathological relevance, given their structural similarity to those isolated from the brain of PD patients. In particular, we have investigated the relationship between structure and toxicity of these different αS species using a number of cellular readouts, in both primary rat cortical neurons and human SH-SY5Y neuroblastoma cells, following the evolution in time of the observed toxic effects. We have evaluated the ability of αS assemblies to interact with the plasma membrane and the involvement of specific membrane components in the binding of the various αS species; we then focused on their capacity to perturb the membrane integrity, to induce ROS production and Ca^{2+} dyshomeostasis. Furthermore, we verified the degree of internalization of the various αS aggregates into the cytosol of neuronal cells and their capacity to induce mitochondrial dysfunction and to impair cell viability. As Ca^{2+} dyshomeostasis is considered to be a crucial early event in PD pathogenesis, we subsequently focused on the study of such dysregulation evoked by αS species, analysing the mechanism of Ca^{2+} entry through the plasma membrane and investigating the possible involvement of membrane proteins, such as voltage-gated channels, the glutamate receptors-channels AMPARs and NMDARs, and PrP^{C}, that may play a role as mediators of Ca^{2+} dysregulation. Evidences accumulated from the analysis of this range of cellular readouts clearly indicate that the OB* are the most deleterious species, causing cellular dysfunction with fast kinetics; furthermore, fibrillar assemblies resulted to have a slight immediate toxic effect, thus we investigated the molecular basis of their toxicity, evaluating their ability to slowly release small toxic oligomeric assemblies upon their binding to the cellular membranes.

Taken together, our results strongly contribute to the definition of the cellular mechanisms of αS neurotoxicity, and expand the possible targets for the design of therapeutic agents for intervention in PD.

2 MATERIALS AND METHODS

2.1 Purification of αS monomers and formation of αS type A* and type B* oligomers, short and long fibrils

The purification of recombinant αS and the formation of the various aggregated species have been performed by the research group headed by Professor Christopher Dobson in Cambridge.

The recombinant human αS was over-expressed in *E.coli* BL21 cells (Agilent, Yarnton, OXF, UK) and purified as a monomeric fraction. To prepare type A* oligomers (OA*), the monomeric αS was incubated at 37°C for 48 h at a concentration of 3 mg/ml with 10 molar equivalents of epigallocatechin gallate (EGCG) in PBS buffer at pH 7.4 (Enrnhoefer *et al*., 2008; Fusco *et al*., 2017). αS samples were further purified with a run of size exclusion chromatography prior incubation with EGCG. After incubation and before performing any type of analysis, monomers of αS were removed with multiple filtration steps using 100 kDa cutoff membranes. Analytical ultracentrifugation analyses of OA* indicated a molecular mass of approximately 340 kDa on average (corresponding to an average of approximately 24 protein molecules).

αS Type B* oligomers (OB*) were prepared by resuspending 6 mg of the lyophilized monomeric protein in PBS buffer at pH 7.4 to yield a final concentration of ca. 800 μM (12mg/ml) and passed through a 0.22 μm cutoff filter (Millipore, Feltham, LDN, UK) before performing an incubation at 37 °C for 20-24 h under quiescent conditions to avoid acceleration of fibrils formation (Chen *et al*., 2015). In order to remove fibrillar species possibly formed despite such precautions, samples were subjected to ultracentrifugation for 60 min at 90,000 rpm (using a TLA-120.2 Beckman rotor; 288,000*g*). The excess of monomeric protein and the small oligomers were removed by means of multiple filtration steps, using 100kDa cut off membranes. The concentrations of the final solutions of oligomers were estimated from the absorbance at 275 nm by using a molar extinction coefficient of 5600 M^{-1} cm^{-1}, as previously reported (Chen *et al*., 2015). The oligomeric samples were found to be stable for days and were used in the first two days after the production.

Long fibrillar samples (also referred to as f0) were prepared by incubating monomeric αS at 70 μM (1 mg/ml) in PBS buffer pH 7.4 (0.1 M ionic strength) containing 0.01% NaN_3

at 37 °C, under constant agitation (New Brunswick Scientific Innova 43; Eppendorf AG, Hamburg, Germany; 200 rpm) for 4-6 days. After this time, each sample was centrifuged (15 min at 16100*g*) and the fibrillar pellet washed twice with PBS before being resuspended into the appropriate volume of PBS. As clumping of fibrils was observed, a second generation of long f1 fibrils (LF) was prepared by incubating 100 µM monomeric (M) αS with 10 µM of f0 sonicated for 1 min (cycles of 0.3 s of active sonication followed by 0.7 s of passive interval) with Sonopuls HD 2070 (Bandelin, Berlin, Germany), in 500 µl PBS at 37 °C under quiescent conditions for 13-15 h and then centrifuged as described above for the generation of f0. Samples of short f1 fibrils (SF) were generated by sonicating long f1 fibrils for 20 s using the same apparatus and settings. The concentration of fibrils was estimated by measuring the absorbance at 275 nm using $\varepsilon_{275} = 5600\ M^{-1}\ cm^{-1}$ after disaggregating an aliquot by the addition of guanidinium chloride to a final concentration of 4 M. N-terminal acetylation of WT αS was performed as previously reported (Fusco *et al*., 2017). Briefly, a plasmid carrying the components of the NatB complex (Addgene, Watertown, MA, USA) was co-expressed with the pT7-7 plasmid encoding for the αS described above, following the protocol described by Johnson and coworkers (Johnson *et al*., 2010).

2.2 Biophysical analyses of the various αS species

2.2.1 AFM

All images were acquired at room temperature in air typically using intermittent contact mode on a Nanowizard II atomic force microscope (JPK instruments, Berlin, Germany) except for the analysis of OA* and OB* samples, which were acquired using tapping mode in a Multimode 8 atomic force microscope (Bruker, Massachusetts, USA). The different αS species (0.1-1 µM, 10 µl) were applied onto a layer of freshly cleaved mica and allowed to air-dry. The samples were washed with water to remove any salts and dried again before imaging. Images were processed with Gwyddion open source software (http://www.gwyddion.net).

2.2.2 Far-UV circular dichroism (CD)

Far-UV circular dichroism (CD) spectra of the different αS species were acquired in PBS at 20 °C between 200 nm and 250 nm, using a scan speed of 50 nm min^{-1} and a bandwidth of 1 nm. 10 accumulations were recorded for each sample, using a 1 mm path length cuvette and a J-810 spectropolarimeter (Jasco, Tokyo, Japan), equipped with a thermostated cell holder.

2.2.3 Fourier Transform - Infrared Spectroscopy (FT-IR)

FT-IR spectra of the different αS species (100-400 μM) were acquired in PBS and analysed in a Bruker BioATRCell II using a Bruker Equinox 55 FT-IR spectrophotometer (Bruker Optics Limited, UK) equipped with a liquid nitrogen cooled mercury cadmium telluride (MCT) detector and a silicon internal reflection element (IRE). For each spectrum, 256 interferograms were recorded at 2 cm^{-1} resolution. Data processing of the amide I region (1720-1580 cm^{-1}) was performed with the Opus software package (Bruker Optics Limited, UK) and consisted of a background subtraction of the buffer spectra, atmospheric compensation and baseline subtraction. All absorbance spectra were normalized for comparison.

2.2.4 X-ray diffraction

Protein stalks were prepared by air drying 10 μL of ~800 μM of the different αS species between two wax-filled capillary ends mounted in a Petri dish, as described previously (Morris *et al*., 2012). X-rays were generated using MICROSTAR microfocus rotating anode X-ray generator and the diffraction data was collected on a X8 Proteum system (Bruker AXS). The data was subsequently analysed on PROTEUM 2 software suite.

2.2.5 Thioflavin T (ThT) and ANS fluorescence

Fluorescence measurements were performed in a 2 x 10 mm path length cuvette, using a Varian Cary Eclipse fluorimeter (Palo Alto, CA, USA) in a temperature-controlled cell holder. ThT fluorescence was monitored by exciting the sample at 446 nm and recording the emission fluorescence spectrum between 460 to 600 nm (5nm slitwidths). Each

protein species (10 μM) was incubated with ThT (50 μM, ε_{416nm} = 26620 M^{-1} cm^{-1}) in PBS for 30 min before performing the measurement. The degree of hydrophobicity of the oligomers was evaluated using the fluorescent dye 8-anilino-1-naphthalenesulfonate (ANS), which binds to hydrophobic patches on the surfaces of solvent-exposed protein aggregates. Such binding was monitored by exciting the sample at 350 nm and recording the emission spectrum between 400 to 650 nm (5nm slitwidths). Each protein species (5 μM) was incubated with ANS (250 μM, ε_{350nm} = 5000 M^{-1} cm^{-1}) in PBS for 30 min before recording the spectra.

2.3 Dot-blot analysis

Dot-blot analysis of αS species were performed by spotting 2.0 μl (0.36 mg/ml) of each conformer onto a 0.2 μm nitrocellulose membrane. After blocking (1.0% bovine serum albumin in TBS/TWEEN 0.1%) the blots were probed with 1:1200 diluted rabbit anti-oligomer (A11) polyclonal antibodies (AHB0052, Thermo Fisher Scientific, Waltham, MA, USA), or with 1:1000 rabbit anti-amyloid fibrils (OC) polyclonal antibodies (AB2286, Sigma-Aldrich, St. Louis, MO, USA) or with 1:250 diluted mouse anti-αS monoclonal antibodies (sc12767, Santa Cruz Biotechnology, CA, USA). Then, the blots were incubated with 1:3000 diluted HRP-conjugated anti-rabbit or anti-mouse secondary antibodies (AB6721 and AB6728, Abcam, Cambridge, UK). The immunolabelled dots were detected using a SuperSignalWest Dura (Pierce, Rockford, IL, USA) and ImageQuant™ TL software (GE Healthcare UK Limited).

2.4 Cell culture and analyses

2.4.1 Cell culture

Authenticated human neuroblastoma SH-SY5Y cells were purchased from A.T.C.C. (Manassas, VA, USA) and cultured in Dulbecco's Modified Eagle's Medium (DMEM), F-12 Ham with 25mM 4-(2-Hydroxyethyl)piperazine-1-ethanesulfonic acid (HEPES) and $NaHCO_3$ (1:1) supplemented with 10% fetal bovine serum (FBS), 1.0mM glutamine and 1.0% penicillin and streptomycin solution. Cells were maintained in a 5.0% CO_2 humidified atmosphere at 37° C and grown until 80% confluence for a maximum of 20

passages and tested to ensure that they were free form mycoplasma contamination. Primary rat cortical neurons were purchased from Thermo Fisher Scientific, plated and maintained in neuronal basal plus medium (Gibco, Thermo Fisher Scientific) supplemented with GlutaMAX (Gibco) at the concentration of 0.5 mM and 2% (v/v) and a serum-free complement, B-27 (Gibco). Cells were maintained at 37 °C in a 5.0% CO_2 humidified atmosphere. Every 4 days, medium was partially replaced with fresh one. All the experiments were performed 12-16 days after plating, as previously reported (Cascella *et al*., 2017).

2.4.2 Measurement of intracellular ROS

αS species were added to the cell culture medium of SH-SY5Y cells seeded on glass coverslips for 15 min at increasing concentrations (0.03, 0.1, 0.3, 1.0 and 3.0 μM, monomer equivalents). In another set of experiments, 0.3 μM OB* were added to the cell culture medium for different lengths of time (0, 5, 10, 15, 30 and 60 min). After treatment, cells were loaded with 5 μM 2′,7′-dichlorodihydrofluorescein diacetate for 10 min (CM-H_2DCFDA, Thermo Fisher Scientific), to detect and quantify intracellular levels of hydrogen peroxide as a ROS marker. This dye can passively diffuse into cells, where intracellular esterases cleave its acetate groups and then its thiol-reactive chloromethyl group reacts with intracellular glutathione and other thiols. Subsequent oxidation yields a fluorescent adduct that is trapped inside the cells. Cells were then fixed in 2.0% (v/v) buffered paraformaldehyde for 10 min at room temperature and the fluorescence was then detected after excitation at 488 nm by a TCS SP5 scanning confocal microscopy system (Leica Microsystems, Mannheim, Germany) equipped with an argon laser source. A series of 1.0 μm thick optical sections (1024 × 1024 pixels) was taken through the cell depth for each sample using a Leica Plan Apo 63× oil immersion objective and projected as a single composite image by superimposition. The confocal microscope was set at optimal acquisition conditions, e.g., pinhole diameters, detector gain and laser powers. Settings were maintained constant for each analysis.

2.4.3 Measurement of intracellular Ca^{2+}

In all the experiments described in this work, the intracellular Ca^{2+} levels were measured by using the fluorescent probe Fluo-4 AM (Thermo Fisher Scientific). This dye, thanks to the presence of the acetoxymethyl (AM) ester group is able to cross the plasma membrane; once inside the cells, esterases cleave the acetyl groups, thus allowing the release of the indicator molecules. Fluo-4 AM fluorescence increases upon binding to Ca^{2+} ions. In a set of experiments, αS species were added to the culture medium of SH-SY5Y cells seeded on glass coverslips for 15 min at various concentrations (0.03, 0.1, 0.3, 1.0 and 3.0 μM, monomer equivalents); cells were also treated with 0.3 μM OB* in medium without Ca^{2+}. In another set of experiments, 0.3 μM (monomer equivalents) OB*, SF and LF were added to the cell culture medium of SH-SY5Y cells for 0, 5, 10, 15, 30, 60 and 180 min and to that of primary rat cortical neurons for 0, 5, 15, 60 and 180 min. In another set of experiments, SH-SY5Y cells were pre-treated with 0.05% trypsin on ice for 10 min and then treated with OB*, SF and LF at 0.3 μM (monomer equivalents) for 0, 5, 10, 15, 30, 60, 120 and 180 min. Cells were also pre-treated for 60 min with 5 μM 6-cyano-7-nitroquinoxaline-2,3-dione (CNQX), a competitive antagonist of AMPARs or with 10 μM memantine (mem), a low-affinity antagonist of NMDARs, or with 10 μM cadmium (Cd^{2+}) ions (Sigma-Aldrich), competitive blockers of VOC Ca^{2+} channels, and then treated with 0.3 μM (monomer equivalents) OB* for 15 min. In another set of experiments, SH-SY5Y cells were pre-treated with 10 μM mem for 60 min, and then treated with OB*, SF and LF (0.3 μM, monomer equivalents) for different lengths of time (0, 5, 10, 15, 30, 60 and 180 min). In another set of experiments, SH-SY5Y cells were treated with increasing concentrations of mem (0.1 μM, 0.5 μM, 1.0 μM, 5.0 μM, 10 μM and 50 μM) for 60 min, and then treated with OB* and SF for 15 min at 0.3 μM (monomer equivalents). Finally, SH-SY5Y cells were pre-treated with 1:250 diluted mouse anti-PrP^C monoclonal antibodies (sc-47730, Santa Cruz Biotechnology) for 30 min, and then treated with OB* (0.3 μM, monomer equivalents) for different lengths of time (0, 5, 10, 15, 30, 60 and 180 min). The cells were then loaded with 10 μM fluo-4 AM and the cytosolic Ca^{2+} levels were measured by the scanning confocal fluorescence microscopy system previously described, after excitation at 488 nm. The fluorescence intensities were expressed as the percentage of that measured in untreated cells.

2.4.4 Alteration of membrane permeability by the different αS species

The disruption of the plasma membrane integrity was evaluated by using the fluorescent dye calcein-AM (Thermo Fisher Scientific), a cell-permeant probe that can be converted to a green-fluorescent calcein after acetoxymethyl ester hydrolysis by intracellular esterases. Briefly, when cultured cells are incubated with the acetoxymethyl (AM) ester of calcein, the neutral ester crosses the plasma membrane. Once internalized, cytosolic esterases hydrolyze calcein-AM to the free acid form whose carboxyl groups trap and retain the fluorophore inside the cytosolic compartment. A decrease in green fluorescence intensity indicates calcein release, thus providing an evidence of plasma membrane damage. The membrane integrity disruption was assessed in SH-SY5Y cells and primary rat cortical neurons seeded on glass coverslips, loaded with 1.0 μM calcein-AM for 30 min at 37 °C and then treated for 60 min with the different αS species at 0.3 μM (monomer equivalents). In another set of experiments, OB* were added to the culture medium of SH-SY5Y cells at 0.3 μM (monomer equivalents) for different lengths of time (0, 5, 10, 15, 30 and 60 min). The membrane integrity disruption was also assessed in SH-SY5Y cells treated for 60 min with N-acetylated αS species (M, OA* and OB*) at 0.3 μM (monomer equivalents). In another set of experiments, cells were pre-treated with 0.05% trypsin on ice for 10 min and then treated with OB*, SF and LF at 0.3 μM (monomer equivalents) for 60 min. Cells were then fixed as previously reported and the emitted fluorescence was detected after excitation at 488 nm by the confocal scanning system previously described. The fluorescence intensities were expressed as the percentage of that measured in untreated cells.

2.4.5 Imaging and quantification of αS species bound to the plasma membrane

SH-SY5Y cells seeded on glass coverslips were treated with αS species (OB*, SF and LF) at 0.3 μM (monomer equivalents) for 10 min, or pre-treated with 0.05% trypsin on ice for 10 min, and after washing twice with PBS treated with the αS assemblies at the same concentration. In another set of experiments, cells were pre-treated for 48h with 25 μM D-threo-1-phenyl-2-decanoylamino-3-morpholino-1-propanol (PDMP, Sigma-Aldrich), or with 1:250 diluted mouse anti-PrP^C monoclonal antibodies (sc47730, Santa Cruz Biotechnology) for 30 min, and then treated with αS aggregates at 0,3 μM (monomer

equivalents) for 10 minutes. After incubation, the cells were washed with PBS, counterstained with 5.0 μg/ml Alexa Fluor 633-conjugated wheat germ agglutinin (W21404, Thermo Fisher Scientific) for 15 min at 37 °C, and then fixed with 2.0% (v/v) paraformaldehyde for 10 min at room temperature. To detect only the species bound to the cell surface, the cellular membrane was not permeabilized, thus preventing antibody internalization. After washing twice with PBS, the presence of αS species bound to cellular membranes was detected by incubating the cells with 1:250 diluted rabbit polyclonal anti-αS antibodies (ab52168, Abcam) for 60 min at 37° C, and subsequently with 1:1000 diluted Alexa Fluor 488-conjugated anti-rabbit secondary antibodies (A-11034, Thermo Fisher Scientific) for 60 min at 37° C. Fluorescence emission was detected after double excitation at 488 nm and 633 nm by the TCS SP8 scanning confocal microscopy system previously described, equipped with an argon laser source, using a Leica Plan Apo 63× oil immersion objective. Three apical sections were projected as a single composite image by superimposition. The colocalization of αS species and cell membranes was estimated for regions of interest in 30-32 cells, and the Pearson's value was calculated via the use of ImageJ (NIH, Bethesda, MD, USA) and JACOP plugin (http://rsb.info.nih.gov) software (Rasband WR).

2.4.6 Analysis of αS species colocalizing with GM1

SH-SY5Y cells seeded on glass coverslips were treated with OB*, SF and LF for 10 min at 0.3 μM (monomer equivalents). Cells were washed with PBS and the monosialoganglioside GM1 was then counterstained with 4.5 μg/ml Alexa Fluor 647-conjugated CTX-B (C34778, Thermo Fisher Scientific); cells were then fixed with 2.0% (v/v) buffered paraformaldehyde for 10 min at room temperature, then the aggregates were detected by treating cells with 1:250 diluted rabbit polyclonal anti-αS antibodies (ab52168, Abcam) for 60 min at 37° C, and finally with 1:1000 diluted Alexa Fluor 488-conjugated anti-rabbit secondary antibodies (A-11034, Thermo Fisher Scientific) for 60 min at 37° C. Fluorescence emission was detected after double excitation at 647 nm and 488 nm by the TCS SP8 scanning confocal microscopy system previously described. The colocalization of αS species with GM1 was then estimated for regions of interest in 30–32 cells, and the Pearson's correlation coefficient was calculated via the use of ImageJ

(NIH, Bethesda, MD, USA) and JACOP plugin (http://rsb.info.nih.gov) software (Rasband WR).

2.4.7 Analysis of αS species colocalizing with different membrane proteins

SH-SY5Y cells and primary rat cortical neurons seeded on glass coverslips were treated for 10 min with αS species at 0.3 μM (monomer equivalents). After fixation in 2.0% (v/v) buffered paraformaldehyde, cells were incubated with 1:250 diluted rabbit anti-αS polyclonal antibodies (ab52168, Abcam), together with 1:250 diluted mouse anti-PrP^C monoclonal antibodies (sc47730, Santa Cruz Biotechnology) or 1:800 diluted mouse anti-NMDARs monoclonal antibodies (320700, Thermo Fisher Scientific) for 60 min at 37 °C, and then with 1:1000 diluted Alexa Fluor 488- and 633- conjugated anti-rabbit and anti-mouse secondary antibodies (A-11034 and A-21052, Thermo Fisher Scientific) for 60 min at 37 °C. Fluorescence emission was detected after double excitation at 488 and 633 nm by confocal microscopy as described above. The colocalization of αS species with PrP^C and NMDARs was estimated for regions of interest in 30–32 cells, and the Pearson's correlation coefficient was calculated via the use of ImageJ (NIH, Bethesda, MD, USA) and JACOP plugin (http://rsb.info.nih.gov) software (Rasband WR).

2.4.8 Confocal microscopy analysis for the internalization of αS species

αS species were added to the culture medium of SH-SY5Y cells seeded on glass coverslips typically for 60 min at 0.3 μM (monomer equivalents). In a set of experiments, OB* and SF were added to the culture medium of SH-SY5Y cells seeded on glass coverslips for 60 min at increasing concentrations (0.03 μM, 0.1 μM, 0.3 μM, 1.0 μM, and 3.0 μM). After incubation, the cells were washed with PBS, counterstained with 5.0 μg/ml Alexa Fluor 633-conjugated wheat germ agglutinin (W21404, Thermo Fisher Scientific) for 15 min at 37 °C and fixed with 2.0% (v/v) buffered paraformaldehyde. The plasma membrane was then permeabilized with a 3.0% (v/v) glycerol solution for 7 min and αS was then detected by treating cells with 1:250 diluted rabbit anti-αS polyclonal antibodies (ab52168, Abcam) for 60 min at 37° C and then with 1:1000 diluted Alexa-Fluor-488-conjugated anti-rabbit secondary antibodies (A-11034, Thermo Fisher

Scientific) for 60 min at 37° C. In a set of experiments, OB*, SF and LF were added to the cell culture medium at 0.3 μM (monomer equivalents) for 30 min, and then polyclonal A11 (AHB0052, Thermo Fisher Scientific) or OC (AB2286, Sigma-Aldrich) conformation-sensitive antibodies were added for 24 h to the extracellular medium (in a molar ratio of 1:2.5). The cells were then counterstained with 5.0 μg/ml Alexa Fluor 633-conjugated wheat germ agglutinin (W21404, Thermo Fisher Scientific), fixed and permeabilized as previously reported and then αS was detected by treating cells with 1:250 diluted rabbit anti-αS polyclonal antibodies (ab52168, Abcam) for 60 min at 37° C and then with 1:1000 diluted Alexa-Fluor-488-conjugated anti-rabbit secondary antibodies (A-11034 Thermo Fisher Scientific) for 60 min at 37° C. In another set of experiments, OB*, SF and LF at 0.3 μM (monomer equivalents) were added to the cell culture medium of SH-SY5Y cells seeded on glass coverslips for different lengths of time (0, 3, 6, 14 and 24 h). The cells were then counterstained with 5.0 μg/ml Alexa Fluor 633-conjugated wheat germ agglutinin (W21404, Thermo Fisher Scientific), fixed and permeabilized as previously reported and then αS was detected by treating cells with with 1:250 diluted rabbit anti-oligomer (A11) polyclonal antibodies (AHB0052, Thermo Fisher Scientific) for 60 min at 37° C, and then with 1:1000 diluted Alexa-Fluor-488-conjugated anti-rabbit secondary antibodies (A-11034 Thermo Fisher Scientific) for 60 min at 37° C. In another set of experiments, cells were pre-treated with 0.05% trypsin on ice and, after washing twice with PBS, treated for 60 min with OB*, SF and LF at 0.3 μM (monomer equivalents). The cells were then counterstained with 5.0 μg/ml Alexa Fluor 633-conjugated wheat germ agglutinin (W21404, Thermo Fisher Scientific), fixed and permeabilized as previously reported and αS was then detected with 1:250 diluted rabbit anti-αS polyclonal antibodies (ab52168, Abcam) and with 1:1000 diluted Alexa-Fluor-488-conjugated anti-rabbit secondary antibodies (A-11034, Thermo Fisher Scientific), as reported previously. Fluorescence emission was detected after double excitation at 633 nm and 488 nm by the scanning confocal microscopy system described above.

2.4.9 Analysis of the mitochondrial status with the MTT reduction inhibition assay

The ability of the different αS species to impair cell metabolic activity was assessed on SH-SY5Y cells and primary rat cortical neurons seeded in 96-well plates, 24 h after their

addition to the cell culture medium at 0.3 μM (monomer equivalents), by the 3-(4,5-dimethylthiazol-2-yl)-2,5-diphenyltetrazolium bromide (MTT) assay. SH-SY5Y cells were also treated for 24 h with αS species (M, OA* and OB*) derived from the N-acetylated αS protein at 0.3 μM (monomer equivalents). In a set of experiments, αS species were added to the culture medium of SH-SY5Y cells at 0.3 μM (monomer equivalents) for different lengths of time (0, 1, 3, 5 and 24 h) and the MTT assay was then assessed. In another set of experiments, OB*, SF and LF at 0.3 μM (monomer equivalents) were added to the culture medium of SH-SY5Y cells and, following 30 min of treatment, polyclonal A11 (AHB0052, Thermo Fisher Scientific) or OC (AB2286, Sigma-Aldrich) conformation-sensitive antibodies were added for 24 h to the extracellular medium (in a molar ratio of 1:2.5), and the MTT assay was then performed. The effect of A11 and OC antibodies alone were also analysed as a negative control. In another set of experiments, SH-SY5Y cells were pre-treated for 30 min with 1:250 diluted mouse anti-PrP^C monoclonal antibodies (sc47730, Santa Cruz Biotechnology), and then treated with OB* at 0,3 μM (monomer equivalents) for 24 h. The effect of anti-PrP^C antibodies alone was also tested as a control. After all the different treatments, the cell culture medium was removed, cells were washed with PBS and the MTT solution (0.5 mg/ml in RPMI) was added to the cells for 4 h. The medium was then aspirated, and the formazan product was solubilized with cell lysis buffer (20% sodium dodecyl sulfate (SDS), 50% N, N-dimethylformamide, pH 4.7) for 1 h. The absorbance values of blue formazan were determined at 590 nm. Cell viability was expressed as the percentage of MTT reduction in treated cells as compared to untreated cells.

2.4.10 Measurement of caspase-3 activity

The extent of the activation of the apoptotic process in SH-SY5Y cells was evaluated by confocal microscopy analysis of caspase-3 activity. αS species were added to the culture medium of SH-SY5Y cells seeded on glass coverslips for 24 h at 0.3 μM (monomer equivalents). In another set of experiments, αS species were added to the cell culture medium for different lengths of time (0, 1, 3, 5 and 24 h) at 0.3 μM (monomer equivalents). After treatment, the cell culture medium was removed and replaced with the FAMFLICA™ caspases 3&7 solution (caspase 3&7 FLICA kit FAM-DEVDFMK, Immunochemistry Technologies, LLC, Bloomington, MN) for 60 min and the emitted

fluorescence was detected after excitation at 488 nm by the confocal scanning system previously described. The fluorescence intensities were expressed as the percentage of that measured in untreated cells.

2.4.11 Hoechst staining

The activation of the apoptotic pathway was also investigated by Hoechst 33342 dye staining (62249, Thermo Fisher Scientific). Hoechst dye is a cell-permeant nuclear counterstain emitting blue fluorescence when bound to double-stranded DNA. This dye is used to identify the presence of condensed pycnotic nuclei in apoptotic cells. SH-SY5Y cells seeded on glass coverslips were treated for 24 h with αS species at 0.3 μM (monomer equivalents), and then incubated with 20 μg/ml Hoechst 33342 dye for 15 min at 37 °C and fixed with 2% (v/v) buffered paraformaldehyde. Blue fluorescence was detected after excitation at 405 nm by the TCS SP8 scanning confocal microscopy system equipped with a diode laser source.

2.4.12 Analysis of the kinetics of toxicity using the different cellular readouts

The different intracellular fluorescence intensities associated with ROS levels, Ca^{2+} influx, calcein leakage, αS internalization, caspase-3 activation and MTT reduction were plotted *versus* the time elapsed after αS addition to the cell culture medium and the resulting kinetic plots were analysed with a procedure of best fitting using a single exponential function of the form:

$$F(t) = F(eq) + A \exp(-k\,t) \quad (1)$$

where *F(t)* is the intracellular fluorescence at time t as a percentage of that observed in untreated cells, *F(eq)* is the same fluorescence at the apparent equilibrium (time ∞), *A* is the amplitude of the exponential fluorescence change as a percentage of that observed in untreated cells, and *k* is the apparent rate constant in s^{-1}.

The intracellular fluorescence intensities associated with Ca^{2+} influx evoked by SF and LF in SH-SY5Y cells, or induced by OB* after a pre-treatment with 0.05% trypsin, with

10 μM mem, with increasing concentration of mem, or with the anti-PrP^C antibodies, as well as the internalization of αS species recognized by the A11 antibodies, were plotted *versus* the time elapsed after αS addition to the cell medium and the resulting kinetic plots were analysed with a procedure of best fitting using a sigmoidal function of the form

$$F(t) = F(eq) + \frac{F(0) - F(eq)}{1 + (\frac{kt}{A})^B} \quad (2)$$

where *F(t)* is the intracellular fluorescence at time t as a percentage of that observed in untreated cells, *F(0)* is the same fluorescence at time zero, *F(eq)* is the same fluorescence at the apparent equilibrium (time ∞), *A* is the amplitude of the fluorescence change as a percentage of that observed in untreated cells, *k* is the apparent rate constant in s^{-1} and B is the slope of the sigmoidal function at time *t*.

2.4.13 Statistical analysis

Statistical analysis was performed with GraphPad Prism 5.0 (GraphPad Software Inc., La Jolla, CA, USA). All data were expressed as means ± standard error of mean (S.E.M). Comparisons between the different groups were performed by a one-way analysis of variance (ANOVA) followed by Bonferroni's post comparison test. *P*-values lower than 0.05, 0.01 and 0.001 were considered to be statistically significant, very significant and extremely significant, respectively.

3 RESULTS

Section I

In the first part of this work, we focused on the comparative analysis of a range of highly stable and well-defined αS assemblies, including the monomer (M), two forms of oligomers (OA* and OB*), and two different fibrillar species, called short (SF) and long fibrils (LF). We monitored the evolution in time of the more relevant toxic effects exerted by these different species on human neuroblastoma cells and primary rat cortical neurons, using a range of different readouts of cellular dysfunction.

We have found that, at early incubation times with the cells, oligomeric species with a partial cross-β structure and a high solvent-exposed hydrophobicity, here referred to as OB*, are the most toxic species to neuronal cells, whereas the monomeric protein and hydrophilic and disordered oligomers, called OA*, were unable to cause any alteration in cellular functionality. We have also observed that αS fibrils can induce the same cytotoxicity as OB*, but only after prolonged incubation times with the cells, and at a rate dependent on their length. Thus, we hypothesized that the late toxic effects of αS fibrils could be associated with their ability to release small hydrophobic oligomers presenting a cross-β structure, similar to the OB*, that are particularly efficient in crossing neuronal membranes and rapidly induce neurotoxicity. To corroborate our hypothesis, we counterstained the αS assemblies internalized by neuronal cells after long times of exposure with an antibody that specifically recognizes oligomers of different proteins or peptides, independently of their primary sequence. Thus, the results obtained in the first part of this work reveal that the intrinsic neurotoxicity of αS species results principally from oligomeric species, formed early during the aggregation process, but also released from mature fibrils, upon their interaction with the plasma membrane of neuronal cells.

3.1 Morphological and structural characterization of the different αS assemblies

The morphological and structural characterization of the different αS species have been performed by the research group of Professor Christopher Dobson in Cambridge. Briefly, samples of each of the highly stable αS species described in this study (M, OA*, OB*, SF and LF) were produced as previously reported and then analysed with AFM (**Figure 22A-E**). Both OA* and OB* oligomers appeared as globular assemblies with a spherical shape and with similar average heights, 5.1 ± 0.8 nm (n = 300) and 4.3 ± 0.9 nm (n = 300), respectively, in good agreement with the dimensions previously obtained by cryo-EM 3D reconstruction methods (Chen *et al*., 2015). Opposite, the SF and LF showed an elongated morphology, with averaged heights of 5.0 ± 2.6 nm and 6.2 ± 3.8 nm, respectively, and average lengths of 57 nm and 520 nm, respectively (**Figure 22F**). The secondary structure content was also evaluated, together with the cross-β structure, the tinctorial properties and the solvent-exposed hydrophobicity by far-UV CD and FT-IR spectroscopy, X-ray diffraction, ThT fluorescence and ANS fluorescence, respectively (**Figure 22G-K**). Using far-UV CD and FT-IR spectroscopy, the OA* resulted to have a predominantly disordered secondary structure with similar spectra to those of the monomeric protein, while OB*, SF and LF presented a β-sheet core (**Figure 22G,H**), with an average of ~ 30-35 % of the protein sequence in a β-sheet conformation for OB*, and ~ 65 % for the fibrillar species, as found previously (Chen *et al*., 2015; Fusco *et al*., 2017). Despite the smaller β-sheet core of OB*, these species display X-ray diffraction pattern typical of amyloid structures (Chiti and Dobson, 2017), reflecting a cross-β structure with an inter-strand spacing of 4.6 Å and an inter-sheet distance of 8.9 Å, closely similar to the values of 4.6 and 9.4 Å, respectively, exhibited by the fibrils (**Figure 22I**). However, their cross-β structure is still rudimentary and not completely regular and compact, as compared to the fibrillar assemblies, resulting in substantial differences in ThT staining (**Figure 22J**). Interestingly, the OB*, SF and LF samples all generated a similar level of ANS fluorescence intensity and a virtually identical blue-shift of the wavelength of maximum emission, indicating a similar and high degree of solvent-exposed hydrophobic surface area. In contrast, the M and OA* species had a very low hydrophobic surface exposed to the solvent according to ANS fluorescence (**Figure 22K**).

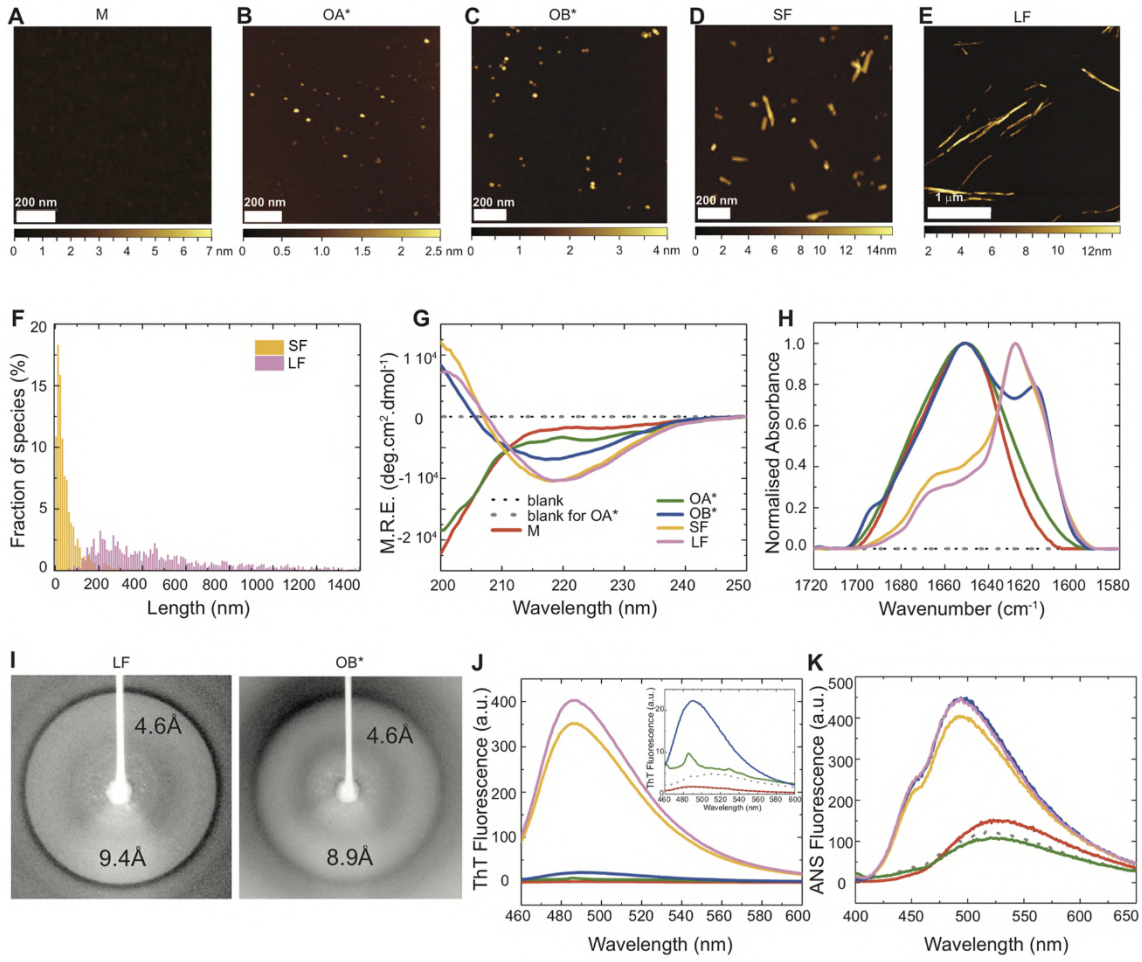

Figure 22 - Morphological and structural characterization of the different αS species. (A-E) AFM images (height data) of the various αS species: M, OA*, OB* SF and LF. The white and colored bars represent the length and height scales, respectively. (**F**) The length distribution of the different fibril population as estimated by AFM. Far-UV CD spectra **(G)**, FT-IR spectra **(H)**, X-ray diffraction patterns (**I**), ThT fluorescence spectra **(J)**, ANS fluorescence spectra **(K)** of the indicated αS species. Inset in (**J**) is the same plot on an expanded *y* scale to show details for M, OA* and OB*.

3.2 αS species show different abilities to induce ROS production

The generation of intracellular ROS is one of the earliest biochemical changes evoked by deleterious protein aggregates, including αS, as already reported (Canevari *et al*., 2004; Gandhi and Abramov, 2012; Deas *et al*., 2016). Here, we analysed the ability of the previously described αS species to induce ROS production, by adding them for 15 min at increasing concentrations to the extracellular medium of the SH-SY5Y cells. At a concentration of 0.3 μM (monomer equivalents), we found that only OB* and, to a lesser extent, SF generated a significant increase (360±15% and 198±12%, respectively) in ROS production relative to untreated cells (**Figure 23A**). A similar trend has been observed at lower protein concentrations (0.03 μM and 0.1 μM), in a dose dependent manner; opposite, at higher protein concentrations, intracellular ROS levels did not increase in the presence of any of the αS samples (**Figure 23B**). This effect seems to be the consequence of the agglutination process to which aggregated αS species are subject at high concentrations, as previously reported (Buell *et al*., 2014).

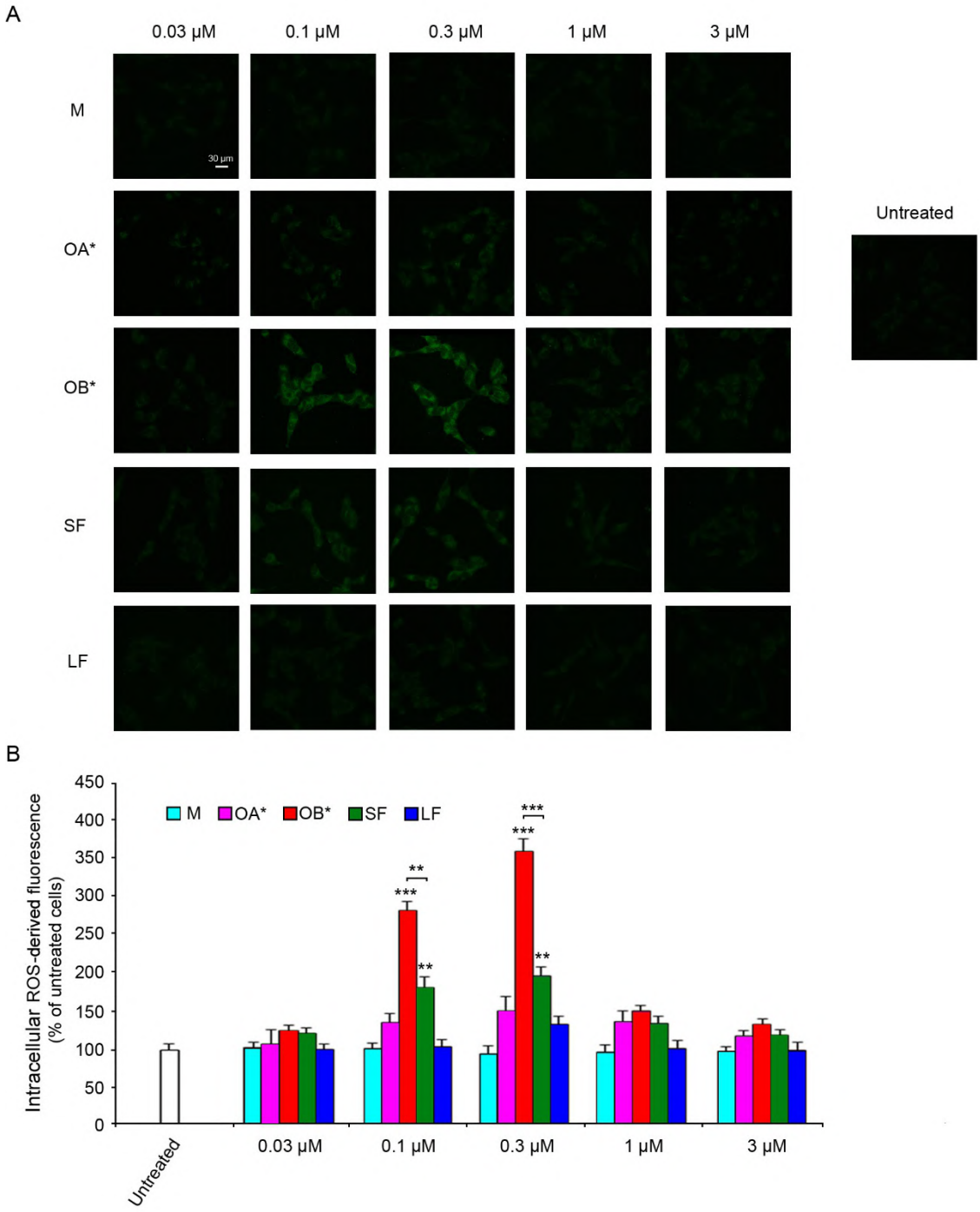

Figure 23 - ROS production in cells exposed to the different αS species. (A) Representative confocal microscope images showing intracellular ROS levels in SH-SY5Y cells treated for 15 min with the indicated αS species at the indicated αS concentrations. Untreated cells are also shown. The green fluorescence arises from the CM-H2DCFDA probe that has reacted with ROS. **(B)** The results of a semi-quantitative analysis of the intracellular ROS-derived fluorescence, expressed as the percentage of the values for untreated cells. Experimental errors are S.E.M. Samples were analysed by one-way ANOVA followed by Bonferroni's multiple comparison test relative to untreated cells (**P < 0.01, ***P < 0.001) unless otherwise indicated. 200–250 cells were analysed per condition in total.

3.3 αS species show different abilities to induce Ca^{2+} dyshomeostasis

We then analysed the effects of the different αS species on the disruption of cytosolic Ca^{2+} homeostasis, another early event in the cascade of biochemical changes responsible for the cytotoxicity of a wide range of misfolded amyloid aggregates, including those of αS (Orrenius *et al*., 2003; Danzer *et al*., 2007; Demuro *et al*., 2010; Zampagni *et al*., 2011; Angelova *et al*., 2016). At a concentration of 0.3 μM (monomer equivalents) OB* and, to a lesser extent, SF evoked a significant (380±15% and 230±10%, respectively) influx of Ca^{2+} ions in SH-SY5Y cells (**Figure 24A,B**). The sharp increase in cytosolic Ca^{2+} levels caused by 0.3 μM OB* was not observed when SH-SY5Y cells were cultured in a Ca^{2+}-free medium, indicating that the influx of Ca^{2+} ions was exclusively from the extracellular medium and it was not released from the intracellular stores (**Figure 24A**). These findings indicate that the different αS species have distinct abilities to induce cellular dysfunction(s) in human neuroblastoma cells at early incubation times. In particular, while M and OA* were unable to induce any increase in intracellular Ca^{2+} levels, the OB* species and, to a much lesser extent, the SF samples evoked the rapid loss of Ca^{2+} homeostasis. A very similar trend was observed at lower protein concentrations (0,1 μM), but not at higher concentrations, at which the agglutination probably occurs (Buell *et al*., 2014).

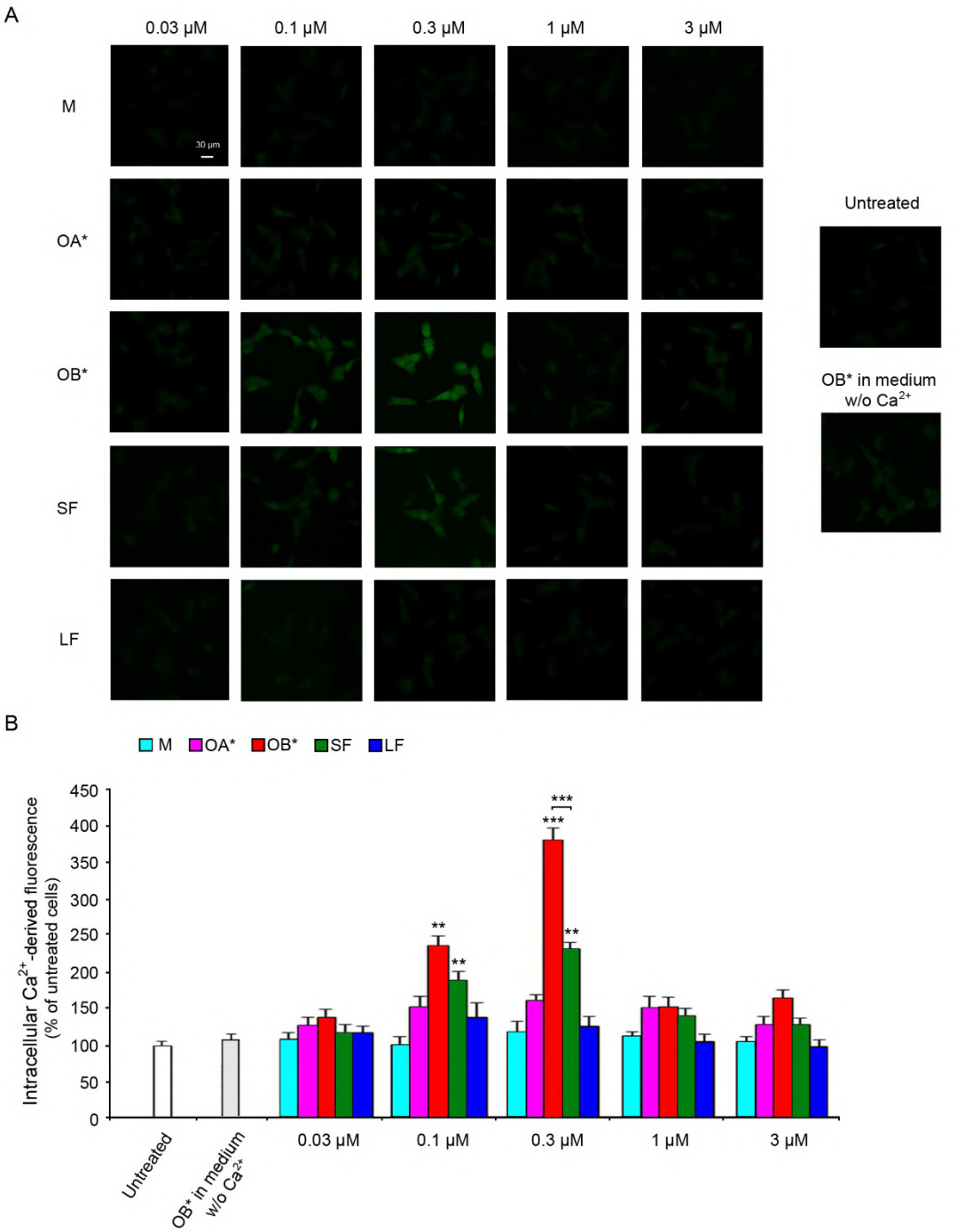

Figure 24 - Ca^{2+} influx evoked in cells by the different αS species. (A) Representative confocal microscope images showing intracellular Ca^{2+} levels in SH-SY5Y cells treated for 15 min with the indicated αS species at the indicated αS concentrations. Untreated cells and cells treated with 0.3 µM OB* in medium without (w/o) Ca^{2+} are also shown. Cells were then loaded with Fluo-4 AM probe. **(B)** The results of a semi-quantitative analysis of the intracellular Ca^{2+}-derived fluorescence, expressed as the percentage of the values for untreated cells. Experimental errors are S.E.M. Samples were analysed by one-way ANOVA followed by Bonferroni's multiple comparison test relative to untreated cells (**P < 0.01, ***P < 0.001), unless otherwise indicated. 200–250 cells were analysed per condition in total.

3.4 αS species show different abilities to disrupt plasma membrane integrity

The ability of αS misfolded aggregates to permeabilize cellular membranes is considered a key event in the cascade of toxic events leading to neuronal cell death (Stafanovic *et al*., 2014). Thus, we analysed the ability of the previously reported αS species to destabilize the plasma membrane integrity of both human SH-SY5Y cells and primary rat cortical neurons, by monitoring the release of the fluorescent probe calcein-AM, loaded into the cells, as previously reported (Papadopoulos *et al*., 1994). The different αS species were added for 60 min to the culture medium at 0.3 μM (monomer equivalents), as previously reported data indicated that this is the concentration at which the most significant effects could be detected. Thus, we found that OB* and, to a less extent, SF generated a significant leakage of calcein (63±4% and 36±5% in SH-SY5Y cells and 73±2% and 40±2% in primary cortical neurons, respectively, as reported in **Figure 25A,B**). By contrast, the other αS species induced only a slight and not significant release of calcein after 60 min from their addition to the culture medium (**Figure 25A,B**).

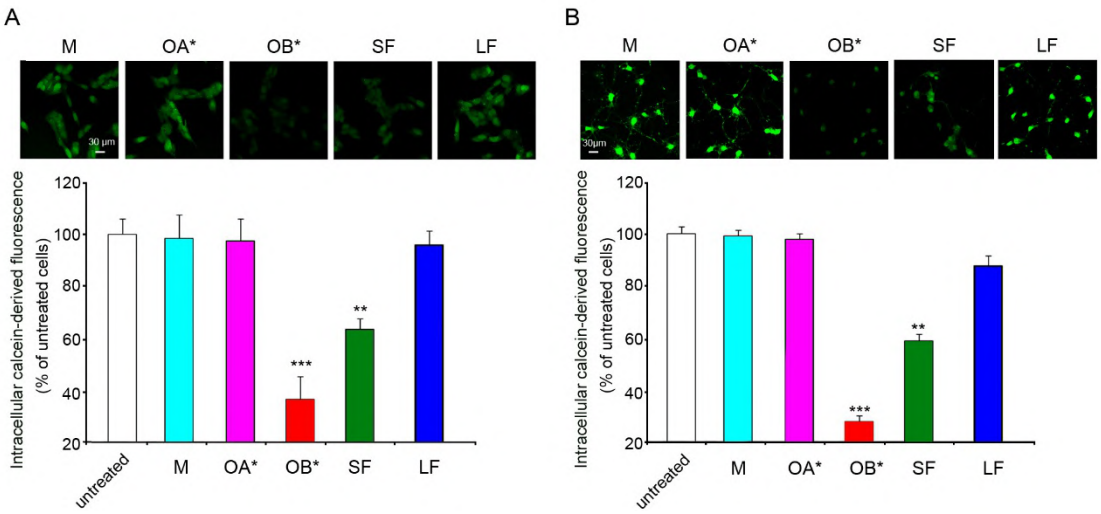

Figure 25 - Disruption of the plasma membrane integrity by the different αS species. (A-B) Representative confocal microscope images showing SH-SY5Y cells (**A**) and primary rat cortical neurons (**B**) loaded with the calcein-AM probe for 30 min and then treated for 60 min with the indicated αS species at a concentration of 0.3 μM (monomer equivalents). The results of a semi-quantitative analysis of the green fluorescence signal, expressed as the percentage of the values for untreated cells. Experimental errors are S.E.M. Samples were analysed by one-way ANOVA followed by Bonferroni's multiple comparison test relative to untreated cells (**P < 0.01, ***P < 0.001). 200–250 cells were analysed per condition in total.

3.5 αS species display different abilities to penetrate cells

We then assessed whether the different αS aggregates interacted with the plasma membrane and were internalized into the cytosol of SH-SY5Y cells, following a 60 min treatment at a concentration of 0.3 μM (monomer equivalents). The plasma membranes (red channel) and αS species (green channel) were counterstained and subsequently analysed at the apical, median and basal planes parallel to the coverslip by confocal scanning microscopy (**Figure 26**). Higher intracellular αS levels were detected upon treatment with OB*, with respect to SF and LF (1300±400%, 600±50% and 300±15%, respectively) (**Figure 26**), relative to the signal of endogenous αS revealed in untreated cells, taken as 100% (**Figure 27C**). The ratio between the protein signal at the median planes and the total protein signal of the apical, median and basal planes revealed that 70±3%, 12±1% and 6±1% of the OB*, SF and LF samples were internalized after 60 min of incubation, respectively (**Figure 26**). Thus, 88±1% and 94±1% of the fluorescence signal arising from αS was localized at the plasma membrane in the cells exposed to SF and LF samples, respectively. By contrast, the M and OA* samples added to the media weakly interacted with the cellular membranes or entered the cells (**Figure 26**). The dose-dependent analysis revealed that the OB* and, to a lesser extent, the SF were able to cross the cellular membrane at a concentration of 0.3 μM, with a bell-shaped protein concentration dependence (**Figure 27**). In particular, the OB* showed a similar trend for both the intracellular and the total αS-derived fluorescence (**Figure 27D,E**), suggesting that the total quantity of the oligomers that was internalized inside the cells is directly proportional to the total amount of oligomers interacting with the plasma membrane. By contrast, the total quantity of SF bound to the membrane was much higher than the fraction that appeared to be internalized at any αS concentration (**Figure 27D,E**). Indeed, concentrations higher than 0.3 μM resulted in an increase in the number of fibrils bound to the cell membrane but not in the quantity of internalized protein (**Figure 27D,E**). Thus, these results indicate that the cellular dysfunctions induced by the OB* and SF at early incubation times are directly correlated with the extent to which the different species have been internalized by the cells. The quantity of internalized species is in turn directly proportional the quantity of αS interacting with the plasma membrane for OB*, but not for SF.

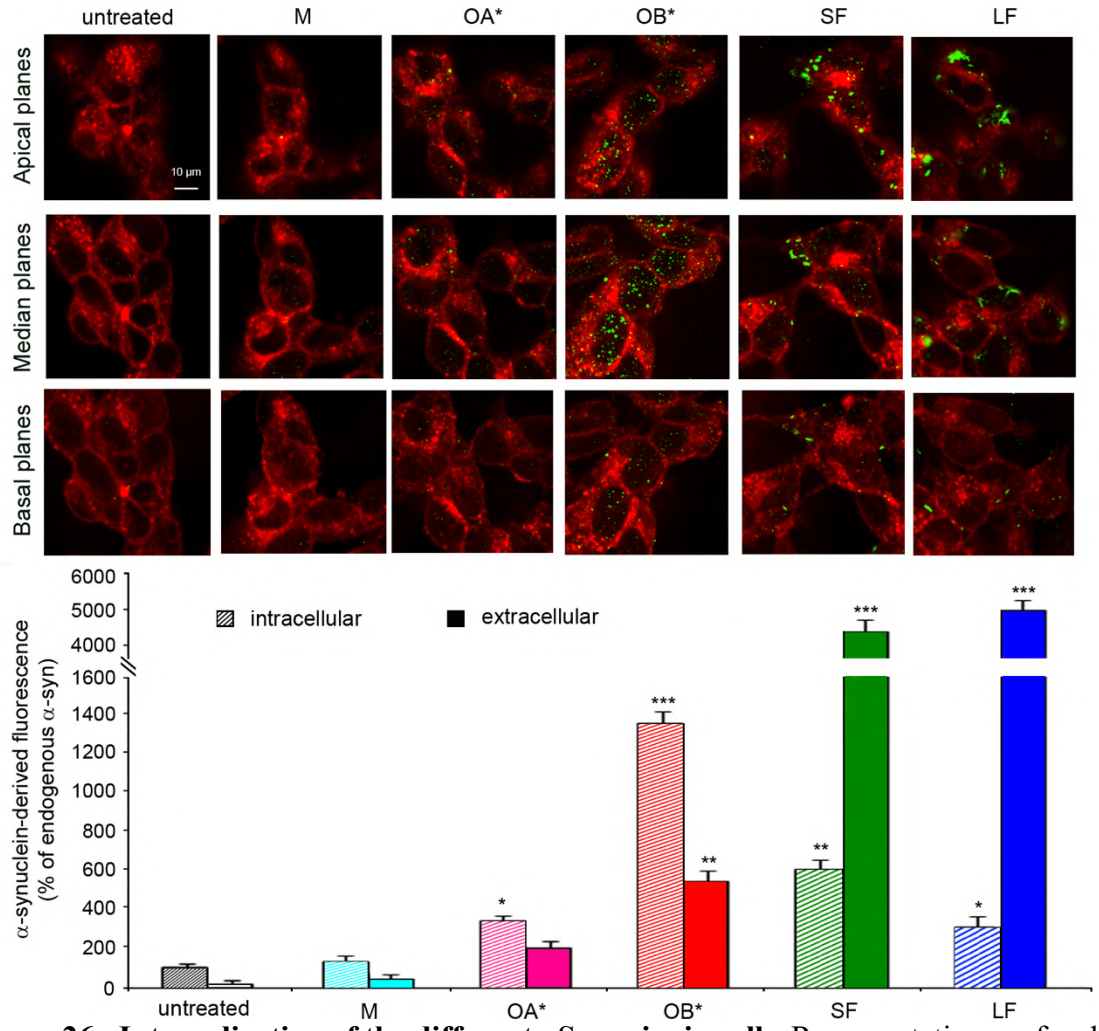

Figure 26 - Internalization of the different αS species in cells. Representative confocal scanning microscope images showing the basal, median and apical sections of SH-SY5Y cells treated for 60 min with the indicated αS species at 0.3 µM (monomer equivalents). Untreated cells are also shown. Red and green fluorescence indicates the cell membranes and the αS species revealed with polyclonal anti-αS antibodies (ab52168), respectively. The results of a semi-quantitative analysis of the intracellular and extracellular αS-derived fluorescence, expressed as the percentage of endogenous αS fluorescence. Experimental errors are S.E.M. Samples were analysed by one-way ANOVA followed by Bonferroni's multiple comparison test relative to untreated cells (*P < 0.05, **P < 0.01, ***P< 0.001). 200–250 cells were analysed per condition in total.

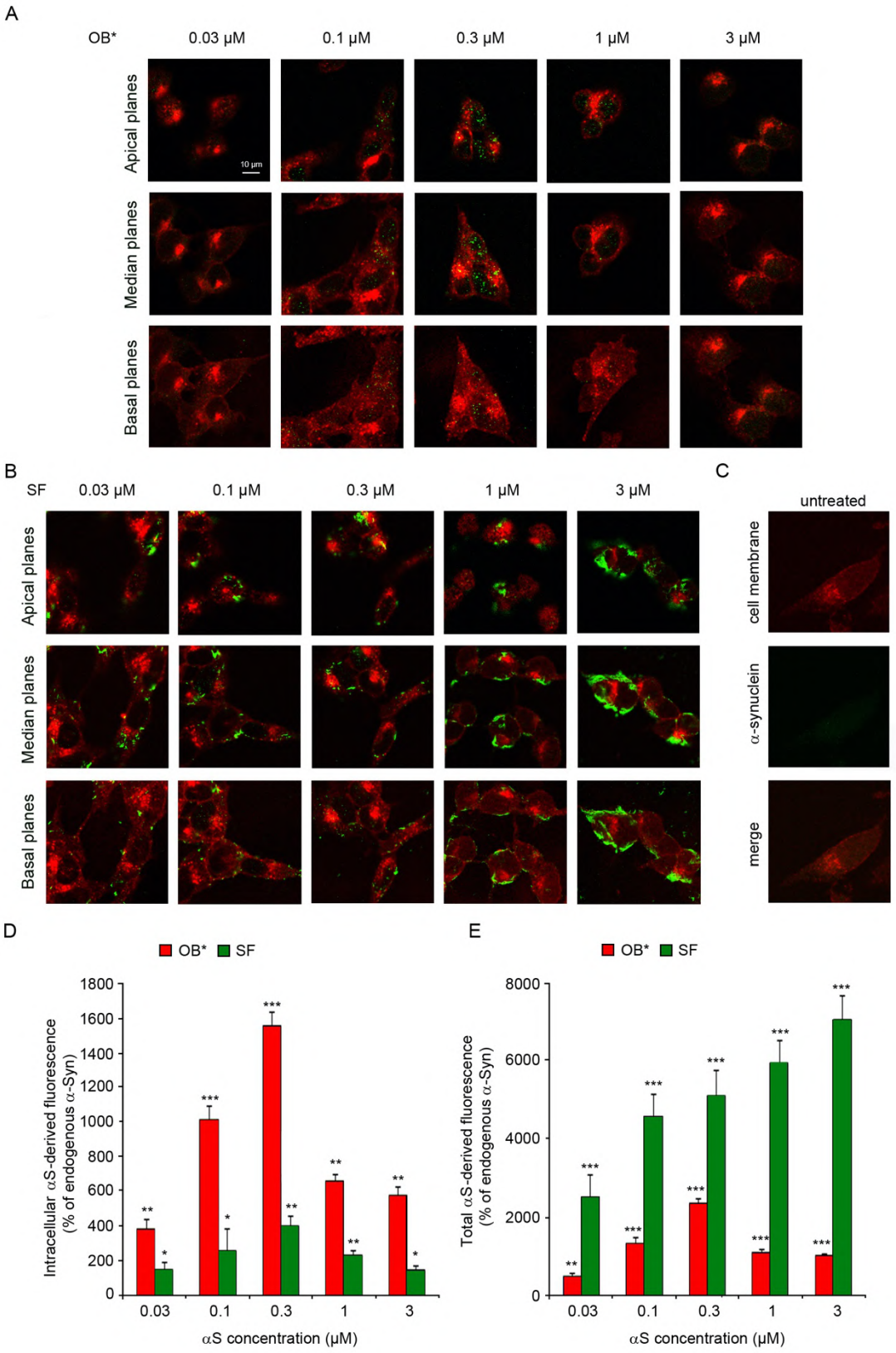

Figure 27 - Internalization of different αS species in cells. (A-B) Representative confocal scanning microscope images showing the basal, median and apical sections of SH-SY5Y cells treated for 60 min with OB* **(A)** and SF **(B)** at the indicated αS concentrations. Red and green fluorescence indicates the cell membranes and the αS species revealed with rabbit anti-αS polyclonal antibodies (ab52168), respectively. **(C)** Representative confocal scanning microscope images showing the cell membrane (red),

the endogenous αS (green) and the merge of all sections of untreated SH-SY5Y cells. **(D-E)** The results of a semi-quantitative analysis of the green fluorescence signal derived from intracellular **(D)** and total **(E)** αS-derived fluorescence, expressed as the percentage of endogenous αS fluorescence. Experimental errors are S.E.M. Samples were analysed by one-way ANOVA followed by Bonferroni's multiple comparison test relative to untreated cells (*P < 0.05, **P < 0.01, ***P < 0.001). 200–250 cells were analysed per condition in total.

3.6 Different αS species show distinct abilities to induce mitochondrial dysfunction and caspase-3 activation

We then assessed whether the different abilities of the various αS aggregates to induce cytosolic ROS production and Ca^{2+} dysregulation also resulted in distinct capacities to induce metabolic impairment and cell death. We firstly measured the reduction of 3-(4,5-dimethylthiazol-2-yl)-2,5 diphenyltetrazolium bromide (MTT), a widely employed indicator of mitochondrial dysfunction (Mosmann, 1983), that is an indirect measure of cellular viability.

Briefly, the various αS species were added at 0,3 μM (monomer equivalents) for 24 h to the culture medium of SH-SY5Y cells and primary rat cortical neurons. After the treatment, we observed that OB* evoked a significant decrease of the ability of neuronal cells to reduce MTT, by 28±2% in SH-SY5Y cells and by 26±1% in primary neurons, respectively (**Figure 28A**). Similarly, MTT reduction decreased by 23±2% and 24±2%, respectively, upon treatment for 24 h with 0.3 μM SF (**Figure 28A**); LF also caused a similar decrease, by 18±2% and 21±2%, respectively, whereas M and OA* did not cause any considerable change in mitochondrial activity (**Figure 28A**).

A similar trend was observed for caspase-3 activity, a crucial component of the apoptotic machinery, measured by the fluorescent FAM-DEVD-FMK FLICA dye, which binds covalently to the active caspase-3 in living cells (Thornberry *et al*., 1997). The treatment of SH-SY5Y cells with OB*, SF and LF (0,3 μM, monomer equivalents) for 24 h induced a caspase-3 activation of 370±30%, 300±20% and 260±25%, respectively. Opposite, M and OA* did not cause any appreciable increase in the activation of this enzyme (**Figure 28B**).

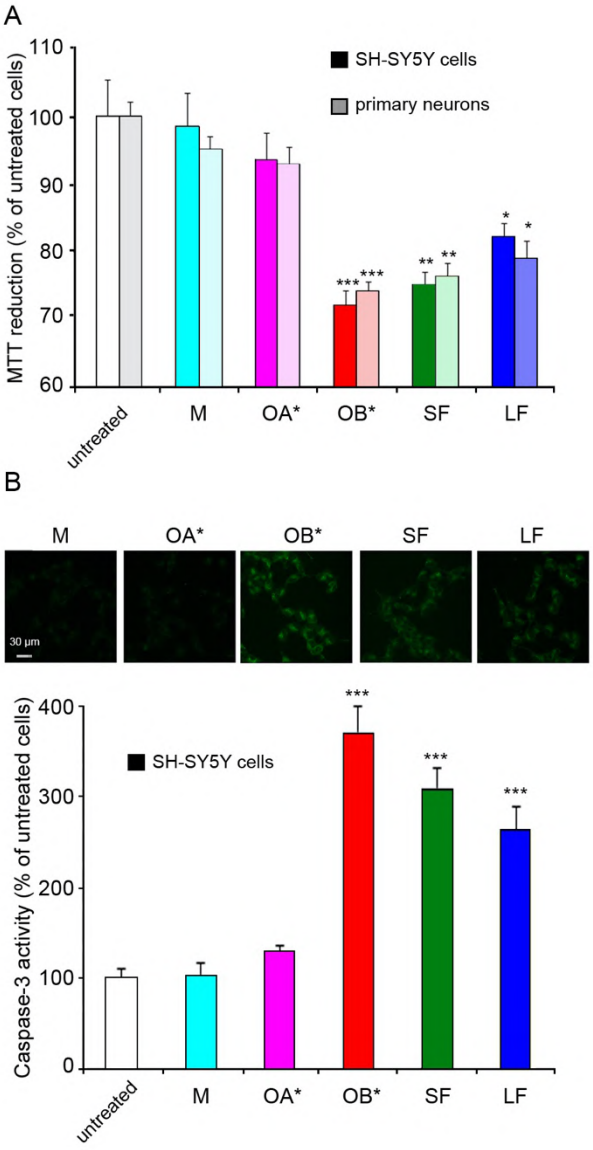

Figure 28 - Impairment of cell viability after exposure to the different αS species. **(A)** MTT reduction in SH-SY5Y cells and primary rat cortical neurons treated for 24 h with the indicated αS species at a concentration of 0.3 µM (monomer equivalents). **(B)** Representative confocal microscope images showing caspase-3 activity in SH-SY5Y cells treated for 24 h with the indicated αS species at 0.3 µM. The results of a semi-quantitative analysis of the caspase-3-derived fluorescence, expressed as the percentage of the values for untreated cells. Experimental errors are S.E.M. Samples were analysed by one-way ANOVA followed by Bonferroni's multiple comparison test relative to untreated cells (*P < 0.05, **P < 0.01, ***P < 0.001). 150.000-200.000 cells (**A**) and 200–250 cells (**B**) were analysed per condition in total.

Furthermore, αS species that resulted to cause a significant toxic effect in neuronal cells, were also stained with the apoptotic marker Hoechst 33342, which binds to the highly condensed chromatin present in the nuclei of apoptotic cells, giving rise to a strong

fluorescence signal and allowing the visualization of abnormal nuclei (Downs and Wilfinger, 1983). Samples of OB*, SF and LF were added for 24 h at a concentration of 0.3 μM to the culture medium of SH-SY5Y cells before staining. Fluorescence microscopy images indicated that the nuclei of the cells treated with OB* and, to a lesser extent, SF were prominently stained with the dye and often appeared abnormal in shape, whereas LF caused a minor nuclear condensation and chromatin fragmentation, as showed in **Figure 29**.

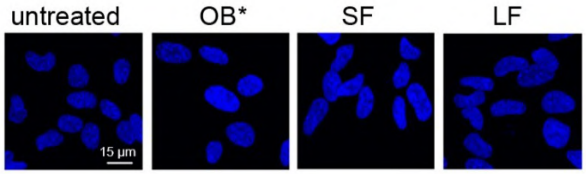

Figure 29 - Chromatin condensation after exposure to different αS species. Representative confocal microscope images of SH-SY5Y cells treated for 24 h with OB*, SF and LF at 0.3 μM (monomer equivalents) and then stained with Hoechst 33342.

3.7 N-acetylated αS species exert the same toxicity as the non-acetylated forms

It has been reported that αS purified from both normal and pathological brain tissue is N-terminally acetylated (Anderson *et al*., 2006); this co-translational modification is widely considered to be a general mechanism for stabilizing the α-helical structure in a range of proteins and peptides, including αS. Thus, we analysed key markers of toxicity, by testing N-acetylated M, OA* and OB* on SH-SY5Y cells; thus, we observed that N-acetylated OB* had the same ability to induce calcein leakage (**Figure 30A**) and the impairment of the mitochondrial functionality (**Figure 30B**) of the non-acetylated assemblies; similarly, M and OA* did not exert any toxic effect on neuronal cells (**Figure 30A,B**).

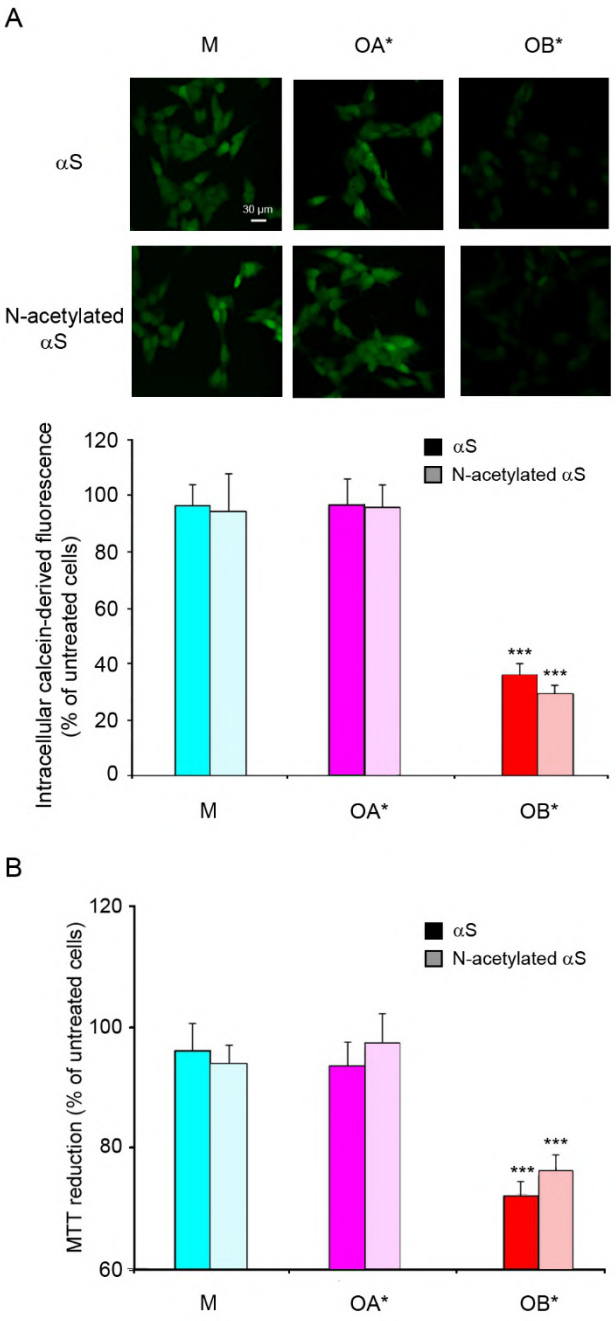

Figure 30 - Analysis of the toxicity evoked by non-acetylated and N-acetylated αS species. (A) Representative confocal microscope images showing SH-SY5Y cells loaded with calcein-AM probe for 30 min and then treated for 60 min with the non-acetylated (αS) and N-acetylated αS species (M, OA* and OB*) at a concentration of 0.3 µM (monomer equivalents). The results of a semi-quantitative analysis of the calcein-derived green fluorescence signal, expressed as the percentage of the values for untreated cells. (**B**) MTT reduction in SH-SY5Y cells treated for 24 h with the indicated non-acetylated (αS) and N-acetylated αS species (M, OA* and OB*) at a concentration of 0.3 µM (monomer equivalents). Experimental errors are S.E.M. Samples were analysed by one-way ANOVA followed by Bonferroni's multiple comparison test relative to untreated cells (***$P < 0.001$). 200–250 cells (**A)** and 150.000-200.000 cells **(B)** were analysed per condition in total.

3.8 Different αS species exert their toxicity on neuronal cells with distinct kinetics

Time-course analysis of intracellular Ca^{2+} increase

The previously reported data strongly suggest that αS cytotoxicity could be related to the time of exposure of the cells to the deleterious aggregates. Thus, we monitored the different readouts of cellular impairment for different lengths of time after treatment of neuronal cells with 0.3 μM (monomer equivalents) OB*, SF and LF.

As Ca^{2+} dyshomeostasis is widely considered to be a key early event in the αS cytotoxicity, we monitored its dysregulation by incubating both SH-SY5Y and primary rat cortical neurons with OB*, SF and LF for different lengths of time (0, 5, 10, 15, 30, 60 and 180 min for SH-SY5Y cells and 0, 5, 15, 60 and 180 for primary rat cortical neurons). In neuroblastoma cells, OB* determined a significant increase in intracellular Ca^{2+} levels already after 10 min of treatment, whereas SF became effective after 15 min and LF after 30 min. In all cases, Ca^{2+} influx came to a plateau for long times of exposure (180 min), when they induced an increase of 510±50%, 340±20% and 240±15%, respectively, relative to untreated cells (**Figure 31A,C**). Furthermore, we found an exponential kinetics for OB*, with an apparent rate constant of $1.1(\pm0.1)\bullet10^{-3}$ s^{-1}, but sigmoidal kinetics for both SF and LF, as reported in **Figure 31C**. In primary rat cortical neurons, all the three species induced an extremely significant increase of intracellular Ca^{2+} concentration already after 15 min of treatment; after 180 min, the increase in intracellular Ca^{2+} levels, with respect to untreated cells, was of 660±40%, 570±30% and 360±15%, respectively (**Figure 31B,D**). In this cell line we analysed the influx of Ca^{2+} ions only at a limited number of key time-points, and when we plotted the normalized Ca^{2+}-derived fluorescence as a function of time, we obtained an exponential trend for all the three species, with the OB* being the most rapid and the LF being the slowest, with apparent rate constant of $1.8(\pm0.3)\bullet10^{-3}$ s^{-1} (OB*), $1.1(\pm0.2)\bullet10^{-3}$ s^{-1} (SF) and $0.8(\pm0.1)\bullet10^{-3}$ s^{-1} (LF) (**Figure 31D**). Furthermore, these observations clearly indicate that cortical neurons are more susceptible to αS cytotoxicity with respect to neuroblastoma cells at early incubation times.

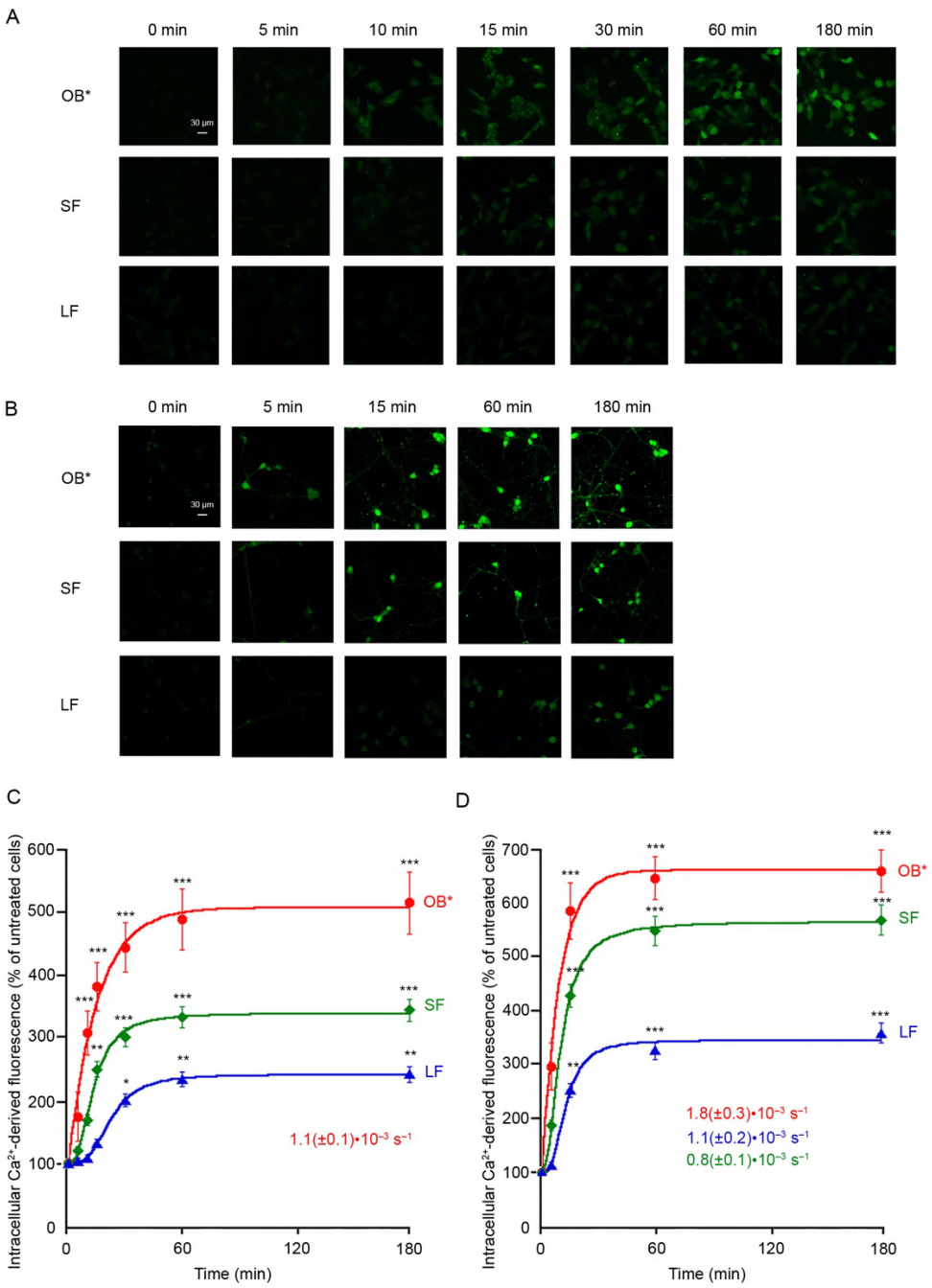

Figure 31 - Time-course analysis of Ca^{2+} influx evoked by OB*, SF and LF. (**A-B**) Representative confocal microscope images showing intracellular Ca^{2+} levels in SH-SY5Y cells (**A**) and primary rat cortical neurons (**B**) treated for different lengths of time (0, 5, 10, 15, 30, 60 and 180 min in SH-SY5Y cells and 0, 5, 15, 60 and 180 min in primary neurons) with αS species at 0.3 µM (monomer equivalents). Cells were then loaded with Fluo-4 AM probe. **(C-D)** The results of a semi-quantitative analysis of Ca^{2+}-derived fluorescence, expressed as the percentage of the values for untreated cells, in SH-SY5Y cells (**C**) and primary rat cortical neurons (**D**). The continuous lines through the experimental points represent the best fits to exponential and sigmoidal functions, reported in detail in the "Materials and Methods" section. Experimental errors are S.E.M. Samples were analysed by one-way ANOVA followed by Bonferroni's multiple

comparison test relative to untreated cells (*P < 0.05, **P < 0.01, ***P < 0.001). 200–250 cells were analysed per condition in total.

Time-course analysis of cell viability impairment

We then evaluated the kinetic profiles of late markers of cytotoxicity, caspase-3 activation and MTT reduction, following incubation of SH-SY5Y cells for different lengths of time (0, 1, 3, 5 and 24 h) with 0.3 μM (monomer equivalents) OB*, SF and LF. The time-course analysis of caspase-3 activation revealed an exponential kinetics for OB*, with an apparent rate constant of $6.1(\pm1.8)\bullet10^{-5}$ s^{-1}. Opposite, the increase in caspase-3 activation was found to be linear for both SF and LF, as reported in **Figure 32A,B**. The analysis of MTT reduction revealed an exponential decay for all the three species, with apparent rate constants of $3.1(\pm0.5)\bullet10^{-5}$ s^{-1} (OB*), $6.1(\pm0.4)\bullet10^{-5}$ s^{-1} (SF) and $6.5(\pm1.8)\bullet10^{-5}$ s^{-1} (LF), as shown in **Figure 32C**. Thus, we observed a similar order of rates for the three species, with the OB* being the most rapid and the LF the slowest (**Figure 32A-C**). This observation is in good agreement with the previously reported evidences on Ca^{2+} dysregulation, even if we observed faster kinetics for the increase in intracellular Ca^{2+} levels (**Figure 31A-D**), with respect to caspase-3 activation and MTT reduction, for all the analysed αS assemblies.

Taken together, these data strongly indicate that OB* are by far the most toxic species among the αS assemblies analysed in this study.

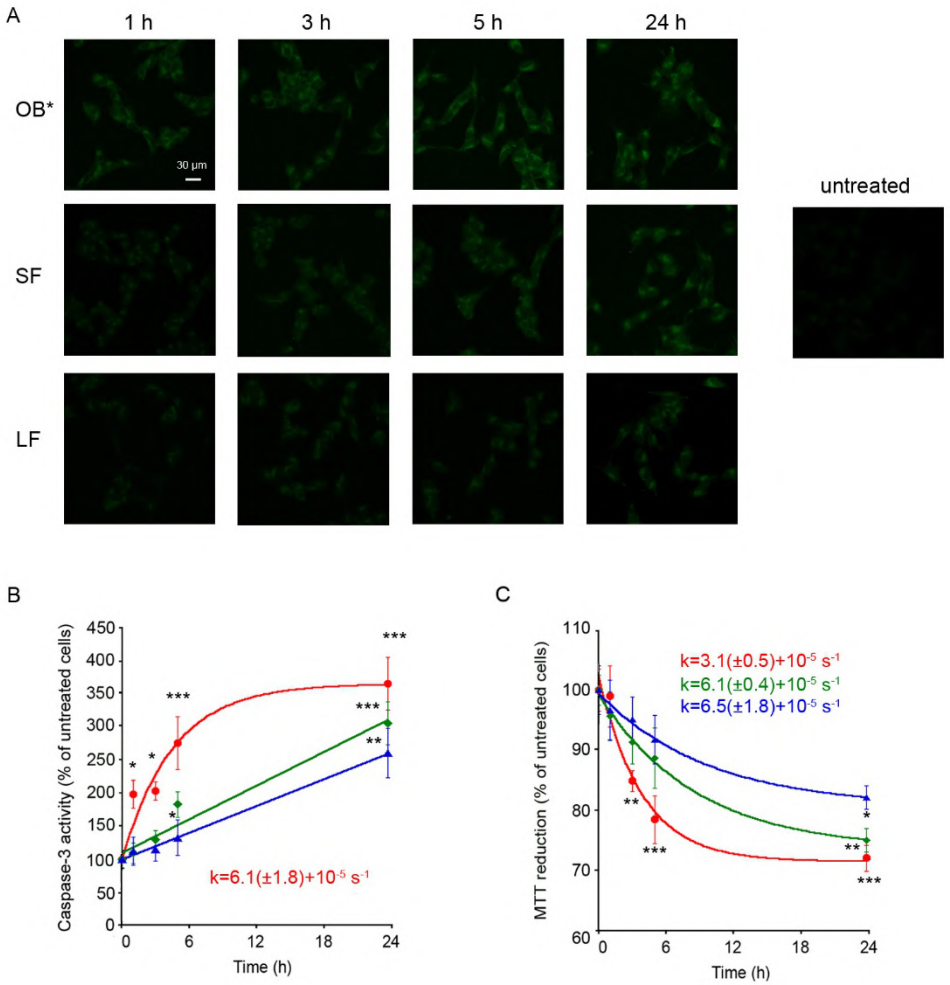

Figure 32 - Time-course analysis of caspase-3 activity and MTT reduction evoked by OB*, SF and LF. (A) Representative confocal microscope images showing caspase-3 activation in SH-SY5Y cells treated with the different αS species at a concentration of 0.3 µM (monomer equivalents) for the indicated lengths of time. Untreated cells are also shown. After treatment, the cells were loaded with FAM-FLICA™ Caspases 3&7 solution. (**B,C**) Time-course analysis of caspase-3 activity (**B**) and MTT reduction (**C**) in SH-SY5Y cells treated for different lengths of time (0, 1, 3, 5 and 24 h) with OB*, SF and LF at 0.3 µM (monomer equivalents). The fluorescence signals in (**B**) are expressed as the percentage of the values for untreated cells. The continuous lines through the data in (**B,C**) represent the best fits to single-exponential or linear functions, reported in detail in the "Materials and Methods" section. Experimental errors are S.E.M. Samples were analysed by one-way ANOVA followed by Bonferroni's multiple comparison test relative to untreated cells (*P < 0.05, **P < 0.01, ***P < 0.001). 200–250 cells (**A,B**) and 150.000-200.000 cells (**C**) were analysed per condition.

Time-course analysis of other readouts describing OB*-induced cytotoxicity

All the previously reported data demonstrate that OB* are the most toxic species among the analysed αS aggregates; for this reason, we evaluated the kinetic profiles of other important readouts of cellular toxicity evoked by such aggregates. In particular, we monitored the evolution in time of intracellular ROS production, calcein leakage and αS internalization, treating SH-SY5Y cells with 0.3 μM (monomer equivalents) OB* for 0, 5, 10, 15, 30 and 60 min. Thus, we found a rapid increase of intracellular ROS production, whose evolution in time followed a single exponential kinetics, with an apparent rate constant of $1.0(\pm0.1)\bullet10^{-3}$ s^{-1}) (**Figure 33A upper panel, B**). We also monitored the release of calcein, that followed an exponential decay in time, with an apparent rate constant of $5.8(\pm2.1)\bullet10^{-4}$ s^{-1} (**Figure 33A middle panel, C**) and resulted to be very similar to those obtained for αS internalization ($6.3(\pm1.9)\bullet10^{-4}$ s^{-1}), as reported in **Figure 33A lower panel, D**.

Taken together, these evidences indicate that, already in the first 60 min of treatment, small αS oligomeric assemblies with a large solvent-exposed hydrophobicity and high β-sheet content progressively and irreversibly impair the functionality of neuronal cells.

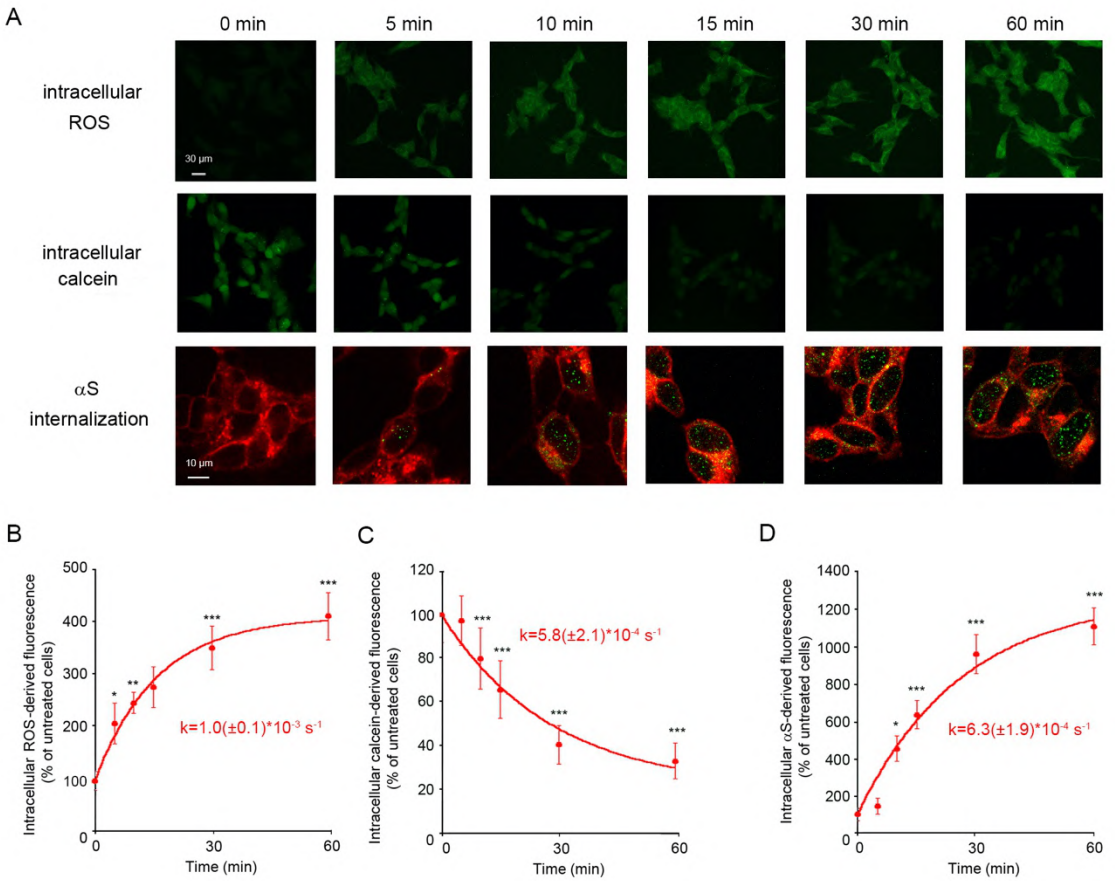

Figure 33 - Time-course analysis of the different parameters describing the cytotoxicity of OB*. (A) Representative confocal microscope images showing intracellular ROS, calcein leakage and αS internalization in SH-SY5Y exposed to OB* at a concentration of 0.3 µM (monomer equivalents) for the indicated lengths of time. (**B-D**) Kinetic plots reporting the fluorescence associated with intracellular ROS **(B)**, calcein leakage **(C)** αS internalization **(D)**, versus time elapsed following addition of 0.3 µM OB* (monomer equivalents) to the SH-SY5Y cell medium, after subtracting the fluorescence measured for untreated cells. The fluorescence signals are expressed as the percentage of the values for untreated cells. The continuous lines through the data represent the best fits to single-exponential functions, reported in detail in the "Materials and Methods" section. Experimental errors are S.E.M. Samples were analysed by one-way ANOVA followed by Bonferroni's multiple comparison test relative to untreated cells (*P < 0.05, **P < 0.01, ***P < 0.001). 200–250 cells were analysed per condition in total.

3.9 The neurotoxicity of αS fibrils is associated with their ability to release toxic oligomers

The previously reported data clearly indicate that OB* are by far the most harmful αS assemblies among those analysed in this work; furthermore, our experimental evidences strongly suggest that αS fibrils, and especially the SF, have the intrinsic capacity to induce cell viability impairment, thus causing the same sequence of toxic events as those observed for the OB* in neuronal cells, although with much slower rates. As it was previously reported that αS fibrils were able to release small oligomeric assemblies *in vitro* (Cremades *et al*., 2012), we tried to establish whether fibrillar cytotoxicity could be attributed to their intrinsic capacity to release small oligomeric assemblies upon their interaction with cellular membranes. To this aim, we probed the nature of the internalized protein species by confocal microscopy experiments, and in particular by labelling such aggregates with the polyclonal conformation-sensitive A11 antibody. This conformation-sensitive antibody was originally raised against prefibrillar $A\beta_{42}$ oligomers, but it has been widely reported to label oligomers of many different proteins or peptides, regardless of their amino acid sequence, because it recognizes a generic epitope common to prefibrillar oligomers and not fibrils, monomers or natively folded precursor proteins (Kayed *et al*., 2003). In good agreement with previously reported data (Chen *et al*., 2015), we observed that the A11 antibody had a much higher affinity for OB* than for OA*, SF or LF forms of αS (Chen *et al*., 2015), as reported in the dot-blot analysis (**Figure 34A**). The absence of an A11-positive cross-reaction of the SF in the dot-blot assay exclude the possibility that a significant fraction of OB* species was present in the SF sample, also at micromolar concentrations. In the same dot-blot experiment, we tested the immunoreactivity of αS species with the OC antibody, previously reported to selectively recognize amyloid fibrils, but not monomeric proteins or prefibrillar assemblies (Kayed *et al*., 2007). Our results are in good agreement with these evidences, as the OC recognized SF and LF, but not OA* and OB* (**Figure 34A**).

We then tested the nature of the internalized αS assemblies by confocal microscopy experiments, after treating human neuroblastoma cells with OB*, SF and LF at 0.3 μM (monomer equivalents) for different lengths of time (0, 3, 6, 15 and 24 h). After 3 h of treatment with OB*, we measured an extremely significant increase (470±40%) in A11-positive intracellular species at median planes parallel to the coverslip, as compared to untreated cells (**Figure 34B,C**). The percentage of OB* internalized by the cells, with

respect to the total amount of assemblies detected by the A11 antibody was calculated from the ratio between the intracellular fluorescence at the median planes and the total fluorescence at all the basal, median and apical planes, and resulted to be 68±6%. This is in good agreement with previously reported data (**Figure 26**), obtained in cells counterstained with the αS sequence-specific polyclonal antibody. Interestingly, the cells exposed to SF and LF for 3 h also showed a significant increase (240±20% and 125±8%, respectively) in the intracellular A11-positive signal (**Figure 34B,C**), indicating the presence in the cells of αS oligomeric assemblies, similar to OB*. The vast majority of the A11-derived fluorescence signal was located inside the cells (87±7% and 97±6% for SF and LF, respectively), suggesting that the A11-positive oligomers, presumably released from fibrillar assemblies, were able to cross the plasma membrane, as observed for the OB* species. The quantity of intracellular A11-positive signal was then monitored as a function of time, and we found an exponential kinetics for OB*, giving the maximum intracellular levels after 6 h of treatment, but sigmoidal kinetics for both SF and LF, with maximal intracellular levels reached only after 24 h of treatment, as reported in **Figure 34B,C**.

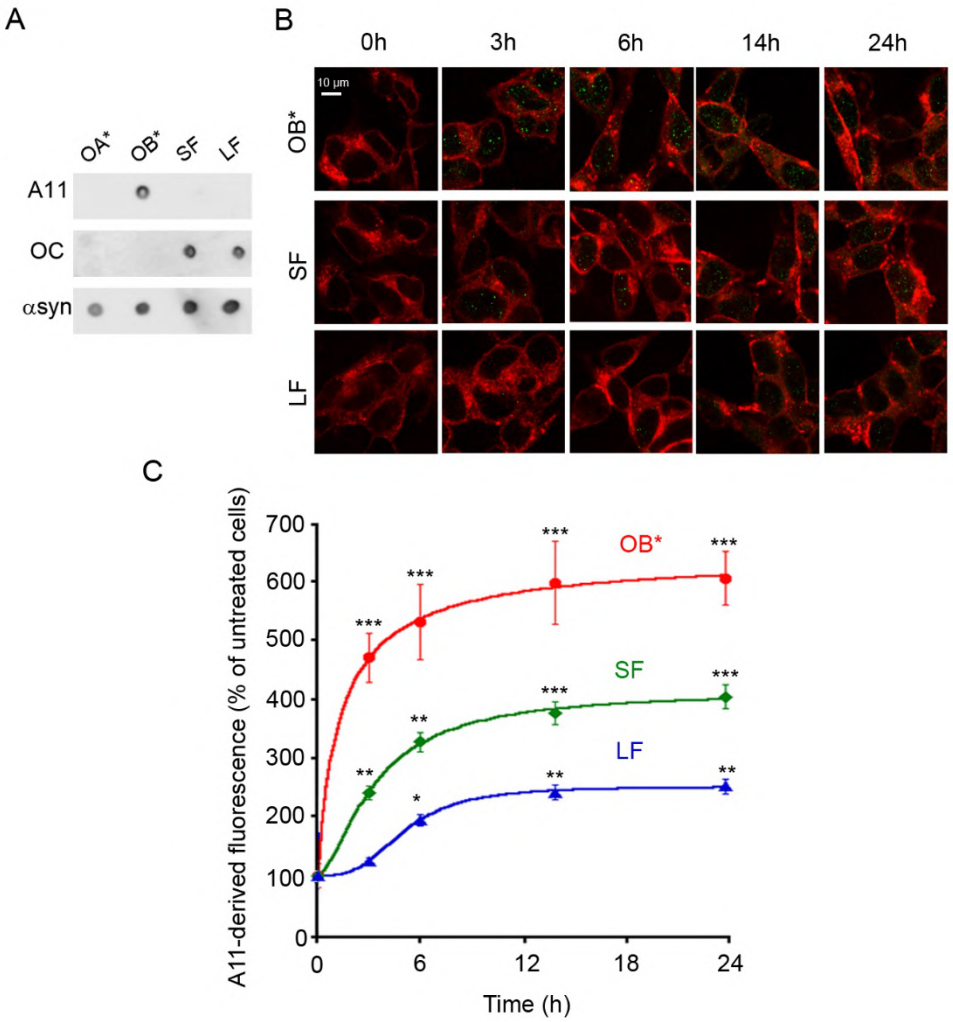

Figure 34 - Analysis of neurotoxic αS species with A11 antibody and confocal microscopy. (A) Dot-blot analysis of αS species probed with conformational specific antibodies A11 (AHB0052, top), OC (AB2286, middle) and polyclonal anti-αS (ab52168, bottom) antibodies. **(B)** Representative confocal scanning microscope images showing the median sections of SH-SY5Y cells treated for the indicated lengths of time with the indicated αS species at a concentration of 0.3 μM (monomer equivalents). Red and green fluorescence indicates the cell membranes and the A11-positive prefibrillar oligomers, respectively. **(C)** Kinetic plots reporting A11-derived intracellular fluorescence following the addition of the indicated αS species at 0.3 μM (monomer equivalents). The continuous lines through the experimental points represent the best fits to exponential and sigmoidal functions, reported in detail in the "Materials and Methods" section. Experimental errors are S.E.M. Samples were analysed by one-way ANOVA followed by Bonferroni's multiple comparison test relative to untreated cells (*P < 0.05, **P < 0.01, ***P < 0.001). 200–250 cells were analysed per condition in total (**B-C**).

Taken together, these data strongly indicate that the internalized species are in all cases oligomeric, as they are bound by the A11 antibody, thus suggesting that fibrillar assemblies are able to release small toxic oligomers upon their interaction with the plasma

membrane. To further corroborate this hypothesis, we performed another set of experiments, in which SH-SY5Y neuroblastoma cells were exposed to OB*, SF and LF (at a concentration of 0.3 μM, monomer equivalents, for 30 min) and then a 2.5-fold excess of A11 antibody was added to the same culture media for 24 h. The A11 antibody was found to reduce the internalization of OB* by 65±3%, as revealed by targeting intracellular αS with the αS sequence-specific polyclonal antibody (Figure **35A,B**), and to completely abolish the associated cytotoxicity, as revealed by the MTT reduction inhibition assay (**Figure 35C**). The A11 antibody was also found to suppress both the SF and LF internalization by 85±2% and 82±3%, respectively (**Figure 35A,B**), and completely prevent their toxicity (**Figure 35C**). The same experiments were performed using the conformation-sensitive OC antibody, previously found to react with SF and LF, but not with OB* (**Figure 34A**). This antibody significantly reduced the intracellular αS-specific antibody signal arising from SF and LF (by 76±4% and 65±6%, respectively) and their cytotoxicity (by ~ 55% and 70%, respectively), without affecting the intracellular fluorescence (reduced only by 7±5%) and the cytotoxicity (reduced only by 3±3%) evoked by OB* (**Figure 35B,C**).

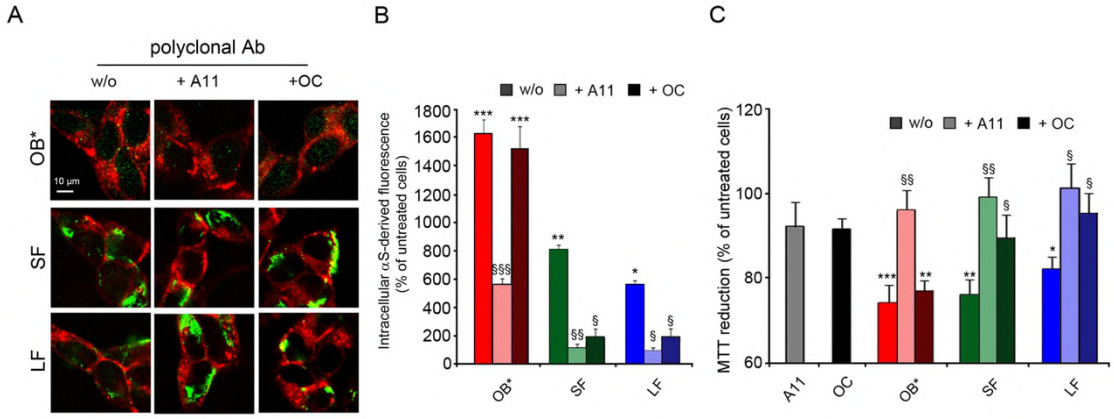

Figure 35 - Analysis of neurotoxic αS species with antibodies and confocal microscopy. (A) Representative confocal scanning microscope images showing the median sections of SH-SY5Y cells treated for 24 h with the indicated αS species at 0.3 μM (monomer equivalents), in the absence or presence of A11 and OC antibodies (1:2.5 molar ratio). Red and green fluorescence indicates the cell membranes and the αS species revealed with polyclonal anti-αS antibodies (ab52168), respectively. **(B)** The results of a semi-quantitative analysis of the green fluorescence signal derived from intracellular αS species relative to the images showed in panel A. The intracellular αS-derived fluorescence is expressed as the percentage of untreated cells. (**C**) MTT reduction in SH-SY5Y cells treated for 24 h with the indicated αS species at 0.3 μM (monomer equivalents) in the absence or presence of A11 and OC antibodies (1:2.5 molar ratio).

Experimental errors are S.E.M. Samples were analysed by one-way ANOVA followed by Bonferroni's multiple comparison test relative to untreated cells (*P < 0.05, **P < 0.01, ***P < 0.001) and to cells treated with the αS species without antibodies (§P < 0.05, §§P < 0.01, §§§P < 0.001). 200–250 cells (**A-B**), and 150.000-200.000 cells **(C)** were analysed per condition in total.

Moreover, a plot of the degree of MTT reduction measured in the previously reported different conditions against the fraction of internalized αS species using the data obtained for OB*, SF and LF in the absence or in the presence of the A11 and OC antibodies, revealed a very significant negative correlation (r = 0.85, p < 0.001) (**Figure 36**).

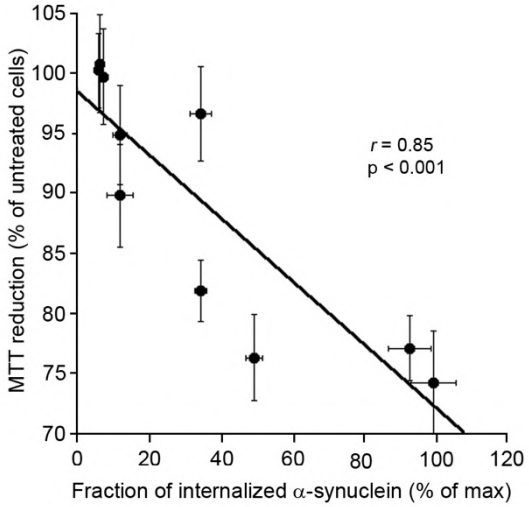

Figure 36 - Dependence of MTT reduction on the αS internalization in cells treated with αS species. MTT reduction values reported in **Figure 35C** plotted against the αS internalization-derived fluorescence values reported in **Figure 35B**, relative to cells treated with OB*, SF and LF in the absence or in the presence of A11 and OC antibodies (1:2.5 molar ratio). The fraction of internalized αS species is expressed as the percentage of the maximum fluorescence found in cells treated with OB*.

Section II

In the first part of this study, we showed that isolated oligomers (OB*), rich in β-sheet secondary structure and with high solvent-exposed hydrophobic surface, are highly toxic to neuronal cells. We also demonstrated that amyloid fibrils, referred to as SF and LF, impair neuronal functionality thanks to their ability to release small oligomeric assemblies upon the interaction with cellular membranes.

Taking into account these evidences, in the second part of this study we focused on the detailed analysis of the ability of toxic αS assemblies to interact with neuronal membranes, thus inducing their disruption and the subsequent Ca^{2+} dysregulation, a crucial early event in the pathogenesis of PD. We also investigated the involvement of the various membrane components, in particular the exposed proteins, on the interaction of the different αS species with the plasma membrane. Our analysis showed that the removal of the proteins exposed on the cell membrane transiently delayed the early Ca^{2+} influx, but not the sustained late one caused by αS oligomers in neuronal cells. In particular, OB* accumulate on the plasma membrane in close proximity of PrP^C, subsequently inducing an increase of intracellular Ca^{2+} influx in cells by both channel-independent and channel-dependent mechanisms. A prompt and transient Ca^{2+} influx was triggered by NMDARs, followed by a massive ionic dysregulation probably due to the disruption of the plasma membrane integrity. Accordingly, the pharmacological inhibition of NMDARs, as well as PrP^C blockade, caused a transient delay in the influx of Ca^{2+} ions. In contrast, αS fibrils caused Ca^{2+} dyshomeostasis with slower kinetics with respect to oligomers, and the ionic alterations were not rescued by the blockade of NMDARs or the removal of the exposed proteins in neuronal membranes.

Overall, the data accumulated in the second part of this work shed light into the interplay between αS aggregates and the plasma membrane of neuronal cells, thus expanding the range of molecular targets for therapeutic intervention in PD.

3.10 αS species show different abilities to interact with neuronal membranes

The different cytotoxicity evoked by αS OB* and fibrils seems to be related to their distinct ability to interact with target cells. To corroborate this hypothesis, we evaluated the different binding affinity of OB*, SF and LF to cellular membranes. Briefly, the plasma membranes (red channel) and αS species (green channel) were counterstained and analysed at the apical sections parallel to the coverslip by confocal scanning microscopy (**Figure 37A**). After 10 min of treatment at 0.3 μM (monomer equivalents), OB* showed a higher colocalization with cellular membranes (49.7±3.4%), with respect to SF and LF (26,2±1.2% and 8,7±1.7%, respectively) (**Figure 37B**). To further define the early phases of membrane interaction, and to clarify the involvement of the different membrane components, we firstly removed the proteins exposed on the outer surface of the plasma membrane by incubating the cells for 10 min with 0.05% trypsin on ice; SH-SY5Y cells were then treated with αS species for 10 min at 0.3 μM (monomer equivalents). Importantly, the pre-treatment with diluted trypsin exclusively led to the removal of the exposed proteins, without affecting cell viability (data not shown). Our results showed that trypsin pre-treatment significantly reduce the interaction of OB* and SF with the plasma membrane (~ 60% and 40%, respectively), without affecting the ability of LF to colocalize with the cellular surface (**Figure 37A,B**). Given the previously reported ability of αS to interact with the monosialoganglioside GM1 (Martinez *et al*., 2007), we investigated its possible involvement in the interaction of the various αS assemblies with the plasma membrane by incubating the cells for 48 h in culture medium containing 25 μM PDMP, a glucosylceramide synthase inhibitor that blocks the natural synthesis of GM1. Its removal resulted in a quite significant reduction in the interaction of OB* with target cells (~20%), without affecting those of SF and LF (**Figure 37A,B**). The combined action of GM1 depletion and exposed proteins removal significantly affected the ability of SH-SY5Y cells to recruit OB* and SF (by ~ 80% and 45%, respectively), as reported in **Figure 37B**.

Overall, these results indicate that the ability of different αS species, and in particular OB*, to interact with target cells depends not only on their specific structural properties (surface-exposed hydrophobicity and β-sheet content), but also on the biochemical features of the membranes they interact with, and primarily on their protein composition.

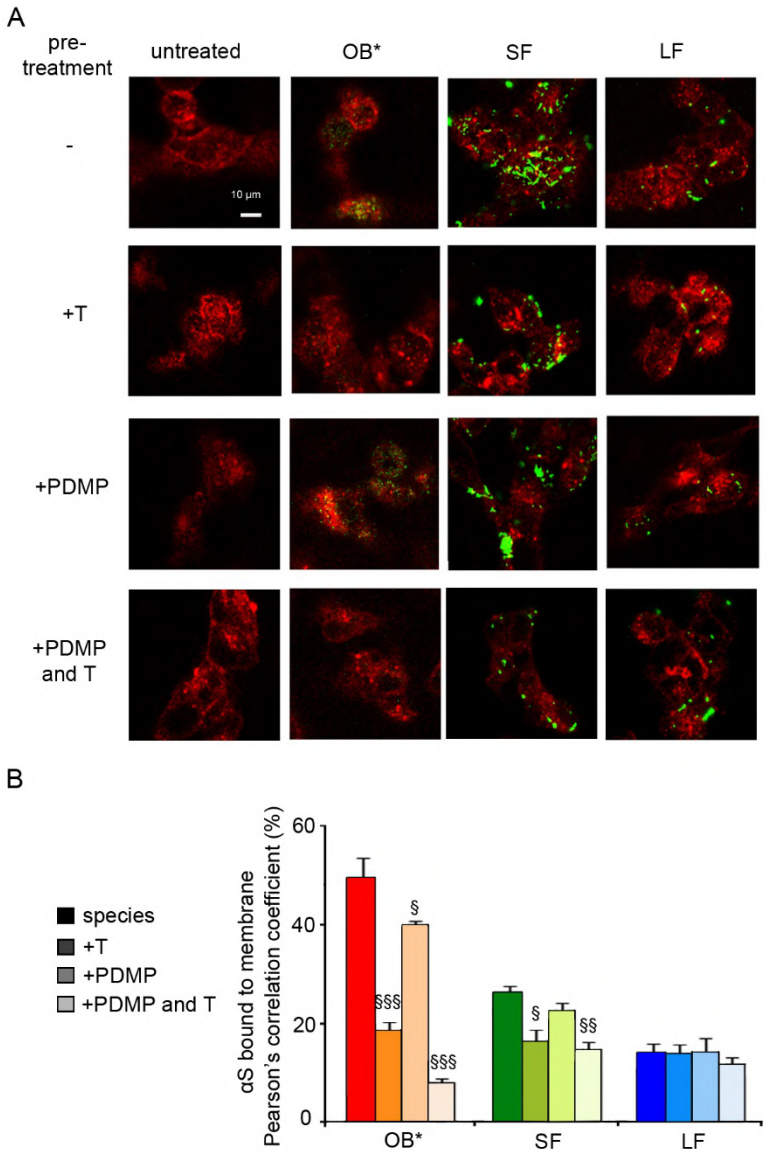

Figure 37 - Analysis of the interaction of the different αS species with the plasma membrane. (**A**) Representative confocal scanning microscope images of the apical sections of SH-SY5Y cells treated for 10 min with αS species at 0.3 µM (monomer equivalents) in the absence or in the presence of a pre-treatment with 0.05% trypsin (T) for 10 min, or with 25 µM PDMP for 48 h, or with 0.05% T and PDMP. Red and green fluorescence indicates the cell membranes and the αS species revealed with polyclonal anti-αS antibodies (ab52168), respectively. (**B**) The histograms show the colocalization on regions of interest (30-32 cells) using the ImageJ (NIH, Bethesda, MD, USA) and JACOP plugin (rsb.info.nih.gov) software. Experimental errors are S.E.M. Samples were analysed by one-way ANOVA followed by Bonferroni's multiple comparison test relative to cells treated with αS species without any pre-treatment (§$P < 0.05$, §§$P < 0.01$, §§§$P < 0.001$).

The evidence of an involvement of membrane proteins in the interaction of OB* with the plasma membrane was also confirmed by the analysis of the ability of αS species to be

internalized into the cytosol of SH-SY5Y cells. After 60 min of treatment at 0.3 μM (monomer equivalents) with OB*, SF and LF, the plasma membranes (red channel) and αS species (green channel) were counterstained and then analysed by confocal scanning microscopy. High intracellular protein levels were detected with the rabbit anti-αS polyclonal antibodies at the median planes parallel to the coverslip for OB* (1300±100%), with respect to SF and LF (500±100% and 270±40%, respectively), relative to the fluorescent signal of endogenous αS in untreated cells, assumed to be 100% (**Figure 38A**), in accordance to the previously reported data showed in **Section 1** (**Figure 26**). On the other hand, trypsin pre-treatment significantly reduced the internalization of OB*, without affecting that of SF and LF, as reported in **Figure 38A**. Similar results were obtained by examining the ability of αS species to disrupt plasma membrane integrity of SH-SY5Y cells, by monitoring the release of the fluorescent probe calcein-AM, previously loaded into the cells. Following a treatment of 10 min with 0.05% trypsin on ice, αS species were added to the culture medium of SH-SY5Y cells at 0.3 μM (monomer equivalents) (**Figure 38B**). After 60 min, we observed that OB* and, to a lesser extent, SF, generated a significant leakage of calcein (67,9±3,6% and 42,3±6,1% respectively; **Figure 38B**), in good agreement with previously reported data (**Section 1**, **Figure 25A**). This effect was significantly prevented by the removal of exposed membrane proteins in cells treated with OB*, in which we observed a reduction of calcein leakage of ~ 40%. Also in this case, we did not observe any significant change in cells treated with SF and LF in the presence or absence of membrane proteins (**Figure 38B**).

Taken together, these data indicate that the mechanism by which αS species interact with the cells is very different, and suggest that a specific membrane protein(s) might be involved in the early interaction of the oligomers but not fibrils with neuronal cells.

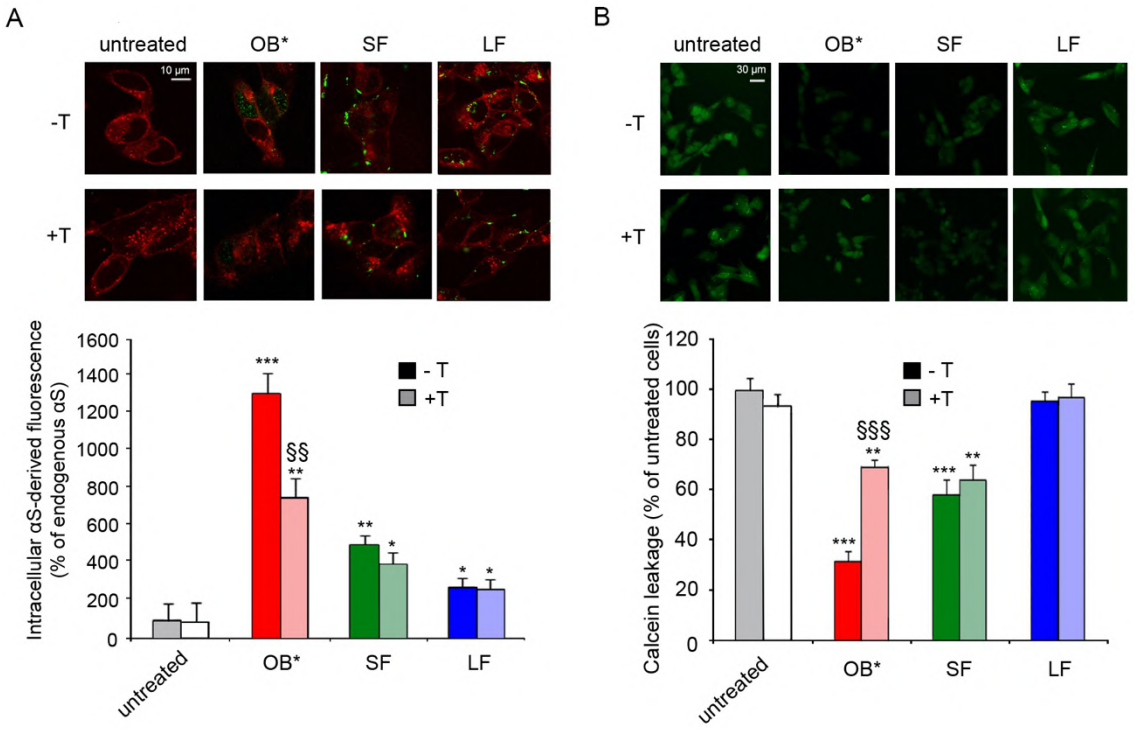

Figure 38 - Involvement of exposed membrane proteins in the internalization of the different αS species and in their ability to permeabilize cellular membranes. (A) Representative confocal scanning microscope images showing the median sections of SH-SY5Y cells treated for 60 min with the indicated αS species at 0.3 µM (monomer equivalents), in the absence or in the presence of a pre-treatment for 10 min with 0.05% trypsin (T) on ice. Red and green fluorescence indicates the cell membranes and the αS species revealed with rabbit anti-αS antibodies (ab52168), respectively. The results of a semi-quantitative analysis of the intracellular αS-derived fluorescence, expressed as the percentage of endogenous αS fluorescence. **(B)** Representative confocal microscope images showing SH-SY5Y cells loaded with the calcein-AM probe for 30 min and then treated for 60 min with the indicated αS species at 0.3 µM (monomer equivalents). The results of a semi-quantitative analysis of the calcein-derived green fluorescence signal, expressed as the percentage of the values for untreated cells. Experimental errors are S.E.M. Samples were analysed by one-way ANOVA followed by Bonferroni's multiple comparison test relative to untreated cells (*$P < 0.05$, **$P < 0.01$, ***$P < 0.001$), or to cells treated with the same αS species, without pre-treatment with trypsin (§§$P < 0.01$, §§§$P < 0.001$). 200–250 cells were analysed per condition in total.

In order to better characterize the involvement of GM1 in the interaction of the analysed αS species with the plasma membrane of SH-SY5Y cells, we evaluated the degree of colocalization between αS aggregates and such ganglioside. GM1 (red channel) was labelled with the cholera toxin subunit B (CTX-B), a component of a heat-labile enterotoxin produced by *Vibrio cholerae*, and αS aggregates (green channel) were counterstained with the rabbit anti-αS polyclonal antibodies (ab52168). SH-SY5Y cells were treated with the various αS species for 10 min at a concentration of 0.3 μM (monomer equivalents). The degree of colocalization, reported as the percentage values of the Pearson's correlation coefficient, was found to be 32.17±3.40% for OB*, 39.43±5.11% for SF and 22.0±1.67% for LF (**Figure 39A,B**). The modest degree of colocalization with all the three species could suggest a minor involvement of this monoganglioside in the binding of αS aggregates to the plasma membrane at early incubation times with the cells.

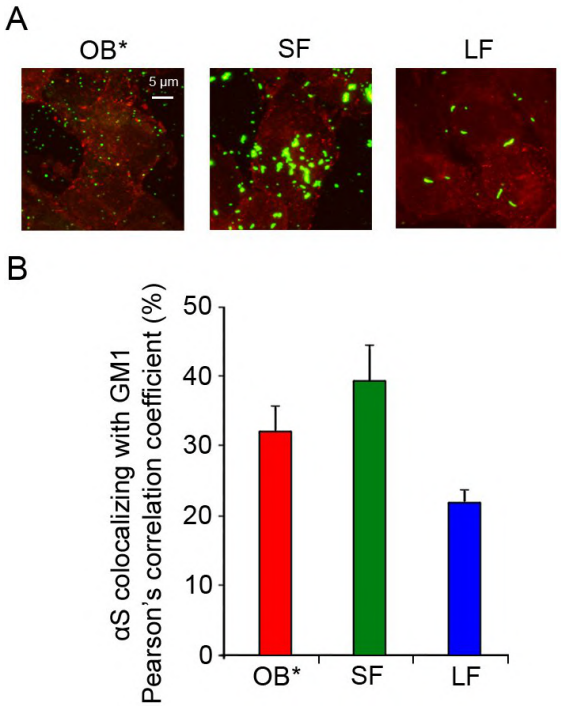

Figure 39 - Analysis of the colocalization of the different αS species with GM1. (**A**) Representative confocal microscope images of SH-SY5Y cells treated for 10 min with the indicated αS species at 0.3 μM (monomer equivalents), in which the GM1 was counterstained with CTX-B. (**B**) Histogram showing the percentage of colocalization on regions of interest (30-32 cells) using the ImageJ (NIH, Bethesda, MD, USA) and JACOP plugin (rsb.info.nih.gov) software. Experimental errors are S.E.M.

3.11 Different αS species induce Ca^{2+} dyshomeostasis by distinct molecular mechanisms

Given the evidence of a major involvement of membrane proteins in the early interaction of αS species (OB* and, to a lesser extent, SF) with target cells, we further explored the possible implication of such proteins in αS-mediated Ca^{2+} dyshomeostasis. Thus, we incubated the cells for 10 minutes with 0.05% trypsin on ice, and then with αS species for different lengths of time (0, 5, 10, 15, 30, 60, 120 and 180 min, respectively) at 0.3 μM (monomer equivalents). Confocal microscopy images showed that trypsin caused a significant reduction of Ca^{2+} influx until 60 min of treatment with OB*, as compared to cells not pre-treated with trypsin (**Figure 40A**). After longer times of exposure this effect was no more observed, thus confirming that membrane proteins could be involved in the early phases of Ca^{2+} entry induced by OB*. We then plotted the normalized Ca^{2+}-derived fluorescence, quantified as the percentage of the value measured for untreated cells, as a function of time. In good agreement with previously reported data, we obtained an exponential kinetics for OB* (**Section 1**, **Figure 31C**), with the maximum increase after 60 min, whereas a sigmoidal one was observed in cells pre-treated with trypsin, as reported in **Figure 40C**. In this case, the half-maximal increase in Ca^{2+}-derived fluorescence was estimated to occur after 77.6±17.3 min after treatment with OB*. On the other hand, the removal of the exposed membrane proteins did not significantly affect the influx of Ca^{2+} ions evoked by SF and LF, with sigmoidal kinetics, neither at early nor at longer incubation times with human neuroblastoma cells (**Figures 40B,D and 41A,B**). These data suggest that the mechanism by which αS species cause Ca^{2+} dysregulation in neuronal cells is different and that a specific membrane protein(s) might be involved in the early Ca^{2+} dysregulation evoked by the oligomers, but not by fibrillar assemblies.

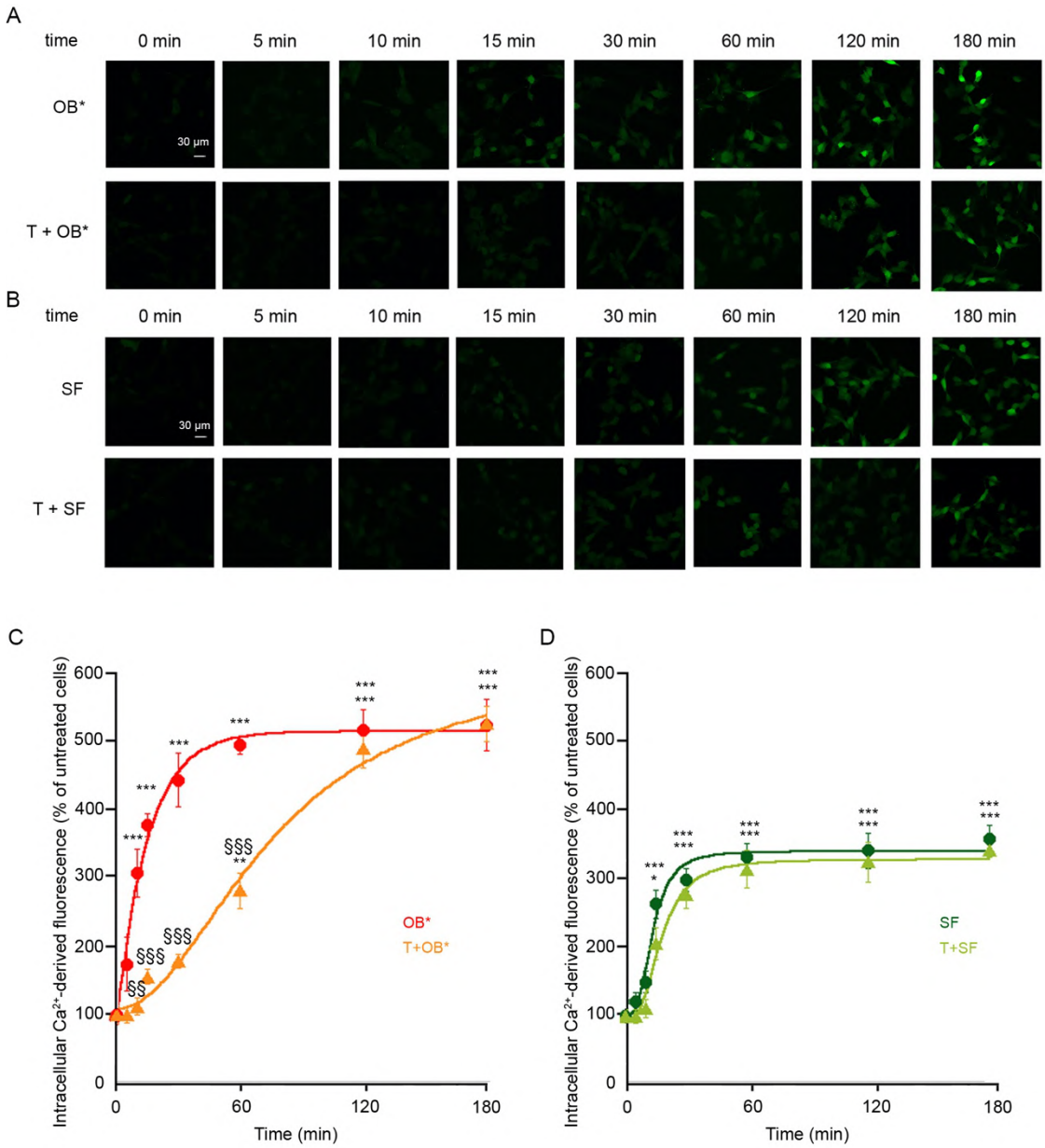

Figure 40 - Effect of trypsin pre-treatment on Ca^{2+} influx induced by OB* and SF. (**A**) Representative confocal microscope images showing SH-SY5Y pre-treated for 10 min with 0.05% trypsin (T) and then treated for the indicated lengths of time with the indicated αS species at a concentration of 0.3 µM (monomer equivalents). Cells were then loaded with Fluo-4 AM probe. (**B**) The results of a semi-quantitative analysis of Ca^{2+}-derived fluorescence, expressed as the percentage of the values for untreated cells. The continuous lines through the experimental points represent the best fits to exponential and sigmoidal functions, reported in detail in the "Materials and Methods" section. Experimental errors are S.E.M. Samples were analysed by one-way ANOVA followed by Bonferroni's multiple comparison test relative to untreated cells (*P < 0.05, **P < 0.01, ***P < 0.001), or relative to cells treated with OB* for the same length of time, without pre-treatment with trypsin (§§P < 0.01, §§§P < 0.001). 200–250 cells were analysed per condition in total.

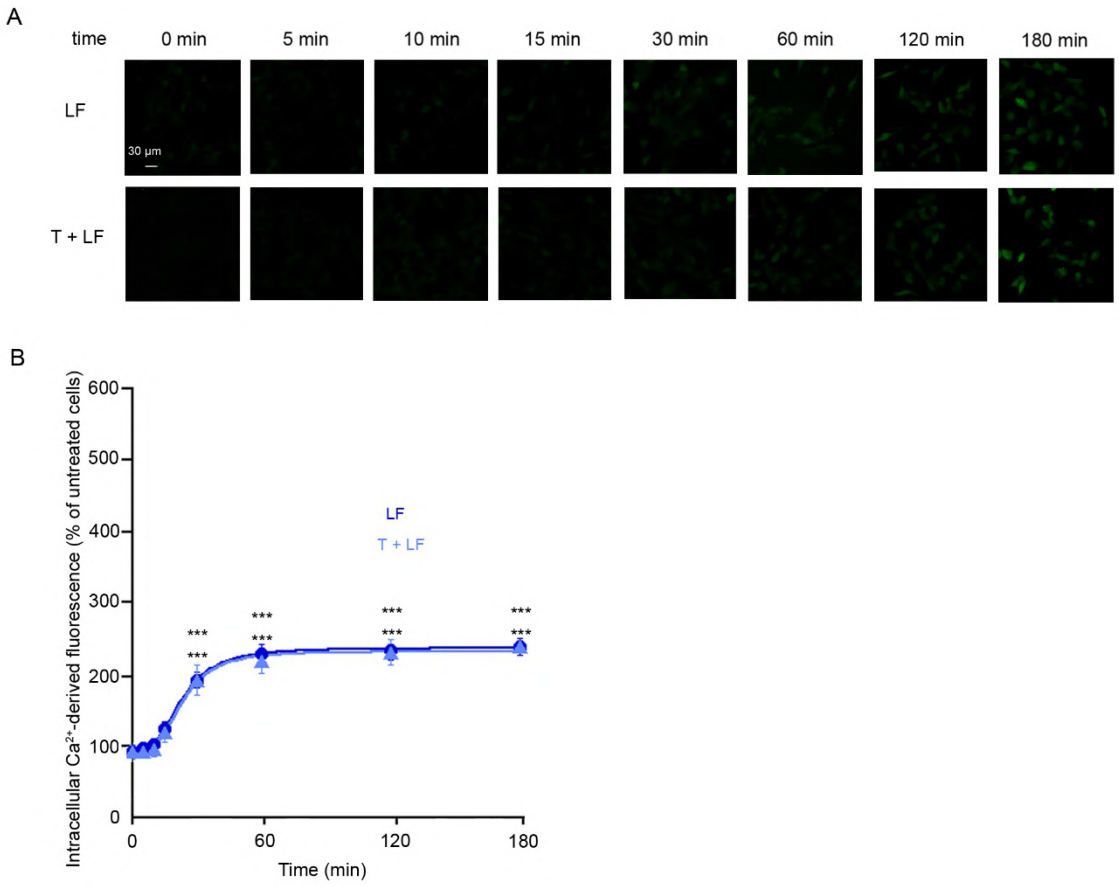

Figure 41 - Effect of trypsin pre-treatment on Ca^{2+} influx induced by LF. (**A**) Representative confocal microscope images showing SH-SY5Y pre-treated for 10 min with 0.05% trypsin (T) and then treated for the indicated lengths of time with LF at a concentration of 0.3 µM (monomer equivalents). Cells were then loaded with Fluo-4 AM probe. (**B**) The results of a semi-quantitative analysis of Ca^{2+}-derived fluorescence was expressed as the percentage of the values for untreated cells. The continuous lines through the experimental points represent the best fits to a sigmoidal function, reported in detail in the "Materials and Methods" section. Experimental errors are S.E.M. Samples were analysed by one-way ANOVA followed by Bonferroni's multiple comparison test relative to untreated cells (***P < 0.001). 200–250 cells were analysed per condition in total.

3.12 αS species colocalize with specific glutamatergic receptors

It has been reported that misfolded αS protein oligomers are able to cause a massive increase in intracellular Ca^{2+}, possibly with a pore-forming mechanism (Danzer *et al*., 2007), or an alteration in membrane conductance due to leak channel formation (Feng *et al*., 2010), consistent with *in vitro* evidence demonstrating the formation of pore-like structures in synthetic membranes (Lashuel *et al*., 2002). Some studies focused on the interaction between αS species and the ionotropic glutamate-receptors NMDARs,

associated to the impairment of hippocampal functions (Diógenes *et al*., 2012; van Diegglen *et al*., 2019). On the other hand, other researchers identified the VOCs as main targets of αS toxic assemblies, whose interaction could be responsible for a massive increase in intracellular Ca^{2+} levels (Adamczyk and Strosznajder, 2006; Ronzitti *et al*., 2014). Given the evidence reported above about a major involvement of exposed membrane proteins in the early phases of Ca^{2+} influx induced by OB* and not by fibrils, we decided to focus the study on such oligomeric assemblies. Thus, we analysed the possible involvement of VOCs or glutamate receptors-channels AMPARs and NMDARs in the mechanism of Ca^{2+} entry induced by αS aggregates, by incubating SH-SY5Y cells with specific channels inhibitors (mem, CNQX and Cd^{2+} ions) and then with OB* (0.3 μM, monomer equivalents) (**Figure 42A,B**). Mem is a low-affinity antagonist of NMDARs, CNQX is a competitive antagonist of AMPARs and Cd^{2+} ions are competitive blockers of VOCs. Briefly, SH-SY5Y cells were pre-treated for 60 min with 10 μM mem, 5.0 μM CNQX, or with 10 μM Cd^{2+} ions, and then treated for 15 min with OB* (0.3 μM, monomer equivalents). Pre-treatment with mem and, to a lesser extent, CNQX, determined a significant decrease in Ca^{2+}–associated fluorescence (**Figure 42A,B**). These data suggested that the blockade of glutamate receptors-channels was able to impair the early Ca^{2+} influx evoked by αS species, indicating a possible involvement of NMDARs and, to a lesser extent, AMPARs in this stage of Ca^{2+} dyshomeostasis. Interestingly, Cd^{2+} ions were not able to decrease the influx of Ca^{2+} ions induced by the oligomers, thus suggesting that VOCs are not involved in the early phases of such process. To gain deeper insight on αS binding to NMDARs embedded into the plasma membrane, we investigated by confocal microscopy whether these assemblies were able to bind to the plasma membrane in close proximity to such receptor-channels in neuronal cells, where they are particularly abundant. Our results showed a high degree of colocalization of OB* (green channel) with NMDARs (red channel) in both primary rat cortical neurons and SH-SY5Y cells (56.0±3% and 58.01±4.41%, respectively) (**Figure 42C**). The degree of colocalization with the NMDARs was also evaluated for fibrillar assemblies in SH-SY5Y cells and, unexpectedly, it was found to be 61.0±3.27% and 48.0±4.43% in cells treated with SF and LF, respectively, as reported in **Figure 42D**.

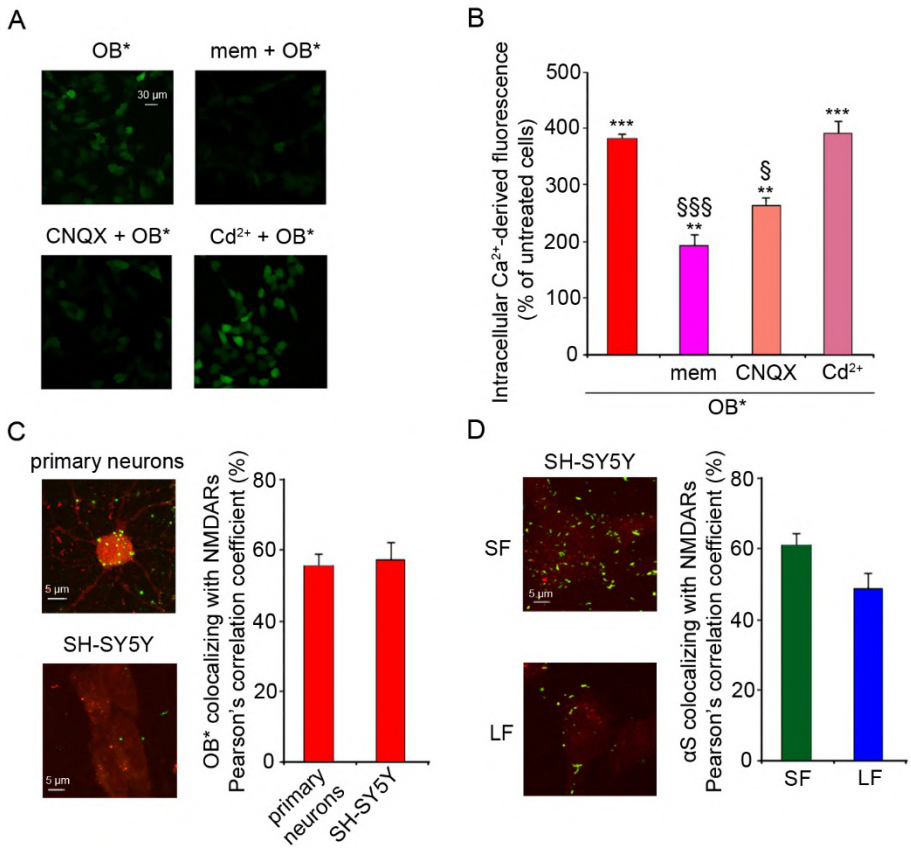

Figure 42 - Effect of the pre-treatment with channels inhibitors on Ca^{2+} influx induced by αS species. (A) Representative confocal microscope images showing SH-SY5Y pre-treated for 60 min with 10 µM mem, 5 µM CNQX and 10 µM Cd^{2+} and then treated for 15 min with OB* at 0.3 µM (monomer equivalents). Cells were then loaded with Fluo-4 AM probe. (**B**) The results of a semi-quantitative analysis of the Ca^{2+}-derived green fluorescence signal, expressed as the percentage of the values for untreated cells. Experimental errors are S.E.M. Samples were analysed by one-way ANOVA followed by Bonferroni's multiple comparison test relative to untreated cells (*P < 0.05, ***P < 0.001), or relative to cells treated with OB*, without pre-treatment with channels inhibitors (§P < 0.05, §§§P < 0.001). 200-250 cells were analysed per condition in total. (**C-D**) Representative confocal microscope images of primary neurons and SH-SY5Y cells treated with OB* (**C**) and with SF and LF (**D**) for 10 min. Red and green fluorescence indicates the NMDARs, detected with mouse anti-NMDARs monoclonal antibodies (320700) and the αS species, revealed with rabbit anti-αS polyclonal antibodies (ab52168), respectively. The histograms show the percentage of colocalization on regions of interest (30-32 cells) using the ImageJ (NIH, Bethesda, MD, USA) and JACOP plugin (rsb.info.nih.gov) software. Experimental errors are S.E.M.

3.13 NMDARs are involved in the early Ca^{2+} dysregulation evoked by αS oligomers

Given the significant inhibition of Ca^{2+} entry induced by the OB* following the pre-treatment with mem, we then focused on the study of NMDARs. Thus, we carried out a time-course analysis of Ca^{2+} dyshomeostasis in SH-SY5Y cells exposed to αS species for different lengths of time (0, 5, 10, 15, 30, 60 and 180 min), after a pre-treatment of 60 min with 10 μM mem (**Figure 43A**). We then plotted the normalized Ca^{2+}-derived fluorescence, quantified as the percentage of the value measured for untreated cells, as a function of time (**Figure 43C**). Interestingly, a lag phase in the fluorescence spike was observed in cells exposed to mem and then treated with OB* in the first 60 min, and the half-maximal increase in Ca^{2+}-derived fluorescence was estimated to occur after 44.3±7.6 min after treatment with OB*. This time is significantly lower than that observed after the removal of the exposed membrane proteins with trypsin (77.6±17.3 min); this evidence suggests that other membrane proteins, not only this specific Ca^{2+} channel, could be involved in the mechanism(s) of Ca^{2+} dysregulation induced by OB* in the first 60 min of treatment. A slight but not significant effect of mem was observed in cells exposed to SF (**Figure 43B**), as noted also in the kinetic plots (**Figure 43D**), despite the high degree of colocalization observed with NMDARs (**Figure 42D**). Finally, no effect was detected in cells treated with LF (**Figure 44A,B**), excluding the involvement of NMDARs in Ca^{2+} dyshomeostasis triggered by such species. These findings suggest that the Ca^{2+} influx induced by protein misfolded oligomers with a large solvent-exposed hydrophobicity and high β-sheet content occurs in two steps: a first rapid step, where Ca^{2+} entrance increases due to glutamatergic receptor stimulation, followed by a delayed one, where a channel-independent mechanism, possibly resulting from bilayer disassembly, is involved. On the contrary, the dysregulation of Ca^{2+} homeostasis evoked by fibrils seems to be exclusively associated to a receptor-independent mechanism of interaction with the plasma membrane.

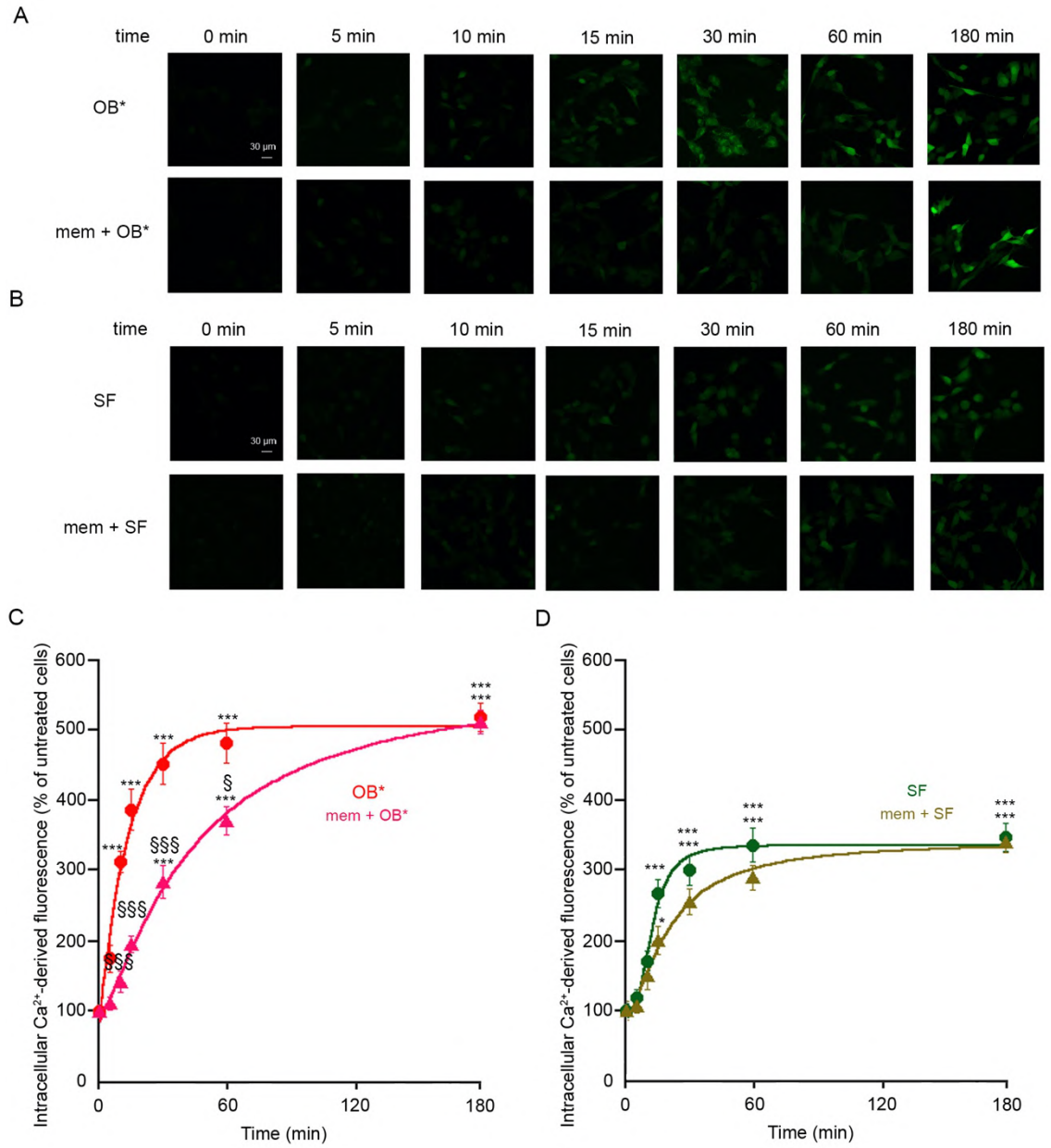

Figure 43 - Effect of mem pre-treatment on Ca^{2+} influx induced by OB* and SF. (**A**) Representative confocal microscope images showing SH-SY5Y pre-treated for 60 min with 10 µM mem and then treated for the indicated lengths of time with the indicated αS species at a concentration of 0.3 µM (monomer equivalents). Cells were then loaded with Fluo-4 AM probe. (**B**) The results of a semi-quantitative analysis of Ca^{2+}-derived fluorescence, expressed as the percentage of the values for untreated cells. The continuous lines through the experimental points represent the best fits to exponential and sigmoidal functions, reported in detail in the "Materials and Methods" section. Experimental errors are S.E.M. Samples were analysed by one-way ANOVA followed by Bonferroni's multiple comparison test relative to untreated cells (*P < 0.05, ***P < 0.001), or relative to cells treated with OB* for the same length of time, without pre-treatment with trypsin (§P < 0.05, §§§P < 0.001). 200–250 cells were analysed per condition in total.

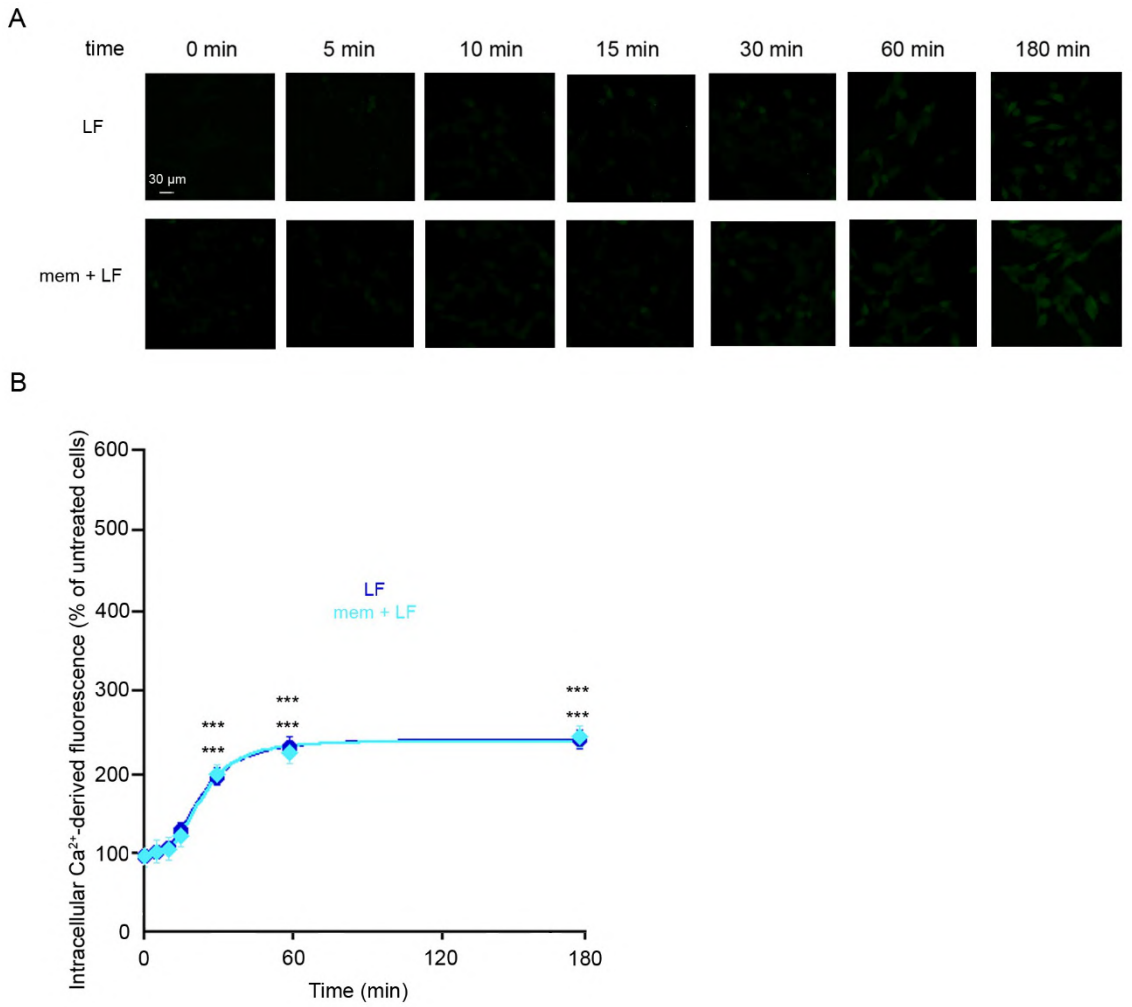

Figure 44 - Effect of mem pre-treatment on Ca^{2+} influx induced by LF. (**A**) Representative confocal microscope images showing SH-SY5Y pre-treated for 60 min with 10 µM mem and then treated for the indicated lengths of time with LF at a concentration of 0.3 µM (monomer equivalents). Cells were then loaded with Fluo-4 AM probe. (**B**) The results of a semi-quantitative analysis of Ca^{2+}-derived fluorescence, expressed as the percentage of the values for untreated cells. The continuous lines through the experimental points represent the best fits to a sigmoidal function, reported in detail in the "Materials and Methods" section. Experimental errors are S.E.M. Samples were analysed by one-way ANOVA followed by Bonferroni's multiple comparison test relative to untreated cells (***P < 0.001). 200–250 cells were analysed per condition in total.

Taking into account the evidence of a role of NMDARs on Ca^{2+} dysregulation evoked by OB*, we performed a dose-response analysis of the blockade of such channels (**Figure 45A**). SH-SY5Y cells were pre-treated with increasing concentrations of mem (0, 0.1, 0.5, 1.0, 5.0, 10.0, and 50.0 μM) for 60 min, and then treated with OB* for 15 min (**Figure 45A, upper panel**). We then plotted the normalized Ca^{2+}-derived fluorescence, quantified as the percentage of the value measured in untreated cells, as a function of mem concentration (**Figure 45B, left plot**). The blockade of the NMDARs was able to produce a significant and dose-dependent decrease in Ca^{2+} influx evoked by OB* (**Figure 45A upper panel, B left plot**). Furthermore, we estimated the half maximal inhibitory concentration (IC_{50}) of such blockade, that resulted to be 1.65±1.22 μM. The same experiment was performed with SF, but neither high nor low doses of mem were able to affect significantly the influx of Ca^{2+} ions from the extracellular medium after a treatment of 15 min (**Figure 45A lower panel, B right plot**); thus, it was not possible to calculate the IC_{50} in such conditions. Taken together, these results confirm the involvement of NMDARs in the early Ca^{2+} entry evoked by oligomers, but not fibrils.

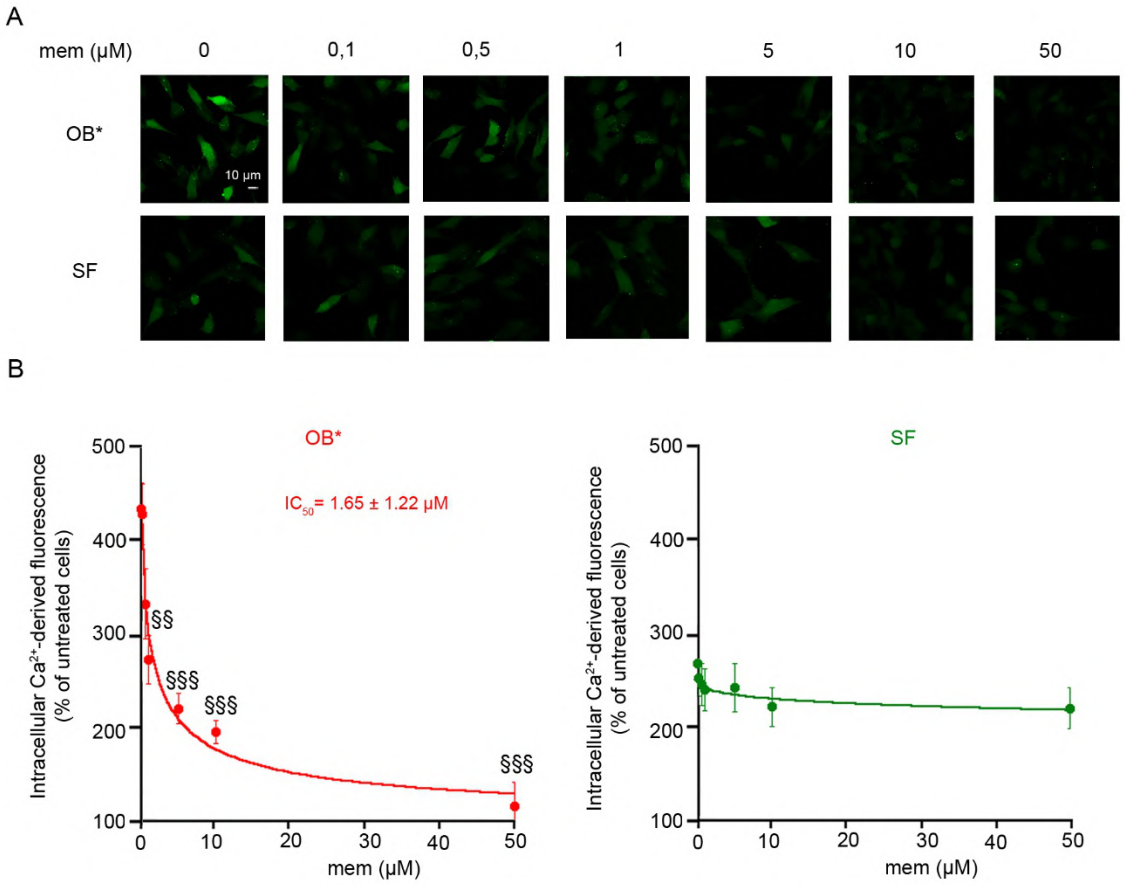

Figure 45 - Effect of mem pre-treatment on Ca^{2+} influx induced by OB* and SF. (**A**) Representative confocal microscope images showing SH-SY5Y pre-treated for 60 min with increasing concentrations of mem (0.1 μM, 0.5 μM, 1.0 μM, 5.0 μM, 10 μM and 50 μM), and then treated for 15 min with the indicated αS species at a concentration of 0.3 μM (monomer equivalents). Cells were then loaded with Fluo-4 AM probe. (**B**) The results of a semi-quantitative analysis of Ca^{2+}-derived fluorescence, expressed as the percentage of the values for untreated cells. The continuous red line through the experimental points represents the best fit to a sigmoidal function, reported in detail in the "Materials and Methods" section. Experimental errors are S.E.M. Samples were analysed by one-way ANOVA followed by Bonferroni's multiple comparison test relative to cells treated with OB* for the same length of time, without pre-treatment with mem (§§P < 0.01, §§§P < 0.001). 200–250 cells were analysed per condition in total.

3.14 PrP^C mediates the recruitment of αS oligomers at the plasma membrane of neuronal cells

For a more exhaustive comprehension of the molecular mechanisms leading to Ca^{2+} dysregulation evoked by the OB*, we analysed in more detail their interaction with the plasma membrane. In particular, we evaluated the possible role of PrP^C in such interaction. We first assessed their degree of colocalization, after treating SH-SY5Y cells with OB* for 10 min at 0.3 μM (monomer equivalents). The percentage value of the Pearson's correlation coefficient resulted to be 69.17±4.20% (**Figure 46A**); we then removed the proteins exposed on the cell membrane surface by incubating SH-SY5Y cells for 10 minutes with 0.05% trypsin, and then we treated SH-SY5Y cells with OB* for 10 min. Such treatment significantly reduced the degree of colocalization with PrP^C that resulted to be 31.19±5.40% (**Figure 46A**). We also depleted the cellular membrane of GM1 by incubating the cells for 48 h in culture medium containing 25 μM PDMP, and then with OB* for 10 min; this treatment resulted in a slight, but not significant, reduction in the degree of colocalization between OB* and PrP^C (58.66±4.75%) (**Figure 46A**). Taken together, these data are in good agreement with those reported in **Figure 37**, in which we examined the involvement of the different membrane components in the binding of the various αS assemblies. To better assess this point, we analysed in more detail the specific role of the PrP^C in the mechanism of membrane binding of OB*. Briefly, we pre-treated primary rat cortical neurons and SH-SY5Y cells with 1:250 diluted anti PrP^C mouse monoclonal antibodies for 30 min and then we treated cells with OB* at 0.3 μM for 10 min. Thus, we evaluated the degree of colocalization of OB* with target cells. The plasma membranes (red channel) and OB* (green channel) were counterstained and analysed at the apical sections parallel to the coverslip by confocal scanning microscopy (**Figure 46B**). A large number of species (taken as 100%) were observed to be associated with the plasma membranes of both primary neurons and SH-SY5Y cells, in good agreement to previously reported data (**Figure 37**) but their number was significantly decreased in the presence of the anti PrP^C antibody (by ~ 40%) (**Figure 46B**). These data clearly indicate that the cellular prion protein is an important mediator of the recruitment of OB* at the surface of neuronal membranes at early incubation times with the cells.

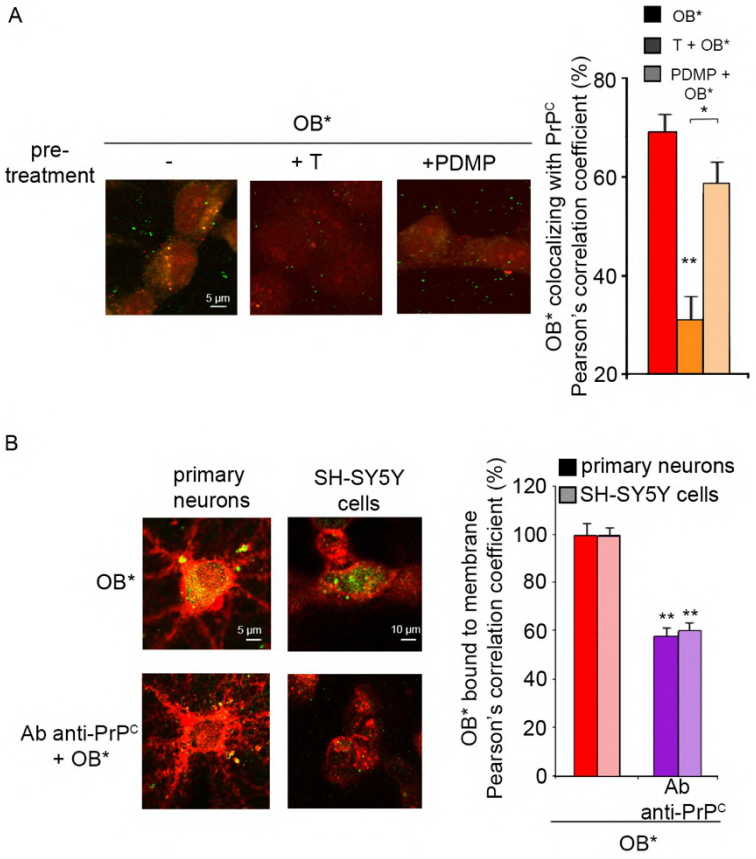

Figure 46 - OB* colocalize with PrP^C. **(A)** Representative confocal microscope images of SH-SY5Y cells treated with OB* for 10 min, in the absence or presence of a pre-treatment with 0.05% trypsin (T) for 10 min, or with 25 µM PDMP for 48 h. Red and green fluorescence indicates the PrP^C detected with mouse anti-PrP^C monoclonal antibodies (Ab anti-PrP^C, sc47730) and the OB*, revealed with rabbit anti-αS polyclonal antibodies (ab52168), respectively. (**B**) Representative confocal scanning microscope images of the apical sections of SH-SY5Y cells treated for 10 min with OB* at 0.3 µM (monomer equivalents) in the absence or presence of a pre-treatment with 1:250 diluted anti-PrP^C antibodies. Red and green fluorescence indicates the cell membranes and the OB*, detected with the rabbit anti-αS polyclonal antibodies (ab52168), respectively. The histograms show the colocalization on regions of interest (30-32 cells) using the ImageJ (NIH, Bethesda, MD, USA) and JACOP plugin (rsb.info.nih.gov) software. Experimental errors are S.E.M. Samples were analysed by one-way ANOVA followed by Bonferroni's multiple comparison test relative to cells treated with OB* without any pre-treatment, unless otherwise indicated (*$P < 0.05$, **$P < 0.01$).

3.15 PrP^C blockade partially prevents the early Ca^{2+} influx evoked by αS oligomers

We then assessed whether the blockade of the PrP^C could rescue the Ca^{2+} dysregulation induced by OB*. Thus, we pre-treated SH-SY5Y cells with 1:250 diluted mouse anti-PrP^C monoclonal antibodies for 30 min and then we treated cells with OB* at 0.3 μM for different lengths of time (0, 5, 10, 15, 30, 60 and 180 min) (**Figure 47A**). We then plotted the normalized Ca^{2+}-derived fluorescence, quantified as the percentage of the value measured for untreated cells, as a function of time, obtaining a sigmoidal kinetics in cells pre-treated with anti-PrP^C antibodies, as reported in **Figure 47B**. A lag phase in the fluorescence spike was observed in the first 30 min, and the half-maximal increase in Ca^{2+}-derived fluorescence was estimated to occur after 61.55±27 min after treatment with OB*. This time is intermediate between those previously reported after the removal of the exposed membrane proteins with trypsin (77.6±17.3 min) and after the pharmacological blockade of NMDARs (44.3±7.6 min). Taken together, these evidences suggest that different membrane proteins, in particular the PrP^C, are involved in the early interaction of αS oligomers with the membrane of target cells, thus influencing the prompt Ca^{2+} influx of which NMDARs are primary mediators. This step is then followed by an unspecific interaction with the neuronal membranes, responsible for the disassembly of the lipid bilayer, that causes in turn a channel-independent and sustained massive Ca^{2+} influx.

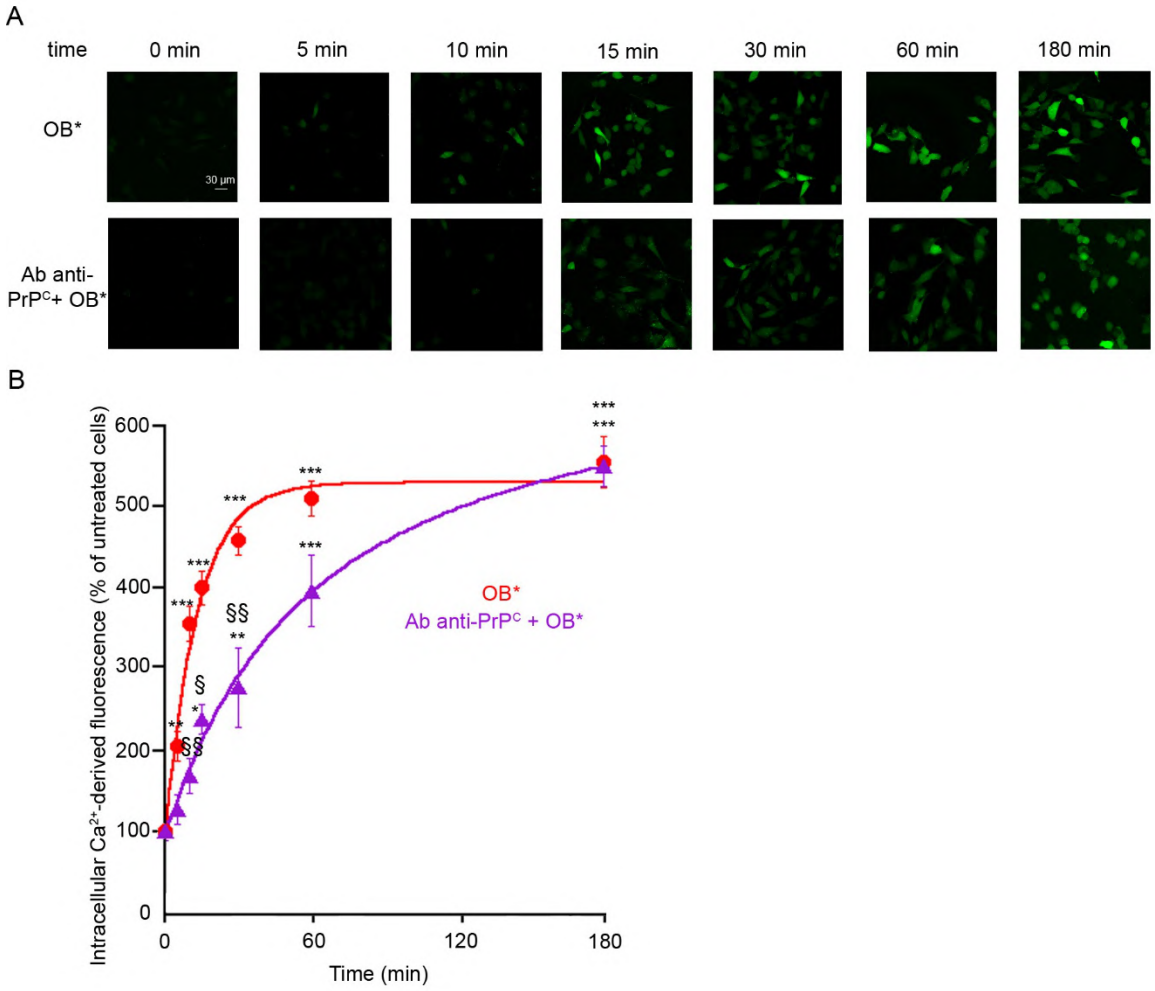

Figure 47 - Effect of PrP^C blockade on Ca^{2+} influx induced by OB*. (**A**) Representative confocal microscope images showing SH-SY5Y pre-treated for 30 min with 1:250 diluted mouse anti-PrP^C monoclonal antibodies (sc47730) and then treated for the indicated lengths of time with OB* at a concentration of 0.3 µM (monomer equivalents). Cells were then loaded with Fluo-4 AM probe. (**B**) The results of a semi-quantitative analysis of Ca^{2+}-derived fluorescence, expressed as the percentage of the values for untreated cells. The continuous lines through the experimental points represent the best fits to exponential and sigmoidal functions, reported in detail in the "Materials and Methods" section. Experimental errors are S.E.M. Samples were analysed by one-way ANOVA followed by Bonferroni's multiple comparison test relative to untreated cells (*$P < 0.05$, **$P < 0.01$, ***$P < 0.001$), or relative to cells treated with OB* for the same length of time, without pre-treatment with anti-PrP^C antibodies (§$P < 0.05$, §§$P < 0.01$). 200–250 cells were analysed per condition in total.

We finally tested whether PrP^C blockade with its specific antibody could reduce the impairment of mitochondrial functionality evoked by OB*, previously shown to occur (**Section 1, Figure 28**). SH-SY5Y cells were pre-treated for 30 min with 1:250 diluted

anti-PrP^C antibody, and then treated with OB* at 0.3 μM for 24 h. The antibody was also tested as a control (**Figure 48**). In the presence of OB*, the ability of neuroblastoma cells to reduce MTT resulted to be decreased to 75.54±6.02% with respect to untreated cells (taken as 100%), in good agreement with previously reported data (**Figure 28**). The pre-treatment with the anti-PrP^C antibodies did not induce any significant reduction of the cytotoxicity, as compared to cells treated with OB* (**Figure 48**). These data are in good agreement with those previously obtained from the analysis of Ca^{2+} dysregulation after prolonged times of exposure to the oligomers.

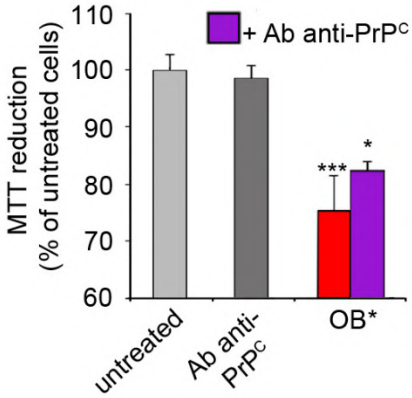

Figure 48 - Effect of PrP^C blockade on the cytotoxicity induced by OB*. MTT reduction in SH-SY5Y cells treated for 24 h with OB* at 0.3 μM (monomer equivalents) in the absence or presence of a pre-treatment with 1:250 diluted mouse anti-PrP^C monoclonal antibodies (Ab anti-PrP^C, sc47730). Experimental errors are S.E.M. Samples were analysed by one-way ANOVA followed by Bonferroni's multiple comparison test relative to untreated cells (*$P < 0.05$, and ***$P < 0.001$). 150.000-200.000 cells were analysed per condition in total.

4 DISCUSSION

α-Synucleinopathies are a subgroup of neurodegenerative diseases defined by the abnormal accumulation of insoluble aggregates, both in neurons and in glial cells, whose major component is the protein αS. Among them, PD is the most widespread; it is the second most common neurodegenerative disorder after AD, and it is characterized by the progressive loss of dopaminergic neurons in the SNpc (Dickson, 2012) with the resulting motor disturbances, such as bradykinesia, muscular rigidity, resting tremor, postural instability and gait impairment (Kalia *et al*., 2015).

This work is focused on αS, a natively unfolded protein that, under specific conditions, can undergo a complex aggregation process, leading to the formation of a wide range of assemblies such as oligomers, protofibrils and fibrils. Aggregated αS is the major constituent of proteinaceous inclusions called LBs and LNs, the most relevant neuropathological hallmarks of PD (Forno *et al*., 1996; Spillantini *et al*., 1998). αS predominantly resides at synaptic terminals (Maroteaux *et al*., 1988), where it has been found to act as a key regulator of SNARE complex assembly, inter-membrane dynamics, and vesicular fusion (Burré *et al*., 2010; Benksey *et al*., 2016), even if its precise function remains still elusive. In the pathological state, αS loses its native unfolded structure and further aggregates into β-sheet-rich assemblies. These species have long been considered to exert their toxicity intracellularly, but several studies have subsequently indicated the presence of a significant extracellular pool of αS (El-Agnaf *et al*., 2003; Paleologou *et al*., 2009; Tokuda *et al*., 2010; Cao *et al*., 2019; Stefanis *et al*., 2019). However, the use of αS as a diagnostic biomarker, with its measurement in CSF and plasma has not produced significant results (Heinzel *et al*., 2014; Atik *et al*., 2016), even if it supports the idea that extracellular αS assemblies play a crucial role in synucleinopathies (Lee *et al*., 2014). A wide range of studies, based on both *in vitro* and *in vivo* experimental evidences, as well as the analysis of biofluids from human PD patients, clearly suggest that certain forms of prefibrillar oligomers, formed at the very early stages of the aggregation process, are highly toxic to neuronal cells, and seem to play a crucial role in the development of the disease (Winner *et al*., 2011; Cremades *et al*., 2012; Kalia *et al*., 2013; Chen *et al*., 2015; Horrocks *et al*., 2016; Ingelsson *et al*., 2016). The toxicity exerted by oligomeric assemblies is thought to be based on their ability to aberrantly

interact with lipid bilayers, leading to their destabilization (Danzer *et al*., 2007; Lorenzen *et al*., 2014). Furthermore, many studies focused on the evaluation of total and oligomeric αS in CSF, demonstrated that total αS is decreased in PD patients as compared to healthy controls, while oligomeric assemblies are significantly increased in PD subjects (Parnetti *et al*., 2016; Majbour *et al*., 2016). Thus, CSF levels of total and oligomeric αS seem to reflect the progression of the disease and their adequate measurement could represent a valid biomarker for the diagnosis on PD. However, several other researches proposed that the fibrillar assemblies, formed at the later steps of αS aggregation, could be able to induce neurodegeneration (Luk *et al*., 2012; Peelaerts *et al*, 2015; Prusiner *et al*., 2015; Woerman *et al*., 2015) and also to lead to the spreading of the pathology (Desplats *et al*., 2009; Hansen *et al*., 2011; Luk *et al*., 2012b; Peelaerts *et al*., 2015). The discovery and characterization of different αS assemblies with peculiar structural characteristics, referred to as 'strains' have led to the hypothesis that such strains could account for the different clinicopathological traits within synucleinopathies (Bousset *et al*., 2013); notably, Peelaerts and coworkers showed that distinct αS strains displayed differential seeding capacities, inducing strain-specific pathology and neurotoxic phenotypes upon their inoculation in rat SN; among them, only fibrillar assemblies exhibited perpetual behavioural and aggravated neurotoxic phenotypes *in vivo* (Peelaerts *et al*., 2015).

As the number of PD cases is rapidly increasing and this disease is nowadays one of the leading source of disability, it is extremely urgent to identify the nature and structure of the different pathogenic αS species, in order to clarify their precise role in neurodegeneration and to design therapeutic strategies able to specifically target pathogenic assemblies, thus slowing the progression of the disease. However, the *in vitro* isolation of specific types of aggregates, especially oligomers, is particularly difficult, given their transient nature and the complexity of the whole aggregation process, in which multiple species are generated simultaneously and rapidly convert into new different assemblies (Chen *et al*., 2015; Cremades *et al*., 2017). Importantly, during the aggregation process, different pathways compete each other, occurring simultaneously (Kaylor *et al*., 2005; Heise *et al*., 2005), whereas in other situations certain pathways are preferentially favored in spite of others. αS monomer can form a large variety of oligomeric and fibrillar species that differ in structure, size and morphology (Uversky, 2003; Cremades *et al*., 2012; Chen *et al*., 2015). Hence, both toxic (Danzer *et al*., 2007; Hinault *et al*., 2010; Cremades *et al*., 2012) and nontoxic (Qin *et al*., 2007; Ehrnhoefer *et al*., 2008; Zhou *et al*., 2010; Pieri *et al*., 2012; Pieri *et al*., 2016) αS oligomers have been described.

Importantly, it has been recently observed that, under specific aggregation conditions, it is possible to direct αS aggregation to follow specific pathways, thus leading to the formation of structurally different types of assemblies, such as kinetically trapped oligomers, that can be further stabilized by the use of chemical agents and then isolated for a detailed structural and morphological characterization (Chen *et al*., 2015; Fusco *et al*., 2017). In particular, the formation of such oligomers have been allowed by the usage of lyophilization, a widely employed technique (Danzer *et al*., 2007; Gihem *et al*., 2011; Celej *et al*., 2012; Lorenzen *et al*., 2014; Chen *et al*., 2015) that leads to a significant increase in the intermolecular interactions between protein molecules. The derived oligomers have a β-sheet folding core, together with the ability to interact with lipid bilayers and to induce membrane permeabilization (Gihem *et al*., 2011; Lorenzen *et al*., 2014; Chen *et al*., 2015; Fusco *et al*., 2017). These species are particularly relevant as they are highly toxic to neuronal cells (Chen *et al*., 2015; Deas *et al*., 2016; Angelova *et al*., 2016) and, when they are added to the culture medium of model neurons, they perfectly reproduce the neuropathological hallmarks of PD (Devine *et al*., 2011; Deas *et al*., 2016; Angelova *et al*., 2016), thanks to their strong similarity to oligomeric assemblies formed *in vivo* (Cremades *et al*., 2017).

In this study we have compared five different αS species: M, OA*, OB*, SF and LF, representative of the five main populations that have been previously reported to progressively form during αS fibrillization, and referred to as M, OA, OB, and fibrils (Cremades *et al*., 2012). Indeed, Cremades and coworkers used single-molecule fluorescence techniques to reveal the presence of two considerable different oligomeric species formed during fibril assembly. These two types of oligomers were denoted as type A and type B (Cremades *et al*., 2012). Type A oligomers (OA) were found to grow through monomer addition, but also to convert into type B oligomers (OB), with a rate of structural conversion with a half-time of about 35 h, a long time necessary for the transition from a largely unstructured oligomer to a β-sheet-rich one. Both types of oligomers were tested for their ability to induce ROS production. The exposure of both neurons and astrocytes to OB and, to a lesser extent, to OA, evoked a significant increase in cytoplasmic ROS production (Cremades *et al*., 2012). A similar trend has been observed in a subsequent study performed by Chen and coworkers, in which the same oligomeric assemblies were described in more detail, by using a wide range of spectroscopic techniques, AFM, and EM (Chen *et al*., 2015). In such work, fibrillar assemblies have also been analysed, and they resulted to induce a modest increase in ROS

production, lower than that observed in the presence of β-sheet rich oligomers (Chen *et al*., 2015). On the contrary, the monomer did not produce considerable changes in ROS production in cultured cells (Cremades *et al*., 2012; Chen *et al*., 2015). The study of this early biochemical toxic modification induced by misfolded amyloid species is particularly important, as the massive generation of free radicals has itself been reported to trigger in turn the production of aberrant misfolded proteins, and to induce abnormal mitochondrial function, and the stimulation of apoptotic pathways in neuronal cells (Nakamura *et al*., 2011). OA* and OB* are analogous to the OA and OB that accumulate during the formation of the particular fibrillar polymorph used in this study (Cremades *et al*., 2012; Chen *et al*., 2015; Fusco *et al*., 2017). In accordance to previously reported evidences, our results indicate that only the OB* were able to induce a significant and rapid increase in ROS levels. Similarly, a wide range of studies showed the ability of αS oligomeric assemblies to exert the same toxic effect (Deas *et al*., 2016; Whiten *et al*., 2018; Huges *et al*., 2019). Moreover, also PFFs were found to increase the mitochondrial ROS production (Tapias *et al*., 2017). Together with ROS production, a massive dysregulation of Ca^{2+} homeostasis has been observed at early incubation times following the addition of OB* and, to a lesser extent, SF, to the culture medium of both SH-SY5Y human neuroblastoma cells and primary rat cortical neurons, in agreement with previously reported results (Angelova *et al*., 2016; Deas *et al*., 2016). The abnormal and prolonged intracellular Ca^{2+} elevation occurring within neuronal cells is widely considered a crucial early event in the pathogenesis of PD. Accordingly, many studies previously demonstrated that αS is able to induce Ca^{2+} dyshomeostasis, both in its unfolded monomeric state and in the aggregated one. Different mechanisms have been proposed to explain Ca^{2+} dysregulation evoked by these species, such as the increase in membrane permeability and a pore formation mechanism (Volles *et al*., 2001; Volles and Lanbury, 2002; Danzer *et al*., 2007).

Another commonly reported measurement of the cytotoxicity of amyloid oligomers is the extent to which they disrupt lipid membranes (Bemporad and Chiti, 2012). Thus, in order to gain insight into the precise molecular mechanisms by which OB* and, to a lesser extent, SF exert their toxicity at early incubation times, we monitored the internalization of all the analysed αS species at 60 min after their addition to the culture medium of SH-SY5Y human neuroblastoma cells. A major internalization of the OB* and, to a lesser extent, SF and LF was observed, which resulted in the perturbation of the cellular membranes and in the release of intracellular molecules in cells treated with only OB*

and SF, as probed by the study of calcein leakage. These data are in good agreement with previously reported evidences on the ability of αS oligomers to disrupt synthetic lipid vesicles (Volles *et al*., 2001; van Rooijen BD *et al*., 2009; Lorenzen *et al*., 2014), and with the observations by Chen and coworkers, showing that OB were much more efficient in permeabilizing lipid vesicles than monomeric or fibrillar forms of αS at the same mass concentration (Chen *et al*., 2015). However, other researchers reported that αS oligomers were not able to permeabilize lipid membranes, whereas membrane permeabilization occurred only following treatment with fibrillar structures (Pieri *et al.*, 2012).

Many groups investigated the internalization of αS species inside the cells. Cremades and collaborators observed a rapid and efficient uptake of monomeric, oligomeric and fibrillar αS species into both neurons and astrocytes (Cremades *et al*., 2012). In a recent work, Masaracchia and coworkers reported that both monomeric and fibrillar αS is internalized by neuroglioma cells, with the monomeric protein accumulating in the perinuclear area, and the fibrillar one in large cytosolic inclusions, after 24 h of treatment (Masaracchia *et al*., 2018). Moreover, a recent study confirmed the internalization of both oligomeric and fibrillar αS in primary neurons (Froula *et al*., 2019). Although the fate of αS aggregates once they enter the cells needs to be investigated in more detail, the uptake of OB* was found to result in mitochondrial dysfunction and apoptosis, in agreement with previous studies (Angelova *et al*., 2016; Deas *et al*., 2016). The ability of αS oligomers formed *in vitro*, or overexpressed in cultured cells, to induce cell death has been widely demonstrated by many other experimental evidences (Chen *et al*., 2007; Danzer *et al*., 2007; Tetzlaff *et al*., 2008; Näsström *et al*., 2011). The fibrillar structures were also reported to induce toxicity, but only at relatively longer incubation times with respect to OB*, whereas the M and OA* species did not exert any toxic effect on the cells at all the experimental times reported in this study. Accordingly, it was previously demonstrated that cells exposed to neuron-derived αS assemblies showed signs of apoptosis, such as nuclear fragmentation and caspase-3 activation, both *in vitro* and *in vivo* (Desplats *et al*., 2009). Moreover, a wide range of studies previously showed that soluble oligomers have a higher cytotoxicity as compared to the fibrillar form of the protein (Stöckl *et al*., 2013). Taken together, our results indicate that αS species with a β-sheet core and solvent-exposed hydrophobic surfaces are able to induce cellular dysfunctions, with the levels of observed cytotoxicity depending on the specific type of aggregate. These data are also in good agreement with previously reported observations on the ability of the OB* to disrupt the lipid bilayers by anchoring to the cellular membrane through the unstructured N-

terminal fragment, and then inserting their high structured β-sheet core in the interior of the bilayers (Fusco *et al*., 2017; Cascella *et al*., 2019). Thus, our experimental evidences demonstrate that most of the OB* interacting with the membrane of neuronal cells are rapidly internalized, although on a time scale slower than that observed for Ca^{2+} influx and ROS formation, that are the earliest perturbations caused by the oligomers. In contrast, the fibrillar assemblies appear to be mostly localized at the surface of the plasma membrane on the timescale of the experiments reported here. Moreover, the quantity of fibrillar species bound to membranes was observed to be much greater than that expected from the level of cellular dysfunction observed here. Therefore, our data suggest that extracellular fibrils are weakly toxic themselves, and the association between SF or LF and cellular membranes is not sufficient to explain their cytotoxicity, and that preferentially small aggregated species are internalized by neuronal cells. Thus, the cytotoxic capacity of the fibrillar assemblies seems to correlate directly with the quantity of αS that interacts with the cellular membranes in a manner that is sufficient to cause the disruption of Ca^{2+} homeostasis and an increased ROS production, and also to be taken up within the cells. We subsequently focused on the analysis of the internalized species by using confocal microscopy and the A11 antibody, which is specific for soluble prefibrillar oligomers of different proteins and peptides, independently of their sequence (Kayed *et al*., 2003). Thus, we found that the internalized species were A11-positive in all cases, not only when the cells were treated with OB*, but also with SF and LF species that are themselves A11-negative, as revealed by dot-blot analysis. Moreover, the apparent steady-state levels of A11-positive species detected inside the cells, which were found to depend on the length of the fibrils, also correlate with the toxicity induced in the cells after prolonged times of exposure, when we observed that all αS species containing cross-β structure were toxic to similar extents. Accordingly, the appearance of A11-positive aggregates from the fibrillar species is relatively slow, with rates that closely match the time course of toxicity. Moreover, the addition of the A11 antibody to the cells was able to prevent αS internalization, as well as the cytotoxic effects of both toxic oligomers and fibrils on neuronal viability. Taken together, these data demonstrate that SF and LF are able to generate toxic oligomeric species when added to the extracellular medium of neuronal cells, upon their association with cellular membranes. Accordingly, Cremades and coworkers previously reported that fibrillar assemblies incubated *in vitro* under near-physiological conditions (pH 7.4, 37 °C) in monomer-free buffer were able to disaggregate, thus leading to the release of small oligomeric assemblies (Cremades *et al*.,

2012); this process is likely to be enhanced in the presence of cells. The dissociation of αS fibrils into soluble species able to bind to neuronal membranes, including both oligomers and monomers, has also been recently observed to occur under conditions close to physiological (Skamris *et al*., 2019). Our finding that SF are more toxic, and exert their effects more rapidly than LF, can be attributed to the fact that they have a higher proportion of fibrillar ends at the same mass concentration. As oligomers release occur from fibril ends, this feature will result in a more rapid release of higher levels of oligomers in the shorter fibrils. Moreover, LF showed a lower diffusion capacity in the cellular medium, and a reduced ability to interact with the cells, than SF. These conclusions are in line with previous reports obtained with the amyloid beta (Aβ) peptide associated with AD, that have revealed the lipid-mediated depolymerization of nontoxic fibrils of Aβ into toxic A11-positive oligomers, which were also shown to resemble the oligomers formed *de novo* during fibrils assembly (Martins *et al*., 2008). These results are also in agreement with the general proposition that any fibrillar species that accumulate in tissue can represent a source of soluble toxic oligomeric assemblies (Cremades *et al*., 2012; Tipping *et al*., 2015), and consistent with the *in vivo* observation of the leakage of Aβ oligomers from fibrils (Lesné *et al*., 2006; Koffie *et al*., 2009). In particular, it has been reported that the toxicity observed in a mouse model expressing the Aβ peptide was proportional to the quantity of oligomers released from amyloid plaques (Lesné *et al*., 2006). Furthermore, those plaques were shown to be surrounded by a halo of oligomeric Aβ that interacts with synapses and contributes to their loss (Koffie *et al*., 2009). Taken together, these results suggest that fibrils, also formed by different proteins, can release oligomers that can in turn contribute to the toxicity associated with fibril spreading. Some αS fibrils have been previously observed to be taken up by cells (Volpicelli-Daley *et al*., 2011; Brahic *et al*., 2016) and possibly contribute to pathology spreading to nearby neurons, triggering protein aggregation in recipient cells (Desplats *et al*., 2009; Luk *et al*., 2012b; Masuda-Suzukake *et al*., 2013; Peelaerts *et al*., 2015; Prusiner *et al*., 2015; Froula *et al*., 2019). In a recent study, it has been reported that the same SF were able to induce PD-like pathology by a spreading process when injected in brains of healthy mice, evoking the reduction of striatal dopamine terminals, the massive loss of dopaminergic neurons in the SN, as well as several motor disturbances. Opposite, the OB* were only able to induce toxicity in the region of brain injection, without signs of seeding or spreading, as it was expected given their kinetically trapped nature (Froula *et al*., 2019). It is possible, however, that the OB-like species that can be released from

fibrils, in addition to contribute to the induction of toxicity, could also enhance the generation of new aggregates, as they might have elongation capabilities similar to those of their fibrillar precursors.

In the second part of this study, we have focused our attention on the analysis of the αS assemblies previously found to be toxic for neuronal cells. We have firstly investigated in detail the mechanism of interaction with the plasma membrane of target cells. Many researches have previously focused on the analysis of the interaction of different αS conformers with the lipid components of the plasma membrane; the monomeric form of the protein has been shown to bind to anionic phospholipids (Stöckl *et al*., 2008), mainly because of the attractive electrostatic interactions between such lipids and multiple positively charged lysine residues that are present in the N-terminal region of αS (Zarbiv *et al*., 2014). The binding of αS oligomeric assemblies has been also associated with the presence of negatively charged lipids for the same reason (Volles *et al*., 2001; Stefanovic *et al*., 2014), and some experimental evidences suggested that the N-terminal region of αS might retain its membrane binding properties also in the fibrillar state (Chaari *et al*., 2013). The monosialogangliosides (GMs), and in particular the GM1 subtype, are a group of lipids extensively analysed for their ability to associate with αS. However, their capacity to recruit αS at the plasma membrane is still controversial; while some researchers found a high degree of association (Martinez *et al*., 2007; Park *et al*., 2009), others did not observe any binding of αS to membranes containing the ganglioside GM1, even at high concentrations (Garten *et al*., 2015). On the timescale of the experiments studied here, we found that GM1 depletion resulted in a quite significant reduction in the interaction of OB* with target cells, without affecting those of both fibrillar assemblies. Moreover, it has been reported that extracellular αS can also act as a specific ligand for different cell surface receptors. The binding of αS assemblies, and in particular oligomers, to these protein interactors has been proposed to be responsible not only for their association with the plasma membrane, but also for their internalization and, importantly, for the transmission of aberrant signal pathways into cells, thus evoking a wide range of biochemical toxic reactions, including Ca^{2+} dysregulation, ROS production, synaptic dysfunction, finally culminating in neurodegeneration. Accordingly, here we have found that the removal of the proteins exposed on the plasma membrane of target cells significantly prevented the binding of OB* and, to a much lesser extent, of SF, to the lipid bilayer. Furthermore, the internalization of OB* and the loss of membrane permeability they evoked were significantly counteracted. Opposite, no effect was found in cells

treated with LF. These observations could be ascribed to the presence of a higher number of open active ends on oligomeric assemblies with respect to fibrils, which are responsible for a higher and rapid interaction with the lipid bilayer of neuronal cells, and in particular with specific components of the plasma membrane, such as the exposed proteins. On the contrary, the binding of the fibrillar aggregates was less specific and poorly influenced by any change in the composition of the plasma membrane. This evidence was particularly verified for LF, that have a lower proportion of fibrillar ends at the same mass concentration with respect to SF, as reported before. These findings are in good agreement with previously discussed evidences on the different kinetics showed by the analysed αS assemblies in inducing cellular dysfunction, with the OB* being the most rapid and the LF the slowest. We subsequently shed light into the mechanism of Ca^{2+} entry through the plasma membrane, in order to investigate the possible involvement of membrane proteins. Thus, we removed them pre-treating cells with diluted trypsin. Our results suggested that these proteins were implicated in the early phases of Ca^{2+} entry induced by OB*, but not in the one evoked by fibrils, as we did not find any difference in the kinetics of Ca^{2+} dyshomeostasis. Many experimental evidences suggest that αS oligomers are able to modulate the activity of membrane channels, such as the voltage-dependent ones, possibly with a direct interaction (Adamczyk and Strosznajder, 2006; Ronzitti *et al*., 2014); the ability to alter the functionality of glutamatergic receptors has also been investigated. Thus, large oligomeric assemblies, added to the culture medium of hippocampal neurons resulted in a significant increase in the AMPARs-mediated excitatory post-synaptic currents, whereas the application of the monomeric protein did not affect the activity of such receptor-channels (Hüls *et al*., 2012). Moreover, other groups investigated the ability of αS aggregates to interact with, or modulate the activity, of NMDARs. In particular, Diogenes and coworkers proposed a complex model in which αS oligomers activate, directly or indirectly, the NMDARs, thus increasing basal synaptic transmission and impairing LTP (Diógenes *et al*., 2012). Here, we demonstrated the involvement of NMDARs in the early phases of Ca^{2+} dyshomeostasis induced by αS oligomers, but not fibrils, in neuroblastoma cells; in particular, we found that the pharmacological inhibition of such glutamatergic receptors transiently delayed the Ca^{2+} influx induced by OB*. Furthermore, we showed that αS oligomers and fibrils all accumulate in close proximity to NMDARs, but only the OB* were able to modulate their activity. This effect, in good agreement with previously reported evidences, can be attributed to the fact that oligomeric assemblies have a higher number of open ends, and

are generally more active than the fibrillar species and abler to rapidly interfere with specific membrane components. However, we cannot posit a direct interaction between αS species and receptor-channels in our experimental conditions, as the resolution of confocal microscopy is limited. Despite this observation, our findings are relevant because suggest that oligomers with large solvent-exposed hydrophobicity and high β-sheet content promptly stimulate glutamatergic Ca^{2+} channels. We also demonstrated that, after a prolonged exposure to OB*, the pharmacological blockade of NMDARs was no more effective in preventing Ca^{2+} influx, thus suggesting that a generic mechanism of destabilization and disassembly of the lipid membrane probably occurs and causes a massive influx of Ca^{2+} ions. Furthermore, the idea that NMDARs could be involved only in the early phases of Ca^{2+} dyshomeostasis is also consistent with a robust body of evidence indicating that the addition of high concentrations of recombinant αS to the culture medium of dopaminergic neurons leads to a significant reduction in NR1 subunits of NMDARs (fundamental for the assembly and the functionality of such channels) on the cell surface (Cheng *et al*., 2011). Accordingly, in a recent study, Yu and coworkers demonstrated the αS oligomers added to culture medium of dopaminergic cells at a concentration of 0.4 μM (very similar to that used in the experiments described in this study) induced the clathrin-mediated internalization of the same NR1 subunit after 60 min of treatment (Yu *et al*., 2019). The activation of NMDARs without a direct interaction with any channel subunit is also consistent with the observations of Ferreira and coworkers, that proposed a complex mechanism in which αS oligomers directly interact with PrP^C, thus leading to a complex signal transduction pathway, finally cultminating in the phosphorylation of NMDARs by the Src family tyrosine kinase Fyn, evoking a massive increase of intracellular Ca^{2+} levels, ultimately triggering synaptic dysfunction in hippocampal neurons (Ferreira *et al*., 2017). Accordingly, Fyn activation has also been described as a critical step of the PrP^C signalling cascade for the modulation of intracellular Ca^{2+} levels in neuronal cells exposed to hydrogen peroxide (Krebs *et al*., 2007).

Many studies focused on the identification of the specific proteins, located at the surface of the plasma membrane, interacting with αS assemblies. Among them, PrP^C has been widely proposed to be a receptor of both oligomeric and fibrillar species, even if its role is still controversial. Some researchers postulated a direct interaction of misfolded αS with PrP^C, responsible for its transfer between cells (Aulić *et al*., 2017; Urrea *et al*., 2017); similarly, others found a higher uptake of fibrillar αS in murine neuroblastoma cells

overexpressing PrP^C as compared to those ablated for the same protein (De Cecco and Legname, 2018). Importantly, PrP^C has been widely described as a receptor for β-amyloid (Aβ) oligomers in AD (Laurén *et al*., 2009; Ganzinger *et al*., 2014); their interaction possibly mediates the neurotoxic effects of such assemblies, culminating in neurodegeneration and cell death (Laurén *et al*., 2009; Scott-McKean *et al*., 2016). Here, we found a high degree of colocalization at the plasma membrane surface between OB* and PrP^C, that was significantly reduced, as expected, by the removal of the exposed proteins with diluted trypsin and poorly influenced by GM1 depletion at early incubation times with the cells, in good agreement with previously reported evidences on the ability of the plasma membrane to recruit αS oligomeric species. We also demonstrated that PrP^C was directly involved in the binding of OB* to the lipid bilayer, as its blockade with a specific antibody significantly prevented the interaction with the plasma membrane at the experimental times reported in this study. Thus, our results are in good agreement with those obtained by many other groups and with aggregates formed from different proteins and peptides, confirming the prominent role of PrP^C as a generalized conformation-specific receptor for misfolded aggregates of disease-associated proteins (Watts *et al*., 2018). However, the contribution of Prp^C in the pathogenesis of neurodegenerative disorders remains to be further validated, but could be highly relevant as a target for therapeutic intervention. In this study we have observed that PrP^C blockade also resulted in a significant reduction of the early Ca^{2+} entry evoked by oligomeric assemblies, with a trend that was very similar to the one observed after the pharmacological inhibition of NMDARs. These observations support the hypothesis that the cytotoxicity of OB* at early incubation times is caused by a receptor-mediated mechanism, independent of pore formation and membrane permeabilization, but still sufficient to trigger a large influx of Ca^{2+} ions. Opposite, after prolonged incubation times, a more generalized and unspecific mechanism of pore formation, membrane perturbation and disruption probably occurs, finally culminating in mitochondrial dysfunction and cell death, that are not prevented by PrP^C blockade. Thus, the experimental evidences accumulated in this study suggest that the cytotoxic effect of αS misfolded oligomers with a β-sheet core and solvent-exposed hydrophobic surfaces may not be exclusively related to a single mechanism, but more likely to a collection of mechanisms involving membrane proteins at the very early stages.

Concluding remarks and future perspectives

In this study, we analysed in detail the toxic capacity of different αS conformers on neuronal cells. We showed that small soluble oligomeric species with a rudimentary cross-β structure and high solvent-exposed hydrophobicity, generated during fibril formation, are by far the most toxic forms of αS. Our results provide important information on the toxic capacity of αS fibrils: together with the well-characterized and extensively described capability to transfer from neuron-to-neuron, contributing to the spreading and diffusion of LB pathology in different brain areas, we demonstrated their ability to release small oligomeric species, that cause in turn an immediate and severe neuronal dysfunction. Thus, molecules that are able to prevent the formation of toxic oligomers of αS during the aggregation process, such as aminosterols (Perni *et al*., 2017; Perni *et al*., 2018), or to interact directly with these toxic species, such as the A11 antibody, or to prevent their release from the fibrillar assemblies, like the OC antibody, are able to suppress their cytotoxic capability. These features are of considerable interest in the design of possible therapeutic strategies targeting αS misfolded aggregates, but also other systems in which the aggregation and accumulation of specific proteins and peptides is linked to neurodegeneration. However, the mechanism by which αS fibrils release toxic oligomers upon membrane binding, as well as the nature of the A11-positive αS species internalized by the cells, must be described in more detail, and in the near future we will address these issues with a range of different biochemical and biophysical techniques.

In the second part of this study we have analysed in detail the mechanism of interaction of toxic αS conformers with the plasma membrane of neuronal cells. Our results clearly indicate that the cytotoxicity of αS oligomers is not only an inherent feature of misfolded protein assemblies linked to their specific structural properties (surface-exposed hydrophobicity and β-sheet content), but it is also dependent on the biochemical features of the cellular membranes they interact with, and so it can be described as a property emerging from their complex interplay. These evidences are in good agreement with those reported in other studies, in which toxic aggregates from different proteins were analysed, together with specific membrane components potentially influencing their interaction with the lipid bilayer (Evangelisti *et al*., 2016; Cascella *et al*., 2017). Here, we have also identified the NMDARs as mediators of the early Ca^{2+} dyshomeostasis evoked by αS oligomeric assemblies, that was transiently delayed by the pharmacological blockade of

such channels. We finally demonstrated the central role of PrP^C for the recruitment of harmful oligomers at the plasma membrane, and for the initiation of the complex cascade of toxic pathways they generate in neuronal cells. However, the precise molecular mechanisms underlying the cytotoxicity of αS oligomers upon their interaction with PrP^C must be described in more detail, and in the near future we would like to define the molecular basis of this process and also to validate this hypothesis in animal models of PD. A deeper understanding of the interplay between αS, PrP^C and other membrane proteins may be extremely useful for the development of novel strategies for therapeutic intervention in PD and α-synucleinopathies in general.

5 REFERENCES

Abeliovich A, Schmitz Y, Farinas I, Choi-Lundberg D, Ho WH *et al*. (2000) Mice lacking a-synuclein display functional deficits in the nigrostriatal dopamine system. *Neuron* **25**:239-252.

Abbasi N, Mohajer B, Abbasi S, Hasanabadi P, Abdolalizadeh A *et al*. (2018) Relationship between cerebrospinal fluid biomarkers and structural brain network properties in Parkinson's disease. *Mov Disord.* **33**:431-39.

Adamczyk A, Strosznajder JB (2006) Alpha-synuclein potentiates Ca^{2+} influx through voltage-dependent Ca^{2+} channels. *Neuroreport.* **17**:1883-1886.

Ahn BH, Rhim H, Kim SY, Sung YM, Lee MY *et al*. (2002) α-Synuclein interacts with phospholipase D isozymes and inhibits pervanadate-induced phospholipase D activation in human embryonic kidney-293 cells. *J Biol Chem*. **277**:12334-12342.

Ahn TB, Kim SY, Kim JY, Park SS, Lee DS *et al*. (2008) Alpha synuclein gene duplication is present in sporadic Parkinson disease. *Neurology* **70**:43-49.

Ai SX, Xu Q, Hu YC, Song CY, Guo JF *et al*. (2014) Hypomethylation of SNCA in blood of patients with sporadic Parkinson's disease. *J Neurol Sci*. **337**:123-128.

Ammal Kaidery NS, Tarannum B, Thomas B (2013) Epigenetic landscape of Parkinson's disease: emerging role in disease mechanisms and therapeutic modalities *Neurotherapeutics* **10**:698-708.

Anderson JP, Walker DE, Goldstein JM, de Laat R, Banducci K *et al*. (2006) Phosphorylation of Ser-129 is the dominant pathological modification of alpha-synuclein in familial and sporadic Lewy body disease. *J Biol Chem*. **281**:29739-29752.

Angelova PR, Ludtmann MH, Horrocks MH, Negoda A, Cremades N *et al*. (2016) Ca^{2+} is a key factor in alpha-synuclein-induced neurotoxicity. *J Cell Sci*. **129**:1792-1801.

Anwar S, Peters O, Millership S, Ninkina N, Doig N *et al*. (2011) Functional alterations to the nigrostriatal system in mice lacking all three members of the synuclein family. *J Neurosci*. **31**:7264-7274.

Apetri MM., Maiti NC, Zagorski MG, Carey PR, Anderson VE (2006) Secondary structure of alpha-synuclein oligomers: characterization by raman and atomic force microscopy. *J Mol Biol*. **355**:63-71.

Ascherio A, Chen H, Weisskopf MG, O'Reilly E, McCullough ML *et al*. (2006) Pesticide exposure and risk for Parkinson's disease. *Ann Neurol*. **60**:197-203.

Ascherio A, Weisskopf MG, O'Reilly EJ, McCullough ML, Calle EE *et al*. (2004) Coffee consumption, gender, and Parkinson's disease mortality in the cancer prevention study II cohort: the modifying effects of estrogen. *Am J Epidemiol.* **160**:977-84.

Askanas V, Engel WK, Alvarez RB, McFerrin J, Broccolini A (2000) Novel immunolocalization of a-synuclein in human muscle of inclusion-body myositis, regenerating and necrotic muscle fibers, and at neuromuscular junctions. *J Neuropathol Exp Neurol.* **59**:592-598.

Atik A, Stewart T, Zhang Y (2016) Alpha-Synuclein as a Biomarker for Parkinson's Disease. *Brain Pathol*. **26**:410-418.

Aulić S, Masperone L, Narkiewicz J, Isopi E, Bistaffa E *et al*. (2017) α-synuclein amyloids hijack prion protein to gain cell entry, facilitate cell-to-Cell spreading and block prion replication. *Sci Rep.* **7**:10050.

Autere J, Moilanen JS, Finnilä S, Soininen H, Mannermaa A *et al*. (2004) Mitochondrial DNA polymorphisms as risk factors for Parkinson's disease and Parkinson's disease dementia. *Hum Genet.* **115**:29-35.

Bae EJ, Ho DH, Park E, Jung JW, Cho K *et al*. (2013) Lipid peroxidation product 4-hydroxy-2-nonenal promotes seeding-capable oligomer formation and cell-to-cell transfer of alpha-synuclein. *Antioxid Redox Signal.* **18**:770-783.

Balaban RS (2009) The role of Ca^{2+} signaling in the coordination of mitochondrial ATP production with cardiac work. *Biochim Biophys Acta* **1787**:1334-1341.

Bannister AJ, Kouzarides T (2011) Regulation of chromatin by histone modifications. *Cell Res.* **21**:381–395.

Barone P, Poewe W, Albrecht S, Debieuvre C, Massey D *et al*. (2010) Pramipexole for the treatment of depressive symptoms in patients with Parkinson's disease: a randomised, double-blind, placebo-controlled trial. *Lancet Neurol* **9**:573-80.

Bartels T, Choi JG, Selkoe DJ (2011) α-Synuclein occurs physiologically as a helically folded tetramer that resists aggregation. *Nature* **477**:107-110.

Bartels T, Kim NC, Luth ES, Selkoe DJ (2014) N-alpha-acetylation of α-synuclein increases its helical folding propensity, GM1 binding specificity and resistance to aggregation. *PLoS ONE* **9**:e103727.

Bellucci A1, Navarria L, Zaltieri M, Falarti E, Bodei S *et al*. (2011) Induction of the unfolded protein response by α-synuclein in experimental models of Parkinson's disease. *J Neurochem*. **116**:588-605.

Bemporad F, Chiti F (2012) Protein misfolded oligomers: experimental approaches, mechanism of formation, and structure-toxicity relationships. *Chem Biol*. **19**:315–327.

Betarbet R, Sherer TB, MacKenzie G, Garcia-Osuna M, Panov AV, Greenamyre JT (2000) Chronic systemic pesticide exposure reproduces features of Parkinson's disease. *Nat Neurosci*. **3**:1301-1306.

Betarbet R, Canet-Aviles RM, Sherer TB, Mastroberardino PG, McLendon C *et al*. (2006) Intersecting pathways to neurodegeneration in Parkinson's disease: effects of the pesticide rotenone on DJ-1, α-synuclein, and the ubiquitin-proteasome system. *Neurobiol Dis.* **22**:404-420.

Bengoa-Vergniory N, Roberts RF, Wade-Martins R, Alegre-Abarrategui J (2017) Alpha-synuclein oligomers: a new hope. *Acta Neuropathol.* **134**:819-838.

Benilova I, Karran E, De Strooper B (2012) The toxic Aβ oligomer and Alzheimer's disease: an emperor in need of clothes. *Nat Neurosci*. **15**:349-357.

Benskey MJ, Perez RG, Manfredsson FP (2016) The contribution of alpha synuclein to neuronal survival and function – Implications for Parkinson's disease. *J Neurochem*. **137**:331-59.

Bennett MC, Bishop JF, Leng Y, Chock PB, Chase TN *et al*. (1999) Degradation of α-synuclein by proteasome. *J Biol Chem.* **274**:33855-33858.

Bernardi P, Rasola A, Forte M, Lippe G (2015) The mitochondrial permeability transition pore: channel formation by F-ATP synthase, integration in signal transduction, and role in pathophysiology. *Physiol Rev.* **95**:1111-1155.

Berridge MJ (1998) Neuronal calcium signaling. *Neuron* **21**:13-26.

Betzer C, Lassen LB, Olsen A, Kofoed RH, Reimer L *et al*. (2018) α-synuclein aggregates activate calcium pump SERCA leading to calcium dysregulation. *EMBO Rep.* **19**:e44617.

Bieschke J, Russ J, Friedrich RP, Ehrnhoefer DE, Wobst H *et al*. (2010) EGCG remodels mature α-synuclein and amyloid-β fibrils and reduces cellular toxicity. *Proc Natl Acad Sci USA* **107**:7710-7715.

Bindoff LA, Birch-Machin M, Cartlidge NE, Parker WD Jr, Turnbull DM (1989) Mitochondrial function in Parkinson's disease. *Lancet* **2**:49.

Blesa J, Trigo-Damas I, Quiroga-Varela A, Jackson-Lewis VR (2015) Oxidative stress and Parkinson's disease. *Front Neuroanat.* **9**:91.

Bousset L, Pieri L, Ruiz-Arlandis G, Gath J, Jensen PH *et al*. (2013) Structural and functional characterization of two alpha-synuclein strains. *Nat Commun.* **4**:2575.

Braak H, Del Tredici K, Bratzke H, Hamm-Clement J, Sandmann-Keil D *et al*. (2002) Staging of the intracerebral inclusion body pathology associated with idiopathic Parkinson's disease (preclinical and clinical stages), *J Neurol.* **249** Suppl 3:III/1-5.

Braak H, Del Tredici K, Rüb U, de Vos RA, Jansen Steur EN *et al*. (2003a) Staging of brain pathology related to sporadic Parkinson's disease. *Neurobiol Aging* **24**:197-211.

Braak H, Rüb U, Gai WP, Del Tredici K (2003b) Idiopathic Parkinson's disease: possible routes by which vulnerable neuronal types may be subject to neuroinvasion by an unknown pathogen. *J Neural Transm*. **110**:517-536.

Brahic M, Bousset L, Bieri G, Melki R, Gitler AD (2016) Axonal transport and secretion of fibrillar forms of α-synuclein, $A\beta_{42}$ peptide and HTTExon 1. *Acta Neuropathol.* **131**:539-548.

Brás IC, Lopes LV, Outeiro TF (2018) Sensing α-synuclein from the outside via the prion protein: implications for neurodegeneration. *Mov Disord.* **33**:1675-1684.

Breydo L, Wu JW, Uversky VN (2012) α-Synuclein misfolding and Parkinson's disease. *Biochim Biophys Acta* **1822**:261-285.

Bridi JC, Hirth F (2018) Mechanism of α-synuclein induced synaptopathy in Parkinson's disease. *Front Neurosci.* **12**:80.

Brini M, Calì T, Ottolini D, Carafoli E (2014) Neuronal calcium signalling: function and dysfunction. *Cell Mol Life Sci.* **71**:2787-2814.

Brooks DJ, Pavese N (2011) Imaging biomarkers in Parkinson's disease. *Prog Neurobiol.* **95**:614-28.

Brown DR (2007) Interactions between metals and a-synuclein—Function or artefact? *FEBS J*. **274**:3766-3774.

Bucciantini M, Giannoni E, Chiti F, Baroni F, Formigli L *et al*. (2002) Inherent toxicity of aggregates implies a common mechanism for protein misfolding diseases. *Nature* **416**:507-511.

Buell AK, Galvagnion C, Gaspar R, Sparr E, Vendruscolo M *et al*. (2014) Solution conditions determine the relative importance of nucleation and growth processes in α-synuclein aggregation. *Proc Natl Acad Sci USA* **111**:7671-7676.

Burré J, Sharma M, Tsetsenis T, Buchman V, Etherton MR *et al*. (2010) α-Synuclein promotes SNARE-complex assembly in vivo and in vitro. *Science* **329**:1663-1667.

Burré J, Vivona S, Diao J, Sharma M, Brunger AT *et al*. (2013) Properties of native brain α-synuclein. *Nature* **498**:E4–E6; discussion E6-E7.

Burré J, Sharma M, Südhof TC (2014) α-Synuclein assembles into higher-order multimers upon membrane binding to promote SNARE complex formation. *Proc Natl Acad Sci USA* **111**:E4274-83.

Burré J, Sharma M, Südhof TC (2018) Cell Biology and Pathophysiology of α-Synuclein. *Cold Spring Harb Perspect Med*. **8**:a024091.

Bussell R Jr, Ramlall TF, Eliezer D (2005) Helix periodicity, topology, and dynamics of membrane-associated α-synuclein. *Protein Sci*. **14**:862-872.

Buttner S, Faes L, Reichelt WN, Broeskamp F, Habernig L *et al*. (2013) The Ca^{2+}/Mn^{2+} ion-pump PMR1 links elevation of cytosolic Ca^{2+} levels to α-synuclein toxicity in Parkinson's disease models. *Cell Death Differ*. **20**:465-477.

Cabin DE, Shimazu K, Murphy D, Cole NB, Gottschalk W *et al*. (2002) Synaptic vesicle depletion correlates with attenuated synaptic responses to prolonged repetitive stimulation in mice lacking α-synuclein. *J Neurosci*. **22**:8797-8807.

Calì T, Ottolini D, Negro A, Brini M (2012) α-Synuclein controls mitochondrial calcium homeostasis by enhancing endoplasmic reticulum-mitochondria interactions. *J Biol Chem.* **287**:17914-17929.

Calì T, Ottolini D, Brini M (2014) Calcium signalling in Parkinson's disease. *Cell Tissue Res*. **357**:439-454.

Calo L, Wegrzynowicz M, Santivañez-Perez J, Spillantini MG (2016) Synaptic failure and α-synuclein. *Mov Disord*. **31**:169-177.

Cannell IG, Kong YW, Bushell M (2008) How do microRNAs regulate gene expression? *Biochem Soc Trans*. **36**:1224-1231.

Cao JX, Zhang HP, Du LX (2013) Influence of environmental factors on DNA methylation. *Yi Chuan*. **35**:839-846.

Cao Z, Wu Y, Liu G, Jiang Y, Wang X *et al*. (2019) α-Synuclein in salivary extracellular vesicles as a potential biomarker of Parkinson's disease. *Neurosci Lett*. **696**:114-120.

Cenci MA (2014) Presynaptic mechanisms of l-DOPA-induced dyskinesia: the findings, the debate, and the therapeutic implications. *Front Neurol*. **5**:242.

Cascella R, Evangelisti E, Bigi A, Becatti M, Fiorillo C *et al*. (2017) Soluble oligomers require a ganglioside to trigger neuronal calcium overload. *J Alzheimers Dis*. **60**:923-938.

Cascella R, Perni M, Chen SW, Fusco G, Cecchi C *et al*. (2019) Probing the Origin of the Toxicity of Oligomeric Aggregates of α-Synuclein with Antibodies. *ACS Chem Biol*. **14**:1352-1362.

Catterall WA (2011) Voltage-gated calcium channels. *Cold Spring Harb Perspect Biol*. **3**:a003947.

Celej MS, Sarroukh R, Goormaghtigh E, Fidelio GD, Ruysschaert JM *et al*. (2012) Toxic prefibrillar α-synuclein amyloid oligomers adopt a distinctive antiparallel β-sheet structure. *Biochem J*. **443**:719-726.

Chaari A, Horchani H, Frikha F, Verger R, Gargouri Y *et al*. (2013) Surface behaviour of alpha-synuclein and its interaction with phospholipids using the Langmuir monolayer

technique: a comparison between monomeric and fibrillar alpha-synuclein. *Int J Biol Macromol*. **58**:190-198.

Chan CS, Guzman JN, Ilijic E, Mercer JN, Rick C *et al*. (2007) “Rejuvenation” protects neurons in mouse models of Parkinson's disease. *Nature* **447**:1081-1086.

Chandra S, Chen X, Rizo J, Jahn R, Südhof TC (2003) A broken α-helix in folded α-Synuclein. *J Biol Chem*. **278**:15313-15318.

Chandra S, Fornai F, Kwon HB, Yazdani U, Atasoy D *et al*. (2004) Double-knockout mice for α- and β-synucleins: Effect on synaptic functions. *Proc Natl Acad Sci USA* **101**:14966-14971.

Chapman ER (2002) Synaptotagmin: a Ca^{2+} sensor that triggers exocytosis? *Nat Rev Mol Cell Biol*. **3**:498-508.

Chartier-Harlin MC, Dachsel JC, Vilariño-Güell C, Lincoln SJ, Leprêtre F *et al*. (2011) Translation initiator EIF4G1 mutations in familial Parkinson disease. *Am J Hum Genet*. **89**:398-406.

Chen H, Zhang SM, Schwarzschild MA, Hernán MA, Ascherio A (2005) Physical activity and the risk of Parkinson disease. *Neurology* **64**:664-669.

Chen H, Huang X, Guo X, Mailman RB, Park Y *et al*. (2010) Smoking duration, intensity, and risk of Parkinson disease. *Neurology* **74**:878-884.

Chen L, Feany MB (2005) α-Synuclein phosphorylation controls neurotoxicity and inclusion formation in a Drosophila model of Parkinson disease. *Nat Neurosci*. **8**:657-663.

Chen L, Jin J, Davis J, Zhou Y, Wang Y *et al*. (2007) Oligomeric α-synuclein inhibits tubulin polymerization. *Biochem Biophys Res Commun*. **356**:548-553.

Chen L, Periquet M, Wang X, Negro A, McLean PJ *et al*. (2009) Tyrosine and serine phosphorylation of α-synuclein have opposing effects on neurotoxicity and soluble oligomer formation. *J Clin Invest*. **119**:3257-3265.

Chen M, Margittai M, Chen J, Langen R (2007) Investigation of α-synuclein fibril structure by site-directed spin labeling. *J Biol Chem*. **282**:24970-24979.

Chen RH, Wislet-Gendebien S, Samuel F, Visanji NP, Zhang G *et al*. (2013) α-Synuclein membrane association is regulated by the Rab3a recycling machinery and presynaptic activity. *J Biol Chem*. **288**:7438-7449.

Chen SW, Drakulic S, Deas E, Ouberai M, Aprile FA *et al*. (2015) Structural characterization of toxic oligomers that are kinetically trapped during α-synuclein fibril formation. *Proc Natl Acad Sci USA* **112**:E1994-E2003.

Cheng F, Li X, Li Y, Wang C, Wang T (2011) α-Synuclein promotes clathrin-mediated NMDA receptor endocytosis and attenuates NMDA-induced dopaminergic cell death. *J Neurochem*. **119**:815-25.

Chinta SJ, Mallajosyula JK, Rane A, Andersen JK (2010) Mitochondrial α-synuclein accumulation impairs complex I function in dopaminergic neurons and results in increased mitophagy in vivo. *Neurosci Lett*. **486**:235-239.

Chiti F, Dobson CM (2006) Protein misfolding, functional amyloid, and human disease. *Annu Rev Biochem*. **75**:333-366.

Chiti F, Dobson CM (2017) Protein Misfolding, Amyloid Formation, and Human Disease: A Summary of Progress Over the Last Decade. *Annu Rev Biochem.* **86**:27-68.

Choi DH, Kim YJ, Kim YG, Joh TH, Beal MF *et al*. (2011) Role of matrix metalloproteinase 3-mediated alpha-synuclein cleavage in dopaminergic cell death. *J Biol Chem.* **286**:14168-14177.

Choi YR, Cha SH, Kang SJ, Kim JB, Jou I et al. (2018) Prion-like Propagation of α-Synuclein Is Regulated by the FcγRIIB-SHP-1/2 Signaling Pathway in Neurons. *Cell Rep*. **22**:136-148.

Ciryam P, Tartaglia GG, Morimoto RI, Dobson CM, Vendruscolo M (2013) Widespread aggregation and neurodegenerative diseases are associated with supersaturated proteins. *Cell Rep*. **5**:781-790.

Cole NB, Dieuliis D, Leo P, Mitchell DC, Nussbaum RL (2008) Mitochondrial translocation of α-synuclein is promoted by intracellular acidification. *Exp. Cell Res*. **314**: 2076-2089.

Colla E, Jensen PH, Pletnikova O, Troncoso JC, Glabe C *et al*. (2012a) Accumulation of toxic α-synuclein oligomer within endoplasmic reticulum occurs in α-synucleinopathy in vivo. *J. Neurosci*. **32**:3301-3305.

Colla E, Coune P, Liu Y, Pletnikova O, Troncoso JC *et al*. (2012b) Endoplasmic reticulum stress is important for the manifestations of α-synucleinopathy in vivo. *J Neurosci*. **32**:3306-3320.

Comellas G, Lemkau LR, Nieuwkoop AJ, Kloepper KD, Ladror DT *et al*. (2011) Structured regions of α-synuclein fibrils include the early-onset Parkinson's disease mutation sites. *J Mol Biol*. **411**:881-895.

Conway KA, Harper JD, Lansbury PT (1998) Accelerated in vitro fibril formation by a mutant α-synuclein linked to early-onset Parkinson disease. *Nat Med*. **4**:1318-1320.

Conway KA, Lee SJ, Rochet JC, Ding TT, Harper JD *et al*. (2000) Accelerated oligomerization by Parkinson's disease linked α-synuclein mutants. *Ann N Y Acad Sci*. **920**:42-45.

Conway KA, Rochet JC, Bieganski RM, Lansbury Jr PT (2001) Kinetic stabilization of the α-synuclein protofibril by a dopamine- α-synuclein adduct. *Science* **294**:1346-1349.

Cookson MR (2012a) Cellular effects of LRRK2 mutations. *Biochem Soc Trans*. **40**: 1070-1073.

Cookson MR (2012b) Parkinsonism due to mutations in PINK1, parkin, and DJ-1 and oxidative stress and mitochondrial pathways. *Cold Spring Harb Perspect Med*. **2**:a009415.

Cooper AA, Gitler AD, Cashikar A, Haynes CM, Hill KJ *et al*. (2006) α-Synuclein blocks ER-Golgi traffic and rab1 rescues neuron loss in Parkinson's models. *Science* **313**:324-328.

Cremades N, Cohen SI, Deas E, Abramov AY, Chen AY *et al*. (2012) Direct observation of the interconversion of normal and toxic forms of alpha-synuclein. *Cell* **149**:1048-1059.

Cremades N, Dobson CM (2018) The contribution of biophysical and structural studies of protein self-assembly to the design of therapeutic strategies for amyloid diseases. *Neurobiol Dis*. **109**:178-190.

Crowther RA, Daniel SE, Goedert M (2000) Characterisation of isolated alpha synuclein filaments from substantia nigra of Parkinson's disease brain. *Neurosci Lett*. **292**:128-130.

Cuervo AM, Stefanis L, Fredenburg R, Lansbury PT, Sulzer D (2004) Impaired degradation of mutant alpha-synuclein by chaperone-mediated autophagy. *Science* **305**:1292-1295.

Cull-Candy S, Brickley S, Farrant M (2001) NMDA receptor subunits: diversity, development and disease. *Curr Opin Neurobiol*. **11**:327-35.

Dalfó E, Barrachina M, Rosa JL, Ambrosio S, Ferrer I (2004) Abnormal α-synuclein interactions with rab3a and rabphilin in diffuse Lewy body disease. *Neurobiol Dis.* **16**: 92-97.

Danzer KM, Haasen D, Karow AR, Moussaud S, Habeck M *et al*. (2007) Different species of α-synuclein oligomers induce calcium influx and seeding. *J Neurosci*. **27**:9220-9232.

Day JJ, Sweatt JD (2010) DNA methylation and memory formation *Nat Neurosci*. **13**:1319-1323.

de Carvalho Aguiar P, Sweadner KJ, Penniston JT, Zaremba J *et al*. (2004) Mutations in the Na^+/K^+−ATPase α3 gene ATP1A3 are associated with rapid-onset dystonia parkinsonism. *Neuron* **43**:169-175.

De Cecco E, Legname G (2018) The role of the prion protein in the internalization of α-synuclein amyloids. *Prion* **12**:23-27.

de Lau LM, Breteler MM (2006) Epidemiology of Parkinson's disease. *Lancet Neurol*. **5**:525–35.

Deas E, Cremades N, Angelova PR, Ludtmann MH, Yao Z *et al*. (2016) α-Synuclein oligomers interact with metal ions to induce oxidative stress and neuronal death in Parkinson's disease. *Antioxid Redox Signal*. **24**:376-391.

Demartino GN, Gillette TG (2007) Proteasomes: machines for all reasons. *Cell* **129**:659-662.

Desplats P, Lee HJ, Bae EJ, Patrick C, Rockenstein E *et al*. (2009) Inclusion formation and neuronal cell death through neuron-to-neuron transmission of α-synuclein. *Proc Natl Acad Sci USA* **106**:13010-13015.

Devi L, Raghavendran V, Prabhu BM, Avadhani NG, Anandatheerthavarada HK (2008) Mitochondrial import and accumulation of α-synuclein impair complex I in human dopaminergic neuronal cultures and Parkinson disease brain. *J Biol Chem*. **283**:9089-9100.

Devine MJ, Gwinn K, Singleton A, Hardy J (2011) Parkinson's disease and α-synuclein expression. *Mov Disord*. **26**:2160-2168.

Di Maio R, Barrett PJ, Hoffman EK, Barrett CW, Zharikov A *et al*. (2016) α-Synuclein binds to TOM20 and inhibits mitochondrial protein import in Parkinson's disease. *Sci Transl Med*. **8**:342ra78.

Dickson DW (2012) Parkinson's disease and parkinsonism: neuropathology. *Cold Spring Harb Perspect Med*. **2**:a009258.

Ding TT, Lee SJ, Rochet JC, Lansbury PT Jr (2002) Annular alpha-synuclein protofibrils are produced when spherical protofibrils are incubated in solution or bound to brain-derived membranes. *Biochemistry* **41**:10209-10217.

Diógenes MJ, Dias RB, Rombo DM, Vicente Miranda H, Maiolino F *et al*. (2012) Extracellular alpha-synuclein oligomers modulate synaptic transmission and impair LTP via NMDA-receptor activation. *J Neurosci*. **32**:11750-11762.

Dobson CM (2003) Protein folding and misfolding. *Nature* **426**:884-890.

Doty RL, Shaman P, Dann M (1984) Development of the University of Pennsylvania Smell Identification Test: a standardized microencapsulated test of olfactory function. *Physiol Behav*. **32**:489-502.

Doty RL (2012) Olfactory dysfunction in Parkinson disease. *Nat Rev Neurol*. **8**:329-339.

Downs TR, Wilfinger WW (1983) Fluorometric quantification of DNA in cells and tissue. *Anal Biochem*. **131**:538-547.

Doxakis E (2010) Post-transcriptional regulation of α-synuclein expression by mir-7 and mir-153. *J Biol Chem*. **285**:12726-12734.

Driver JA, Logroscino G, Gaziano JM, Kurth T (2009) Incidence and remaining lifetime risk of Parkinson disease in advanced age. *Neurology* **72**:432-38.

Dryanovski DI, Guzman JN, Xie Z, Galteri DJ, Volpicelli-Daley LA *et al*. (2013) Calcium entry and α-synuclein inclusions elevate dendritic mitochondrial oxidant stress in dopaminergic neurons. *J Neurosci*. **33**:10154-10164.

Dufty BM, Warner LR, Hou ST, Jiang SX, Gomez-Isla T *et al*. (2007) Calpain-cleavage of α-synuclein: connecting proteolytic processing to disease-linked aggregation. *Am J Pathol*. **170**:1725-1738.

Edwards TL, Scott WK, Almonte C, Burt A, Powell EH *et al*. (2010) Genome-wide association study confirms SNPs in SNCA and the MAPT region as common risk factors for Parkinson disease. *Ann Hum Genet*. **74**:97-109.

Ehrnhoefer DE, Bieschke J, Boeddrich A, Herbst M, Masino L *et al*. (2008) EGCG redirects amyloidogenic polypeptides into unstructured, off-pathway oligomers. *Nat Struct Mol Biol*. **15**:558-566.

Eisenberg D, Jucker M (2012) The amyloid state of proteins in human diseases. *Cell* **148**:1188-1203.

El-Agnaf OM, Salem SA, Paleologou KE, Cooper LJ, Fullwood NJ *et al*. (2003) α-Synuclein implicated in Parkinson's disease is present in extracellular biological fluids, including human plasma, *FASEB J*. **17**:1945-1947.

Eliezer D, Kutluay E, Bussell R, Browne G (2001) Conformational properties of α-synuclein in its free and lipid-associated states. *J Mol Biol*. **307**:1061-1073.

Ellis CE, Schwartzberg PL, Grider TL, Fink DW, Nussbaum RL (2001) α-Synuclein is phosphorylated by members of the Src family of protein-tyrosine kinases. *J Biol Chem*. **276**:3879-3884.

Emmanouilidou E, Melachroinou K, Roumeliotis T, Garbis SD, Ntzouni M *et al*. (2010) Cell-produced-synuclein is secreted in a calcium dependent manner by exosomes and impacts neuronal survival. *J Neurosci*. **30**:6838-6851.

Eschbach J, von Einem B, Müller K, Bayer H, Scheffold A *et al*. (2015) Mutual exacerbation of peroxisome proliferator-activated receptor γ coactivator 1α deregulation and α-synuclein oligomerization. *Ann Neurol.* **77**:15-32.

Eusebi P, Hansson O, Paciotti S, Orso M, Chiasserini D *et al*. (2017) Diagnostic utility of cerebrospinal fluid α-synuclein in Parkinson's disease: a systematic review and meta-analysis. *Mov Disord*. **32**:1389-400.

Evangelisti E, Cascella R, Becatti M, Marrazza G, Dobson CM et al. (2016) Binding affinity of amyloid oligomers to cellular membranes is a generic indicator of cellular dysfunction in protein misfolding diseases. Sci Rep. 6:32721.

Fagerqvist T, Näsström T, Ihse E, Lindström V, Sahlin C *et al*. (2013) Off-pathway α-synuclein oligomers seem to alter α-synuclein turnover in a cell model but lack seeding capability in vivo. *Amyloid* **20**:233-244.

Fairfoul G, McGuire LI, Pal S, Ironside JW, Neumann J *et al*. (2016) Alpha-synuclein RT-QuIC in the CSF of patients with alpha-synucleinopathies. *Ann Clin Transl Neurol*. **3**:812-818.

Fandrich M, Dobson CM (2002) The behaviour of polyamino acids reveals an inverse side chain effect in amyloid structure formation. *EMBO J*. **21**:5682-5690.

Fang F, Chen H, Feldman AL, Kamel F, Ye W *et al*. (2012) Head injury and Parkinson's disease: a population-based study. *Mov Disord*. **27**:1632-1635.

Fang F, Yang W, Florio JB, Rockenstein E, Spencer B *et al*. (2017) Synuclein impairs trafficking and signaling of BDNF in a mouse model of Parkinson's disease. *Sci Rep*. **7**:3868.

Fares MB, Ait-Bouziad N, Dikiy I, Mbefo MK, Jovičić A *et al*. (2014) The novel Parkinson's disease linked mutation G51D attenuates in vitro aggregation and membrane binding of α-synuclein, and enhances its secretion and nuclear localization in cells. *Hum Mol Genet*. **23**:4491-4509.

Faustini G, Longhena F, Varanita T, Bubacco L, Pizzi M *et al*. (2018) Synapsin III deficiency hampers α-synuclein aggregation, striatal synaptic damage and nigral cell loss in an AAV-based mouse model of Parkinson's disease. *Acta Neuropathol*. **136**:621-639.

Feng LR, Federoff HJ, Vicini S, Maguire-Zeiss KA (2010) α-Synuclein mediates alterations in membrane conductance: a potential role for α-synuclein oligomers in cell vulnerability. *Eur J Neurosci*. **32**:10-17.

Ferreira DG, Temido-Ferreira M, Vicente Miranda H, Batalha VL, Coelho JE *et al*. (2017) α-synuclein interacts with PrP^C to induce cognitive impairment through mGluR5 and NMDAR2B, *Nat Neurosci*. **20**:1569-1579.

Ferreira, ST, Klein WL (2011) The Aβ oligomer hypothesis for synapse failure and memory loss in Alzheimer's disease. *Neurobiol Learn Mem*. **96**:529-543.

Ferreira ST, Clarke JR, Bomfim TR, De Felice FG (2014) Inflammation, defective insulin signaling, and neuronal dysfunction in Alzheimer's disease. *Alzheimers Dement*. **10**:S76-S83.

Fitzpatrick AW, Debelouchina GT, Bayro MJ, Clare DK, Caporini MA *et al*. (2013) Atomic structure and hierarchical assembly of a cross-beta amyloid fibril. *Proc Natl Acad Sci USA* **110**:5468-5473.

Flavin WP, Bousset L, Green ZC, Chu Y, Skarpathiotis S *et al*. (2017) Endocytic vesicle rupture is a conserved mechanism of cellular invasion by amyloid proteins. *Acta Neuropathol*. **134**:629-653.

Fontaine SN, Zheng D, Sabbagh JJ, Martin MD, Chaput D *et al*. (2016) DnaJ / Hsc 70 chaperone complexes control the extracellular release of neurodegenerative- associated proteins. *EMBO Mol Med*. **35**:1537-1549.

Forno LS (1996) Neuropathology of Parkinson's disease. *J Neuropathol Exp Neurol*. **55**:259-272.

Freundt EC, Maynard N, Clancy EK, Roy S, Bousset L *et al*. (2012) Neuron-to-neuron transmission of α-synuclein fibrils through axonal transport. *Ann Neurol*. **72**:517-524.

Froula JM, Henderson BW, Gonzalez JC, Vaden JH, Mclean JW *et al*. (2018) α-Synuclein fibril-induced paradoxical structural and functional defects in hippocampal neurons. *Acta Neuropathol Commun*. **6**:35.

Froula JM, Castellana-Cruz M, Anabtawi NM, Camino JD, Chen SW *et al*. (2019) Defining α-synuclein species responsible for Parkinson's disease phenotypes in mice. *J Biol Chem*. **294**:10392-10406.

Fujita Y, Ohama E, Takatama M, Al-Sarraj S, Okamoto K (2006) Fragmentation of Golgi apparatus of nigral neurons with α-synuclein-positive inclusions in patients with Parkinson's disease. *Acta Neuropathol*. **112**:261-265.

Funayama M, Ohe K, Amo T, Furuya N, Yamaguchi J *et al*. (2015) CHCHD2 mutations in autosomal dominant late-onset Parkinson's disease: a genome-wide linkage and sequencing study. *Lancet Neurol*. **14**:274-282.

Furukawa K, Matsuzaki-Kobayashi M, Hasegawa T, Kikuchi A, Sugeno N *et al*. (2006) Plasma membrane ion permeability induced by mutant α-synuclein contributes to the degeneration of neural cells. *J Neurochem.* **97**:1071-1077.

Fusco G, De Simone A, Gopinath T, Vostrikov V, Vendruscolo M *et al*. (2014) Direct observation of the three regions in α-synuclein that determine its membrane-bound behaviour. *Nat Commun*. **5**:3827.

Fusco G, Pape T, Stephens AD, Mahou P, Costa AR *et al*. (2016) Structural basis of synaptic vesicle assembly promoted by α-synuclein. *Nat Commun*. **7**:12563.

Fussi N, Höllerhage M, Chakroun T, Nykänen NP, Rösler TW *et al*. (2018) Exosomal secretion of α-synuclein as protective mechanism after upstream blockage of macroautophagy. *Cell Death Dis*. **9**:757.

Galvagnion C, Buell AK, Meisl G, Michaels TC, Vendruscolo M *et al*. (2015) Lipid vesicles trigger alpha-synuclein aggregation by stimulating primary nucleation. *Nat Chem Biol*. **11**:229-234.

Games D, Valera E, Spencer B, Rockenstein E, Mante M *et al*. (2014) Reducing C-terminal-truncated alpha-synuclein by immunotherapy attenuates neurodegeneration and propagation in Parkinson's disease-like models. *J Neurosci*. **34**:9441-9454.

Gandhi S, Wood-Kaczmar A, Yao Z, Plun-Favreau H, Deas E *et al*. (2009) PINK1-associated Parkinson's disease is caused by neuronal vulnerability to calcium-induced cell death. *Mol Cell*. **33**:627-638.

Ganzinger KA, Narayan P, Qamar SS, Weimann L, Ranasinghe RT *et al*. (2014) Single-molecule imaging reveals that small amyloid-β_{1-42} oligomers interact with the cellular prion protein (PrP^C). *Chembiochem*. **15**:2515-2521.

Gao L, Tang H, Nie K, Wang L, Zhao J *et al*. (2015) Cerebrospinal fluid alpha-synuclein as a biomarker for Parkinson's disease diagnosis: a systematic review and meta-analysis. *Int J Neurosci*. **125**:645-54.

Gao X, Chen H, Schwarzschild MA, Ascherio A (2011) Use of ibuprofen and risk of Parkinson disease. *Neurology* **76**:863-869.

Garcia-Reitböck P, Anichtchik O, Bellucci A, Iovino M, Ballini C, Fineberg E, Ghetti B, Della Corte L, Spano P, Tofaris GK, Goedert M, Spillantini MG (2010) SNARE protein redistribution and synaptic failure in a transgenic mouse model of Parkinson's disease. *Brain* **133**:2032-2044.

Garten M, Prévost C, Cadart C, Gautier R, Bousset L *et al*. (2015) Methyl-branched lipids promote the membrane adsorption of α-synuclein by enhancing shallow lipid-packing defects. *Phys Chem Chem Phys*. **17**:15589-15597.

Gath J, Habenstein B, Bousset L, Melki R, Meier BH *et al*. (2012) Solid state NMR sequential assignments of alpha-synuclein. *Biomol NMR Assign*. **6**:51-55.

Ge Y, Xu K (2016) Alpha-synuclein contributes to malignant progression of human meningioma via the Akt/mTOR pathway. *Cancer Cell Int*. **16**:86.

George JM, Jin H, Woods WS, Clayton DF (1995) Characterization of a novel protein regulated during the critical period for song learning in the zebra finch. *Neuron* **15**:361-372.

Giannoccaro MP, La Morgia C, Rizzo G, Carelli V (2017) Mitochondrial DNA and primary mitochondrial dysfunction in Parkinson's disease. *Mov Disord*. **32**:346-363.

Giasson BI, Duda JE, Murray IV, Chen Q, Souza JM *et al*. (2000) Oxidative damage linked to neurodegeneration by selective α-synuclein nitration in synucleinopathy lesions. *Science* **290**:985-989.

Giasson BI, Murray IV, Trojanowski JQ, Lee VM (2001) A hydrophobic stretch of 12 amino acid residues in the middle of α-synuclein is essential for filament assembly. *J Biol Chem*. **276**:2380-2386.

Gibb WR, Lees AJ (1988) The relevance of the Lewy body to the pathogenesis of idiopathic Parkinson's disease. *J Neurol Neurosurg Psychiatry* **51**:745-752.

Giehm L, Oliveira CL, Christiansen G, Pedersen JS, Otzen DE (2010) SDS-induced fibrillation of alpha-synuclein: an alternative fibrillation pathway. *J Mol Biol*. **401**:115-133.

Giehm L, Svergun DI, Otzen DE, Vestergaard B (2011) Low-resolution structure of a vesicle disrupting α-synuclein oligomer that accumulates during fibrillation. *Proc Natl Acad Sci USA* **108**:3246-3251.

Gitler AD, Bevis BJ, Shorter J, Strathearn KE, Hamamichi S *et al*. (2008) The Parkinson's disease protein α-synuclein disrupts cellular Rab homeostasis. *Proc Natl Acad Sci USA* **105**:145-150.

Glickman MH, Ciechanover A (2002) The ubiquitin–proteasome proteolytic pathway: destruction for the sake of construction. *Physiol Rev*. **82**:373-428

Goedert M (2001) Alpha-synuclein and neurodegenerative diseases. *Nat Rev Neurosci*. **2**:492-501.

Goers J, Manning-Bog AB, McCormack AL, Millett IS, Doniach S *et al*. (2003) Nuclear localization of alpha-synuclein and its interaction with histones. *Biochemistry* **42**:8465-8471.

Gold A, Turkalp ZT, Munoz DG (2013) Enteric alpha-synuclein expression is increased in Parkinson's disease but not Alzheimer's disease. *Mov Disord*. **28**:237-41.

Gorbatyk OS, Li S, Nguyen FN, Manfredsson FP, Kondrikova G *et al*. (2010) α-Synuclein expression in rat substantia nigra phospholipase D2 toxicity and nigral neurodegeneration. *Mol Ther*. **18**:1758-1768.

Gosavi N, Lee HJ, Lee JS, Patel S, Lee SJ (2002) Golgi fragmentation occurs in the cells with prefibrillar α-synuclein aggregates and precedes the formation of fibrillar inclusion. *J Biol Chem*. **277**:48984-48992.

Ghosh D, Singh PK, Sahay S, Jha NN, Jacob RS *et al*. (2015) Structure based aggregation studies reveal the presence of helix-rich intermediate during α-synuclein aggregation. *Sci Rep*. **5**:9228.

Grace AA, Bunney BS (1983) Intracellular and extracellular electrophysiology of nigral dopaminergic neurons-3. Evidence for electrotonic coupling. *Neuroscience* **10**:333–335; 337-348.

Gräff J, Tsai L-H (2013) Histone acetylation: molecular mnemonics on the chromatin. *Nat Rev Neurosci*. **14**:97-111.

Greten-Harrison B, Polydoro M, Morimoto-Tomita M, Diao L, Williams AM *et al*. (2010) αβγ-Synuclein triple knockout mice reveal age-dependent neuronal dysfunction. *Proc Natl Acad Sci USA* **107**:19573-19578.

Grosch J, Winkler J, Kohl Z (2016) Early degeneration of both dopaminergic and serotonergic axons – a common mechanism in Parkinson's disease. *Front Cell Neurosci.* **10**:293.

Guardia-Laguarta C, Area-Gomez E, Rüb C, Liu Y, Magrané J *et al*. (2015) α-Synuclein is localized to mitochondria-associated ER membranes. *J Neurosci.* **34**:249-259.

Guerrero-Ferreira R, Taylor NM, Mona D, Ringler P, Lauer ME *et al*. (2018) Cryo-EM structure of α-synuclein fibrils. *eLife* **7**:e36402.

Guilliams T, El-Turk F, Buell AK, O'Day EM, Aprile FA *et al*. (2013) Nanobodies raised against monomeric α-synuclein distinguish between fibrils at different maturation stages. *J Mol Biol*. **425**:2397-2411.

Guo JU, Ma DK, Mo H, Ball MP, Jang MH *et al*. (2011) Neuronal activity modifies the DNA methylation landscape in the adult brain. *Nat Neurosci*. **14**:1345-1351.

Guo JT, Chen AQ, Kong Q, Zhu H, Ma CM *et al*. (2008) Inhibition of vesicular monoamine transporter-2 activity in α-synuclein stably transfected SH-SY5Y cells. *Cell Mol Neurobiol*. **28**:35-47.

Gureviciene I, Gurevicius K, Tanila H (2007) Role of α-synuclein in synaptic glutamate release. *Neurobiol Dis*. **28**:83-89.

Gureviciene I, Gurevicius K, Tanila H (2009) Aging and α-synuclein affect synaptic plasticity in the dentate gyrus. *J Neural Transm.* **116**:13-22.

Guzman JN, Sánchez-Padilla J, Chan CS, Surmeier DJ (2009) Robust pacemaking in substantia nigra dopaminergic neurons. *J Neurosci*. **29**:11011-11019.

Haas RH, Nasirian F, Nakano K, Ward D, Pay M *et al*. (1995) Low platelet mitochondrial complex I and complex II/III activity in early untreated Parkinson's disease. *Ann Neurol*. **37**:714-722.

Halliday G, Lees A, Stern M (2011) Milestones in Parkinson's disease—Clinical and pathologic features. *Mov Disord*. **26**:1015-1021.

Hansen C, Angot E, Bergström AL, Steiner JA, Pieri L *et al*. (2011) α-Synuclein propagates from mouse brain to grafted dopaminergic neurons and seeds aggregation in cultured human cells. *J Clin Invest*. **121**:715-725.

Hashimoto M, Yoshimoto M, Sisk A, Hsu LJ, Sundsmo M *et al*. (1997) NACP, a synaptic protein involved in Alzheimer's disease, is differentially regulated during megakaryocyte differentiation. *Biochem Biophys Res Commun*. **237**:611-616.

Hayden EY, Teplow DB (2013) Amyloid β-protein oligomers and Alzheimer's disease. *Alzheimers Res Ther*. **5**:60.

Healy DG, Falchi M, O'Sullivan SS, Bonifati V, Durr A *et al*. (2008) Phenotype, genotype, and worldwide genetic penetrance of LRRK2-associated Parkinson's disease: a case-control study. *Lancet Neurol*. **7**:583-90.

Heinzel S, Gold M, Deuschle C, Bernhard F, Maetzler W *et al*. (2014) Naturally occurring alpha-synuclein autoantibodies in Parkinson's disease: sources of (error) variance in biomarker assays. *PLoS One* **9**:e114566.

Heise H, Hoyer W, Becker S, Andronesi OC, Riedel D *et al*. (2005) Molecular-level secondary structure, polymorphism, and dynamics of full-length alpha-synuclein fibrils studied by solid-state NMR. *Proc Natl Acad Sci USA* **102**:15871-15876.

Heman-Ackah SM, Manzano R, Hoozemans JJ, Scheper W, Flynn R *et al*. (2017) α-Synuclein induces the unfolded protein response in Parkinson's disease SNCA triplication iPSC-derived neurons. *Hum Mol Genet*. **26**:4441-4450.

Henderson MX, Peng C, Trojanowski JQ, Lee VMY (2018) LRRK2 activity does not dramatically alter α-synuclein pathology in primary neurons, *Acta Neuropathol Commun*. **6**:45.

Henderson MX, Trojanowski JQ, Lee VMY (2019) α-Synuclein pathology in Parkinson's disease and related α-synucleinopathies. *Neurosci Lett*. **709**:134316.

Hinault MP, Cuendet AF, Mattoo RU, Mensi M, Dietler G *et al*. (2010) Stable α-synuclein oligomers strongly inhibit chaperone activity of the Hsp70 system by weak interactions with J-domain co-chaperones. *J Biol Chem*. **285**:38173-38182.

Hogan DB, Fiest KM, Roberts JI, Maxwell CJ, Dykeman J *et al*. (2016) The prevalence and incidence of dementia with Lewy bodies: a systematic review. *Can J Neurol Sci*. **43**:S83-95.

Holmes BB, DeVos SL, Kfoury N, Li M, Jacks R *et al*. (2013) Heparan sulfate proteoglycans mediate internalization and propagation of specific proteopathic seeds. *Proc Natl Acad Sci USA* **110**:E3138-47.

Hong Z, Shi M, Chung KA, Quinn JF, Peskind ER *et al*. (2010) DJ-1 and α-synuclein in human cerebrospinal fluid as biomarkers of Parkinson's disease. *Brain* **133**:713-26.

Hoozemans JJM, van Haastert ES, Eikelenboom P, de Vos RAI, Rozemuller JM *et al*. (2007) Activation of the unfolded protein response in Parkinson's disease. *Biochem. Biophys Res Commun.* **354**:707-711.

Horrocks MH, Lee SF, Gandhi S, Magdalinou NK, Chen SW *et al*. (2016) Single-molecule imaging of individual amyloid protein aggregates in human biofluids. *ACS Chem Neurosci*. **7**:399-406.

Hoyer W, Cherny D, Subramaniam V, Jovin TM (2004) Impact of the acidic C-terminal region comprising amino acids 109–140 on α-synuclein aggregation in vitro. *Biochemistry* **43**:16233-16242.

Huang Z, Xu Z, Wu Y, Zhou Y (2011) Determining nuclear localization of alpha-synuclein in mouse brains. *Neuroscience* **199**:318-332.

Hughes AJ, Daniel S, Lees A (2001) Improved accuracy of clinical diagnosis of Lewy body. *Neurology* **57**:1497-1499.

Hughes CD, Choi ML, Ryten M, Hopkins L, Drews A *et al*. (2019) Picomolar concentrations of oligomeric alpha-synuclein sensitizes TLR4 to play an initiating role in Parkinson's disease pathogenesis. *Acta Neuropathol*. **137**:103-120.

Hüls S, Högen T, Vassallo N, Danzer KM, Hengerer B, Giese A, Herms J (2012) AMPA-receptor-mediated excitatory synaptic transmission is enhanced by iron-induced α-synuclein oligomers. *J Neurochem*. **117**:868-78.

Hurley MJ, Brandon B, Gentleman SM, Dexter DT (2013) Parkinson's disease is associated with altered expression of CaV1 channels and calcium-binding proteins. *Brain* **136**:2077-2097.

Ibáñez P, Bonnet AM, Débarges B, Lohmann E, Tison F *et al*. (2004) Causal relation between α-synuclein gene duplication and familial Parkinson's disease. *Lancet* **364**:1169-1171.

Ilijic E, Guzman JN, Surmeier DJ (2011) The L-type channel antagonist isradipine is neuroprotective in a mouse model of Parkinson's disease. *Neurobiol Dis*. **43**:364-371.

Imai Y, Soda M, Takahashi R (2000) Parkin suppresses unfolded protein stress-induced cell death through its E3 ubiquitin-protein ligase activity. *J Biol Chem*. **275**:35661-35664.

Ingelsson M (2016) Alpha-synuclein oligomers - neurotoxic molecules in Parkinson's disease and other Lewy body disorders. *Front Neurosci*. **10**:408.

Israeli E, Yakunin E, Zarbiv Y, Hacohen-Solovich A, Kisos H *et al*. (2011) α-Synuclein expression selectively affects tumorigenesis in mice modeling Parkinson's disease. *PLoS One* **6**:e19622.

Iwata A, Maruyama M, Akagi T, Hashikawa T, Kanazawa I *et al*. (2003) Alpha-synuclein degradation by serine protease neurosin: implication for pathogenesis of synucleinopathies. *Hum Mol Genet*. **12**:2625-2635.

Jakes R, Spillantini MG, Goedert M (1994) Identification of two distinct synucleins from human brain. *FEBS Lett*. **345**:27-32.

Jang A, Lee H, Suk JE, Jung JW, Kim KP *et al*. (2010) Non-classical exocytosis of α-synuclein is sensitive to folding states and promoted under stress conditions. *J Neurochem*. **113**:1263-1274.

Jang HS, Shin WJ, Lee JE, Do JT (2017) CpG and Non-CpG Methylation in Epigenetic Gene Regulation and Brain Function. *Genes (Basel)* **8**:148.

Jankovic J (2008) Parkinson's disease: clinical features and diagnosis. *J Neurol Neurosurg Psychiatry* **79**:368-376.

Janowska MK, Wu KP, Baum J (2015) Unveiling transient protein-protein interactions that modulate inhibition of alpha-synuclein aggregation by beta-synuclein, a pre-synaptic protein that co-localizes with alpha-synuclein. *Sci Rep*. **5**:15164.

Jenco JM, Rawlingson A, Daniels B, Morris AJ (1998) Regulation of phospholipase D2: Selective inhibition of mammalian phospholipase D isoenzymes by α- and β-synucleins. *Biochemistry* **37**:4901-4909.

Ji H, Liu YE, Jia T, Wang M, Liu J *et al*. (1997) Identification of a breast cancer-specific gene, BCSG1, by direct differential cDNA sequencing. *Cancer Res*. **57**:759–764.

Jiang P, Gan M, Yen SH, McLean PJ, Dickson DW (2017) Impaired endo-lysosomal membrane integrity accelerates the seeding progression of α-synuclein aggregates, *Sci Rep*. **7**:7690.

Jiang Z, de Messieres M, Lee JC (2013) Membrane remodeling by α-synuclein and effects on amyloid formation. *J Am Chem Soc*. **135**:15970-15973.

Jimenez JL, Guijarro JI, Orlova E, Zurdo J, Dobson CM *et al*. (1999) Cryo-electron microscopy structure of an SH3 amyloid fibril and model of the molecular packing. *EMBO J*. **18**:815-821.

Jin H, Kanthasamy A, Ghosh A, Yang Y, Anantharam V *et al*. (2011) α-Synuclein negatively regulates protein kinase Cd expression to suppress apoptosis in dopaminergic neurons by reducing p300 histone acetyltransferase activity. *J Neurosci*. **31**:2035-2051.

Johnson M, Coulton AT, Geeves MA, Mulvihill DP (2010) Targeted amino-terminal acetylation of recombinant proteins in E. coli. *PLoS ONE* **5**:e15801.

Kalia LV, Kalia SK, McLean PJ, Lozano AM, Lang AE (2013) α-Synuclein oligomers and clinical implications for Parkinson disease. *Ann Neurol*. **73**:155-169.

Kalinderi K, Bostantjopoulou S, Fidani L (2016) The genetic background of Parkinson's disease: current progress and future prospects. *Acta Neurol Scand*. **134**:314-326.

Kamp F, Beyer K (2006) Binding of α-synuclein affects the lipid packing in bilayers of small vesicles. *J Biol Chem*. **281**:9251-9259.

Kang L, Moriarty GM, Woods LA, Ashcroft AE, Radford SE *et al*. (2012) N-terminal acetylation of α-synuclein induces increased transient helical propensity and decreased aggregation rates in the intrinsically disordered monomer. *Protein Sci*. **21**:911-917.

Karpowicz RJ Jr, Haney CM, Mihaila TS, Sandler RM, Petersson EJ *et al*. (2017) Selective imaging of internalized proteopathic α-synuclein seeds in primary neurons reveals mechanistic insight into transmission of synucleinopathies. *J Biol Chem*. **292**: 13482-13497.

Kawashima M, Suzuki SO, Doh-ura K, Iwaki T (2000) α-Synuclein is expressed in a variety of brain tumors showing neuronal differentiation. *Acta Neuropathol.* **99**:154-160.

Kayed R, Head E, Thompson JL, McIntire TM, Milton SC *et al*. (2003) Common structure of soluble amyloid oligomers implies common mechanism of pathogenesis. *Science* **300**:486-489.

Kayed R, Head E, Sarsoza F, Saing T, Cotman CW *et al*. (2007) Fibril specific, conformation dependent antibodies recognize a generic epitope common to amyloid fibrils and fibrillar oligomers that is absent in prefibrillar oligomers. *Mol Neurodegener*. **26**:2-18.

Kaylor J, Bodner N, Edridge S, Yamin G, Hong DP *et al*. (2005) Characterization of oligomeric intermediates in alpha-synuclein fibrillation: FRET studies of Y125W/Y133F/Y136F alpha-synuclein. *J Mol Biol*. **353**:357-372.

Kim S, Jeon BS, Heo C, Im PS, Ahn TB *et al*. (2004) α-Synuclein induces apoptosis by altered expression in human peripheral lymphocyte in Parkinson's disease. *FASEB J.* **18**:1615-1617.

Kim J, Inoue K, Ishii J, Vanti WB, Voronov SV *et al*. (2007) A MicroRNA feedback circuit in midbrain dopamine neurons. *Science* **317**:1220-1224.

Kim, HY, Cho MK, Kumar, A., Maier, E., Siebenhaar C *et al*. (2009) Structural properties of pore-forming oligomers of α-synuclein. *J Am Chem Soc.* **131**:17482-17489.

Kirik D, Rosenblad C, Burger C, Lundberg C, Johansen TE *et al*. (2002) Parkinson-like neurodegeneration induced by targeted overexpression of α-synuclein in the nigrostriatal system. *J Neurosci.* **22**:2780-2791.

Kisos H, Pukaß K, Ben-Hur T, Richter-Landsberg C *et al*. (2012) Increased neuronal α-synuclein pathology associates with its accumulation in oligodendrocytes in mice modeling α-synucleinopathies, *PLoS One* **7**:e46817.

Kitada T, Asakawa S, Hattori N, Matsumine H, Yamamura Y *et al*. (1998) Mutations in the parkin gene cause autosomal recessive juvenile parkinsonism. *Nature* **392**:605-608.

Klucken J, Poehler AM, Ebrahimi-Fakhari D, Schneider J, Nuber S *et al*. (2012) Alpha-synuclein aggregation involves a bafilomycin A_1-sensitive autophagy pathway. *Autophagy* **8**:754-766.

Knowles TP, Fitzpatrick AW, Meehan S, Mott HR, Vendruscolo M *et al*. (2007) Role of intermolecular forces in defining material properties of protein nanofibrils. *Science* **318**:1900-1903.

Koffie RM, Meyer-Luehmann M, Hashimoto T, Adams KW, Mielke ML *et al*. (2009) Oligomeric amyloid beta associates with postsynaptic densities and correlates with excitatory synapse loss near senile plaques. *Proc Natl Acad Sci USA* **106**:4012-4017.

Kontopoulos E, Parvin JD, Feany MB (2006) α-Synuclein acts in the nucleus to inhibit histone acetylation and promote neurotoxicity. *Hum Mol Genet*. **15**:3012-3023.

Krebs B, Wiebelitz A, Balitzki-Korte B, Vassallo N, Paluch S *et al*. (2007) Cellular prion protein modulates the intracellular calcium response to hydrogen peroxide. *J Neurochem*. **100**:358-367.

Krüger R, Kuhn W, Muller T, Woitalla D, Graeber M *et al*. (1998) Ala30Pro mutation in the gene encoding α-synuclein in Parkinson's disease. *Nat Genet*. **18**:106-108.

La Rovere RM, Roest G, Bultynck G, Parys JB (2016) Intracellular Ca^{2+} signaling and Ca^{2+} microdomains in the control of cell survival, apoptosis and autophagy. *Cell Calcium* **60**:74-87.

Labbé C, Betancor OL, Ross OA (2016) Epigenetic regulation in Parkinson's disease. *Acta Neuropathol*. **132**:515-30.

Lamb CA, Yoshimori T, Tooze SA (2013) The autophagosome: origins unknown, biogenesis complex. *Nat Rev Mol Cell Biol*. **14**:759-774.

Larsen KE, Schmitz Y, Troyer MD, Mosharov E, Dietrich P *et al*. (2006) α-Synuclein overexpression in PC12 and chromaffin cells impairs catecholamine release by interfering with a late step in exocytosis. *J Neurosci*. **26**:11915-11922.

Lashuel HA, Petre BM, Wall J, Simon M, Nowak RJ *et al*. (2002) α-Synuclein, especially the Parkinson's disease-associated mutants, forms pore-like annular and tubular protofibrils. *J Mol Biol*. **322**:1089-1102.

Lashuel HA, Overk CR, Oueslati A, Masliah E (2013) The many faces of α-synuclein: from structure and toxicity to therapeutic target. *Nat Rev Neurosci*. **14**:38-48.

Laurén J, Gimbel DA, Nygaard HB, Gilbert JW, Strittmatter SM (2009) Cellular prion protein mediates impairment of synaptic plasticity by amyloid-beta oligomers. *Nature* **457**:1128-1132.

Lautenschläger J, Stephens AD, Fusco G, Ströhl F, Curry N *et al*. (2018) C-terminal calcium binding of α-synuclein modulates synaptic vesicle interaction. *Nat Commun*. **9**:712.

Lavedan C, Leroy E, Dehejia A, Buchholtz S, Dutra A *et al*. (1998) Identification, localization and characterization of the human γ-synuclein gene. *Hum Genet*. **103**:106-112.

Layfield R, Tooth D, Landon M, Dawson S, Mayer J *et al*. (2001) Purification of poly-ubiquitinated proteins by S5a-affinity chromatography. *Proteomics* **1**:773-777.

Lázaro DF, Dias M1, Carija A, Navarro S, Madaleno CS *et al*. (2016) The effects of the novel A53E alpha-synuclein mutation on its oligomerization and aggregation. *Acta Neuropathol. Commun*. **4**:128.

Lee A, Gilbert RM (2016) Epidemiology of Parkinson Disease. *Neurol Clin.* **34**:955-965.

Lee HJ, Khoshaghideh F, Patel S, Lee SJ (2004) Clearance of α-synuclein oligomeric intermediates via the lysosomal degradation pathway. *J Neurosci*. **24**:1888-1896.

Lee HJ, Suk JE, Bae EJ, Lee JH, Paik SR *et al*. (2008) Assembly-dependent endocytosis and clearance of extracellular α-synuclein. *Int J Biochem Cell Biol*. **40**:1835-1849.

Lee HJ, Cho ED, Lee KW, Kim JH, Cho SG *et al*. (2013) Autophagic failure promotes the exocytosis and intercellular transfer of α-synuclein. *Exp Mol Med*. **45**:e22.

Lee HJ, Bae EJ, Lee SJ (2014) Extracellular α- synuclein- a novel and crucial factor in Lewy body diseases. *Nat Rev Neurol*. **10**:92-98.

Lee JC, Lai BT, Kozak JJ, Gray HB, Winkler JR (2007) α-Synuclein tertiary contact dynamics. *J Phys Chem B* **111**:2107-2112.

Lee JG, Takahama S, Zhang G, Tomarev SI, Ye Y (2016) Unconventional secretion of misfolded proteins promotes adaptation to proteasome dysfunction in mammalian cells. *Nat Cell Biol*. **18**:765-776.

Lee S, Imai Y, Gehrke S, Liu S, Lu B (2012) The synaptic function of LRRK2. *Biochem Soc Trans*. **40**:1047-51.

Lesage S, Drouet V, Majounie E, Deramecourt V, Jacoupy M *et al*. (2016) Loss of VPS13C function in autosomal-recessive parkinsonism causes mitochondrial dysfunction and Increases PINK1/Parkin-dependent mitophagy. *Am J Hum Genet*. **98**:500-513.

Lesage S, Condroyer C, Klebe S, Lohmann E, Durif F *et al*. (2012) EIF4G1 in familial Parkinson's disease: pathogenic mutations or rare benign variants? *Neurobiol Aging*. **33**:e1-e5.

Lewis PA, Spillane JE (2019) The Molecular and Clinical Pathology of Neurodegenerative Disease – Chapter 3, Parkinson's Disease. 83-121.

Li QX, Campbell BC, McLean CA, Thyagarajan D, Gai WP *et al*. (2002) Platelet α- and γ-synucleins in Parkinson's disease and normal control subjects. *J Alzheimers Dis*. **4**:309-315.

Li W, West N, Colla E, Pletnikova O, Troncoso JC *et al*. (2005) Aggregation promoting C-terminal truncation of alpha-synuclein is a normal cellular process and is enhanced by the familial Parkinson's disease-linked mutations. *Proc Natl Acad Sci USA* **102**:2162-2167.

Li WW, Yang R, Guo JC, Ren HM, Zha XL *et al*. (2007) Localization of α-synuclein to mitochondria within midbrain of mice. *NeuroReport* **18**:1543-1546.

Li X, Hoffmann M, Garen CR, Cortez LM, Petersen NO *et al*. (2019) Early stages of aggregation of engineered α-synuclein monomers and oligomers in solution. *Sci Rep*. **9**:1734.

Linazasoro, G, Borg M, Tijssen MAJ, Bressman SB, Dobyns WB *et al*. (2002) Pathogenesis of Parkinson's disease: dopamine, vesicles and α-synuclein. *Nat Rev Neurosci*. **3**:932-942.

Liu CW, Giasson BI, Lewis KA, Lee VM, Demartino GN *et al*. (2005) A precipitating role for truncated α-synuclein and the proteasome in α-synuclein aggregation: implications for pathogenesis of Parkinson disease. *J Biol Chem.* **280**:22670-22678.

Liu S, Ninan I, Antonova I, Battaglia F, Trinchese F *et al*. (2004) α-Synuclein produces a long-lasting increase in neurotransmitter release. *EMBO J.* **23**:4506-4516.

Liu Q, Emadi S, Shen JX, Sierks MR, Wu J (2013) Human α4β2 nicotinic acetylcholine receptor as a novel target of oligomeric α-synuclein. *PLoS One* **8**:e55886.

Longhena F, Faustini G, Varanita T, Zaltieri M, Porrini V *et al*. (2018) Synapsin III is a key component of α-synuclein fibrils in Lewy bodies of PD brains. *Brain Pathol*. **28**:875-888.

Longhena F, Faustini G, Spillantini MG, Bellucci A (2019) Living in promiscuity: the multiple partners of alpha-synuclein at the synapse in physiology and pathology. *Int J Mol Sci*. **20**:141.

Lorenzen N., Nielsen SB, Buell AK, Kaspersen JD, Arosio P *et al*. (2014) The role of stable α-synuclein oligomers in the molecular events underlying amyloid formation. *J Am Chem Soc*. **136**:3859-3868.

Ltic S, Perovic M, Mladenovic A, Raicevic N, Ruzdijic S *et al*. (2004) α-Synuclein is expressed in different tissues during human fetal development. *J Mol Neurosci*. **22**:199-204.

Lu JH, Ardah MT, Durairajan SS, Liu LF, Xie LX (2011) Baicalein inhibits formation of α-synuclein oligomers within living cells and prevents Aβ peptide fibrillation and oligomerisation. *Chem biochem.* **12**:615-624.

Lu X, Kim-Han J, Harmon S, Sakiyama-Elbert SE, O'Malley KL (2014) The Parkinsonian mimetic, 6-OHDA, impairs axonal transport in dopaminergic axons. *Mol Neurodegener*. **9**:17.

Lucke C, Gantz DL, Klimtchuk E, Hamilton JA (2006) Interactions between fatty acids and α-synuclein. *J Lipid Res*. **47**:1714-1724.

Ludtmann MHR, Angelova PR, Horrocks MH, Choi ML, Rodrigues M *et al*. (2018) α-Synuclein oligomers interact with ATP synthase and open the permeability transition pore in Parkinson's disease. *Nat Commun.* **9**:2293.

Luk KC, Song C, O'Brien P, Stieber A, Branch JR *et al*. (2009) Exogenous α-synuclein fibrils seed the formation of Lewy body-like intracellular inclusions in cultured cells. *Proc Natl Acad Sci USA* **106**:20051-20056.

Luk KC, Kehm VM, Zhang B, O'Brien P, Trojanowski JQ *et al*. (2012a) Intracerebral inoculation of pathological α-synuclein initiates a rapidly progressive neurodegenerative alpha-synucleinopathy in mice. *J Exp Med*. **209**:975-986.

Luk KC, Kehm V, Carroll J, Zhang B, O'Brien P *et al*. (2012b) Pathological α-synuclein transmission initiates Parkinson-like neurodegeneration in nontransgenic mice. *Science* **338**:949-953.

Luna E, Decker SC, Riddle DM, Caputo A, Zhang B *et al*. (2018) Differential α-synuclein expression contributes to selective vulnerability of hippocampal neuron subpopulations to fibril-induced toxicity. *Acta Neuropathol*. **135**:855-875.

Lv Z, Krasnoslobodtsev AV, Zhang Y, Ysselstein D, Rochet JC *et al*. (2016) Effect of acidic pH on the stability of α-synuclein dimers. *Biopolymers* **105**:715-724.

Ma KL, Song LK, Yuan YH, Zhang Y, Han N *et al*. (2014) The nuclear accumulation of alpha-synuclein is mediated by importin alpha and promotes neurotoxicity by accelerating the cell cycle. *Neuropharmacology* **82**:132-42.

Mak SK, McCormack AL, Manning-Bog AB, Cuervo AM, Di Monte DA (2010) Lysosomal degradation of α-synuclein in vivo. *J Biol Chem*. **285**:13621-13629.

Machiya Y, Hara S, Arawaka S, Fukushima S, Sato H *et al*. (2010) Phosphorylated α-synuclein at Ser-129 is targeted to the proteasome pathway in a ubiquitin-independent manner. *J Biol Chem*. **285**:40732-40744.

Majbour NK, Vaikath NN, van Dijk KD, Ardah MT, Varghese S *et al*. (2016) Oligomeric and phosphorylated α-synuclein as potential CSF biomarkers for Parkinson's disease. *Mol Neurodegener*. **11**:7.

Mao X, Ou MT, Karuppagounder SS, Kam TI, Yin X *et al*. (2016) Pathological α-synuclein transmission initiated by binding lymphocyte-activation gene 3. *Science* **353**:6307.

Maraganore DM, Lesnick TG, Elbaz A, Chartier-Harlin MC, Gasser T *et al*. (2004) UCHL1 is a Parkinson's disease susceptibility gene. *Ann Neurol*. **55**:512-521.

Maroteaux L, Campanelli JT, Scheller RH (1988) Synuclein: a neuron-specific protein localized to the nucleus and presynaptic nerve terminal. *J Neurosci*. **8**:2804-2815.

Marques SC, Oliveira CR, Pereira CM, Outeiro TF (2011) Epigenetics in neurodegeneration: a new layer of complexity. *Prog Neuropsychopharmacol Biol Psychiatry* **35**:348-355.

Martin I, Kim JW, Lee BD, Kang HC, Xu JC *et al*. (2014) Ribosomal protein s15 phosphorylation mediates LRRK2 neurodegeneration in Parkinson’s disease. *Cell* **157**:472-485.

Martin ZS, Neugebauer V, Dineley KT, Kayed R, Zhang W *et al*. (2012) α-Synuclein oligomers oppose long-term potentiation and impair memory through a calcineurin-

dependent mechanism: relevance to human synucleopathic diseases. *J Neurochem*. **120**:440-452.

Martinat C, Bacci JJ, Leete T, Kim J, Vanti WB *et al*. (2006) Cooperative transcription activation by Nurr1 and Pitx3 induces embryonic stem cell maturation to the midbrain dopamine neuron phenotype. *Proc Natl Acad Sci USA* **103**:2874-2879.

Martinez Z, Zhu M, Han S, Fink AL (2007) GM1 specifically interacts with alpha-synuclein and inhibits fibrillation. *Biochemistry* **46**:1868-1877.

Martins IC, Kuperstein I, Wilkinson H, Maes E, Vanbrabant M *et al*. (2008) Lipids revert inert Abeta amyloid fibrils to neurotoxic protofibrils that affect learning in mice. *EMBO J*. **27**:224-33.

Masaracchia C, Hnida M, Gerhardt E, Lopes da Fonseca T, Villar-Pique A *et al*. (2018) Membrane binding, internalization, and sorting of alpha-synuclein in the cell. *Acta Neuropathol Commun*. **6**:79.

Masliah E, Rockenstein E, Veinbergs I, Mallory M, Hashimoto M *et al*. (2000) Dopaminergic loss and inclusion body formation in α-synuclein mice: implications for neurodegenerative disorders. *Science* **287**:1265-1269.

Masuda-Suzukake M, Nonaka T, Hosokawa M, Oikawa T, Arai T *et al*. (2013) Prion-like spreading of pathological α-synuclein in brain. *Brain* **136**:1128-1138.

Masuda-Suzukake M, Nonaka T, Hosokawa M, Kubo M, Shimozawa A *et al*. (2014) Pathological α-synuclein propagates through neural networks. *Acta neuropathologica commun.* **2**:88.

Matsuo Y, Kamitani T (2010) Parkinson's disease-related protein, α-synuclein, in malignant melanoma. *PLoS One* **5**:e10481.

Mazzulli JR, Xu YH, Sun Y, Knight AL, McLean PJ *et al*. (2011) Gaucher disease glucocerebrosidase and α-synuclein form a bidirectional pathogenic loop in synucleinopathies. *Cell* **146**:37-52.

Mazzulli, JR, Zunke F, Isacson O, Studer L, Krainc D (2016) α-Synuclein-induced lysosomal dysfunction occurs through disruptions in protein trafficking in human midbrain synucleinopathy models. *Proc Natl Acad Sci USA* **113**:1931-1936.

McCann H, Stevens CH, Cartwright H, Halliday GM (2014) α-Synucleinopathy phenotypes. *Parkinsonism Relat Disord*. **20**:S62-S67.

McCoy-Simandle K, Hanna SJ, Cox D (2016) Exosomes and nanotubes: control of immune cell communication. *Int J Biochem Cell Biol.* **71**:44-54.

McKeith IG, Boeve BF, Dickson DW, Halliday G, Taylor JP *et al*. (2017) Diagnosis and management of dementia with Lewy bodies: Fourth consensus report of the DLB Consortium. *Neurology* **89**:88-100.

Mehra S, Sahay S, Maji SK (2019) α-Synuclein misfolding and aggregation: Implications in Parkinson's disease pathogenesis. *BBA - Proteins and Proteomics* **1867** (2019) 890-908.

Melki R (2015) Role of different alpha-synuclein strains in synucleinopathies, similarities with other neurodegenerative diseases. *J Parkinsons Dis*. **5**:217-227.

Miake H, Mizusawa H, Iwatsubo T, Hasegawa M (2002) Biochemical characterization of the core structure of α-synuclein filaments. *J Biol Chem.* **277**:19213-19219.

Mizuno Y, Ohta S, Tanaka M, Takamiya S, Suzuki K *et al*. (1989) Deficiencies in complex I subunits of the respiratory chain in Parkinson's disease. *Biochem Biophys Res Commun*. **163**:1450-1455.

Mizuta I, Satake W, Nakabayashi Y, Ito C, Suzuki S *et al*. (2006) Multiple candidate gene analysis identifies α-synuclein as a susceptibility gene for sporadic Parkinson's disease. *Hum Mol Genet.* **15**:1151-1158.

Morales I, Sanchez A, Rodriguez-sabate C, Rodriguez M (2015) The degeneration of dopaminergic synapses in Parkinson's disease: a selective animal model. *Behav Brain Res*. **289**:19-28.

Morris KL, Serpell LC (2012) X-ray fibre diffraction studies of amyloid fibrils. *Methods Mol. Biol*. **849**:121-136.

Mosmann T (1983) Rapid colorimetric assay for cellular growth and survival: Application to proliferation and cytotoxicity assays. *J Immunol Meth*. **65**:55-63.

Nakai M, Fujita M, Waragai M, Sugama S, Wei J *et al*. (2007) Expression of α-synuclein, a presynaptic protein implicated in Parkinson's disease, in erythropoietic lineage. *Biochem Biophys Res Commun*. **358**:104-110.

Nakajima T, Takauchi S, Ohara K, Kokai M, Nishii R *et al*. (2005) α-synuclein-positive structures induced in leupeptin-infused rats. *Brain Res*. **1040**:73-80.

Nakajo S, Omata K, Aiuchi T, Shibayama T, Okahashi I *et al*. (1990) Purification and characterization of a novel brain-specific 14-kDa protein. *J Neurochem.* **55**:2031-2038.

Nakajo S, Shioda S, Nakai Y, Nakaya K (1994) Localization of phosphoneuroprotein 14 (PNP 14) and its mRNA expression in rat brain determined by immunocytochemistry and in situ hybridization. *Brain Res Mol Brain Res*. **27**:81-86.

Nakamura K, Nemani VM, Azarbal F, Skibinski G, Levy JM *et al*. (2011) Direct membrane association drives mitochondrial fission by the Parkinson disease-associated protein alpha-synuclein. *J Biol Chem.* **286**:20710-20726.

Nakamura T, Yamashita H, Takahashi T *et al*. (2001) Activated Fyn phosphorylates α-synuclein at tyrosine residue 125. *Biochem Biophys Res Commun.* **280**: 1085-1092.

Nedergaard S, Flatman JA, Engberg I (1993) Nifedipine- and omega-conotoxin-sensitive Ca^{2+} conductances in guinea-pig substantia nigra pars compacta neurones. *J Physiol*. **466**: 727-747.

Narkiewicz J, Giachin G, Legname G (2014) In vitro aggregation assays for the characterization of α-synuclein prion-like properties. *Prion* **8**:19-32.

Näsström T, Fagerqvist T, Barbu M, Karlsson M, Nikolajeff F *et al*. (2011) The lipid peroxidation products 4-oxo-2-nonenal and 4-hydroxy-2-nonenal promote the formation of α-synuclein oligomers with distinct biochemical, morphological, and functional properties. *Free Radic Biol Med*. **50**:428-437.

Negro A, Brunati AM, Donella-Deana A, Massimino ML, Pinna LA (2002) Multiple phosphorylation of α-synuclein by protein tyrosine kinase Syk prevents eosin-induced aggregation. *FASEB J*. **16**:210-212.

Nielsen MS, Vorum H, Lindersson E, Jensen PH (2001) Ca^{2+} binding to α-synuclein regulates ligand binding and oligomerization. *J Biol Chem*. **276**:22680-22684.

Nonaka T, Watanabe ST, Iwatsubo T, Hasegawa M (2010) Seeded aggregation and toxicity of α-synuclein and tau: cellular models of neurodegenerative diseases. *J Biol Chem*. **285**:34885-34898.

Noyce AJ, Bestwick JP, Silveira-Moriyama L, Hawkes CH, Giovannoni G *et al*. (2012) Meta-analysis of early nonmotor features and risk factors for Parkinson disease. *Ann Neurol*. **72**:893-901.

Nunnari J, Suomalainen A (2012) Mitochondria: in sickness and in health. *Cell* **148**:1145-1159.

Oliveri V (2019) Toward the discovery and development of effective modulators of α-synuclein amyloid aggregation. *Eur J Med Chem*. **167**:10-36.

Orrenius S, Zhivotovsky B, Nicotera P (2003) Regulation of cell death: the calcium-apoptosis link. *Nat Rev Mol Cell Bio*. **4**:552-565.

Osterberg VR, Spinelli KJ, Weston LJ, Luk KC, Woltjer RL *et al*. (2015) Progressive aggregation of α-synuclein and selective degeneration of Lewy inclusion-bearing neurons in a mouse model of parkinsonism. *Cell Rep*. **10**:1252-1260.

Ouberai MM, Wang J, Swann MJ, Galvagnion C, Guilliams T *et al*. (2013) α-Synuclein senses lipid packing defects and induces lateral expansion of lipids leading to membrane remodeling. *J Biol Chem*. **288**:20883-20895.

Paik SR, Shin HJ, Lee JH, Chang CS, Kim J (1999) Copper(II)-induced self-oligomerization of α-synuclein. *Biochem J*. **340**:821-828.

Paiva I, Jain G, Lázaro DF, Jerčić KG, Hentrich T *et al*. (2018) Alpha-synuclein deregulates the expression of COL4A2 and impairs ER-Golgi function. *Neurobiol Dis.* **119**:121-135.

Paleologou KE, Kragh CL, Mann DM, Salem SA, Al-Shami R *et al*. (2009) Detection of elevated levels of soluble α-synuclein oligomers in post-mortem brain extracts from patients with dementia with Lewy bodies. *Brain* **132**:1093-1101.

Papadopoulos NG, Dedoussis GV, Spanakos G, Gritzapis AD, Baxevanis CN *et al*. (1994) An improved fluorescence assay for the determination of lymphocyte-mediated cytotoxicity using flow cytometry. *J Immunol Meth*. **177**:101-111.

Papp MI, Kahn JE, Lantos PL (1989) Glial cytoplasmic inclusions in the CNS of patients with multiple system atrophy (striatonigral degeneration, olivopontocerebellar atrophy and Shy-Drager syndrome). *J Neurol Sci*. **94**:79-100.

Parihar MS, Parihar A, Fujita M, Hashimoto M, Ghafourifar P (2008) Mitochondrial association of alpha-synuclein causes oxidative stress. *Cell Mol Life Sci.* **65**:1272-1284.

Parihar MS, Parihar A, Fujita M, Hashimoto M, Ghafourifar P (2009) Alpha-synuclein overexpression and aggregation exacerbates impairment of mitochondrial functions by augmenting oxidative stress in human neuroblastoma cells. *Int J Biochem Cell Biol*. **41**: 2015-2024.

Park JY, Kim KS, Lee SB, Ryu JS, Chung KC *et al*. (2009) On the mechanism of internalization of α-synuclein into microglia: roles of ganglioside GM1 and lipid raft. *J Neurochem*. **110**:400-411.

Park G, Tan J, Garcia G, Kang Y, Salvesen G *et al*. (2016) Regulation of histone acetylation by autophagy in Parkinson Disease. *J Biol Chem*. **291**:3531-3540.

Park SM, Jung HY, Kim TD, Park JH, Yang CH *et al*. (2002) Distinct roles of the N-terminal-binding domain and the C-terminal-solubilizing domain of α-synuclein, a molecular chaperone. *J Biol Chem*. **277**:28512-28520.

Parnetti L, Castrioto A, Chiasserini D, Persichetti E, Tambasco N et *al*. (2013) Cerebrospinal fluid biomarkers in Parkinson disease. *Nat Rev Neurol*. **9**:131-140.

Parnetti L, Cicognola C, Eusebi P, Chiasserini D (2016) Value of cerebrospinal fluid α-synuclein species as biomarker in Parkinson's diagnosis and prognosis. *Biomark Med*. **10**:35-49.

Parnetti L, Gaetani L, Eusebi P, Paciotti S, Hansson O *et al*. (2019) CSF and blood biomarkers for Parkinson's disease. *Lancet Neurol*. **18**:573-86.

Pasanem P, Myllykangas L, Siitonem M, Raunio A, Kaakkola S *et al*. (2014) Novel α-synuclein mutation A53E associated with atypical multiple system strophy and Parkinson's disease type pathology. *Neurobiol Aging* **35**:2180.e1-5.

Paumier KL, Luk KC, Manfredsson FP, Kanaan NM, Lipton JW *et al*. (2015) Intrastriatal injection of pre-formed mouse α-synuclein fibrils into rats triggers α-synuclein pathology and bilateral nigrostriatal degeneration. *Neurobiol Dis*. **82**:185-199.

Payton JE, Perrin RJ, Woods WS, George JM (2004) Structural determinants of PLD2 inhibition by α-synuclein. *J Mol Biol*. **337**:1001-1009.

Peelaerts W, Bousset L, Van der Perren A, Moskalyuk A, Pulizzi R *et al*. (2015) α-Synuclein strains cause distinct synucleinopathies after local and systemic administration. *Nature* **522**:340-344.

Pemberton S, Madiona K, Pieri L, Kabani M, Bousset L *et al*. (2011) Hsc70 protein interaction with soluble and fibrillar α-synuclein. *J Biol Chem*. **286**:34690-34699.

Perez RG, Waymire JC, Lin E, Liu JJ, Guo F *et al*. (2002) A role for α-synuclein in the regulation of dopamine biosynthesis. *J Neurosci*. **22**:3090-3099.

Perrin RJ, Woods WS, Clayton DF, George JM (2000) Interaction of human α-synuclein and Parkinson's disease variants with phospholipids. Structural analysis using site-directed mutagenesis. *J Biol Chem*. **275**:34393-34398.

Phillips MJ, Voeltz GK (2016) Structure and function of ER membrane contact sites with other organelles. *Nat Rev Mol Cell Biol.* **17**:69-82.

Pieri L, Madiona K, Bousset L, Melki R (2012) Fibrillar α-synuclein and huntingtin exon 1 assemblies are toxic to the cells. *Biophys J*. **102**:2894-2905.

Pieri L, Chafey P, Le Gall M, Clary G, Melki R *et al*. (2016) Cellular response of human neuroblastoma cells to α-synuclein fibrils, the main constituent of Lewy bodies. *Biochim Biophys Acta*. **1860**:8-19.

Pinho R, Paiva I, Jercic KG, Fonseca-Ornelas L, Gerhardt E *et al*. (2019) Nuclear localization and phosphorylation modulate pathological effects of α-synuclein. *Hum Mol Genet*. **8**:31-50.

Poirier MA, Xiao W, Macosko JC, Chan C, Shin YK *et al*. (1998) The synaptic SNARE complex is a parallel four-stranded helical bundle. *Nat Struct Biol*. **5**:765-769.

Politis M (2014) Neuroimaging in Parkinson disease: from research setting to clinical practice. *Nat Rev Neurol*. **10**:708-722.

Polymeropoulos MH, Lavedan C, Leroy E, Ide SE, Dehejia A *et al*. (1997) Mutation in the α-synuclein gene identified in families with Parkinson's disease. *Science* **276**:2045-2047.

Popoff V, Mardones GA, Bai SK, Chambon V, Tenza D *et al*. (2009) Analysis of articulation between clathrin and retromer in retrograde sorting on early endosomes. *Traffic* **10**:1868-1880.

Portela A, Esteller M (2010) Epigenetic modifications and human disease. *Nat Biotechnol*. **28**:1057-1068.

Postuma RB, Aarsland D, Barone P, Burn DJ, Hawkes CH *et al*. (2012) Identifying prodromal Parkinson's disease: pre-motor disorders in Parkinson's disease. *Mov Disord*. **27**:617-626.

Pranke IM, Morello V, Bigay J, Gibson K, Verbavatz JM *et al*. (2011) α-Synuclein and ALPS motifs are membrane curvature sensors whose contrasting chemistry mediates selective vesicle binding. *J Cell Biol*. **194**:89-103.

Prots I, Grosch J, Brazdis RM, Simmnacher K, Veber V *et al*. (2017) α-Synuclein oligomers induce early axonal dysfunction in human iPSC-based models of synucleinopathies. *Proc Natl Acad Sci USA* **115**:7813-7818.

Prusiner SB, Woerman AL, Mordes DA, Watts JC, Rampersaud R *et al*. (2015) Evidence for alpha-synuclein prions causing multiple system atrophy in humans with parkinsonism. *Proc Natl Acad Sci USA* **112**:5308-5317.

Puopolo M, Raviola E, Bean BP (2007) Roles of subthreshold calcium current and sodium current in spontaneous firing of mouse midbrain dopamine neurons. *J Neurosci*. **27**:645-656.

Qin Z, Hu D, Han S, Reaney SH, Di Monte DA *et al*. (2007) Effect of 4-hydroxy-2-nonenal modification on α-synuclein aggregation. *J Biol Chem*. **282**:5862-5870.

Rappley I, Gitler AD, Selvy PE, LaVoie MJ, Levy BD *et al*. (2009) Evidence that α-synuclein does not inhibit phospholipase D. *Biochemistry* **48**:1077-1083.

Rcom-H'cheo-Gauthier AN, Osborne SL, Meedeniya AC, Pountney DL (2016) Calcium: alpha-synuclein interactions in alpha-synucleinopathies. *Front Neurosci*. **10**:570.

Reijnders JS, Ehrt U, Weber WE, Aarsland D, Leentjens AF (2008) A systematic review of prevalence studies of depression in Parkinson's disease. *Mov Disord*. **23**:183-189.

Rey NL, George S, Steiner JA, Madaj Z, Luk KC *et al*. (2018) Spread of aggregates after olfactory bulb injection of alpha-synuclein fibrils is associated with early neuronal loss and is reduced long term. *Acta Neuropathol*. **135**:65-83.

Reynolds NP, Soragni A, Rabe M, Verdes D, Liverani E *et al*. (2011) Mechanism of membrane interaction and disruption by α-synuclein. *J Am Chem Soc*. **133**:19366-19375.

Richard IH, McDermott MP, Kurlan R, Lyness JM, Como PG *et al*. (2012) A randomized, double-blind, placebo-controlled trial of antidepressants in Parkinson disease. *Neurology* **78**:1229-1236.

Roberts HL, Brown DR (2015) Seeking a mechanism for the toxicity of oligomeric α-synuclein, *Biomolecules* **5**, 282-305.

Rocca WA (2018) The burden of Parkinson's disease: a worldwide perspective. *Lancet Neurol*. **17**:928-929.

Rodriguez L, Marano MM, Tandon A (2018) Import and Export of Misfolded α-synuclein. *Front Neurosci*. **12**:344.

Roncevic D, Palma JA, Martinez J, Goulding N, Norcliffe-Kaufmann L *et al*. (2014) Cerebellar and parkinsonian phenotypes in multiple system atrophy: similarities, differences and survival. *J Neural Transm*. **121**:507-512.

Ronzitti G, Bucci G, Emanuele M, Leo D, Sotnikova TD *et al*. (2014) Exogenous α-synuclein decreases raft partitioning of Cav2.2 channels inducing dopamine release. *J Neurosci*. **34**:10603-10615.

Ross CA, Poirier MA (2005) Opinion: what is the role of protein aggregation in neurodegeneration? *Nat Rev Mol Cell Biol*. **6**:891-898.

Rousseaux MW, de Haro M, Lasagna-Reeves CA, De Maio A, Park J *et al*. (2016) TRIM28 regulates the nuclear accumulation and toxicity of both α-synuclein and tau. *eLife*. **5**:e19809.

Roy S (2017) Synuclein and dopamine: the Bonnie and Clyde of Parkinson's disease. *Nat Neurosci*. **20**:1514-1515.

Sabatini BL, Regehr WG (1987) Timing of neurotransmission at fast synapses in the mammalian brain. *Nature* **384**:170-172.

Sakono M, Zako T (2010) Amyloid oligomers: formation and toxicity of Aβ oligomers. *FEBS J*. **277**:1348-1358.

Salazar SV, Strittmatter SM (2017) Cellular prion protein as a receptor for amyloid-β oligomers in Alzheimer's disease. *Biochem Biophys Res Commun*. **483**:1143-1147.

Sanna G, Del Giudice MG, Crosio C, Iaccarino C (2012) LRRK2 and vesicle trafficking. *Biochem Soc Trans*. **40**:1117-1122.

Sawaya MR, Sambashivan S, Nelson R, Ivanova MI, Sievers SA *et al*. (2015) Linking smoking, coffee, urate, and Parkinson's disease—a role for gut microbiota? *J Parkinsons Dis*. **5**:255-262.

Schrag A, Schott JM (2006) Epidemiological, clinical, and genetic characteristics of early-onset parkinsonism. *Lancet Neurol*. **5**:355-363.

Scott DA, Tabarean I, Tang Y, Cartier A, Masliah E *et al*. (2010) A pathologic cascade leading to synaptic dysfunction in α-synuclein-induced neurodegeneration. *J Neurosci*. **30**:8083-8095.

Scott D, Roy S (2012) α-Synuclein inhibits intersynaptic vesicle mobility and maintains recycling-pool homeostasis. *J Neurosci*. **32**:10129-10135.

Scott-McKean JJ, Surewicz K, Choi JK, Ruffin VA, Salameh AI *et al*. (2016) Soluble prion protein and its N-terminal fragment prevent impairment of synaptic plasticity by Aβ oligomers: Implications for novel therapeutic strategy in Alzheimer's disease. *Neurobiol Dis*. **91**:124-131.

Seirafi M, Kozlov G, Gehring K (2015) Parkin structure and function. *FEBS J*., **282**:2076-2088.

Senior SL, Ninkina N, Deacon R, Bannerman D, Buchman VL *et al*. (2008) Increased striatal dopamine release and hyperdopaminergic-like behavior in mice lacking both α-synuclein and γ-synuclein. *Eur J Neurosci.* **27**:947-957.

Serpell LC, Sunde M, Fraser PE, Luther PK, Morris EP *et al*. (1995) Examination of the structure of the transthyretin amyloid fibril by image reconstruction from electron micrographs. *J Mol Biol*. **254**:113-118.

Serpell LC, Smith JM (2000a) Direct visualisation of the β-sheet structure of synthetic Alzheimer's amyloid. *J Mol Biol*. **299**:225-231.

Serpell, LC, Sunde M, Benson MD, Tennent GA, Pepys MB *et al*. (2000b) The protofilament substructure of amyloid fibrils. *J Mol Biol*. **300**:1033-1039.

Serpell LC, Berriman J, Jakes R, Goedert M, Crowther RA (2000c). Fiber diffraction of synthetic α -synuclein filaments shows amyloid-like cross-β conformation. *Proc Natl Acad Sci USA* **97**:4897-4902.

Skamris T, Marasini C, Madsen KL, Foderà V, Vestergaard B (2019) Early stage alpha-synuclein amyloid fibrils are reservoirs of membrane-binding species. *Sci Rep*. **9**:1733.

Shameli A, Xiao W, Zheng Y, Shyu S, Sumodi J *et al*. (2016) A critical role for alpha-synuclein in development and function of T lymphocytes. *Immunobiology* **221**:333-340.

Sharon R, Goldberg MS, Bar-Josef I, Betensky RA, Shen J *et al*. (2001) α-Synuclein occurs in lipid-rich high molecular weight complexes, binds fatty acids, and shows homology to the fatty acid-binding proteins. *Proc Natl Acad Sci USA* **98**:9110-9115.

Shi M, Liu C, Cook TJ, Bullock KM, Zhao Y *et al*. (2014) Plasma exosomal α-synuclein is likely CNS-derived and increased in Parkinson's disease. *Acta Neuropathol*. **128**:639-650.

Shi Z, Sachs JN, Rhoades E, Baumgart T (2015) Biophysics of α-synuclein induced membrane remodeling. *Phys Chem Chem Phys*. **17**:15561-15568.

Shin EC, Cho SE, Lee DK, Hur MW, Paik SR *et al*. (2000) Expression patterns of α-synuclein in human hematopoietic cells and in Drosophila at different developmental stages. *Mol Cells* **10**:65-70.

Shrivastava AN, Redeker V, Fritz N, Pieri L, Almeida LG *et al*. (2015) α-Synuclein assemblies sequester neuronal α3-Na^+/K^+-ATPase and impair Na^+ gradient. *EMBO J*. **34**:2408-2423.

Simuni T, Sethi K (2008) Nonmotor manifestations of Parkinson's disease. *Ann Neurol.* **64:**65-80.

Singleton A, Farrer M, Johnson J, Singleton A, Hague S *et al*. (2003) α-Synuclein locus triplication causes Parkinson's disease. *Science* **302**:841.

Singleton AB, Farrer MJ, Bonifati V (2013) The genetics of Parkinson's disease: progress and therapeutic implications. *Mov Disord*. **28**:14-23.

Singleton AB, Farrer MJ, Johnson J, Singleton A, Hague S *et al*. (2003) α-Synuclein locus triplication causes Parkinson's disease. *Science* **302**:841.

Smith WW, Jiang H, Pei Z, Tanaka Y, Morita H *et al*. (2005) Endoplasmic reticulum stress and mitochondrial cell death pathways mediate A53T mutant α-synuclein-induced toxicity. *Hum Mol Genet.* **14**:3801-3811.

Snead D, Eliezer D (2014) α-Synuclein Function and Dysfunction on Cellular Membranes. *Exp. Neurobiol.* **23**:292-313.

Sokolov Y, Kozak JA, Kayed R, Chanturiya A, Glabe C *et al*. (2006) Soluble amyloid oligomers increase bilayer conductance by altering dielectric structure. *J Gen Physiol*. **128**:637-647.

Spillantini MG, Crowther RA, Jakes R, Hasegawa M, Goedert M (1998) α-Synuclein in filamentous inclusions of Lewy bodies from Parkinson's disease and dementia with Lewy bodies. *Proc Natl Acad Sci USA* **95**:6469-6473.

Stefanis L, Emmanouilidou E, Pantazopoulou M, Kirik D, Vekrellis K *et al*. (2019) How is alpha-synuclein cleared from the cell? *J Neurochem.* **150**:577-590.

Stefanovic AN, Stöckl MT, Claessens MM, Subramaniam V (2014) α-Synuclein oligomers distinctively permeabilize complex model membranes. *FEBS J.* **281**:2838-50.

Steidl JV, Gomez-Isla T, Mariash A, Ashe KH, Boland LM (2003) Altered short-term hippocampal synaptic plasticity in mutant α-synuclein transgenic mice. *Neuroreport* **14**: 219-223.

Steiner JA, Quansah E, Brundin P (2018) The concept of alpha-synuclein as a prion-like protein: ten years after. *Cell Tissue Res*. **373**:161-173.

Stephens AD, Zacharopoulou M, Kaminski Schierle GS (2019) The cellular environment affects monomeric α-synuclein structure. *Trends Biochem Sci.* **44**:453-466.

Stöckl MT, Fischer P, Wanker E, Herrmann A (2008) α-Synuclein selectively binds to anionic phospholipids embedded in liquid-disordered domains. *J Mol Biol*. **375**:1394-1404.

Stöckl MT, Claessens MM, Subramaniam V (2012) Kinetic measurements give new insights into lipid membrane permeabilization by α-synuclein oligomers. *Mol Biosyst*. **8**:338-45.

Stöckl MT, Zijlstra N, Subramaniam V (2013) α-Synuclein oligomers: an amyloid pore? Insights into mechanisms of α-synuclein oligomer-lipid interactions. *Mol Neurobiol*. **47**:613-621.

Stoessl AJ, Lehericy S, Strafella AP (2014) Imaging insights into basal ganglia function, Parkinson's disease, and dystonia. *Lancet* **384**:532-544.

Sunde M, Serpell LC, Bartlam M, Fraser PE, Pepys MB *et al*. (1997) Common core structure of amyloid fibrils by synchrotron X-ray diffraction. *J Mol Biol*. **273**:729-739.

Sung J Y, Park SM, Lee CH, Um JW, Lee HJ *et al*. (2005) Proteolytic cleavage of extracellular secreted α-synuclein via matrix metalloproteinases. *J Biol Chem*. **280**:25216-25224.

Surguchev A, Surguchov A (2015) Effect of α-synuclein on membrane permeability and synaptic transmission: a clue to neurodegeneration? *J Neurochem*. **132**:619-621.

Surmeier DJ (2007) Calcium, ageing, and neuronal vulnerability in Parkinson's disease. *Lancet Neurol*. **6**:933-938.

Surmeier DJ, Schumacker PT (2013) Calcium, bioenergetics, and neuronal vulnerability in Parkinson's disease. *J Biol Chem*. **288**:10736-10741.

Sutton RB, Fasshauer D, Jahn R, Brunger AT (1998) Crystal structure of a SNARE complex involved in synaptic exocytosis at 2.4 Å resolution. *Nature* **395**:347-353.

Taira T, Saito Y, Niki T, Iguchi-Ariga SM, Takahashi K *et al*. (2004) DJ-1 has a role in antioxidative stress to prevent cell death. *EMBO Rep*. **5**:213-218.

Takahashi T, Yamashita H, Nagano Y, Nakamura T, Ohmori H *et al*. (2003) Identification and characterization of a novel Pyk2/related adhesion focal tyrosine kinase-associated protein that inhibits α-synuclein phosphorylation. *J Biol Chem.* **278**:42225-42233.

Tamo W, Imaizumi T, Tanji K, Yoshida H, Mori F *et al*. (2002) Expression of α-synuclein, the precursor of non-amyloid β component of Alzheimer's disease amyloid, in human cerebral blood vessels. *Neurosci Lett*. **326**:5-8.

Tan YY, Wu L, Zhao ZB, Wang Y, Xiao Q *et al*. (2014) Methylation of α-synuclein and leucine-rich repeat kinase 2 in leukocyte DNA of Parkinson's disease patients. *Parkinsonism Relat Disord*. **20**:308-313.

Tapias V, Hu X, Luk KC, Sanders LH, Lee VM *et al*. (2017) Synthetic alpha-synuclein fibrils cause mitochondrial impairment and selective dopamine neurodegeneration in part via iNOS-mediated nitric oxide production. *Cell Mol Life Sci*. **74**:2851-2874.

Tetzlaff JE, Putcha P, Outeiro TF, Ivanov A, Berezovska O *et al*. (2008) CHIP targets toxic α-synuclein oligomers for degradation. *J Biol Chem*. **283**:17962-17968.

Thayer SA, Usachev YM, Pottorf WJ (2002) Modulating Ca^{2+} clearance from neurons. *Front Biosci*. **7**:d1255-79.

Thome AD, Harms AS, Volpicelli-Daley LA, Standaert DG (2016) MicroRNA-155 Regulates Alpha-Synuclein-Induced Inflammatory Responses in Models of Parkinson Disease. *J Neurosci*. **36**:2383-2390.

Thompson MJ, Balbirnie M, Wiltzius JJ, McFarlane HT, Madsen AØ *et al*. (2007) Atomic structures of amyloid cross-beta spines reveal varied steric zippers. *Nature* **447**:453-457.

Thornberry NA, Rano TA, Peterson EP, Rasper DM, Timkey T *et al*. (1997) A combinatorial approach defines specificities of members of the caspase family and granzyme B. Functional relationships established for key mediators of apoptosis. *J Biol Chem.* **272**:17907-17911.

Tio M, Wen R, Lim YL, Zukifli ZHB, Xie S *et al*. (2017) Varied pathological and therapeutic response effects associated with CHCHD2 mutant and risk variants. *Hum Mutat*. **38**:978-987.

Tipping KW, Karamanos TK, Jakhria T, Iadanza MG, Goodchild SC *et al*. (2015) pH-induced molecular shedding drives the formation of amyloid fibril-derived oligomers. *Proc Natl Acad Sci USA* **112**:5691-5696.

Tofaris GK, Layfield R, Spillantini MG (2001) α-Synuclein metabolism and aggregation is linked to ubiquitin-independent degradation by the proteasome. *FEBS Lett*. **509**:22-26.

Tokuda T, Qureshi MM, Ardah MT, Varghese S, Shehab SA *et al*. (2010) Detection of elevated levels of α-synuclein oligomers in CSF from patients with Parkinson disease. *Neurology* **75**:1766-1772.

Tosatto L, Andrighetti AO, Plotegher N, Antonini V, Tessari I *et al*. (2012) α-Synuclein pore forming activity upon membrane association. *Biochim Biophys Acta* **1818**:2876-2883.

Tran HT, Chung CHY, Iba M, Zhang B, Trojanowski JQ *et al*. (2014) α-Synuclein immunotherapy blocks uptake and templated propagation of misfolded α-synuclein and neurodegeneration. *Cell Rep*. **7**:2054-2065.

Tsigelny IF, Sharikov Y, Wrasidlo W, Gonzalez T, Desplats PA *et al*. (2012) Role of α-synuclein penetration into the membrane in the mechanisms of oligomer pore formation. *FEBS J.* **279**:1000-1013.

Tucci A, Charlesworth G, Sheerin UM, Plagnol V, Wood NW *et al*. (2012) Study of the genetic variability in a Parkinson's Disease gene: *EIF4G1*. *Neurosci Lett*. **518**:19-22.

Tuttle MD, Comellas G, Nieuwkoop AJ, Covell DJ, Berthold DA *et al*. (2016) Solid-state NMR structure of a pathogenic fibril of full-length human α-synuclein. *Nat Struct Mol Biol*. **23**:409-415.

Ueda K, Fukushima H, Masliah E, Xia Y, Iwai A *et al*. (1993) Molecular cloning of cDNA encoding an unrecognized component of amyloid in Alzheimer disease. *Proc Natl Acad Sci USA* **90**:11282-11286.

Ulusoy A, Febbraro F, Jensen PH, Kirik D, Romero-Ramos M (2010) Co-expression of C-terminal truncated alpha-synuclein enhances full-length alpha-synuclein-induced pathology. *Eur J Neurosci*. **32**:409-422.

Urrea L, Segura-Feliu M, Masuda-Suzukake M, Hervera A, Pedraz L *et al*. (2018) Involvement of cellular prion protein in α-synuclein transport in neurons. *Mol Neurobiol*. **55**:1847-1860.

Uversky VN, Li J, Fink AL (2001) Evidence for a partially folded intermediate in alpha-synuclein fibril formation. *J Biol Chem*. 2001, **276**:10737-10744.

Uversky VN, Li J, Souillac P, Millett IS, Doniach S *et al*. (2002) Biophysical properties of the synucleins and their propensities to fibrillate: inhibition of α-synuclein assembly by β- and γ-synucleins. *J Biol Chem*. **277**:11970-11978.

Uversky VN (2003) A protein-chameleon: conformational plasticity of α-synuclein, a disordered protein involved in neurodegenerative disorders. *J Biomol Struct Dyn*. **21**:211-234.

Uversky VN (2007) Neuropathology, biochemistry, and biophysics of α-synuclein aggregation. *J Neurochem*. **103**:17-37.

van Diggelen F, Hrle D, Apetri M, Christiansen G, Rammes G *et al*. (2019) Two conformationally distinct α-synuclein oligomers share common epitopes and the ability to impair long-term potentiation. *PLoS One* **14**:e0213663.

van Rooijen BD, van Leijenhorst-Groener KA, Claessens MM, Subramaniam V (2009) Tryptophan fluorescence reveals structural features of α-synuclein oligomers. *J Mol Biol*. **394**:826-33.

Vargas KJ, Makani S, Davis T, Westphal CH, Castillo PE *et al*. (2014) Synucleins regulate the kinetics of synaptic vesicle endocytosis. *J Neurosci*. **34**:9364-9376.

Varkey J, Isas JM, Mizuno N, Jensen MB, Bhatia VK *et al*. (2010) Membrane curvature induction and tubulation are common features of synucleins and apolipoproteins *J Biol Chem*. **285**:32486-32493.

Vilar M, Chou HT, Luhrs T, Maji SK, Riek-Loher D *et al*. (2008) The fold of α-synuclein fibrils. *Proc Natl Acad Sci USA* **105**:8637-8642.

Vilariño-Güell C, Wider C, Ross OA, Dachsel JC, Kachergus JM *et al*. (2011) *VPS35* mutations in Parkinson disease. *Am J Hum Genet*. **89**:162-167.

Vilariño-Guell C, Rajput A, Milnerwood AJ, Shah B, Szu-Tu C *et al*. (2014) *DNAJC13* mutations in Parkinson disease. *Hum Mol Genet*. **23**:1794-1801.

Villa N, Do A, Hershey JW, Fraser CS (2013) Human eukaryotic initiation factor 4G (eIF4G) protein binds to eIF3c, -d, and -e to promote mRNA recruitment to the ribosome. *J Biol Chem*. **288**:32932-32940.

Villar-Piqué A, da Fonseca TL, Outeiro TF (2016) Structure, function and toxicity of alpha-synuclein: the Bermuda triangle in synucleinopathies. *J Neurosci*. **139**:240-255.

Visanji NP, Marras C, Hazrati L-N, Liu LWC, Lang AE (2014) Alimentary, my dear Watson? The challenges of enteric α-synuclein as a Parkinson's disease biomarker. *Mov Disord*. **29**:444-450.

Vogiatzi T, Xilouri M, Vekrellis K, Stefanis L (2008) Wild type α-synuclein is degraded by chaperone-mediated autophagy and macroautophagy in neuronal cells. *J Biol Chem*. **283**:23542-23556.

Volles MJ, Lee SJ, Rochet JC, Shtilerman MD, Ding TT *et al*. (2001) Vesicle permeabilization by protofibrillar alpha-synuclein: implications for the pathogenesis and treatment of Parkinson's disease. *Biochemistry* **40**:7812-7819.

Volles MJ, Lansbury PT (2002) Vesicle permeabilization by protofibrillar α-synuclein is sensitive to Parkinson's disease-linked mutations and occurs by a pore-like mechanism. *Biochemistry* **41**:4595-4602.

Volpicelli-Daley LA, Luk KC, Patel TP, Tanik SA, Riddle DM *et al*. (2011) Exogenous α-synuclein fibrils induce Lewy body pathology leading to synaptic dysfunction and neuron death. *Neuron* **72**:57-71.

Vyklicky V, Korinek M, Smejkalova T, Balik A, Krausova B *et al*. (2014) Structure, function, and pharmacology of NMDA receptor channels. *Physiol Res*. **63**:191-203.

Waddington CH (2012) The epigenotype. 1942. *Int J Epidemiol*. **41**:10-13.

Wakabayashi K, Tanji K, Mori F, Takahashi H (2007) The Lewy body in Parkinson's disease: Molecules implicated in the formation and degradation of α-synuclein aggregates. *Neuropathology* **27**:494-506.

Wales P, Pinho R, Lazaro DF, Outeiro TF (2013) Limelight on α-synuclein: pathological and mechanistic implications in neurodegeneration. *J Parkinsons Dis*. **3**:415-459.

Walsh DM, Selkoe DJ (2007) Aβ oligomers - a decade of discovery. *J Neurochem*. **101**:1172-1184.

Wang W, Perovic I, Chittuluru J, Kaganovich A, Nguyen LT *et al*. (2011) A soluble α-synuclein construct forms a dynamic tetramer. *Proc Natl Acad Sci USA* **108**:17797-17802.

Wang X, Moualla D, Wright JA, Brown DR (2010) Copper binding regulates intracellular α-synuclein localisation, aggregation and toxicity. *J Neurochem*. **113**:704-714.

Watson JB, Hatami A, David H, Masliah E, Roberts K *et al*. (2009) Alterations in corticostriatal synaptic plasticity in mice overexpressing human α-synuclein. *Neuroscience* **159**:501-513.

Watts JC, Bourkas MEC, Arshad H (2018) The function of the cellular prion protein in health and disease. *Acta Neuropathol*. **135**:159-178.

Waxman EA, Giasson BI (2008) Specificity and regulation of casein kinase-mediated phosphorylation of α-synuclein. *J Neuropathol Exp Neurol*. **67**:402-416.

Webb JL, Ravikumar B, Atkins J, Skepper JN, Rubinsztein DC (2003) α-Synuclein is degraded by both autophagy and the proteasome. *J Biol Chem*. 278:25009-25013.

Wenning GK, Ben Shlomo Y, Magalhaes M, Daniel SE, Quinn NP (1994) Clinical features and natural history of multiple system atrophy. An analysis of 100 cases. *Brain* **117**:835-845.

Wennström M, Surova Y, Hall S, Nilsson C, Minthon L *et al*. (2013) Low CSF levels of both α-synuclein and the α-synuclein cleaving enzyme neurosin in patients with synucleinopathy. *PLoS One* **8**:e53250.

West AB, Moore DJ, Choi C, Andrabi SA, Li X *et al*. (2007) Parkinson's disease-associated mutations in LRRK2 link enhanced GTP-binding and kinase activities to neuronal toxicity. *Hum Mol Genet*. **16**:223-232.

Westphal CH, Chandra SS (2013) Monomeric synucleins generate membrane curvature *J Biol Chem*. **288**:1829-1840.

Whiten DR, Cox D, Horrocks MH, Taylor CG, De S *et al*. (2018) Single-molecule characterization of the interactions between extracellular chaperones and toxic α-synuclein oligomers. *Cell Rep.* **23**:3492-3500.

Wiethoff CM, Wodrich H, Gerace L, Nemerow GR (2005) Adenovirus protein VI mediates membrane disruption following capsid disassembly. *J Virol*. **79**:1992-2000.

Wimalasena K (2011) Vesicular monoamine transporters: structure-function, pharmacology, and medicinal chemistry. *Med Res Rev*. **31**:483-519.

Winner B, Jappelli R, Maji SK, Desplats PA, Boyer L *et al*. (2011) In vivo demonstration that α-synuclein oligomers are toxic. *Proc Natl Acad Sci USA* **108**:4194-4199.

Winslow AR, Chen CW, Corrochano S, Acevedo-Arozena A, Gordon DE *et al*. (2010) α-Synuclein impairs macroautophagy: implications for Parkinson's disease. *J Cell Biol.* **190**:1023-1037.

Woerman AL, Stohr J, Aoyagi A, Rampersaud R, Krejciova Z *et al*. (2015) Propagation of prions causing synucleinopathies in cultured cells. *Proc Natl Acad Sci USA* **112**:4949-4958.

Wood SJ, Wypych J, Steavenson S, Louis JC, Citron M *et al*. (1999) α-Synuclein fibrillogenesis is nucleation-dependent. Implications for the pathogenesis of Parkinson's disease. *J Biol Chem*. **274**:19509-19512.

Wright JA, Wang X, Brown DR (2009) Unique copper-induced oligomers mediate α-synuclein toxicity. *FASEB J*. **23**:2384-2393.

Wu B, Liu Q, Duan C, Li Y, Yu S *et al*. (2011) Phosphorylation of α-synuclein upregulates tyrosine hydroxylase activity in MN9D cells. *Acta Histochem.* **113**:32-35.

Wu KP, Kim S, Fela DA, Baum J (2008) Characterization of conformational and dynamic properties of natively unfolded human and mouse α-synuclein ensembles by NMR: implication for aggregation. *J Mol Biol*. **378**:1104-1115.

Xilouri M., Brekk OR., Stefanis L (2013) α-Synuclein and protein degradation systems: a reciprocal relationship. *Mol Neurobiol*. 47:537-551.

Yankner BA, Duffy LK, Kirschner DA (1990) Neurotrophic and neurotoxic effects of amyloid beta protein: reversal by tachykinin neuropeptides. *Science* **250**:279-282.

Yavich L, Tanila H, Vepsalainen S, Jakala P (2004) Role of α-synuclein in presynaptic dopamine recruitment. *J Neurosci.* **24**:11165-11170.

Yu WH, Dorado B, Figueroa HY, Wang L, Planel E *et al*. (2009) Metabolic activity determines efficacy of macroautophagic clearance of pathological oligomeric α-synuclein. *Am J Pathol*. **175**:736-747.

Yu V, Yang W, Li X, Li X, Yu S (2019) Alpha-synuclein oligomerization increases its effect on promoting NMDA receptor internalization. *Int J Clin Exp Pathol*. **12**:87-100.

Zakharov SD, Hulleman JD, Dutseva EA, Antonenko YN, Rochet JC *et al*. (2007) Helical α-synuclein forms highly conductive ion channels, *Biochemistry* **46**:14369-14379.

Zaltieri M, Grigoletto J, Longhena F, Navarria L, Favero G *et al*. (2015) α-Synuclein and synapsin III cooperatively regulate synaptic function in dopamine neurons. *J Cell Sci*. **128**:2231-2243.

Zampagni M, Cascella R., Casamenti F, Grossi C, Evangelisti E *et al*. (2011) A comparison of the biochemical modifications caused by toxic and non-toxic protein oligomers in cells. *J Cell Mol Med*. **15**:2106-2116.

Zarbiv Y, Simhi-Haham D, Israeli E, Elhadi SA, Grigoletto J *et al*. (2014) Lysine residues at the first and second KTKEGV repeats mediate alpha-synuclein binding to membrane phospholipids. *Neurobiol Dis*. **70**:90-98.

Zarranz JJ, Alegre J, Gómez-Esteban JC, Lezcano E, Ros R *et al*. (2004) The new mutation, E46K, of α-synuclein causes Parkinson and Lewy body dementia. *Ann Neurol*. **55**:164-173.

Zhang L, Yuan Y, Tong Q, Jiang S, Xu Q *et al*. (2016) Reduced plasma taurine level in Parkinson's disease: association with motor severity and levodopa treatment. *Int J Neurosci*. **126**:630-636.

Zhang R, Hu X, Khant H, Ludtke SJ, Chiu W *et al*. (2009) Interprotofilament interactions between Alzheimer's $A\beta_{1-42}$ peptides in amyloid fibrils revealed by cryoEM. *Proc Natl Acad Sci USA* **106**:4653-4658.

Zheng B, Liao Z, Locascio JJ, Lesniak KA, Roderick SS *et al*. (2010) PGC-1α, a potential therapeutic target for early intervention in Parkinson's disease. *Sci Transl Med.* **2**:52ra73.

Zhou B, Wen M, Yu WF, Zhang CL, Jiao L (2015) The diagnostic and differential diagnosis utility of cerebrospinal fluid α –synuclein levels in Parkinson's disease: a meta-analysis. *Parkinsons Dis*. **2015**:567386.

Zhou W, Long C, Reaney SH, Di Monte DA, Fink AL *et al*. (2010) Methionine oxidation stabilizes non-toxic oligomers of α-synuclein through strengthening the auto-inhibitory intra-molecular long-range interactions. *Biochim Biophys Acta* **1802**:322-330.

Zhu M, Qin ZJ, Hu D, Munishkina LA, Fink AL (2006) α-Synuclein can function as an antioxidant preventing oxidation of unsaturated lipid in vesicles. *Biochemistry* **45**:8135-8142.

Zündorf G, Rieser G (2011) Calcium dysregulation and homeostasis of neural calcium in the molecular mechanisms of neurodegenerative diseases provide multiple targets for neuroprotection. *Antioxid Redox Signal*. **14**:1275-88.